AN EVALUATION OF THE USE OF NATURAL STABLE ISOTOPES OF WATER TO TRACK WATER MOVEMENT THROUGH OIL SANDS MINE CLOSURE LANDFORMS

A Thesis Submitted to the College of Graduate Studies and Research in Partial Fulfillment of the Degree of Master of Science in the Department of Civil Engineering, University of Saskatchewan, Saskatoon, Canada

By

Thomas John Baer

PERMISSION TO USE

In presenting this thesis in partial fulfillment of the requirements for a Postgraduate degree from the University of Saskatchewan, I agree that the Libraries of this University may make it freely available for inspection. I further agree that permission for the copying of this thesis in any manner, in whole or in part, for scholarly purposes may be granted by the professor or professors who supervised my thesis work or, in their absence, by the head of the Department or the Dean of the College in which my thesis work was done. It is understood that any copying or publication or use of this thesis or parts thereof for financial gain shall not be allowed without my written permission. It is also understood that due recognition shall be given to me and to the University of Saskatchewan in any scholarly use which may be made of any material in my thesis.

Requests for permission to copy or to make other use of material in this thesis in whole or part should be addressed to:

Head of the Department of Civil Engineering
University of Saskatchewan
57 Campus Drive
Saskatoon, Saskatchewan S7N 5A9
Canada

OR

Dean of the College of Graduate Studies and Research
University of Saskatchewan
107 Administration Place
Saskatoon, Saskatchewan S7N 5A2
Canada

ABSTRACT

Surface mining of oil sands results in extensive land disturbance, earth movement and water usage. After mining, the disturbed landscapes must be reconstructed and reclaimed as natural landforms. There are numerous challenges associated with understanding the responses of these landforms over time, including a need to track and characterize water movement through closure landforms to understand the hydrological responses of these landforms over time. This study attempted to use natural stable isotopes of water (δD and $\delta^{18}O$) to identify and characterize source waters from various closure landforms at an oil sands mine site.

The study area is Syncrude's Mildred Lake mine, an open pit oil sands mine located in northern Alberta. A variety of groundwater, surface water and soil samples from a variety of landforms (overburden dumps, composite and mature fine tailings areas, tailings sand structures and freshwater reservoirs) were collected in an attempt to fully represent the isotopic distribution of waters across the mine site. Laboratory analysis of δD and $\delta^{18}O$ was done on all samples.

The local meteoric water line first established by Hilderman (2011) was redeveloped with additional precipitation data and calculated to be δD=7.0(δ18O) -18.6‰. A natural evaporation line having a slope of 5.3 was calculated for the mine site with samples collected from three surface water ponds on the mine site.

Five primary source waters were identified on the mine site: process affected water/tailings, rainfall, snow, interstitial shale water and Mildred Lake water. It was found that these sources of water generally have unique natural stable water isotope signatures. Process affected water at the site generally had an enriched signature compared to other mine waters. The enrichment was attributed to fractionation from the recycle water circuit and natural evaporation.

The characterizations of these source waters were then used in several hydrogeological examples to demonstrate that natural stable water isotopes can be applied to water balance estimates and to identify water movement processes related to closure landforms.

ACKNOWLEDGEMENTS

I would first off like to thank my supervisor, Dr. Lee Barbour for all his guidance and support throughout my research. He has been a fantastic mentor, supervisor and role model throughout my time working for him. I would also like to thank my committee members Dr. Jim Hendry and Dr. Grant Ferguson for providing me with valuable input and suggestions.

I would like to thank Syncrude Canada Ltd., NSERC and the University of Saskatchewan for providing funding for this project. Thank you again Dr. Jim Hendry for providing lab space and equipment and Erin Schmeling for all her help and guidance in the laboratory. I would like to thank multiple people who assisted in sample collection. Thank you Bryan Koehler, Kathryn Hearson and Dyan Pratt for accompanying me on site and assisting in sample collection. Thank you Dr. Carl Mendoza of the University of Alberta for allowing me to assist with piezometer installations and other projects which provided me with multiple opportunities to collect samples. I would also like to thank Jessica Clark of Syncrude and Wendy Kline of Terracon who collected a variety of water samples across the site which were instrumental to this project. Thank you Warren Zubot and Jessica Clark (once again) for providing site information and data.

Lastly and most importantly, I would like to thank my family and friends for their unwavering support, encouragement and understanding these last two years and throughout my life. I am truly blessed to have these people in my life. Most notably, I would like to thank my parents, Terry and Darlene and my younger brothers, Mitch and Donavan.

TABLE OF CONTENTS

LIST OF FIGURES

LIST OF TABLES

1 INTRODUCTION

The oil sands industry in the Athabasca oil sands region in northern Alberta has experienced rapid growth and development as the global demand for energy has increased. The Canadian Association of Petroleum Producers (CAPP) estimate that oil sands crude oil production will increase from 1.5 million barrels per day in 2010 to 3.0 million barrels per day in 2020 (CAPP, 2011).

In 2011, surface mining accounted for 51% of Alberta's oil production (Government of Alberta 2013). Surface minable oil sands make up about 20% of the oil sands reserves in Alberta and make up only 3% of the total oil sands area (Government of Alberta 2012b). The area available for surface mining in Alberta is approximately 4,800 km^2 in which only about 715 km^2 have been disturbed (Government of Alberta 2012a). Consequently, the surface mining of oil sands is likely to continue for some time.

Oil sands surface mining is often criticized due to the negative environmental impacts and large amounts of land disturbance. Environmental regulations require that all landscapes disturbed by oil sands mining be reclaimed and returned to an equivalent capacity to natural sites.

Potentially, there could be 4,800 km^2 of disturbed and mined landscape in northern Alberta that will require reclamation. The disturbed landscapes commonly referred to as closure landforms include mined out pits, in-pit and above ground tailings/process water storage areas, tailings sand structures and overburden dumps. Closure landforms can be reclaimed as a variety of landforms and ecosystems such as wetlands, forests, and end-pit lakes.

1.1 Problem Description

There are many challenges associated with the reclamation of closure landforms. The Royal Society of Canada (RSC) state that one of the main issues is that the mining process significantly disturbs and alters the original landscape, habitat and hydrology (RSC 2011). It is expected that

the time required for these landscapes to evolve back towards similar biological, geo-technical and hydrological conditions as those that existed prior to the disturbance may take decades to centuries.

The scale of the land disturbances and the long durations involved to ensure that these landscapes are evolving towards an equivalent capacity require that methods be developed to monitor the hydrogeological evolution of these landforms over time. Of particular concern is the challenge of characterizing water movement through these landforms over time with concomitant release from these landforms of constituents of concern.

The water flow and storage characteristics of closure landforms will alter over time. This alteration will affect the rates of release of both water (as surface and as groundwater) and the contaminants to the environment. Additionally, biological and geo-technical characteristics of closure landforms will be affected by the hydrogeological evolution.

As a result, it is important that methods be developed to track water movement through these landforms and understand the physical hydrogeological response of closure landforms over time. A better understanding of these characteristics and processes enables more representative numerical models of landscape performance to be developed. These models provide tools for industry to evaluate alternative closure designs and help to further understand the long term response of closure landforms.

1.2 Research Objectives

Traditionally, water chemistry is employed in hydrogeological studies to characterize groundwater. However, obtaining water chemistry data is expensive and time consuming. An alternative technique to characterize water is to utilize natural stable isotope compositions of water (deuterium/hydrogen and oxygen-18/oxygen-16 pairs).

Natural stable isotopes have been utilized successfully in a multitude of hydrological and hydrogeological applications. Natural occurring deuterium and oxygen-18 profiles have been utilized:

- To determine dominant transport mechanisms through aquitards (Hendry et al. 2011) and in unsaturated zones (Adomako et al. 2010);

- At a regional scale to characterize landscape hydrogeology in both natural (Athanasopoulos 2009, Criss and Davisson 1996) and mine site settings (Douglas 1997); and,
- In other oil sands closure landform studies to interpret flow mechanisms through reclamation covers (Kelln 2008) and to estimate percolation into a shale overburden dump (Hilderman 2011).

It is postulated based on these earlier studies, that it will be possible to characterize oil sands mine site waters using natural deuterium and oxygen-18 signatures. Using these characterizations, flow mechanisms through closure landforms can be further defined to help understand the transient hydrogeological evolution of closure landforms.

The overall goal of this study is to evaluate the applicability of using naturally occuring stable water isotopes to track water movement through oil sands closure landforms. The overall goal will be completed by addressing the following objectives:

- Assemble a site wide catalogue of stable water isotope signatures for the Mildred Lake Mine including water from: tailings (fluid fine tailings, sand tailings and composite tailings), the recycle water circuit, overburden (shale and glacial soils), surface water and meteoric water;
- Interpret this ‘isoscape’ data by identifying and characterizing the processes controlling the isotopic distribution across the site such as changes in the composition of stable water isotopes due to the upgrader processes, fractionation from within the tailings recycle water circuit, the presence of interstitial waters within overburden deposits, etc., and;
- Apply this ‘isoscape’ characterization to illustrate how mixing and flushing processes can be interpreted for oil sands mine closure landforms such as sand tailings and shale overburden.

The objectives were completed by collecting a range of water and soil samples across Syncrude’s Mildred Lake Mine Site. The natural deuterium and oxygen-18 compositions of the water and pore water were determined through a laboratory analysis. Following the laboratory analysis, waters across the site were characterized based on natural stable water isotope composition. The characterizations were then employed to make preliminary estimates on simple flow and water balance mechanisms within closure landforms.

1.3 Site Description

The study area is Mildred Lake Mine site, located about 35 km north of Fort McMurray, Alberta in the Athabasca oil sands region. The mine site is an active open pit mining operation that is owned and operated by Syncrude Canada Ltd. In 2011, The Mildred Lake Mine produced approximately 105 million barrels of crude oil (Syncrude 2012a). An aerial photograph of the mine site is shown in Figure 1.1.

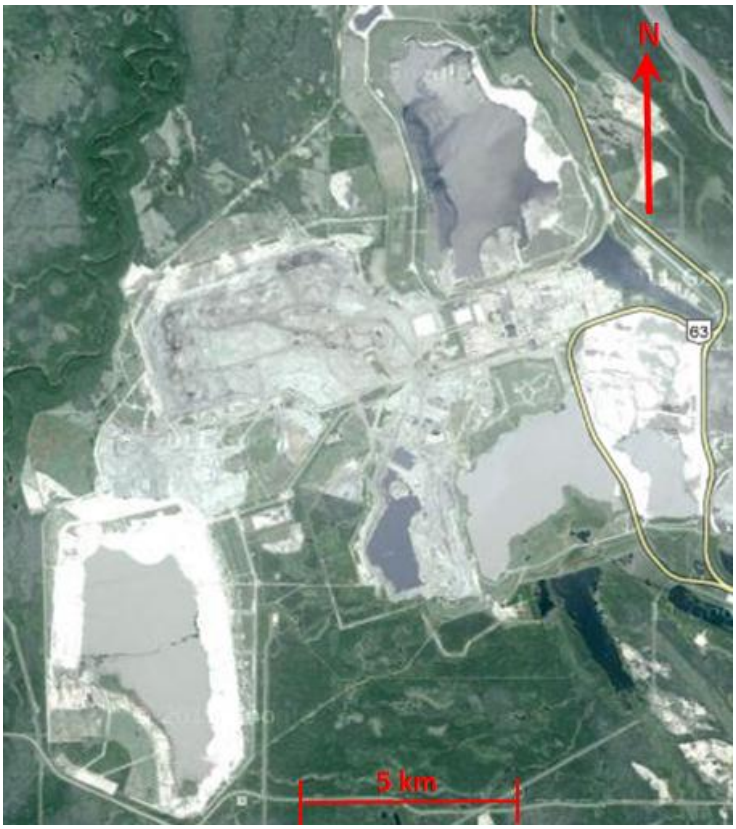

Figure 1.1: Aerial photograph of Mildred Lake Mine Site (Google 2013a)

There are a number of different landforms at the Mildred Lake mine, including tailings sand structures/dykes, above ground and in-pit tailings/process water confining areas, overburden dumps and active mining zones.

A large volume of water is stored on site and used in the extraction and upgrading process. In 2011, the Mildred Lake mine used 308.5 million m^3 of water, in which 38.5 million m^3 was drawn from the Athabasca River. The remaining water balance was made up of recycled process water (Syncrude 2012b).

1.3.1 Overview of mining process

The mining process begins by stripping the overburden material to gain access to the bitumen rich ore. Surface mineable oil sands are located at a maximum depth of about 70 m below ground (RSC 2011). The stripped overburden material is managed on site and stored in mined out pits or as surface deposits called overburden dumps.

The mined ore is transported hydraulically to a mill/upgrader complex for extraction and upgrading. Transporting, extraction and upgrading utilize large volumes of water. Water used in these processes is considered process affected water (PAW) and cannot be released directly to the environment. PAW is stored in tailings management areas and is reused in the transport, extraction and upgrading process.

The ore consists of a mixture of bitumen, water and mineral particles (ie: sand, silt, clay). Once the bitumen is extracted, the leftover tailings which contain mineral soil, PAW and trace amounts of bitumen is stored on site in tailings areas.

1.3.2 Tailings/PAW management areas

Large volumes of PAW and tailings are stored on site within tailings management areas, as shown in Figure 1.2.

The Mildred Lake mine has several tailings areas, consisting of both in-pit and above ground containments. These areas are used to store PAW and waste from the extraction and upgrader process in the form of tailings. The process or recycled water used in the extraction and upgrading process is drawn from the tailings ponds.

Southwest Sand Storage (SWSS) and Mildred Lake Settling Basin (MLSB) are both above ground tailings containment. MLSB is at maximum capacity and is used to store coke and fine tailings in the form of fluid fine tailings and mature fine tailings (Zubot 2010). SWSS is currently operational and stores coarse sand tailings and fluid tailings.

East in-pit (EIP), West in-pit (WIP) and Southwest in-pit (SWIP) are in-pit tailings areas. Both East and West in-pit are approaching maximum capacity and are currently undergoing closure. The northwest corner of East in-pit is currently being used as a reclamation study area called Sandhill Fen,a constructed wetland landform. West in-pit is being converted to an end pit lake, in which the fine tailings will be capped by a layer of fresh water and allowed to consolidate.

Figure 1.2: Tailings and process water areas at Mildred Lake Mine (Google 2013a) Abbreviations: EIP= East in-Pit, WIP= West in-pit, SWIP= Southwest in-pit, SWSS= Southwest Sands Storage, MLSB= Mildred Lake Settling Basin

1.3.3 Overburden dumps

Open pit mining results in the removal of large volumes of overburden to provide access to the bitumen rich ore. The overburden at the Mildred Lake mine site is comprised primarily of shale from the Cretaceous Clearwater Formation and a thin layer of sandstone from the Grand Rapids Formation (Chapman 2008). As a result, the overburden dumps at the Mildred Lake mine site are mainly composed of shale.

South Bison Hills is an overburden dump currently undergoing reclamation and is located south of West in-pit

1.4 Layout of Thesis

This thesis contains a total of six chapters. Chapter 2 is a literature review that covers isotope background and theory and relevant literature on hydrogeology and mine reclamation. Chapter 3 describes the field, lab and analytical materials and methodologies. Chapter 4 presents, discusses

and interprets the compiled data. Chapter 5 applies the interpreted results to practical applications to estimate water balance and flow mechanisms within closure landforms. The final chapter draws conclusions and discusses recommendations from this study.

2 LITERATURE REVIEW

This chapter will summarize relevant literature and background information for this study, including an introduction to the natural stable isotopes of water and background information regarding the Mildred Lake mine site. The information in this section was obtained primarily from journal articles, post-graduate theses, textbooks, scientific reports and select fact and information sheets found on the internet.

2.1 Natural Stable Isotopes of Water

Isotopes are atoms of the same element that have different atomic masses. The difference in mass results in slightly different physical characteristics between isotopes of the same element. The differences in physical properties cause small but measurable changes in isotope composition during physical and chemical reactions (Clark and Fritz 1997).

This study employs natural stable isotopes of water, deuterium (^{2}H or D)/hydrogen (^{1}H) and oxygen-18 (^{18}O)/oxygen-16 (^{16}O). In both cases, the lighter element makes up well over 99% of the natural abundance of the element. These isotope pairs are referred to as natural because both hydrogen and oxygen occur naturally within the water molecule and stable because they do not decay or degrade.

2.1.1 Reporting isotope compositions

Isotopes compositions are expressed as the ratio of heavy isotopes to light isotopes. For example, the deuterium-hydrogen pairing would be written as:

$$R = \frac{D}{H} \tag{2.1}$$

where R refers to the isotope ratio, D is the number of deuterium atoms and H is the number of

hydrogen atoms. A similar ratio can be expressed for the oxygen pairings ($R=^{18}O/^{16}O$).

Isotope compositions are often compared and measured to a reference standard and expressed on a δ (delta) basis in units of ‰ (per mille i.e. parts per thousand). The reasons for this notation include:

- Relative differences in isotope compositions between two samples can be measured more accurately than absolute isotope ratios (Hoefs, 2009);
- Using ratios leads to reporting results with five or more decimal places making ratios impractical to use (Mook 2006), and;
- Reference standards are required for international sample comparison (Mook 2006).

The δ value in units of ‰ for an isotope pairing is calculated by:

$$\delta = \left(\frac{R}{R_{std}} - 1\right) * 1000\ ‰ \tag{2.2}$$

where δ is the isotope composition in ‰, R is the isotope ratio of the sample, and R_{std} is the isotope ratio of the reference standard. In this paper, similar notations to Gat (2010) will be used to report δ-values. The D/H pairing will be reported as δD and the $^{18}O/^{16}O$ paring will be displayed as $\delta^{18}O$.

A negative δ-value indicates that the sample has less of the heavy isotope in comparison to the reference standard. On the other hand, a positive δ-value has more of the heavy isotope present compared to the reference standard. Lower or more negative δ-values are referred to as being isotopically "light" or "depleted" and higher δ-values are called isotopically "heavy" or "enriched".

2.1.2 Standards

The δ-notation requires the use of a reference standard. The most common global standard is the Vienna Standard Mean Ocean Water (VSMOW) standard and unless otherwise stated, all δ-values are referenced to VSMOW (Gat 2010). The accepted isotope ratios of VSMOW are 155.76 ppm for the D/H ratio (de Wit et al. 1980) and 2005.8 ppm for the $^{18}O/^{16}O$ ratio (Baertschi 1976).

2.2 Fractionation

Fractionation events are physical or chemical reactions that cause an alteration in isotope composition (Kendall and Doctor 2011). Fractionation occurs as a result of the differing atomic weights between isotope species which results in the heavier isotopes having a lower mobility and higher bond energy compared to the lighter isotopes (Mook 2006). These differing characteristics cause isotopes to behave differently during chemical and physical reactions, resulting in small but measurable changes in isotope composition between the products and reactants. As temperatures increase these effects become less significant; limiting fractionation at higher temperatures (Gat 1996).

2.2.1 Fractionation in the water cycle

Fractionation of deuterium and oxygen-18 isotopes in the water cycle can be triggered by phase changes, chemical reactions and biological reactions. However, in most natural scenarios chemical and biological reactions cause insignificant alterations in isotope properties of water. This is because the amount of hydrogen and oxygen in water usually far exceeds the geochemical or biological reactants (Savin 1980, Kendall and Doctor 2011). An exception to this is in high temperature and high pressure geo-thermal systems, where increased reactions between rock and water occur (Kendall and Doctor 2011).

2.2.2 Phase change fractionation

The main processes that cause fractionation of naturally occuring stable water isotopes within the water cycle are phase changes (Gat 1996, Kendall and Doctor 2011). Phase changes are the transitions from one physical state (solid, liquid or gas) to another state and include evaporation, condensation, melting and freezing. These physical reactions drive alterations in natural stable water isotope compositions and are responsible for unique signatures within the water cycle.

When fractionation occurs as a result of phase changes the heavy isotope will tend to remain in the lower energy state where there is less molecular movement. Alternatively, light isotopes will transition to the high energy state where there is more molecular movement. The energy states of each phase from the lowest to highest state are solid, liquid and gas. A summary of phase change fractionations is presented in Figure 2.1.

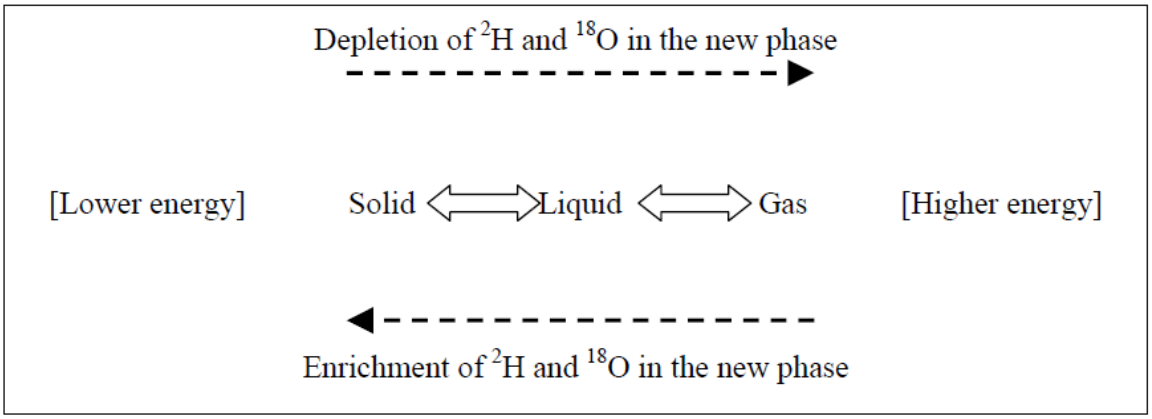

Figure 2.1: Fractionation during a phase change (Hilderman 2011)

An example of phase change fractionation process in the water cycle is evaporation, illustrated in Figure 2.2. When water evaporates, the light isotopes prefer the higher energy gaseous phase and will evaporate more readily than the heavy isotopes. This results in the accumulation of heavier isotopes in the residual water causing it to become enriched as it evaporates. In a similar manner, the vapour produced will be progressively enriched as evaporation progresses and enriches the residual water.

During condensation, the heavy isotopes transition more readily to the liquid phase, resulting in the progressive depletion of the vapour phase. Similar concepts can be applied to all other phase change processes.

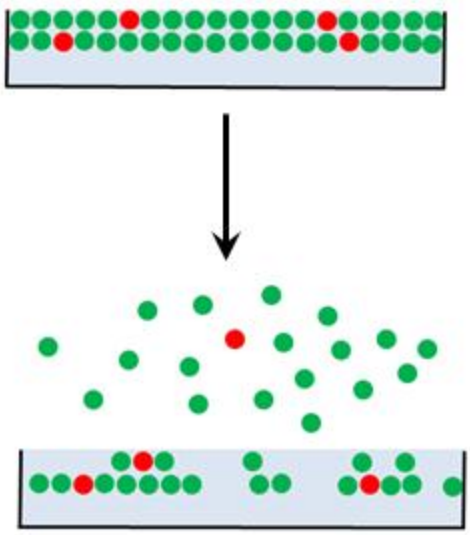

Figure 2.2: Demonstration of evaporation fractionation (green=light isotopes; red=heavy isotopes)

2.2.3 Mathematical description of fractionation

This section will go through the necessary mathematics to understand fractionation as it pertains to this study. Fractionation processes in the natural environment is usually split into two components: equilibrium and kinetic fractionation (Gat 1996, Mook 2001).

Equilibrium fractionation is reversible and is driven by differences in thermodynamic properties between heavy and light molecules. The differing properties result in varying isotope compositions between two phases when the system is in isotopic equilibrium. Clark and Fritz (1997) describe isotope equilibrium as a condition in which chemical equilibrium exists (forward and backward reactions are equal), the product and reactant reservoirs are well mixed and the reaction has proceeded far enough to completely mix the isotopes between the products and reactants.

Mathematically, equilibrium fractionation is described by the equilibrium fractionation factor, α:

$$\alpha_{2-1} = \frac{R_2}{R_1} = \frac{\delta_2 + 1000}{\delta_1 + 1000} \tag{2.3}$$

where $\alpha_{2\text{-}1}$ is the fractionation factor for the reaction and the subscripts 1 and 2 refer to the isotope composition of the reactant and product reservoirs at equilibrium conditions, respectively. A few key concepts regarding the equilibrium fractionation factor include:

- A fractionation factor greater than 1 indicates that the reactant will become depleted throughout the fractionation process, while the product will be enriched compared to the reactant. An example of this is condensation;
- A fractionation factor less than 1 indicates the reactant will become more enriched throughout fractionation, while the product will always be more depleted compared to the source reservoir;
- The fractionation factor for the reverse process is simply the reciprocal of the forward reactions fractionation factor ($\alpha_{condensation}=1/\alpha_{evaporation}$);
- A fractionation factor of 1 indicates no fractionation, and;
- The equilibrium fractionation factor is temperature dependant. Colder temperatures result in more fractionation and produce fractionation factors further away from 1.

Equilibrium fractionation effects have been studied extensively and fractionation factors have been experimentally determined and verified theoretically (Mook 2001). Majoube (1971) and Horita and Wesoloski (1994) have developed relationships for the liquid-vapour equilibrium fractionation factor. They also verified that the factor is dependent on temperature. The relationships developed by Majoube (1971) are displayed in Equations 2.4 and 2.5.

$$\ln(\alpha D_{l-v}) = \left(\frac{24844}{T^2} - \frac{76.248}{T} + 0.0526\right) \tag{2.4}$$

$$\ln\left(\alpha^{18}O_{l-v}\right) = \left(\frac{1137}{T^2} - \frac{0.4156}{T} - 0.0207\right) \tag{2.5}$$

where T is the temperature in K and $\alpha^{18}O$ and αD are the equilibrium fractionation factors for $\delta^{18}O$ and δD, respectively.

Equilibrium fractionation can also be described by the enrichment factor, ε which is derived from the fractionation factor by the following expression:

$$\varepsilon = (\alpha - 1) * 1000\ ‰ \tag{2.6}$$

The enrichment factor is expressed in units of ‰. A negative value is analogous to a fractionation factor less than 1, while a positive fractionation factor is analogous to a fractionation factor greater than 1.

Kinetic fractionation, also called non-equilibrium fractionation results when a system is in a non-equilibrium condition. This can be triggered by a change in temperature or the addition/removal of a reactant/product (Clark and Fritz 1997). Kinetic fractionation is more difficult to experimentally quantify (Mook 2001) and can either enhance or reduce fractionation effects (Clark and Fritz 1997).

Kinetic fractionation during natural evaporation to the atmosphere has been identified as being mainly dependant on relative humidity (Gat 1996, Gonfiantini 1986). Gat (1996) quantifies the kinetic fractionation for natural evaporative processes with the following equation:

$$\epsilon_k = (1 - h) \cdot \theta \cdot n \cdot C_D \tag{2.7}$$

where ε_k is the kinetic enrichment, h is the relative humidity and C_D is the theoretical kinetic enrichment constant and has a value of 28.5‰ for $\delta^{18}O$ and 25.1‰ for δD (Gat 1996, Kendall and Caldwell 1998). The weighting term, θ is a factor dependant on the size of the water body (Kendall and Caldwell 1998). Empirically derived θ-values are shown in Table 2.1.

Table 2.1: Empirically derived θ values

Water Body	θ	Reference
Small Lakes	1	(Gat 1995)
North American Great Lakes	0.88	(Gat et al. 1994)
Eastern Mediterranean Sea	0.5	(Gat et al. 1996)

The n-term also ranges between 0.5 to 1 and accounts for the possibility of stagnant air layers within the evaporation process. For an open body of water, n is equal to 0.5 (Gat 1996). Alternatively, n is approximately equal to 1 when evaporation occurs through a stagnant air layer (Kendall and Caldwell 1998). This includes evaporation which occurs from soils (Barnes and Allison 1988) and leaves (Allison et al. 1985).

Clark and Fritz (1997) suggest that the equilibrium and kinetic fractionation components for natural evaporation can be combined by summing the enrichment factors of each component, as shown below:

$$\epsilon_{tot} = \epsilon_{eq} + \epsilon_k \tag{2.8}$$

where ε_{tot} is the total enrichment, ε_{eq} is the equilibrium enrichment and ε_k is the kinetic enrichment.

The kinetic and equilibrium fractionation factors describe isotopic partitioning between reactant and product reservoirs throughout a chemical reaction. Attempts to model fractionation processes rely on the Rayleigh distillation equation to describe the progressive isotopic enrichment or depletion in a reservoir during a fractionation process. The next section will briefly outline some key concepts of Rayleigh distillation to further demonstrate fractionation and the progressive enrichment/depletion of isotopes.

2.2.4 Rayleigh distillation

The most common application of Rayleigh distillation is in the description of the evaporation of surface water (Gonfiantini 1996, Gat 1996, Kendall and Caldwell 1998) and cloud rain out processes (Kendall and Caldwell 1998, Clark and Fritz 1997). The mathematical equation for open system Rayleigh distillation is:

$$R = R_o f^{\alpha-1} \tag{2.9}$$

where R is the instantaneous isotope ratio of the source reservoir when a fraction, f, of it remains, R_o is the initial isotope ratio of the source reservoir and α is the equilibrium fractionation factor. This equation can be written using δ-notation as follows:

$$(\delta + 1000) = (\delta_o + 1000) f^{\alpha-1} \tag{2.10}$$

Open system Rayleigh distillation occurs when the reaction products are continuously removed from the system and do not interact with the reactants. A plot of an open system Rayleigh distillation process is shown in Figure 2.3. This is a simple representation of a body of surface water undergoing evaporation to the atmosphere. Throughout evaporation, vapour is removed from the system and does not interact with the products. Figure 2.3 shows that as the water body loses mass to evaporation, it becomes progressively enriched. The isotopic composition of the vapour and liquid are related by the fractionation factor, α and therefore the vapour becomes enriched as evaporation progresses. As well, when all the water has evaporated (f=0) the isotopic composition of all the vapour is equivalent to the liquid isotope composition at the beginning of evaporation (f=1). This demonstrates that conservation of mass principles are conserved in the Rayleigh distillation equation.

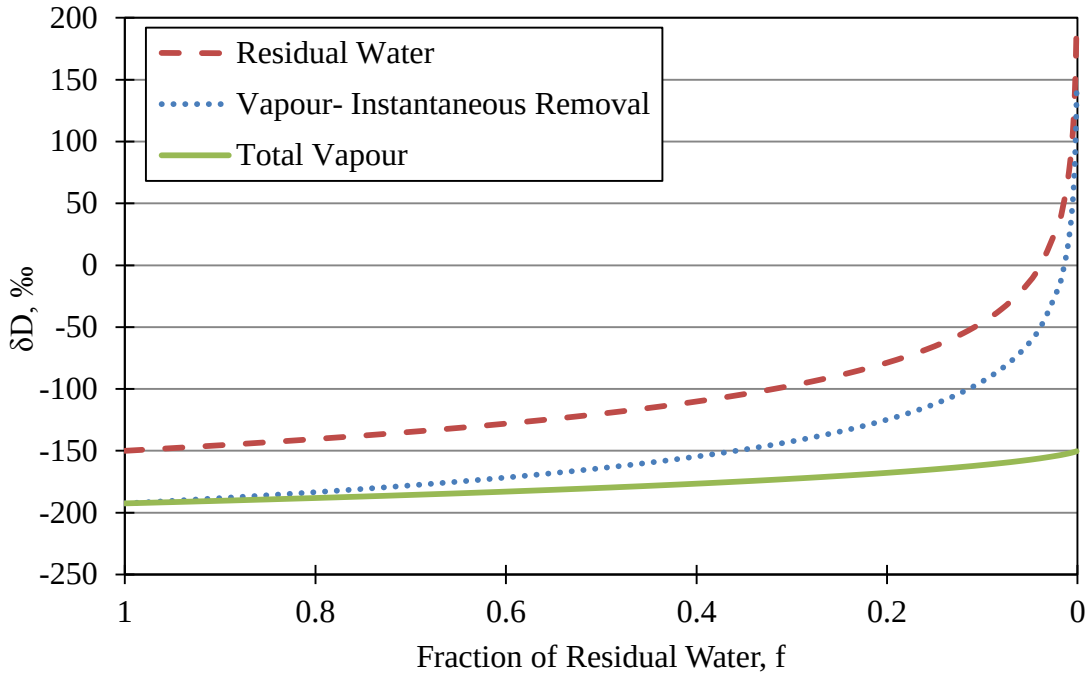

Figure 2.3: Open system Rayleigh distillation, simple representation of the evaporation of surface water to the atmosphere, $\alpha_{v\text{-}l}$=0.95 and δ_o=-150‰

The Rayleigh distillation equation can also be modified and applied to closed systems. A closed system is a system in which the products and reactants are continuously interacting with one another. The closed system Rayleigh equation is:

$$(\delta + 1000) = \frac{(\delta_o + 1000)}{\alpha - f(\alpha - 1)} \tag{2.11}$$

where δ is the isotope composition of the reactants at f, δ_o is the isotope composition of the reactant at f=1, α is the fractionation factor and f is the fraction of reactant remaining. The closed system Rayleigh distillation process is often used to describe the condensation of vapour in a cloud mass (Gat 1996, Kendall and Caldwell 1998). A closed system fractionation process is shown in Figure 2.4.

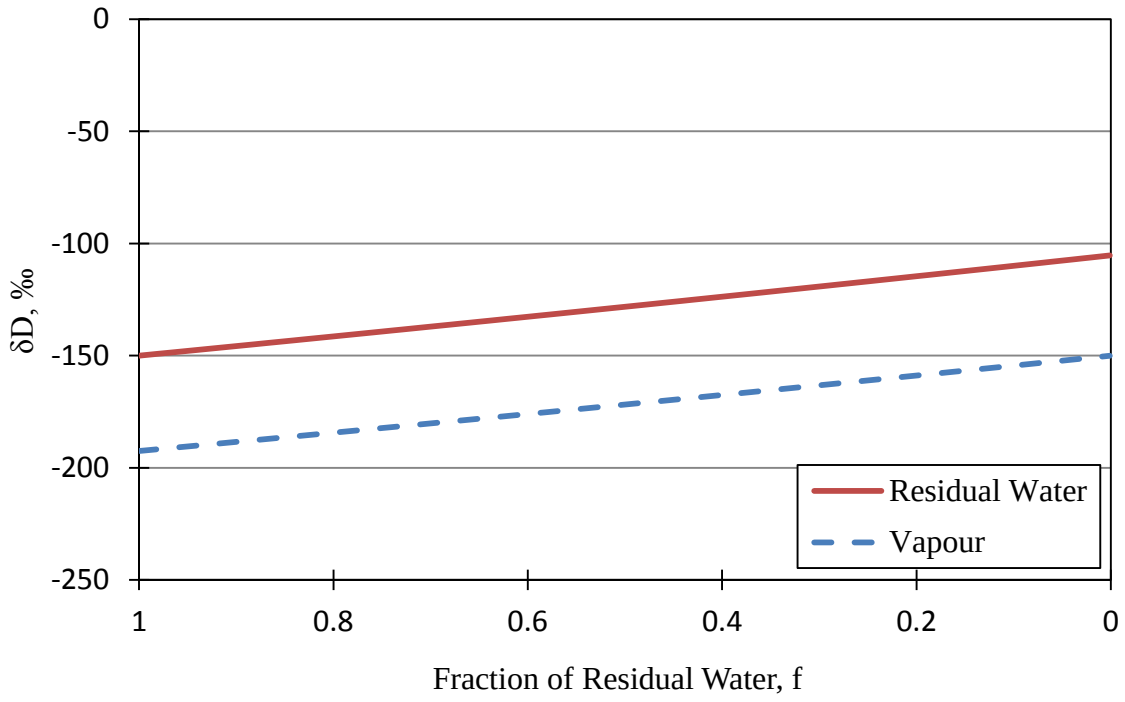

Figure 2.4: Closed system Rayleigh distillation, representation of closed system evaporation, $\alpha_{l\text{-}v}$=0.95, δ_o=-150‰

Less fractionation is observed in a closed system than for an open system because no mass is lost and the vapour and liquid phases are constantly interacting. The liquid and vapour isotope compositions are related by the fractionation factor, producing similar differences between the vapour and liquid phases throughout the reaction. As the liquid evaporates, both the vapour and the liquid enrich progressively. The conservation of mass is demonstrated by the identical isotope compositions of vapour at f=0 and liquid at f=1.

These two simple examples illustrate fractionation processes in the water cycle by showing how a phase change process may alter the isotopic composition of reactant and product reservoirs. Both examples highlight that throughout a fractionation process the isotopic composition of the reactant and product reservoirs will change and a continuous and gradual enrichment/depletion will be observed as the fractionation process advances.

2.3 Isotopic Variations and Fractionation in the Water Cycle

Fractionation processes continue throughout the water cycle as repeated cycles of evaporation and condensation alter the isotope composition of precipitation. The relevant literature pertaining to fractionation and isotope signatures in the hydrosphere will be discussed in this section.

2.3.1 Meteoric Water

The natural stable water isotope composition of meteoric water at the global scale has been extensively studied by multiple researchers, the most notable being Craig (1961) and Dansgaard (1964). Through their work, a linear trend between the deuterium (δD) and oxygen-18 ($\delta^{18}O$) values of meteoric water was established, which is referred to as the global meteoric water line (GMWL) and described mathematically by the following equation:

$$\delta D = 8\left(\delta^{18}O\right) + 10 \tag{2.12}$$

The GMWL is defined empirically using precipitation data collected at various sites worldwide (Gat 2005). δD and $\delta^{18}O$ of local precipitation is controlled by local climatic conditions, the origin of cloud masses, and secondary evaporation during rainfall (Clark and Fritz 1997). These factors ultimately affect the slope and d-excess value (y-intercept of meteoric water line) and cause variations in the meteoric water line for a given region. As a result, the meteoric water line for a specific region or area is developed from analyses of regional precipitation and is referred to as the local meteoric water line (LMWL).

In general, the isotope composition of precipitation for a specific region is often affected by seasonal variations in temperature. This causes cold weather precipitation, in particular snow to be more depleted than warm weather precipitation. This is illustrated in Figure 2.5.

2.3.2 Evaporation and the evaporation line

Most surface waters and shallow groundwater is exposed to natural evaporative processes. The corresponding enrichment follows a line that falls below the LMWL. This distinct line is referred to as the evaporation line (Gat 1981) with a slope typically varying between 2 to 5 in arid regions (Rose 1995). However, Gibson et al. (2005) illustrates that evaporation line slopes of approximately 7 have been observed in northern Canada, demonstrating that slopes of evaporation lines can vary significantly depending on local atmospheric conditions. An illustration of a typical evaporation line is plotted with the LMWL is shown in Figure 2.5.

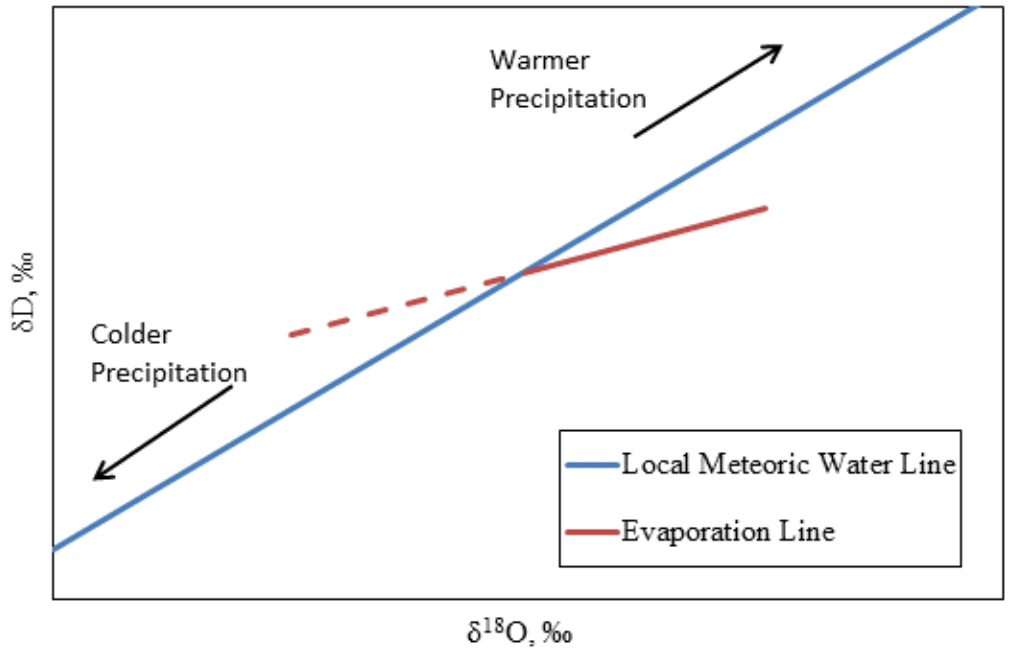

Figure 2.5: Illustration showing evaporation line location with LMWL and relative locations of cold and warm precipitation

Several mathematical models to describe the evaporation line have been developed (Gonfiantini 1986, Craig and Gordon 1965, Gat and Matsui 1991). Estimation of the amount of evaporative loss can be made based on observed evaporative enrichment of surface waters (Gammons et al. 2006, Mayr et al. 2007, Wassenaar et al. 2011, Gibson et al. 1993, Wolfe et al. 2007). These models show that the evaporation line is primarily controlled by temperature, relative humidity and the isotopic composition of atmospheric vapour. Generally, lower relative humidity and higher temperatures result in a shallower slope of the evaporation line. A model to estimate the evaporation line (Gonfiantini 1986) will be presented in Chapter 3 along with techniques to estimate evaporation using field data (Gonfiantini 1986, Ferguson et al. 2007).

Transpiration, which is the evaporative water loss through plants, has been observed to have no fractionation effects (Clark and Fritz 1997, Zimmerman et al. 1967, Barnes and Allison 1988). This indicates that shallow soil with a thick vegetative cover will undergo little fractionation. This is because during the hot summer months, the presence of vegetation results in water losses mainly through transpiration, rather than evaporation. On the other hand, bare shallow soils are more likely to be enriched due to sparse vegetation covers, allowing evaporation to dominate.

2.3.3 Fractionation and enrichment of snowmelt

Snow is typically depleted in comparison to other waters in a given region and it has been observed that a snowpack will undergo changes in natural stable water isotope values over a seasonal cycle. These changes include an enrichment of the snowpack due to evaporation and sublimation (Moser and Stichler 1975, Clark and Fritz 1997) and an enrichment of the snowpack and snowmelt as melting progresses (Earman et al. 2006, Lee et al. 2010, Hoover and Shoemaker 1986, Taylor et al. 2002, Taylor et al. 2001, Clark and Fritz 1997).

Moser and Stichler (1975) observed 1‰ and 0.2‰ enrichments for δD and $\delta^{18}O$ respectively for each percent of snow lost to sublimation during laboratory testing conducted at -10°C. Plotting these enrichments in δD vs. $\delta^{18}O$ space results in a line with a slope of about 5, verifying that sublimation results in fractionation of the snowpack. Despite this, Hilderman (2011) points out that snow is locked in position and mixing does not occur within a snowpack. This results in the outer snow layer or crust that interacts with the atmosphere to become isotopically enriched while the inner core and majority of the snow remains unaltered.

Enrichment during snowmelt has been observed by Taylor et al. (2002). In this study, a progressive enrichment of snowmelt during melting was observed in California, Vermont, Colorado and Alaska, USA. The enrichments in $\delta^{18}O$ ranged from 3.5 to 5.6‰ in snowmelt from the beginning of melt to the end of melt. However, the average $\delta^{18}O$ values of the snowpack were in between the range of snowmelt $\delta^{18}O$ values. This demonstrates that the average $\delta^{18}O$ value of snowmelt is likely similar to the average $\delta^{18}O$ value of the snowpack.

Additionally, Lee et al. (2010) observed a maximum δD enrichment of approximately 45‰ and a $\delta^{18}O$ enrichment of 6‰ in snowmelt from the beginning to the end of melt. The snowpack itself was enriched by 8 to 10‰ in $\delta^{18}O$ and 60 to 70‰ in δD from the beginning to end of snowmelt. This study further showed that the average δD and $\delta^{18}O$ values of the snowpack and snowmelt are generally comparable. The average values of snowmelt and the snowpack were within 5 and 1‰ in δD and $\delta^{18}O$, respectively.

As the above examples illustrate, it can be difficult to quantify and take into account the enrichment of snowmelt due to sublimation, evaporation and melting. Not accounting for snowmelt enrichment can lead to an underestimation of snowmelt contribution to recharge (Earman et al. 2006). In a previous study at the Mildred Lake mine, Kelln (2008) observed $\delta^{18}O$

values of shallow groundwater that was 4‰ more enriched on average than $\delta^{18}O$ values of snow.

2.4 Mixing

Mixing of water from various sources and landforms is ubiquitous within a closure landscape. Examples include mixing of process affected water (PAW) ortailings with recharge water and mixing of snowmelt infiltration with antecedent pore water. Source water compositions within closure landforms can be estimated if the isotope signatures of source waters and isotope compositions of the mixture are known. Like chemical species, δD and $\delta^{18}O$ values follow mass and concentration balance principles and the compositions can be estimated with the following equations:

$$\delta_{mix} Q_{mix} = \delta_1 Q_1 + \delta_2 Q_2 + \ldots \quad (2.13)$$

$$Q_{mix} = Q_1 + Q_2 + \ldots \quad (2.14)$$

where the subscripts mix, 1 and 2 represent the total mixture, first source water and second source water, respectively, Q represents flow rates or volume of each component and δ represents the isotope composition.

For two component mixing, source water compositions can be easily obtained. By dividing both Equations 2.13 and 2.14 by Q_{mix} and then substituting Equation 2.14 into Equation 2.13 results in the following expression:

$$\frac{Q_1}{Q_{mix}} = \frac{\delta_{mix} - \delta_2}{\delta_1 - \delta_2} \quad (2.15)$$

where Q_1/Q_{mix} represents the composition of the first source water. The second source water can be calculated by $1\text{-}Q_1/Q_{mix}$. Estimates using this approach have been utilized by Kelln (2008) to estimate components of antecedent pore water and snowmelt within shallow groundwater.

2.5 Mine Site Overview

This section summarizes the relevant information for the Mildred Lake mine pertaining to mining operations, closure landforms, site water management, and recycle and raw water circuits. This general information will be utilized later in the interpretation of the stable isotope of water signatures for site wide waters.

Operation of the Mildred Lake mine requires the movement of large volumes of earth and water, including both fresh water and PAW during mining, extraction and upgrading. As a result, it is necessary to have a general understanding of the recycle water circuit to hypothesize prevalent fractionation processes within the circuit. This section draws a majority of the information from Zubot (2010).

2.5.1 Mine site geology

The McMurray Formation is composed of shale, sandstone and the ore composed of bitumen impregnated sand. The McMurray Formation is overlain by shale and sandstones from the Cretaceous Clearwater formation and a thin layer of sandstone from the Grand Rapids Formation (Isaac et al. 1982). Muskeg and organic layers overlie the Grand Rapids Formation.

The McMurray Formation is underlain by limestones and shale from the Devonian Waterways Formation and Beaverhill Lake Group (Chapman 2008).

2.5.2 Mining

Mining first consists of stripping the overburden with shovel excavators to get access to the bitumen rich ore in the McMurray formation. The muskeg and organic overburden layers are stored on site and later used in reclamation. The non-organic overburden materials is stockpiled on site and eventually reclaimed or used in tailings dyke and road construction (RSC 2011). Upon completion of mining, the mined out pits are converted to tailings and PAW management areas.

2.5.3 Hydraulic transport

Hydrotransport technology is used to transport the ore from the mining area to the extraction and upgrading plant (Zubot 2010). Once the ore is accessed, haul trucks transport the ore to crushers and cyclofeeders. The cyclofeeders add hot water and sodium hydroxide to the ore to create a slurry mixture (Zubot 2010). The slurry is then transported via pipeline for extraction and upgrading.

2.5.4 Extraction

The purpose of extraction is to separate the bitumen from water, geologic material, salts and other contaminants. The extraction process consists of running the slurry through tumblers where steam, hot water (80°C) and sodium hydroxide is added to the slurry to condition the slurry for

separation. The slurry is then sent to primary separation vessels where the slurry is aerated and the bitumen froth is recovered (Zubot 2010).

Operating temperatures range from 35°C to 75°C throughout the hydrotransport and extraction processes (Zubot 2010). The separated waste materials (water, geologic materials, etc.) are stored in tailings management facilities.

2.5.5 Upgrading

The upgrader converts bitumen into synthetic crude oil that can be further processed at refineries (Zubot 2010). Through this process, natural gas (CH_4) and water are used to produce hydrogen gas (H_2). The hydrogen gas hydrotreats and hydrocracks the bitumen and converts it to synthetic crude oil. In addition to synthetic crude oil, the byproducts of the upgrader include coke and "sour" water and gas (containing nitrogen and sulfur species). The coke is stored at Mildred Lake Settling Basin Cell 5, which is a dyke located on the southwest site of Mildred Lake Settling Basin. The Mildred Lake mine operates sour water treatment facilities and sulfur and ammonia recovery plants to manage and handle the sulfur and nitrogen species (Zubot 2010).

Overall, the oil sands mining process results in significant land disturbance, water use and produces several by-products. Both overburden and waste material are produced in large quantities that need to be managed, stored and eventually reclaimed. These materials include shale, till and organic overburden, PAW, tailings and coke.

2.6 PAW/Tailings Management

The mining and processing of bitumen requires large amounts of water. The Syncrude mine site used about 312 million m^3 of water in 2010. Approximately 89% of this water is recycled water from the upgrading process while the remaining portion of water is drawn from the Athabasca River, about 34 million m^3 (Syncrude 2010).

Along with utilizing and storing large volumes of water, oil sands companies must abide by strict environmental regulations. PAW/tailings cannot be released to the environment and must be contained on site. As a result, large volumes of PAW are stored on site and comprise a majority of the water within a site wide water balance. Management, storage and reclamation of PAW/tailings is an ongoing challenge and the final release following closure remains an unresolved issue.

2.6.1 Fractionations controlling the signature of PAW/tailings

The Mildred Lake mine requires a combination of fresh Athabasca River water and recycled PAW. Fresh water is required for boiler feed water, cooling towers, utilities and potable water. The cooling tower and boiler feed water are used in upgrading and make up the majority of the raw water demand, approximately 75% of the site wide raw water demand in 2003 (Zubot 2010). All imported Athabasca river water used on site is considered PAW and cannot be released to the environment. The only exception to this is treated sanitary sewage, which is released to the Athabasca River.

The hydraulic transport of bitumen and tailings, along with bitumen extraction make up a majority of the water demand on site. However, these processes utilize recycled PAW skimmed from surface of tailings basins (Zubot 2010).

All the uses of PAW and fresh water listed above cause heating of the water and increases in temperature. These waters also undergo evaporation, often under elevated relative humidity conditions within the extraction plant and upgrader. This evaporation results in fractionation throughout these processes. Zubot (2010) acknowledges that steam and evaporative losses occur throughout the extraction and upgrader circuit, further verifying these processes will likely contribute to fractionation of PAW/tailings.

The recycle water circuit circulates PAW from all tailings basins into the Recycle Pond reservoir which supplies PAW to the mine circuit. This circulation through the Recycle Pond results in surface PAW that is relatively well mixed such that the PAW discharged to each tailings basin has gone through similar fractionation processes. Consequently, the PAW of each tailings basin should have similar and comparable δD and $\delta^{18}O$ values if the mine water recycle circuit is the major fractionating process of PAW/tailings.

Evaporation from the tailings basins may also cause fractionation of PAW/tailings. Each tailings basin may have different atmospheric conditions leading to different evaporation rates. Varying pond temperatures and atmospheric relative humidity conditions may also influence the natural evaporation processes between tailings areas. For example, atmospheric data collected by O'Kane Consultants had an average temperature and relative humidity throughout May to September 2012 of approximately 15°C and 68%, respectively at South Bison Hills (O'Kane 2013). The average temperature and relative humidity during this time at Coke Beach

was approximately 16°C and 60%, respectively. These differences in atmospheric conditions may ultimately affect fractionation of δD and $\delta^{18}O$ and affect the slope of the evaporation line. This may contribute to unique δD and $\delta^{18}O$ signatures among the different tailings basins. As a consequence, differences in the natural stable water isotope values between tailings basins may occur as a result of natural evaporation processes rather than from the recycle water circuit.

3 MATERIALS AND METHODS

This section will provide a detailed overview of relevant study area followed by a description of the field and laboratory methods utilized in this study.

3.1 Study Areas

A variety of soil, surface water and groundwater samples were collected from various areas across the mine site. This section will briefly describe the different sampling areas relevant in this study. Locations of tailings and reclamation areas are shown in Figure 3.1.

3.1.1 Tailings areas and the recycle water circuit

The five principle tailings areas on site were mentioned previously in Section 1.3.2. The above ground facilities include Southwest Sand Storage (SWSS) and Mildred Lake Settling Basin (MLSB). The in-pit facilities include West in-pit (WIP), East in-pit (East in-pit) and Southwest in-pit (SWIP). Additional information on the tailings areas can be found in Zubot (2010).

Fine tailings are generally classified as being sand tailings, fluid fine tailings, mature fine tailings and composite tailings. Sand tailings, as the name implies, are composed of sand which settle from fluid tailings and dewater relatively quickly. Upon deposition, sand tailings are used to form perimeter dykes and beaches around above ground tailings basins (Zubot 2010). Sand tailings at the mine site are primarily stored and managed at SWSS.

Fluid fine tailings refer to fine grained tailings (silts and clays) that have recently been discharged into a tailings area. Fine tailings take a much longer time to settle than sand tailings and have very high water contents. Because of the high water contents, fluid fine tailings have fluid like properties. Fine particles in these tailings slowly settle and dewater over several years to form mature fine tailings. Mature fine tailings have a “yogurt” type consistency with water contents generally between 65 to 70% by weight (Zubot 2010). Mildred Lake Settling Basin is

used to store both fluid and mature fine tailings, with volumes of mature fine tailings being dredged and transported to West in-pit for long term storage (Zubot 2010).

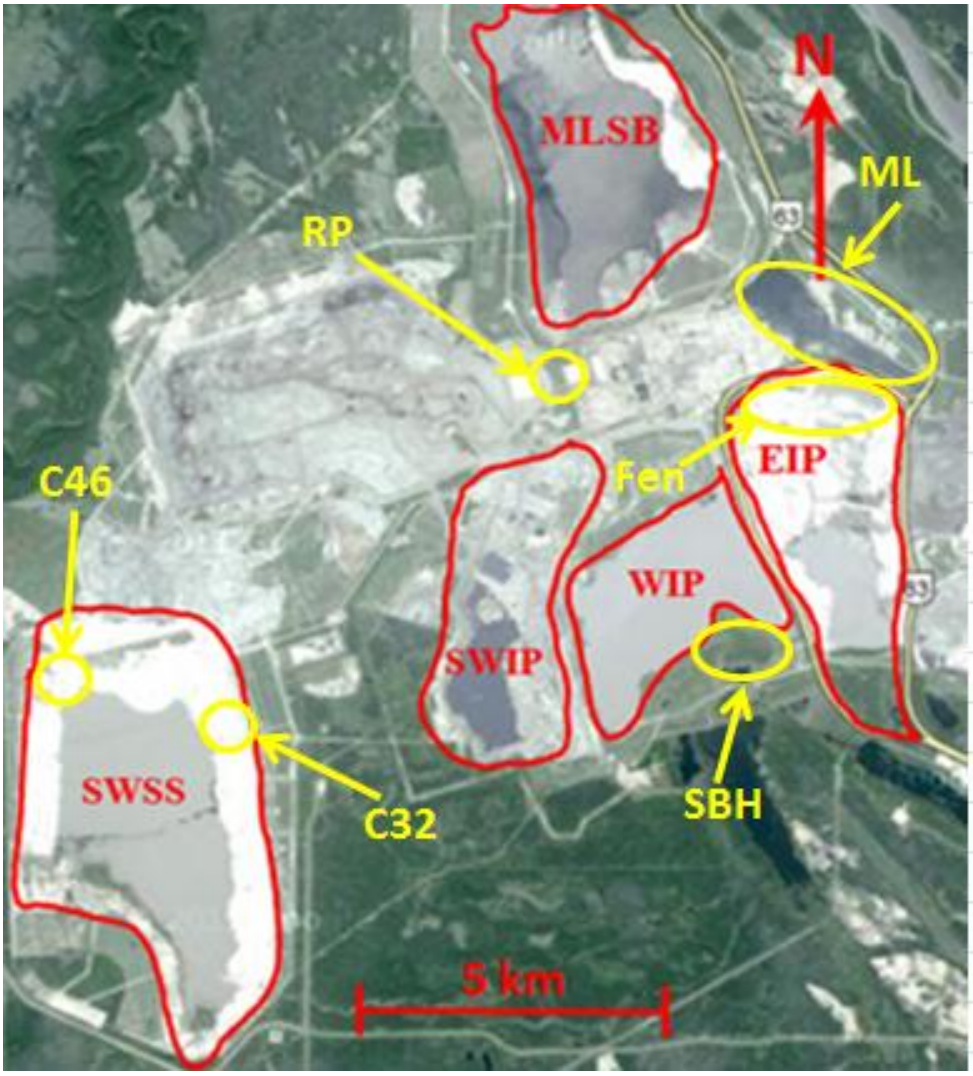

Figure 3.1: Locations of tailings and reclamation areas at the Mildred Lake mine. Acronyms: SWSS=Southwest Sands Storage; C32= SWSS Cell 32; C46= SWSS Cell 46; SWIP=Southwest in-pit; WIP=West in-pit; EIP= East in-pit; MLSB= Mildred Lake Settling Basin; SBH= South Bison Hills; ML=Mildred Lake; Fen=Sandhill Fen; RP=Recycle Pond

Composite tailings are a slurry mixture of sand, mature fine tailings and a coagulant with the goal of rapid dewatering upon deposition to obtain a structurally stable material (Zubot 2010). Composite tailings mixtures are prevalent at East in-pit, which contain a mixture of mature fine

tailings from West in-pit, sand and the coagulant (Barbour, personal communication).

In addition to tailings areas, there were opportunities to sample the Recycle Pond (RP in Figure 3.1), the Effluent Pond and several points within the recycle water circuit.

3.1.2 Tailings Dykes

Tailings dykes are constructed as part of above ground tailings storage facilities. The dykes are either constructed out of overburden material (RSC 2010) or are formed by hydraulic deposition and mechanical reworking of tailings.

SWSS Cells 32 and 46 are shown in Figure 3.1 (C32 and C46). Both these cells are sand tailings dykes that are monitored for environmental research. Research at Cell 32 began in 2000 and has a more established monitoring program than Cell 46, which started research in 2002 (Price 2005). Price (2005) modelled the present hydrogeology of both cells and predicted the flushing of dissolved solids through Cell 32 over time.

Cell 32 and Cell 46 contain an extensive network of piezometers and groundwater wells (Price 2005). A majority of the shallower wells are dry and therefore cannot be used for groundwater sampling. This provides an opportunity to sample vapour in isotopic equilibrium with the piezometers in an effort to estimate the isotopic compositions of unsaturated pore water from the isotope compositions of corresponding vapour samples.

3.1.3 Mildred Lake

Mildred Lake (ML in Figure 3.1) is the fresh water reservoir for the mine site. It is a natural surface water body and water from the Athabasca River is continuously pumped into Mildred Lake to meet the water demands of the mine site. Volumes of water are drawn from the Athabasca river continuously throughout the year (Zubot, personal communication), with total annual water volumes ranging from 34.1 to 41.2 million m^3 between 2007 and 2011 (Syncrude 2012a). Mildred Lake provides an opportunity to collect natural surface water within a close proximity to the mine site.

3.1.4 Overburden Dumps

As the name implies, overburden dumps are essentially large stockpiles of overburden material. These dumps are mainly composed of saline-sodic shale, lean oil sands, glacial lacustrine till or any other geologic material overlying the ore. The current reclamation strategy for saline-sodic

overburden material is to grade the landforms to establish a target hydrology (e.g. drainage networks for perched wetlands), place the reclamation cover and then followed by re-vegetate (Chapman 2008). Overburden dumps are capped with non-sodic soil, generally glacial soils (till or lacustrine clays) and a mixture of organic peat mixed with glacial soils (Boese 2003).

South Bison Hills (SBH in Figure 3.1) is a shale dump that is currently undergoing reclamation and is located just south of West in-pit. Soil cover placement began in 1996 (Boese 2003) and continued until 2001 (Chapman 2008). The dump is currently vegetated with tall grass, shrubs and spruce and aspen trees. Three perched ponds are located on South Bison Hills and are called Bill's Lake, Peat Pond and Golden Pond.

South Bison Hills has been extensively studied in an attempt to understand the hydrogeological evolution of overburden dumps. Chapman (2008) characterized the hydrogeology of South Bison Hills and developed a conceptual flow model to identify key hydrogeological characteristics within the landform. Hilderman (2011) utilized natural δD and salt tracers within South Bison Hills along with a numerical model to estimate net percolation into the dump as well as salt transport characteristics near the shale/soil cover interface. Kelln et al. (2006) examined the hydrological response of South Bison Hill's soil cover over a four year time frame and observed preferential flow paths through the reclamation cover during the spring freshet using natural $\delta^{18}O$ and sulphate tracers.

Hilderman (2011) and Kelln (2008) both studied a research plot that consisted of three areas of 50 by 200 m which have varying soil cover thicknesses and are named D1, D2 and D3. The soil cover depths are shown below in Table 3.1. The glacial till is overlain by the peat/mineral mix in all covers. Each area has an interflow collection system which collects interflow associated with spring snowmelt. An aerial image of South Bison Hills is shown in Figure 3.2.

Table 3.1: Soil cover depths at D1, D2 and D3 covers

Study Area	Peat/Mineral Mix [cm]	Glacial Till [cm]
D1	20	30
D2	15	20
D3	20	80

Figure 3.2: Aerial image of South Bison Hills (Image from Google 2013b)

3.1.5 Sandhill Fen

Sandhill Fen is a reclamation study area on the north side of East in-pit. Construction of the Fen was completed recently in 2011. The Fen overlies composite tailings and has a hummocky topography with two perched wetlands. The hummocks were constructed out of tailings sand or natural sand and were capped with varying depths of leaf, fibric and humic materials. A network of underdrains lies beneath the ground surface to prevent upward movement of PAW/tailings into the root zone. A plan of the Fen and relevant piezometer nests is shown in Fresh water from Mildred Lake is periodically pumped into the Fen to maintain the water level within the wetland. Fresh water pumping into the Fen began on July 7, 2012 and was shut down on September 4, 2012 for the winter. In 2013, fresh water pumping began on May 29.

Figure 3.3.

Fresh water from Mildred Lake is periodically pumped into the Fen to maintain the water level within the wetland. Fresh water pumping into the Fen began on July 7, 2012 and was shut down on September 4, 2012 for the winter. In 2013, fresh water pumping began on May 29.

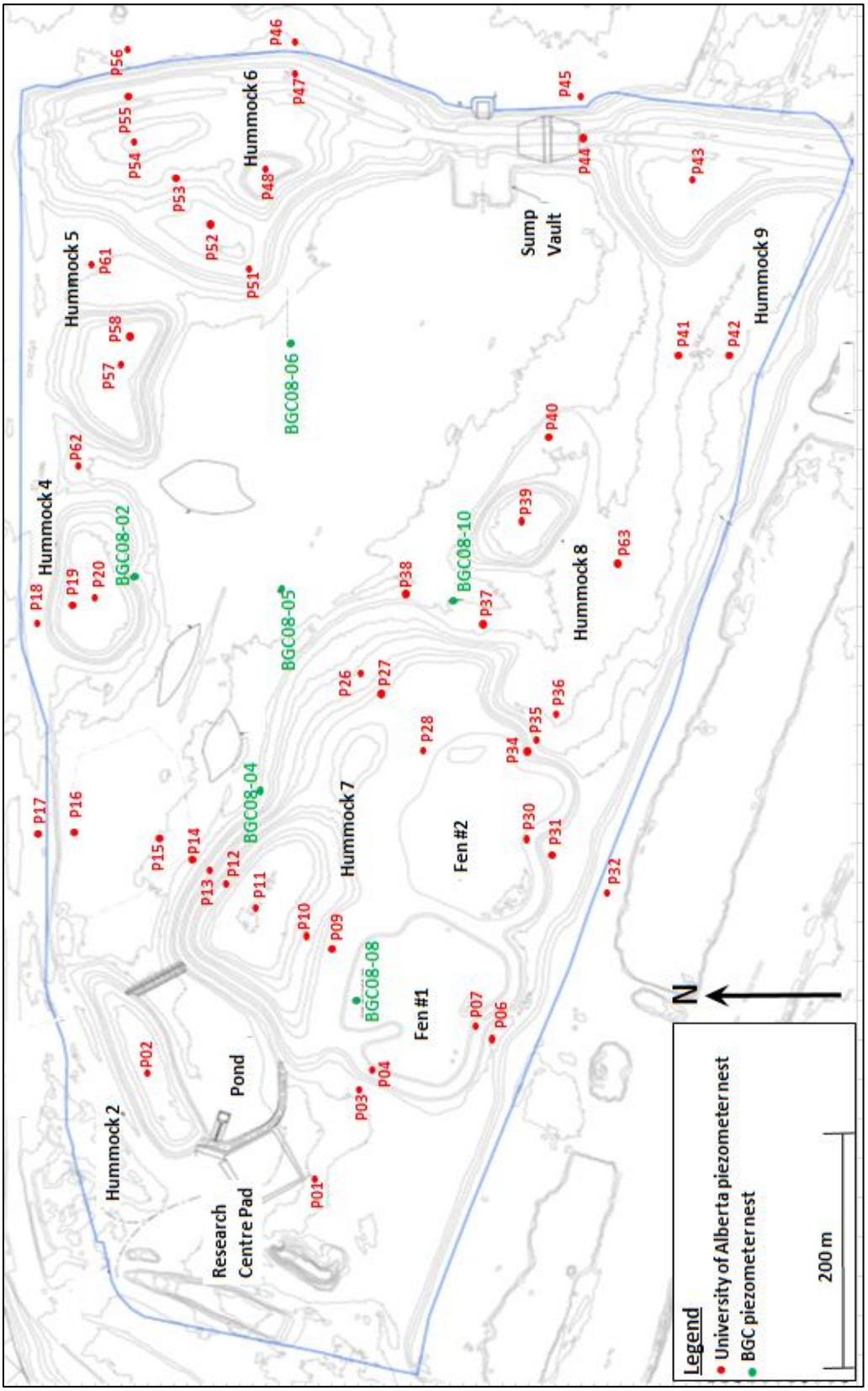

Figure 3.3: Layout of Sandhill Fen and relevant piezometer nests (Plan provided by Syncrude Canada Ltd., reproduced with permission)

3.2 Sampling

A variety of water, vapour and soil samples were collected across site throughout the year. Water samples included groundwater, surface water, meteoric water and process affected/tailings water. Soil samples were collected from several different reclamation sites, including shale dumps, tailings sand dykes, and tailings pits. Vapour samples were collected at select dry wells and piezometers at SWSS Cell 32. The purpose of the sampling program was to collect samples that will fully represent the hydrology of the mine site in an effort to characterize and catalogue site wide waters.

3.2.1 Rainfall sampling

Rainfall is a vital component of the water balance of closure landforms. Rainfall provides water for groundwater recharge which furthermore encourages contaminant flushing. Sampling of rainfall was executed on site to add to local meteoric δD and $\delta^{18}O$ signatures and the local meteoric water line (LMWL) developed by Hilderman (2011).

Rainfall collectors (Figure 3.4) supplied by Dr. Sean Carey of McMaster University, were placed at three of the meteorological stations on the mine site. The bottle system in Figure 3.4 collects the precipitation through the funnel and holds it in the bottle until sampling. The system is designed to prevent atmospheric interaction and evaporation of the sample. The PVC case on the right is open on one end to hold the bottle system and protect it from the environment.

Figure 3.4: Rainfall collectors

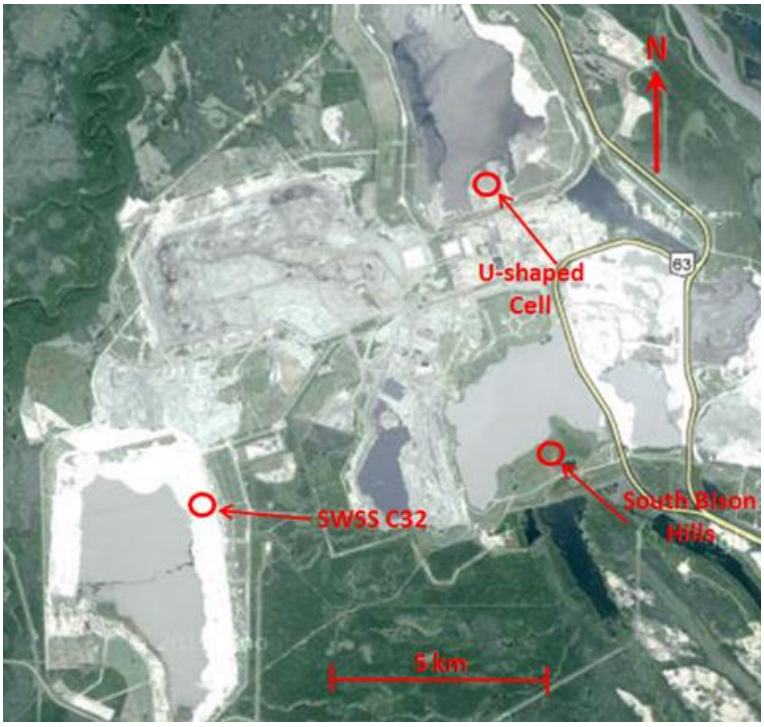

Figure 3.5: Location of rainfall collectors at Mildred Lake mine

The location of the rainfall collectors is shown in Figure 3.5. Each collector was mounted to a fence post at the specified meteorological stations in Figure 3.5. The collectors were placed in the open so there was no interference with collection.

Rainfall sampling began after snowmelt in May 2012 and continued into the autumn of 2012. Collectors were checked after heavy rain events or on a bi-weekly basis when there were no significant rain events. Samples were poured directly from the collectors into sample bottles with zero headspace if possible and sealed immediately.

3.2.2 Snow sampling

Snow makes up a significant component of precipitation and recharge in semi-arid and arid zones (Ireson et al. 2013, Hayashi et al. 2003). Therefore it is vital to be able to characterize snow and snowmelt to develop the LMWL and estimate isotope values of recharge on closure landforms. Snow surveys are performed by Syncrude and O'Kane Consultants across select closure landforms (Clark, personal communication). During these surveys, snow samples were collected in March 2012, January/February 2013 and March 2013 for isotope analysis.

Snow samples were taken from the middle of the snow pack, sealed in large Ziploc® freezer bags and allowed to melt at room temperature. Afterwards, the melt water was poured into a water sample bottle (Clark, personal communication).

3.2.3 Surface water sampling

In addition to Mildred Lake, surface water is present on closure landforms in the form of wetlands, ponds and drainage ditches.

Surface water samples were collected primarily from Mildred Lake and the perched ponds on South Bison Hills (Peat Pond, Golden Pond and Bill's Lake). Sample collection consisted of dipping a sample bottle just beneath the surface and filling to zero head space. Two samples from Mildred Lake were collected on August 15, 2012 and May 19, 2013. Additionally, six samples from Mildred Lake were sampled by Syncrude between May to July 2013 (Hearson, personal communication). Surface water samples at South Bison Hills were collected several times throughout the spring and summer of 2012.

3.2.4 Groundwater sampling

Groundwater samples were collected from several closure landforms, including South Bison Hills, SWSS Cells 32 and 46 and the Sandhill Fen. Samples were drawn from several piezometers, wells, interflow collectors and underdrains on these landforms.

Groundwater sampling at SWSS Cells 32 and 46 included sampling "wet" piezometers and underdrain system discharges. Piezometers and wells monitored by the University of Alberta at SWSS Cells 32 and 46 were collected between July 24 and 26, 2013. Sampling was executed with the University of Alberta using a low-flow sampling apparatus, shown in Figure 3.6.

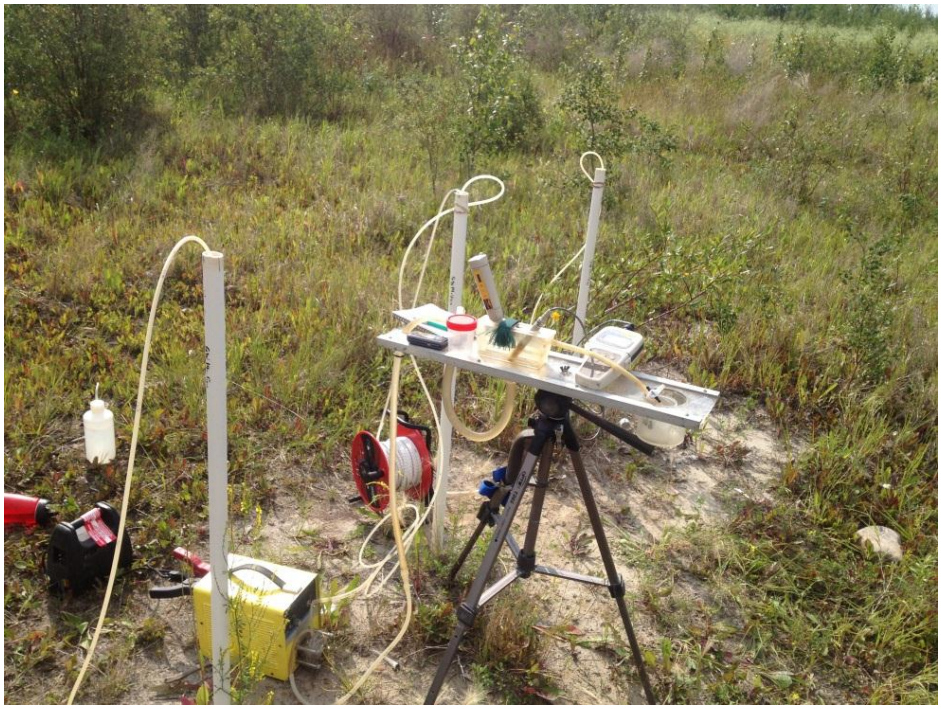

Figure 3.6: Low flow sampling apparatus

Sampling began by pumping water with a peristaltic pump from the well screen at a low flow rate with the objective of pumping at a similar rate that occurs during well recovery. The pH and temperature of pumped water was measured during pumping and water samples were collected once pH and temperature stabilized. A total of six underdrain discharge points at SWSS Cell 32 and one discharge at SWSS Cell 46 were sampled throughout the spring and summer of 2012. The underdrain discharge at Cell 46 is shown in Figure 3.7. Samples were collected by filling a sample bottle with water being discharged by the underdrains.

Figure 3.7: Underdrain discharge at SWSS Cell 46

Groundwater sampling at the Sandhill Fen consisted of sampling piezometers installed by the University of Alberta and BGC Engineering as well as a sump which collects water discharged by the underdrain system. The Fen piezometers monitored by the University of Alberta were sampled on May 16, 2013. The samples were collected with a bailer and piezometers were purged with at least three full bailer buckets of water before sampling. Wells installed by BGC were sampled from June 12 to 14, 2012. Samples were collected with a bailer and were purged until electrical conductivity from the baled water stabilized. A total of seventeen sump samples were collected between December 1, 2011 and July 31, 2013. Sump samples were collected by dropping a bailer into the sump and sampling water near the sump water surface.

Groundwater sampling at South Bison Hills consisted of sampling wells, piezometers and interflow collection systems described by Hilderman (2011). Wells and piezometers were sampled between July 23 and 27, 2012 and were purged if possible. However, a majority of the wells are in low conductivity shale formations resulting in a long well recovery time. Most of the shallow piezometers had little water in them and as a result, purging of these wells was not possible. Samples from the interflow systems were collected with a submersible pump (Clark, personal communication) on June 21, 2012 and July 10, 2012 and throughout the spring and summer of 2013. Additionally, Syncrude sampled a set of wells at South Bison Hills on August

31, 2012. Each well was purged three well volumes before sampling with a bailer (Clark, personal communication).

In addition, the University of Alberta collected samples from select piezometers at SWSS Cells 32 and 46, the Fen and South Bison Hills on September 29 and 30, 2012. Their sampling procedure consisted of sampling with a bailer. Piezometers were purged with two full bailer volumes of water before sample collection (Longval, e-mail communication).

3.2.5 PAW Sampling

Collection of PAW from the surface of tailings ponds and along the recycle circuit was undertaken by Golder Associates (Zubot, personal communication). Samples from tailings ponds surfaces were collected directly by dipping a sample bottle into the ponds with a telescoping metal arm. Tailing ponds sampled include the Recycle Pond, Effluent Pond Mildred Lake Settling Basin, Southwest Sands Storage, East in-pit, and Southwest in-pit.

West in-pit and the North Mine Train were collected from recycle circuit water lines. The lines were purged before sample collection to ensure a representative and non-stagnant sample.

3.2.6 Tailings Profiles

In the spring and summer of 2012, ConeTec collected a series of vertical profiles of tailings at West in-pit and additional profiles from Aurora Settling Basin (ASB), an above ground tailings area at the Aurora mine site (Halferdahl, e-mail communication).

ConeTec used a specialty soft soil/fluid sampler to sample fine tailings at depth. The sampler, which essentially consisted of a pressurized piston, was dropped into the tailings to the required depth. The piston collected the tailings sample and was then lifted above surface and discharged into a bucket and sealed. The tailings samples were then sent to Syncrude's laboratory in Edmonton where they were centrifuged to obtain a solids free water sample (Halferdahl, e-mail communication).

3.2.7 Water sample handling and storage

All water samples were collected in high density polyethylene (HDPE) bottles with zero headspace (if possible) and sealed and were stored at room temperature. Upon analysis, sample

bottles were only opened to extract water and then were re-sealed immediately after sub-sampling.

3.2.8 Soil sampling

Soil sampling for natural stable water isotope analysis of soil pore water was executed at the Fen, Mildred Lake Settling Basin Cell 5 (Coke Beach) and South Bison Hills.

Soil sampling at the Fen occurred throughout the summer of 2012 and on May 1, 2013. Sampling in the summer was done in conjunction with a separate piezometer installation project undertaken by the University of Alberta. The deeper soil samples were collected with a portable drill rig (General 500 Dig'R Mobile) while drilling holes for the piezometers. The drill rig is shown in Figure 3.8.

Figure 3.8: Dig'R Mobile

Solid stem auger flights of three foot lengths were used to drill holes for piezometer installations. Soil samples were collected from the bottom of each auger flight during drilling. The soil at the bottom flight was assumed to roughly represent the soil at the bottom of the drilled hole.

Before sample collection, the outside of the soil sample was visually inspected and any noticeable contamination was scraped off by hand. After the visual inspection, the soil was scraped into a medium Ziploc® freezer bag and sealed, removing as much air as possible. The sample was then double bagged within another sealed Ziploc® bag and stored in a cooler at room

temperature immediately after collection until laboratory analysis could be executed.

Shallow soil sample collection was also undertaken during the summer of 2012 at the Fen using a Dutch hand auger (shown in Figure 3.9). Shallow soil samples were collected at a majority of the piezometer installation locations. Samples were taken at increments of approximately 30 cm or when an alteration in soil type was noticed. Upon sampling, the soil samples were visually inspected and any noticeable contamination was scraped off before collecting the sample. The samples were stored in Ziploc® freezer bags with as much air removed as possible before sealing. The samples were then double bagged with another Ziploc® bag and then stored in a cooler at room temperature.

Figure 3.9: Dutch hand auger used for sampling

A transect of four vertical soil profiles were collected on May 1, 2013 in an effort to capture an isotope profile demonstrating snowmelt infiltration on the Fen. The sampling transect consisted of profiles at the top and bottom of a hummock and two in between the top and bottom profiles. Samples were collected along 2 m deep vertical profiles at 20 cm increments. Samples were collected with a Dutch hand auger in the same manner as described previously in this section.

Coke Beach was sampled at three select locations on May 15, 2013 with a Dutch hand auger. Each location was sampled at 10 cm intervals up to depths of 100 cm. Sample collection techniques were similar to those described earlier in this section. The soil sample was visually inspected and any noticeable contamination was scraped off. Samples were collected in two sealed Ziploc® bags with air removed and stored in a cooler at room temperature.

Soil sampling at South Bison Hills was part of a larger sampling program executed by Syncrude. Soil samples at depths no greater than180 cm were collected in September 2012. A bucket auger was used to collect samples. Samples were vacuum sealed in two heavy duty plastic bags and stored in coolers immediately after sampling (Yarmuch, e-mail communication).

3.2.9 Soil sample handling and storage

Soil samples were stored in two Ziploc® bags with air removed in a cooler at room temperature. Upon laboratory analysis, samples were taken out of the cooler and outer bag removed. The inner bags of samples were only opened to inflate bags with dry air. Once deuterium (δD) and oxygen-18 ($\delta^{18}O$) analyses were complete, samples were deflated, placed in the second Ziploc® bag (air removed) and stored back in the cooler.

It has been demonstrated by Schmeling (unpublished data) that soil samples stored in this manner retain their true isotopic signature for upwards of four months.

3.2.10 Vapour sampling

Vapour samples were collected from select 1" piezometers at SWSS Cell 32 on July 12, 2013. This was a trial program and as a result a variety of purge and sample collection times were tested. Sampling depths ranged from 1.5 to 8 m below ground.

Samples were extracted near the screen of a dry piezometer or near the water surface of a wet piezometer by running a ¼" HDPE tube down the piezometer to the required depth. The top of the piezometer was closed off to prevent atmospheric air from travelling into the piezometer and contaminating the sample.

A 1L Grab Air Sample Pump and tedlar gas sampling bags, both manufactured by SKC Inc. were used for sample collection. The pump was attached to the HDPE tubing and the pump was run to purge the line. Purge times were 30, 45 and 60 seconds; immediately after purging the sample bag was attached to the outlet of the pump for approximately one minute before sampling was complete.

At wet wells, water samples were collected immediately after sample collection to compare to gas samples. Air temperatures were recorded in all wells sampled at the sample depth with a Solinist water level meter. Water and vapour samples were stored in a cooler immediately after collection and isotope analysis was conducted on all gas samples the night of July 12, 2013 to

limit fractionation through the gas sample bags.

3.3 Laboratory Analysis

δD and $\delta^{18}O$ isotope analyses were undertaken on all water and soil pore water samples. Repeat analyses were conducted on approximately 20% of the samples to ensure accurate, consistent and reasonable results. All isotope compositions are referenced to the VSMOW standard.

3.3.1 Los Gatos isotope analyzer

A Los Gatos laser absorption spectrometer operated by Environment Canada was initially going to be used to directly determine liquid isotope values of all water samples collected. However, due to equipment breakdowns and sample back logs, a Picarro isotope analyzer was used to conduct natural stable water isotope analyses on samples collected after mid-June 2012.

3.3.2 Picarro isotope analyzer

A Picarro cavity ring down spectrometer was used to conduct δD and $\delta^{18}O$ analyses on all soil samples and a majority of the water samples. Isotope compositions were determined using liquid-vapour equilibration techniques outlined by Wassenaar et al. (2008). It has been shown by Wassenaar et al. (2008) that the precision and accuracy using liquid-vapour equilibration techniques is comparable to conventional and isotope ratio mass spectrometry (IRMS) techniques.

This technique consists of placing a water or soil sample in an air tight bag, inflating the bag with dry air and sealing the bag. Once the vapour and liquid water are in isotopic equilibrium the vapour from the sample and the vapour from two known water standards are analyzed using the spectrometer.

The Picarro measures δD and $\delta^{18}O$ compositions of vapour of the samples and standards. These compositions along with known liquid δD and $\delta^{18}O$ values of the standard are used to calculate the liquid isotope value of the sample using techniques described in Section 3.3.3. The liquid isotope values of the standards are determined with the Los Gatos liquid isotope analyzer operated by Environment Canada.

3.3.3 Liquid-vapour equilibration: laboratory and analytical procedure

Soil samples, water samples and water standards were prepared by placing a volume of sample in

an air tight re-sealable Ziploc® freezer bag and inflating the bag with dry air. Water sample sizes were approximately 10 mL and soil samples ranged between 100 mL to over 300 mL. Drier soil samples required a larger sample size because of the lower volume of water they contain

Equilibration times for all soil samples were between 3 to 4 days as recommended by Wassenaar et al. (2008). Liquid samples and standards were given at least one hour to equilibrate due to much lower equilibration times associated with water samples (Wassenaar et al. 2008).

After equilibration is complete, the samples were analyzed by the Picarro by drawing the equilibrated vapour from the sample bag with a needle attached to the Picarro inlet. The samples were run for approximately 4 minutes to allow the instruments vapour content, δD and $\delta^{18}O$ readings to stabilize. The recorded vapour isotope compositions recorded were 30 second averages output by the Picarro. Equilibrated standards were run in the same manner.

Two standards are required to relate the sample vapour and liquid isotope values. Standard water samples were run before and after each group of collected samples, as illustrated in Figure 3.10. Standards were rerun every five samples to reduce the error caused by varying room temperatures that occur in the lab throughout the day.

Standard #1	Sample #1	Sample #2	Sample #3	Sample #4	Sample #5	Standard #2

Figure 3.10: Picarro sample analysis order

The relationship between equilibrated liquid and vapour isotope compositions is linear (Picarro, 2009). As a result, a calibration line using the vapour and liquid isotope compositions of the standards was created for each sample set, as shown in Figure 3.11. A separate line for both δD and $\delta^{18}O$ is required. Once the calibration line is established, the liquid isotope values of the samples can be calculated directly using the line equation and the vapour δD and $\delta^{18}O$ values produced by the Picarro.

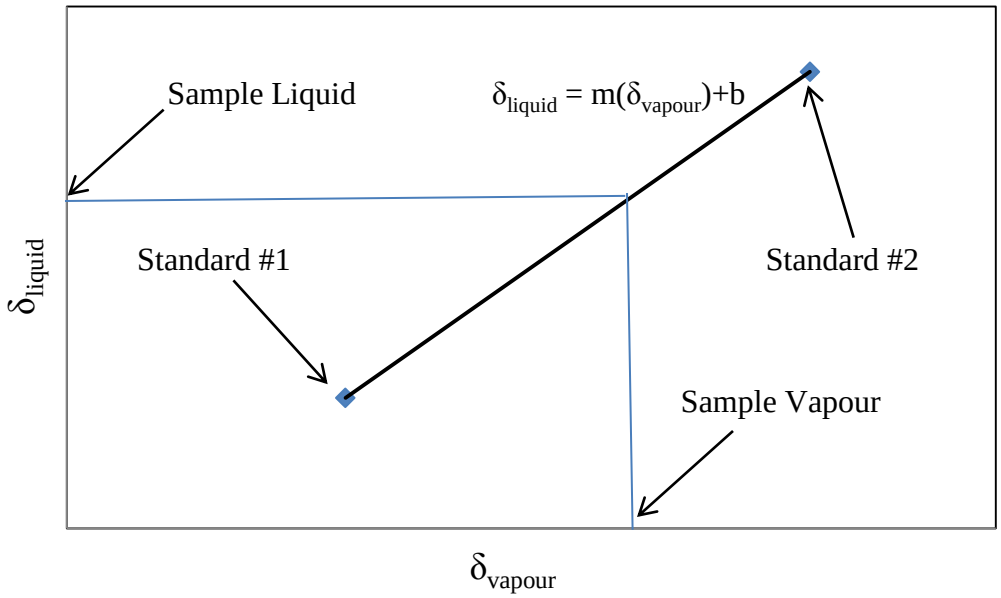

Figure 3.11: Calculating liquid isotope values from vapour isotope values

Repeated tests were undertaken on approximately 15% of the samples to demonstrate the repeatability of the liquid-vapour equilibration method. In the case of liquid samples (n=96), differences between the original and repeat samples varied on average by 1.0‰ and 0.35‰ for δD and $\delta^{18}O$, respectively with normal standard deviations of 0.7‰ and 0.3‰, respectively. Soil samples (n=63) had an original-to-repeat average difference of 1.25‰ and 0.42‰ for δD and $\delta^{18}O$, respectively with normal standard deviations of 1.0‰ and 0.35‰, respectively.

Through analysis of the Picarro data files, no methane or hydrocarbon interference was evident in any of the water or soil samples.

3.3.4 Los Gatos/Picarro comparison

A comparison of the analyses results from the two isotope instruments (Los Gatos and Picarro) was conducted. Twenty random water samples were run on both the Picarro and Los Gatos and the resulting liquid isotope values compared. The comparison produced average absolute differences of 1.0‰ and 0.30‰ for δD and $\delta^{18}O$, respectively. Standard deviations for δD and $\delta^{18}O$ differences were 0.73 and 0.24, respectively. A summary of the individual sample comparisons can be found in Appendix A.

3.4 Data Analysis

This section will summarize the methods used to process the collected data into meaningful and interpretable information including the methods used to establish the LMWL, model the evaporation line and characterize source waters.

3.4.1 Developing the LMWL

The LMWL was redeveloped utilizing similar techniques to Peng et al. (2004) and Athanasopoulos (2009). Both these studies calculated monthly volume weighted isotope compositions of precipitation to develop the LMWL. The monthly values were then plotted in δD vs. $\delta^{18}O$ space and a regression line through the values determined the slope of the LMWL.

This study calculated volume weighted values of rainfall over time frames of roughly two to four weeks. The time frames were dependant on sampling dates which represented the duration of precipitation collection.

Rainfall data from both 2009 and 2012 was used to calculate the volume weighted δD and $\delta^{18}O$ values of rainfall. Rainfall from 2009 was collected at South Bison Hills only, while rainfall from 2012 was collected from three locations (SWSS Cell 32, South Bison Hills and U-shaped cell). To account for this, all rainfall volumes were normalized to the average rainfall volumes collected for each year. By doing this the 2009 and 2012 rainfall datasets were weighted equally when calculating volume weighted δD and $\delta^{18}O$ values of rainfall for LMWL development.

Snow samples were collected from snow surveys in late winter. Because of this δD and $\delta^{18}O$ values of winter precipitation for a given year was calculated as the average of all snow samples collected during that year.

Once the volume weighted rainfall and snow values were calculated, the weighted data points were plotted in δD vs. $\delta^{18}O$ space. A regression line for the data points was generated in Excel (Microsoft 2010) to define the LMWL.

3.4.2 Characterizing source waters

Mine site waters were initially characterized by plotting datasets against the LMWL and comparing the datasets graphically. By comparing the source waters graphically, general trends and differences between the source waters were observed visually. These differences among

source waters include ranges of δD and $\delta^{18}O$ values and the location of source water with respect to the LMWL.

After datasets were visually compared, statistical analyses were executed to support the graphical interpretations. Statistical analyses consisted of first generating quantile plots (probability plots) to determine the distribution of each dataset. Once the statistical distribution was determined, cumulative distribution functions (CDFs) were generated along with box and whisker plots. T-testing was executed to statistically compare data sets.

Quantile plotting was conducted in the statistical analysis program MiniTab 16 (MiniTab Inc. 2012). Quantile plots were generated for both δD and $\delta^{18}O$ values to determine if each dataset adequately fit a normal distribution. An adequate fit was achieved when a P-value greater than 0.05 was achieved. If a normal distribution did not sufficiently describe a dataset, additional probability plots were generated to assess if a log-normal, Weibull or gamma distribution better described the dataset.

Once statistical distributions were established, CDFs and box and whisker plots of δD and $\delta^{18}O$ for each dataset were created in Excel. The theoretical CDF equation for a normal distribution is:

$$f(x) = \frac{1}{2}\left(1 + \text{erf}\left(\frac{x-\mu}{\sqrt{2\pi\sigma^2}}\right)\right) \tag{3.1}$$

where μ is the mean of the data set, σ is the standard deviation of the data set, x defines a value or point for the dataset and f(x) which represents the cumulative distribution of the dataset at x. The f(x) value describes the percentage or fraction of values that will statistically be less than x. The theoretical CDFs created from Equation 3.1 were plotted with the corresponding experimental dataset to visually compare experimental and theoretical curves.

CDFs and box and whisker plots show a range of expected values for each dataset and allows for the comparison of datasets to establish differences and distinctions among different mine waters.

Numerous t-tests were conducted on MiniTab to statistically confirm or refute the similarities and differences among datasets. T-tests statistically compare the means of two datasets to determine if the datasets are equal. A 95% confidence interval was used in the t-tests, meaning a P-value less than 0.05 indicates no correlation between the datasets at that confidence interval. P-value's greater than 0.05 specifies that a dataset may be related at a 95% confidence interval.

3.4.3 Developing and modelling the natural evaporation line

An evaporation line for the surface water samples was empirically established by plotting a regression line through specific data sets. The slope of the regression line was considered to be equivalent to the slope of an evaporation line. A natural evaporation line was established from the isotope signatures for the perched ponds on South Bison Hills. The empirically derived natural evaporation line was then modelled in a similar manner to Gammons et al. (2006) which utilized Gonfiantini's (1986) model to verify the validity of the empirical natural evaporation line.

Gonfiantini's (1986) model utilizes atmospheric conditions such as relative humidity, temperature and the isotopic composition of vapour in the free atmosphere to estimate the natural evaporation line. A summary of the model is provided below. More details and derivations of equations can be found in Gonfiantini (1986).

The model adopts the liquid-vapour transport model established by Craig and Gordon (1965) to estimate isotopic partitioning between the vapour and liquid phases during evaporation to estimate the isotopic composition of an evaporating surface water body. Through this model, the following relationship is established:

$$\delta = \left(\delta_o - \frac{A}{B}\right) f^B + \frac{A}{B} \tag{3.2}$$

where f is the fraction of residual water remaining in the evaporating water body, δ_o is the initial isotopic composition of the water body at f=1 and δ is the isotopic composition of the evaporating water body at f. The parameters A and B can be calculated with the following equations:

$$A = \frac{h\delta_a + \varepsilon_k + \varepsilon/\alpha}{1 - h + \varepsilon_k} \tag{3.3}$$

$$B = \frac{h - \varepsilon_k - \frac{\varepsilon}{\alpha}}{1 - h + \varepsilon_k} \tag{3.4}$$

where h is the relative humidity, δ_a is the isotopic composition of the atmosphere,α is the equilibrium fractionation factor, ε is the equilibrium enrichment factor (ε=α-1), and ε_k is the kinetic enrichment factor.

The model assumes h, δ_a, α, ε and ε_k values remain constant throughout evaporation. α-values were derived by the equilibrium fractionation factor equations derived by Majoube (1971), which are shown in Equations 2.4 and 2.5. Values for ε_k were derived from Equation 2.7.

No atmospheric samples were collected to establish a value for δ_a. However, Jacob and Sonntag (1991) provide a good summary of the isotopic composition of atmospheric vapour and precipitation at Heidelberg, Germany through 1981 to 1988. With this data, relationships between the isotopic composition of precipitation and atmosphere were established:

$$\delta D_{eqvap} = 1.00 \cdot \delta D_{vap} - 2‰ \tag{3.5}$$

$$\delta^{18}O_{eqvap} = 0.90 \cdot \delta^{18}O_{vap} - 1.4‰ \tag{3.6}$$

where the subscript *eqvap* represents the theoretical isotopic compositions of vapour in equilibrium with precipitation calculated from Majoube's (1971) equations and the subscript *vap* is the actual isotopic composition of atmospheric vapour. These relationships were used to estimate average δ_a values.

Initial liquid δD and δ^{18}O values (δ_o) were established as the point of intersection between the LMWL and natural evaporation line. Once the A and B parameters were calculated, the δD and δ^{18}O values of the evaporating water body as a function of the fraction of water lost can be developed. Combining the δD and δ^{18}O functions produces a slope for the evaporation line.

The model described above is a simple model which is used to approximate the slope of the natural evaporation line. Because of its simplicity the model has its downfalls. The model assumes constant atmospheric conditions which results in average h, δ_a, α and ε_k parameters as model inputs. In reality, these values fluctuate diurnally and seasonally, indicating the model may misrepresent the atmospheric conditions at certain times of the day or year. However, because of the models simplicity and attempt to account for differing atmospheric conditions, Gonfiantini's (1986) model provides a good basis to understand the processes controlling evaporation and the slope of the natural evaporation line.

3.4.4 Estimating Evaporation

Along with the development of modelling the natural evaporation line, several researchers have attempted to estimate evaporation rates from surface water bodies by combining water balance and isotope theory concepts (Gibson et al. 1993, Wolfe et al. 2007, Ferguson et al. 2007, Gibson

and Edwards 2002, Rock and Mayer 2007, Gonfiantini 1986). This study will follow concepts and methods developed by Gonfiantini (1986) and Ferguson et al. (2007) to estimate the E/I ratio (evaporation/inflow).

The general water balance equation lakes are:

$$\frac{dV}{dt} = I - O - E \tag{3.7}$$

where V is the lake volume, t is time, dV/dt is the change in lake volume over time, I is the rate of water inflow, O is the rate of water outflow and E is the evaporation rate. The isotope balance for lakes is expressed as:

$$V\frac{d\delta_L}{dt} + \delta_L\frac{dV}{dt} = I\delta_I - O\delta_O - E\delta_E \tag{3.8}$$

where δ_L, δ_I, δ_O and δ_E are natural stable water isotope compositions of the lake, inflows, outflows and evaporated water, respectively. All the flow rates and isotopic compositions can be assessed and estimated from sampling and field data except for the volume and isotopic composition of evaporation (E and δ_E). δ_E can be estimated from an expression provided in Gibson et al. (2002) which uses Craig and Gordon's (1965) evaporation model to estimate δ_E:

$$\delta_E = \frac{\delta_L + h\delta_A - \varepsilon}{1 - h + \varepsilon_K} \tag{3.9}$$

where h is the relative humidity, δ_A is the isotopic composition of the atmosphere, ε is the total enrichment from evaporation and ε_K is the kinetic enrichment from evaporation.

Combining Equations 3.8 and 3.9 leads to the following expression:

$$\frac{E}{I} = \frac{(\delta_L - \delta_I)(1 - h + \varepsilon_K)}{(\delta_L + 1000)\left(\varepsilon_K + \frac{\varepsilon}{\alpha}\right) + h(\delta_A - \delta_L)} \tag{3.10}$$

where E/I is the evaporation to inflow ratio and α is the equilibrium fractionation factor. Equation 3.11 can be used to calculate the E/I ratio of a water body if δD and $\delta^{18}O$ values of the water body, inflows and atmosphere are known along with meteorological data to estimate the equilibrium fractionation factors and kinetic enrichment factors. The E/I ratio can be further supplemented with hydrological data to estimate evaporation volumes.

3.4.5 Vapour to liquid isotope values: theory

The purpose of collecting and analyzing a series of vapour samples was to estimate the in-situ δD and $\delta^{18}O$ composition of pore water surrounding a dry piezometer. This was done successfully in a laboratory setting by Rothfuss et al. (2013) for sand. The vapour was analyzed with a Picarro isotope analyzer and it was shown that the vapour-liquid relationship is well represented by equilibrium fractionation factors published by Majoube (1971), which are shown in Section 2.2.3.

This study utilized a similar approach to that of Rothfuss et al. (2013) to estimate the isotope values of pore water from vapour isotope values. Although Rothfuss et al.'s (2013) methods and calculations were closely followed. However, some additional calculations and corrections had to be adapted to deal with the specific field sampling issues associated with this research study.

The first of these complications is that the Picarro isotope analyzer at the University of Saskatchewan is not calibrated to read true isotope values of vapour directly, while in Rothfuss et al.'s (2013) study the Picarro was calibrated to directly read true isotope values. To account for this, a correction was established using equilibrium fractionation factors (Equations 2.4 and 2.5), liquid standards with known isotope values, and the isotope values of vapour equilibrated with the liquid standards.

The correction was calculated by comparing the differences between the theoretical and experimental δD and $\delta^{18}O$ values of vapour. Three liquid standards were studied. The differences between the experimental and theoretical vapour values among all three samples were approximately equivalent. The Picarro read experimental δD and $\delta^{18}O$ values of vapour that were approximately 14.5 and 4.2‰ more enriched in δD and $\delta^{18}O$, respectively than the theoretical vapour values.

Because the Picarro reported δD and $\delta^{18}O$ values heavier than the theoretical values, a correction factor was subtracted from the experimental values obtained by the Picarro isotope analyzer to theoretically approximate the true isotope values of vapour. This correction equation for δD is shown in Equation 3.11:

$$\delta D_{cor} = \delta D_{exp} - 14.5‰ \tag{3.11}$$

where δD_{cor} is the corrected δD value and δD_{exp} is the experimental δD value of vapour obtained

from the Picarro. A similar equation can be derived for $\delta^{18}O$.

Another complication in the current study is the range of temperatures measured in the field. The observed temperatures at sampling depths ranged from 6 to 13°C. This produces two complications. The first complication is vapour at lower temperatures is saturated at a lower specific humidity than what occurs during equilibration of a water sample at laboratory temperatures. For example, vapour sampling at temperatures of 6 to 13°C would result in a lower specific humidity between 9,500 to 15,000 ppm at a relative humidity of 100%. These specific humidity values are significantly lower than those obtained at temperatures of 22 to 25°C (28,000 to 30,000 ppm at saturation). Schmidt et al. (2010) has shown that specific humidity does affect Picarro outputs in a predictable and linear fashion.

To account for the varying specific humidity between the vapour samples collected in the field and the vapour equilibrated in the laboratory another correction was applied. This correction was applied because the calibration to standard waters is only undertaken at laboratory room temperatures

The correction first utilizes the linear correction proposed by Schmidt et al. (2010) for the relationship between specific humidity and δD and $\delta^{18}O$ compositions output by the Picarro. The average slopes for δD and $\delta^{18}O$ were 0.08 and 0.131 ‰/1,000 ppm, respectively. The correction for δD was calculated with the following equation:

$$\delta D_{cor2} = \delta D_{cor} + \left(30{,}000 - SH_{sample}\right) * 0.08 \ \frac{‰}{1{,}000\ ppm} \tag{3.12}$$

where δD_{cor} is the δD value calculated in Equation 3.11, SH_{sample} is the specific humidity of the vapour sample in ppmv and δD_{cor2} is the new δD of vapour. A similar expression can be established for $\delta^{18}O$. The 30,000 ppmv is the typical humidity observed in equilibrated vapour samples at laboratory room temperatures of 23°C. This value was applied to all vapour samples.

The second obstacle with the field sampling of vapour is the range of temperatures at which liquid-vapour equilibration is occurring. This produces a range of equilibrium fractionation factors, which is demonstrated by the fractionation factor expressions established by Majoube (1971).

These lower in-situ temperatures have to be accounted for in order to establish in-situ pore water isotopic composition. The equilibrium fractionation factor for a known in-situ temperature can be calculated and applied to calculate the liquid isotope compositions using the following equation:

$$\delta_L = (\delta_{cor2} + 1{,}000) * \alpha_{l/v} - 1{,}000 \quad (3.13)$$

where δ_L is the liquid isotopic composition, δ_{cor2} is the isotopic composition calculated in Equation 3.12 and $\alpha_{l/v}$ is the fractionation factor at the sampling temperature.

These corrections were applied to estimate the liquid isotope values from experimental vapour isotope values. The corrections presented assume that the vapour and liquid phases are in equilibrium and remain in equilibrium during sampling. Deviating from equilibrium conditions in the field will produce invalid results.

An example showing how to calculate the liquid isotope composition from the experimental vapour isotope composition using the techniques described in this section is shown in Appendix B.

4 PRESENTATION OF RESULTS

This section will present the results from the field and laboratory programs. The modification of the local meteoric water line (LMWL) developed by Hilderman (2011) will be refined and modified using the collected data. A natural evaporation line will be established for overburden wetlands. Mine site waters will be characterized based on their δD and $\delta^{18}O$ compositions to establish unique signatures for precipitation (snow and rain), interstitial shale pore water, and recycle process affected water (PAW) and tailings. Additionally, an attempt to explain the PAW/tailings signatures and fractionation processes will be provided. δD and $\delta^{18}O$ data of all water and soil samples are shown in Appendix C. Sampling information such as sampling dates and UTM co-ordinates of piezometer nests and drilling locations are shown in Appendix D.

4.1 LMWL for the Mildred Lake mine

4.1.1 Hilderman's (2011) data set and LMWL

Hilderman (2011) collected twenty six rainfall samples from South Bison Hills from May 2009 to the beginning of October 2009 and fourteen snow samples collected in March 2009. The preliminary LMWL developed by Hilderman (2009) using this data set was as follows:

$$\delta D = 6.7(\delta^{18}O) - 29.8 \quad (4.1)$$

Hilderman's (2011) LMWL along with 95% prediction intervals for the LMWL and the plotted precipitation and snow samples are shown in Figure 4.1.

The volume weighted average of rainfall was determined to be -129‰ and -14.9‰ for δD and $\delta^{18}O$, respectively. The average δD and $\delta^{18}O$ values of snow were -194‰ and -25.0‰, respectively. A snow survey at South Bison Hills by Syncrude in 2009 estimated a snow water equivalent (SWE) of 93 mm and the meteorological station at South Bison Hills recorded approximately 220 mm of rainfall.

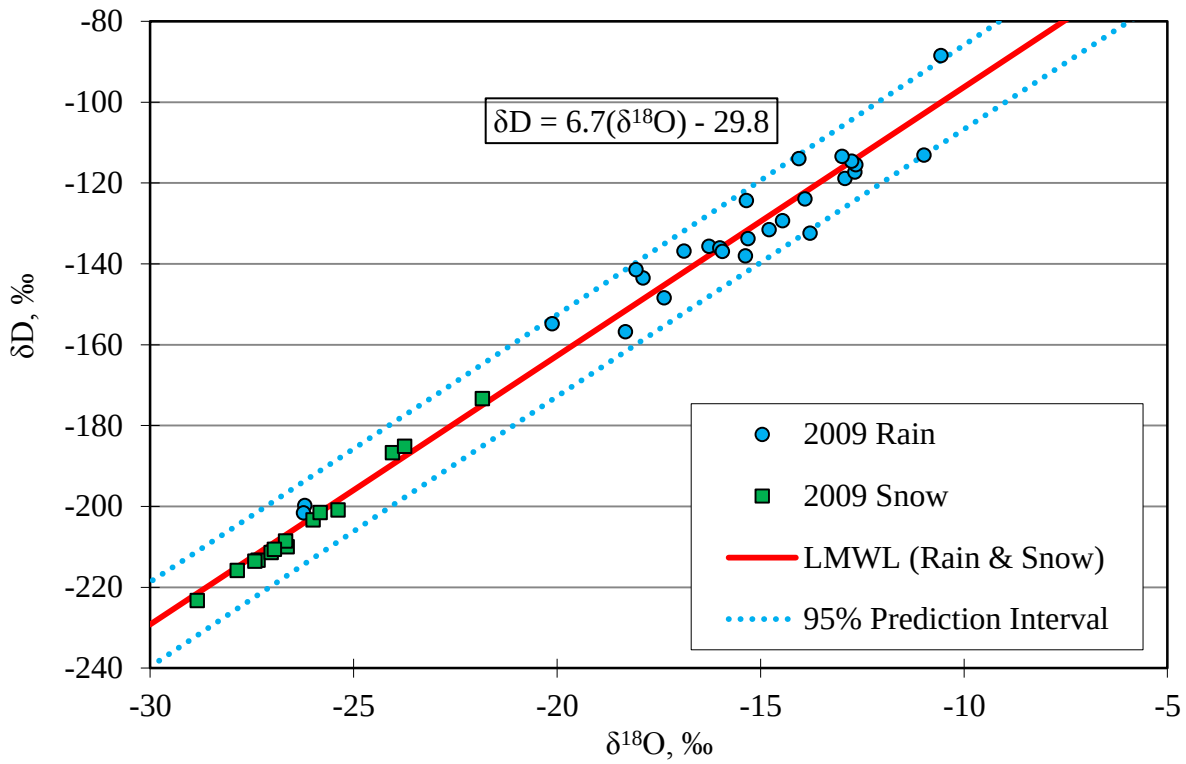

Figure 4.1: Rainfall and snow data set from 2009 and corresponding LMWL (Hilderman 2011)

4.1.2 Modifying the LMWL

Samples of rainfall were collected in the spring and summer of 2012 and snow was sampled 2012 and 2013. Rainfall samples were collected at South Bison Hills, Southwest Sands (SWSS) Cell 32 and U-shaped cell meteorological stations. Snow samples were collected the Mildred Lake mine site and at the Aurora capping study. A summary of the is shown in

Table 4.1. Rainfall amounts were monitored by meteorological stations operated by O'Kane Consultants (Clark, personal communication).

The collected rainfall volumes shown in

Table 4.1 are the volumes of rainfall measured during the sampling duration. Rainfall events that

occurred outside the sampling time, for example in April 2012 before rainfall samplers were installed, are not included in the volume calculations.

Table 4.1: Summary of precipitation data; δD and $\delta^{18}O$ values are volume weighted averages of collected precipitation

	Total collected water volume [mm]	δD, ‰	$\delta^{18}O$, ‰
2012 SWSS Rainfall	200	-119	-14.5
2012 Ucell Rainfall	285	-123	-15.9
2012 30T Rainfall	228	-126	-16.0
2012 Average Rainfall	230	-123	-15.6
2009 Rainfall	220	-129	-14.9
2009 Snow	93	-204	-26.1
2012 Snow	57	-195	-25.0
Jan/Feb 2013 Snow	--	-209	-27.3
March 2013 Snow	126	-212	-27.4
2009 Precipitation	313	-151	-18.2
2012 Precipitation	287	-137	-17.5
2012 Rainfall/2013 March Snow	356	-155	-19.8
2009 and 2012 Average	600	-145	-17.9

** Snow depths given as snow water equivalent (SWE)

There are noticeable differences between the 2009 and 2012 volume weighted δD and $\delta^{18}O$ values of precipitation. Between 2009 and 2012, δD and $\delta^{18}O$ values varied as much as 18‰ and 1.6‰, respectively. Peng et al. (2004) found similar differences between annual volume weighted precipitation for Calgary, AB over a ten year time frame. Over that time frame, Peng et al. (2004) recorded annual isotope values that varied between -15.5 and -19.4‰ for $\delta^{18}O$ and -112 and -149‰ for δD. The reasons for these differences are clear upon analysis of the data set in Peng et al. (2004). Years with a higher fraction of winter precipitation produced more depleted δD and $\delta^{18}O$ values compared to years where there was less winter precipitation. This trend also occurs in the Mildred Lake data set in the present study and is consistent with the greater depletion of cold weather precipitation. A large amount of winter precipitation will contribute significantly to the annual volume weighted averages, resulting in more depleted average δD and $\delta^{18}O$ values.

The refined LMWL was calculated by plotting volume weighted average isotope values of precipitation over a given time frame. A (y-on-x) regression line was then drawn through the volume weighted data set to obtain the LMWL.

Three rainfall sampling locations were operational in 2012, while rainfall was sampled from only one location in 2009. To ensure both the 2009 and 2012 dataset contributed equally to the development of the LMWL, the 2012 datasets for each location were normalized to produce an annual dataset that was equivalent and comparable to the 2009 dataset.

Weighted average δD and $\delta^{18}O$ values of precipitation were calculated over a two to four week time frame, depending on sampling frequency. The weighted average calculations are shown in Appendix E. The resulting LMWL is plotted in Figure 4.2 along with Hilderman's (2011) LMWL. The equation of the refined LMWL was determined to be:

$$\delta D = 7.0(\delta^{18}O) - 18.6‰ \qquad (4.2)$$

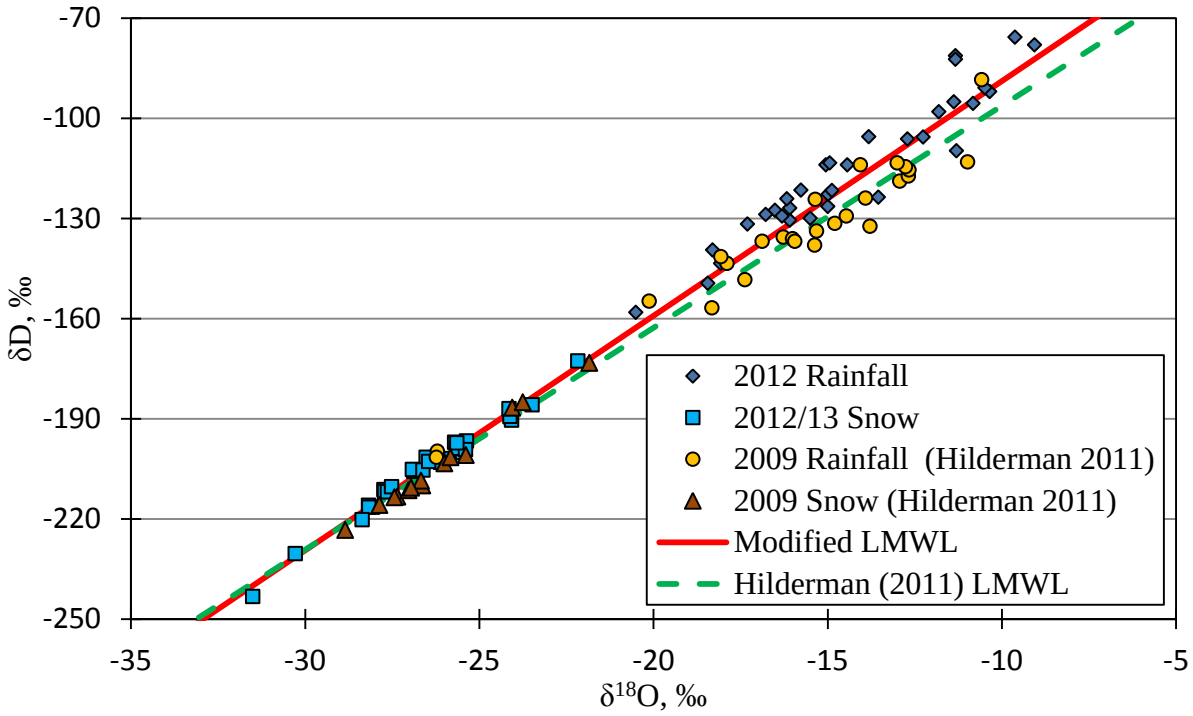

Figure 4.2: Modified LMWL using volume weighted average approach

An annual LMWL for 2009 and 2012 were also developed with the volume weighted approach. Additionally, an LMWL was generated for 2009, 2012 and both years combined by drawing a (y-on-x) regression line through all individual samples collected. Table 4.2 provides a summary of volume weighted and individual sample LMWLs for the Mildred Lake mine along with the volume weighted and individual sample LMWL for Calgary.

The corresponding individual sample and volume weighted LMWLs for the mine site are comparable to each other, but the annual LMWLs for 2009 and 2012 are different. The difference between the two years is well within an acceptable range. Peng et al. (2004) observed annual volume weighted LMWLs with slopes ranging from 7.13 to 8.52 between 1992 and 2001. These differences could be due to annual weather variations which could affect the source water of precipitation (ocean vs. inland) and the rainout of cloud masses.

The volume weighted and individual sample LMWL for the Calgary region vary. Peng et al. (2004) attributed these differences to continental evaporation and re-evaporation of precipitation

between the cloud and ground during rainfall events. This trend was not as distinct in the Mildred Lake mine LMWL.

Table 4.2: Summary of volume weighted and individual sample LMWL's developed for the Mildred Lake mine; Calgary's LMWL (Peng et al. 2004) shown for comparison

LMWL	Years	Volume Weighted LMWL	Individual sample LMWL
Mildred Lake Mine	2009, 2012	$\delta D=7.0(\delta^{18}O)-18.6‰$	$\delta D=7.0(\delta^{18}O)-18.7‰$
Mildred Lake Mine (Hilderman 2011)	2009	$\delta D=6.7(\delta^{18}O)-28.6‰$	$\delta D=6.7(\delta^{18}O)-26.5‰$
Mildred Lake Mine	2012	$\delta D=7.3(\delta^{18}O)-10.9‰$	$\delta D=7.3(\delta^{18}O)-11.6‰$
Calgary, AB (Peng et al. 2004)	1992-2001	$\delta D=7.7(\delta^{18}O)-0.2‰$	$\delta D=7.1(\delta^{18}O)-13.6‰$

Table 4.3 provides a summary of the LMWL for several other regions as well as the new LMWL for the mine site. Both Calgary and Edmonton are located south of the Mildred Lake Mine while Fort Smith is north of the mine site. A trend between the LMWLs is evident where more southern LMWLs have a steeper slope and a higher y-intercept (d-excess) in comparison with the northern regions.

Table 4.3: Comparison of LMWL's from several locations nearby

Location	Years	LMWL
Mildred Lake Mine	2009, 2012	$\delta D=7.0(\delta^{18}O)-18.6‰$
Global Meteoric Water Line	N/A	$\delta D=8.2(\delta^{18}O)+10.6‰$
Calgary, AB (Peng et al. 2004)	1992-2001	$\delta D=7.7(\delta^{18}O)-0.2‰$
Edmonton, AB (Hage et al. 1975)	1962-1966	$\delta D=7.7(\delta^{18}O)+0.4‰$
Fort Smith, NT (Hage et al. 1975)	1962-1966	$\delta D=6.8(\delta^{18}O)-20.9‰$

The slope and d-excess of the mine site LMWL are lower than those of the Global Meteoric Water Line (GMWL). A LMWL with a shallower slope than the GMWL indicates that evaporation regularly occurs during rainfall (Friedman et al. 1962, Clark and Fritz 1997). The shallower slope also indicates that the precipitation may be derived from a coastal source that has gone through several evaporation-condensation cycles and/or that precipitation originates from an inland source, such as forests and lakes (Clark and Fritz 1997).

Merlivat and Jouzel (1979) have shown theoretically that the global d-excess parameter is strongly dependant on the relative humidity at the ocean source. As a result, evaporation processes strongly control the d-excess parameter (Kendall and Coplen 2001). This further demonstrates that local precipitation typically goes through several evaporation cycles or originates from an inland source.

The re-developed mine site LMWL ($\delta D=7.0(\delta^{18}O)-18.6‰$) and 95% prediction intervals for the LMWL is shown in Figure 4.3 along with all meteoric water samples collected. Overall, only a few samples fall outside the 95% prediction intervals for the line.

The two data points that fall well below the lower prediction interval were very small rain events during mid-spring of 2009. The insignificant amounts of rain that occurred during this time likely translated into small sample volumes which would be more susceptible to the influence of evaporation. The two data points that are above the 95% prediction intervals were summer storms that occurred late in June 2012. Meteorological conditions may have been unstable during this rain event and caused inconsistent δD and $\delta^{18}O$ values for that particular rain event.

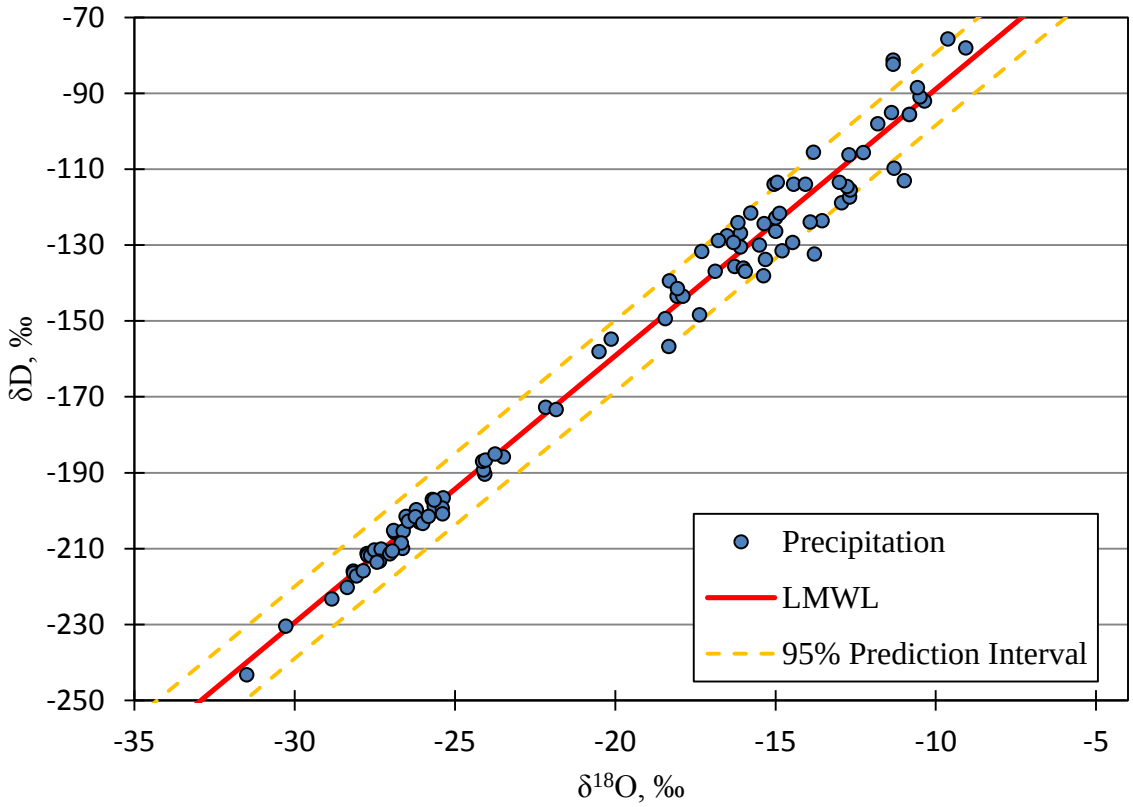

Figure 4.3: Mildred Lake mine LMWL with 95% prediction interval and all meteoric samples

4.2 Developing a Natural Evaporation Line

Three perched ponds on South Bison Hills: Peat Pond, Bill's Lake and Golden Pond were sampled throughout the summer months of 2003 and 2004 by Kelln (2008), in 2009 by Hilderman (2011) and in 2012 and 2013 as part of this study. When plotted against the LMWL a clear evaporative trend is evident, as shown in Figure 4.4. The resulting (y-on-x) regression line produces a natural evaporation line with a slope of 5.3. The natural evaporation line was established using only three small bodies of surface water on South Bison Hills, which indicates that this line may not be representative of other surface water bodies in the region.

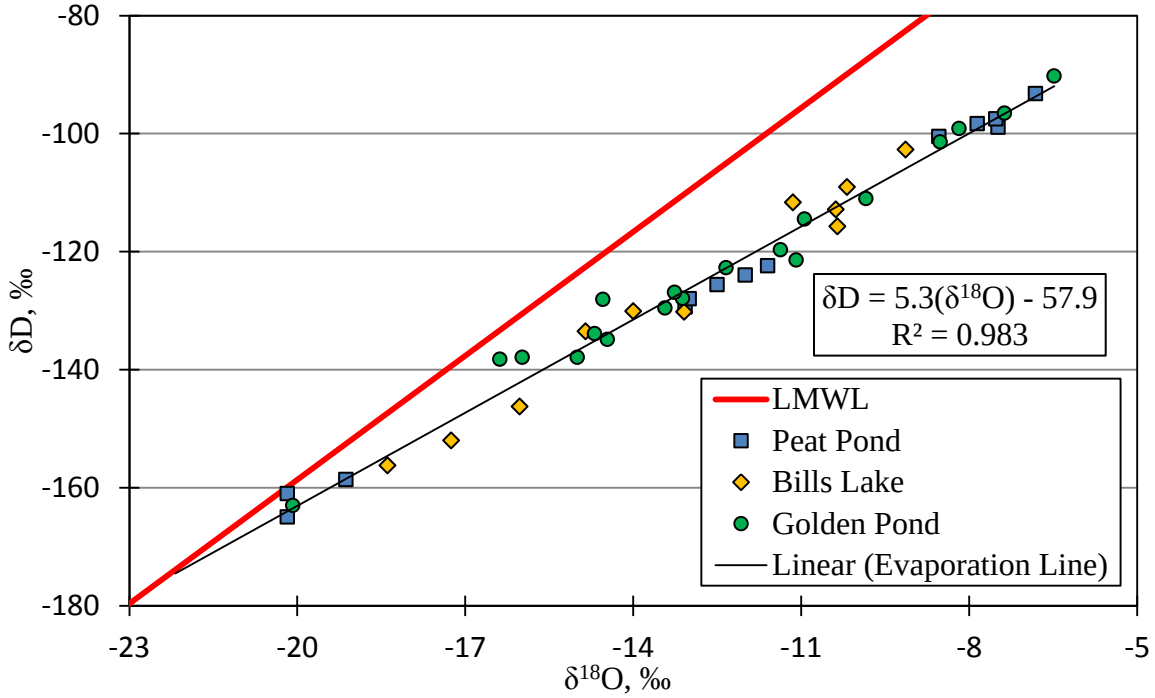

Figure 4.4: South Bison Hills ponds plotted in with LMWL

The natural evaporation line for the Mildred Lake is comparable to the ones established by Wassenaar et al. (2011) for the Okanagan Valley, BC and Gammons et al. (2006) for Butte, Montana, which both have a slope of 5.0. Gibson et al. (2005) found natural evaporation lines was generally between 4.1 to 5.8 for several regions in northern Alberta and the Northwest Territories, further demonstrating that the established natural evaporation line is reasonable.

The natural evaporation line intersects the LMWL at δD and $\delta^{18}O$ values of -175‰ and -22.2‰ respectively. This intersect provides an approximation of the δD and $\delta^{18}O$ composition of the source waters (Gibson et al. 2005). The intersect values are more depleted than the volume weighted averages of precipitation, indicating that a significant component of input water is likely derived from snowmelt.

The natural evaporation line was theoretically estimated using techniques utilized by Gammons et al. (2006), as described in Section 3.4.3. The inputs for the model include air temperature and relative humidity, the initial liquid isotope composition of the pond ($\delta^{18}O_l$ and δD_l) and the isotopic composition of the atmosphere ($\delta^{18}O_a$ and δD_a). The estimated values for each input are displayed in Table 4.4.

Table 4.4: Inputs for natural evaporation line model

Input	Value
Temperature [°C]	15
Relative Humidity [%]	68
δD_l [‰]	-175
$\delta^{18}O_l$ [‰]	-22.2
δD_a [‰]	-214
$\delta^{18}O_a$ [‰]	-29.4

Input values were developed in a similar fashion to Gammons et al. (2006). Temperature and relative humidity inputs were established as being the average recorded values throughout May to September (O'Kane 2013), the season over which a majority of evaporation takes place. Initial liquid isotope values were represented by the point of intersection between the LMWL and natural evaporation line, which provides an approximation of the initial liquid isotope composition of the pond water. Atmospheric isotope values were calculated as discussed in Section 3.4.3 using Equations 3.6 and 3.7.

The model produces a natural evaporation line with a slope of 5.25, which is similar to the empirical slope of 5.3, further verifying the natural evaporation line. Estimations of water lost to evaporation using this model will be developed and discussed in the next chapter.

The three ponds were plotted individually to develop a separate evaporation line for each pond. The resulting slopes for Bill's Lake, Peat Pond, and Golden Pond were 5.7, 5.2 and 5.1, respectively. These differences may be due to differing microclimates at the ponds caused by vegetation and terrain. This may alter humidity, temperatures and wind speeds between the ponds. The plot showing the natural evaporation line for each individual pond can be found in Appendix F.

Peat Pond and Golden Pond have similar evaporation line slopes, while the evaporation line slope of Bill's Lake is considerably steeper. Both Peat Pond and Golden Pond are larger than Bill's Lake and surrounded by small shrubs and grasses.

Bill's Lake on the other hand, is surrounded by aspen trees and thick shrubs. Because of the thick vegetation, transpiration would likely be more prevalent around Bill's Lake on hot days, possibly

causing a micro-climate in which the relative humidity is considerably higher. When the natural evaporation is re-calculated using a relative humidity of 0.75 with all other parameters the same as in Table 4.4, the resulting estimate produces a line with a slope of 5.6, which is similar to the empirical natural evaporation line with a slope of 5.7.

4.3 Statistical Analysis

A series of statistical charts and analyses were conducted on the collected isotope data from each source of mine site water. The statistical analysis included interpretative plotting of cumulative distributions functions (CDFs) and box and whisker plots as well as statistical testing such as t-tests. These tests were executed to evaluate whether the δD and $\delta^{18}O$ signatures from each source of mine water might be considered unique.

This section will initially outline all the statistical analysis prior to establishing unique signatures for source waters by drawing information from the statistical information in conjunction with additional information. The main source waters for the mine site include precipitation (rainfall and snow), interstitial shale water, Athabasca River/Mildred Lake water and PAW/tailings. Additionally, analyses were also conducted on individual tailings deposits as well as specific sampling of interflow and groundwater wells and soil samples collected from different closure landforms.

4.3.1 Probability Analysis

The statistical analyses package MiniTab 16 was used to develop quantile curves (probability curves) for the representative site waters: rainfall, snow, shale pore water, PAW/tailings and Mildred Lake. Additional probability curves for individual tailings sources, interflow and groundwater within different closure landforms were generated in an attempt to develop statistical correlations between the datasets.

A summary of the quantile plot results including normal distribution means, standard deviations and P-values are shown in Appendix G. Generally, a normal distribution fit the data sets adequately (P-values>0.05). When a normal distribution was rejected, the data set was further analyzed to check if the data set followed a lognormal, Weibull or gamma distribution better. In some cases, a lognormal distribution fit a data set marginally better; however, in those scenarios it was decided the improved fit was not sufficient to complicate calculations for marginally better

fits; as a result, a normal distribution was assumed for all data sets.

At a 95% confidence interval, a normal distribution fit the snow, rainfall and deep shale water (>3m) well with P-values greater than 0.10 occurring for both δD and $\delta^{18}O$.

A normal distribution did not describe the Mildred Lake, West in-pit profiles and Aurora Settling Basin profiles well at a 95% confidence interval, with P-values well below 0.05. Despite this, the variance and scatter in these data sets is significantly small in comparison with other datasets (i.e. snow and rain) and therefore δD and $\delta^{18}O$ signatures of these data sets can be developed.

The surface PAW water samples as a whole did not fit a normal distribution well at the 95% confidence interval. However, the PAW samples for individual tailings basins are well represented by a normal distribution (at a 95% confidence interval). The poor fit for the PAW samples as a whole could be due to the differing physical characteristics of each tailings area (such as depth, area and volume) which cause each area to respond differently to environmental events (such as snowmelt and evaporation). Consequently, at the 95% confidence interval, each individual tailings area fit a normal distribution well, but when grouped together, the differences among tailings areas resulted in a poorer fit.

No single distribution fit the interflow samples or the soil and groundwater samples collected from closure landforms such as the Fen, South Bison Hills and SWSS Cell 32 and 46. These sites are known to be influenced by multiple sources of water (e.g. PAW, precipitation, and/or interstitial shale water) and consequently it is not surprising that they are not well fit with a single distribution (at the 95% confidence interval).

4.3.2 Cumulative distribution functions (CDFs) and box and whisker plots

Theoretical and experimental CDFs were generated for the five primary source waters along with box and whisker plots. The theoretical and experimental CDFs can be found in Appendix H. Relevant information from these plots will be presented in the following sections when investigating mine water signatures and characterizations.

4.3.3 T-tests

MiniTab was used to run a series of 2-sample t-tests to compare data sets. T-tests statistically compare data sets. T-test comparisons were run assuming both equal and unequal variances using a 95% confidence interval. A P-value less than 0.05 signified the data sets are unrelated at

the 95% confidence interval. A t-test that outputs a P-value greater than 0.05 indicates the data sets are related at the 95% confidence interval. The results of the t-tests can be found in Appendix I.

It was found that the five primary source water groups were unrelated.

4.4 Water characterization

The main objective of this project was to characterize and classify source waters in closure landforms based on δD and $\delta^{18}O$ signatures. These characterizations of source waters can then be used in multiple applications including water balances, mixing models and evaporation estimates.

4.4.1 Characterization Introduction

Figure 4.5 displays the five mine site source waters plotted with the refined LMWL. Upon visual inspection, the plot illustrates that source waters are generally unique. Additionally, it can be deduced that interstitial shale water (Hilderman 2011), Mildred Lake and PAW/tailings have limited ranges in their δD and $\delta^{18}O$ signatures whereas snow and precipitation display a broader range of values. The uniqueness among source waters and variance is further demonstrated in the CDFs and box and whisker plots shown in Figures 4.6 to 4.9. These figures show a clear distinction between, snow, interstitial shale water, Mildred Lake water and PAW/tailings. They also depict the wide variances for snow and rain, with rainfall having a signature that encompasses PAW/tailings, and interstitial shale water.

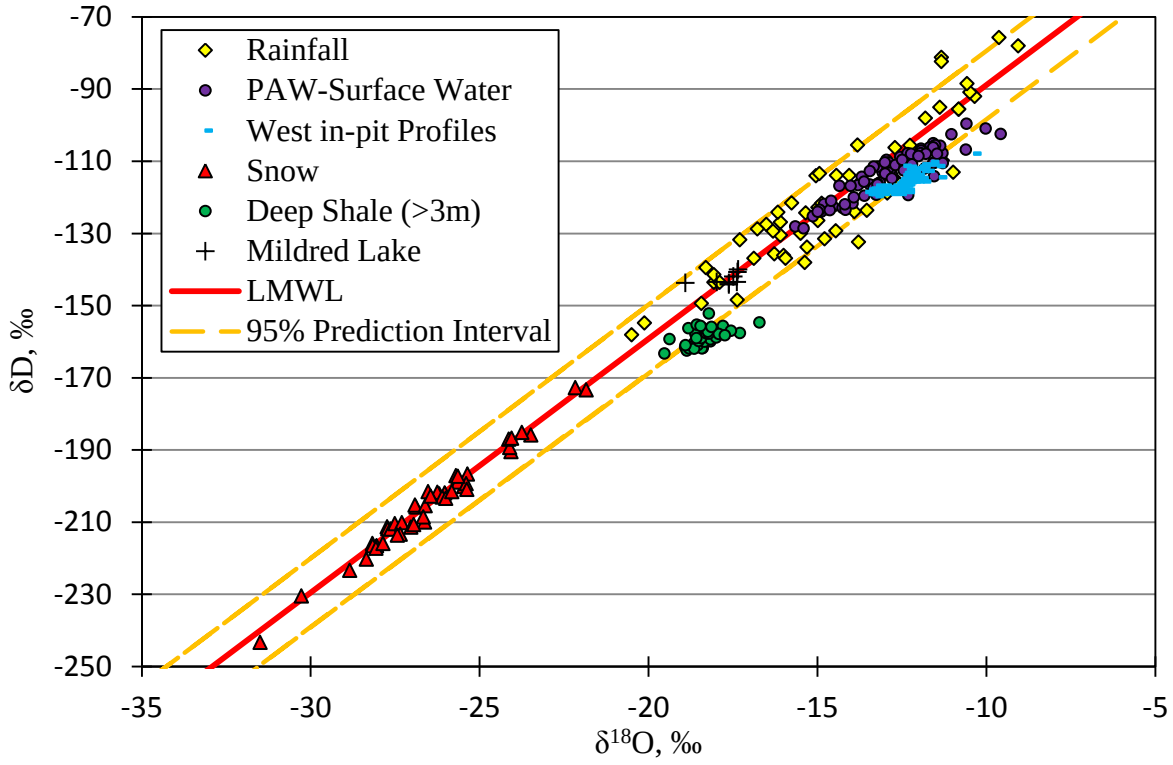

Figure 4.5: Source waters plotted with LMWL

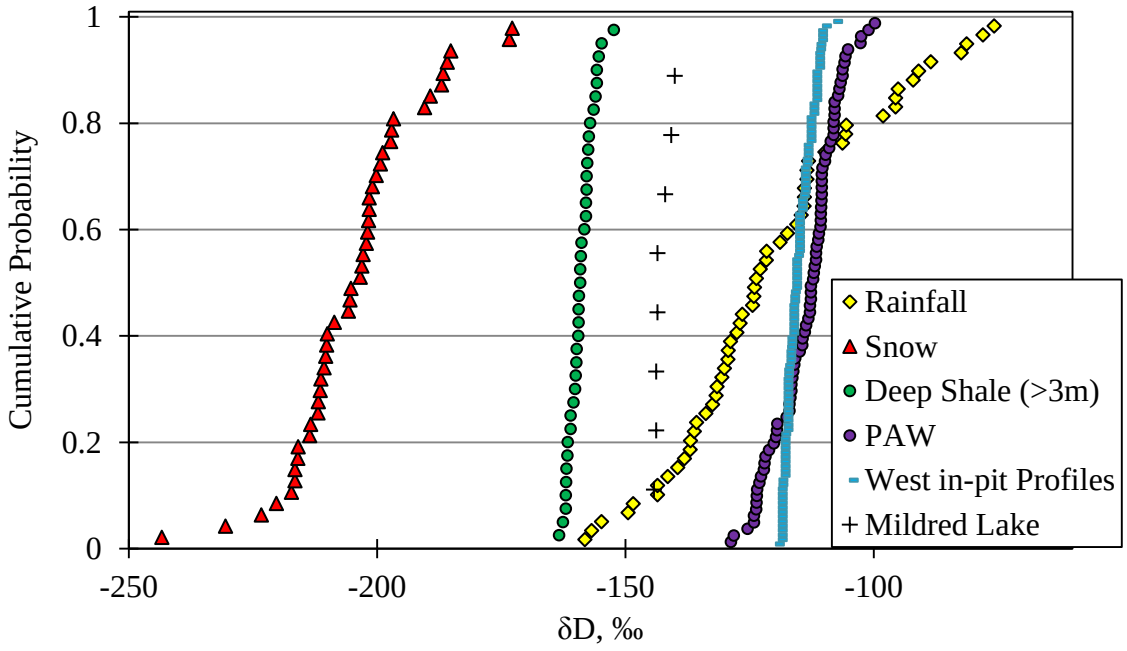

Figure 4.6: Experimental cumulative density functions of Mildred Lake mine waters for δD

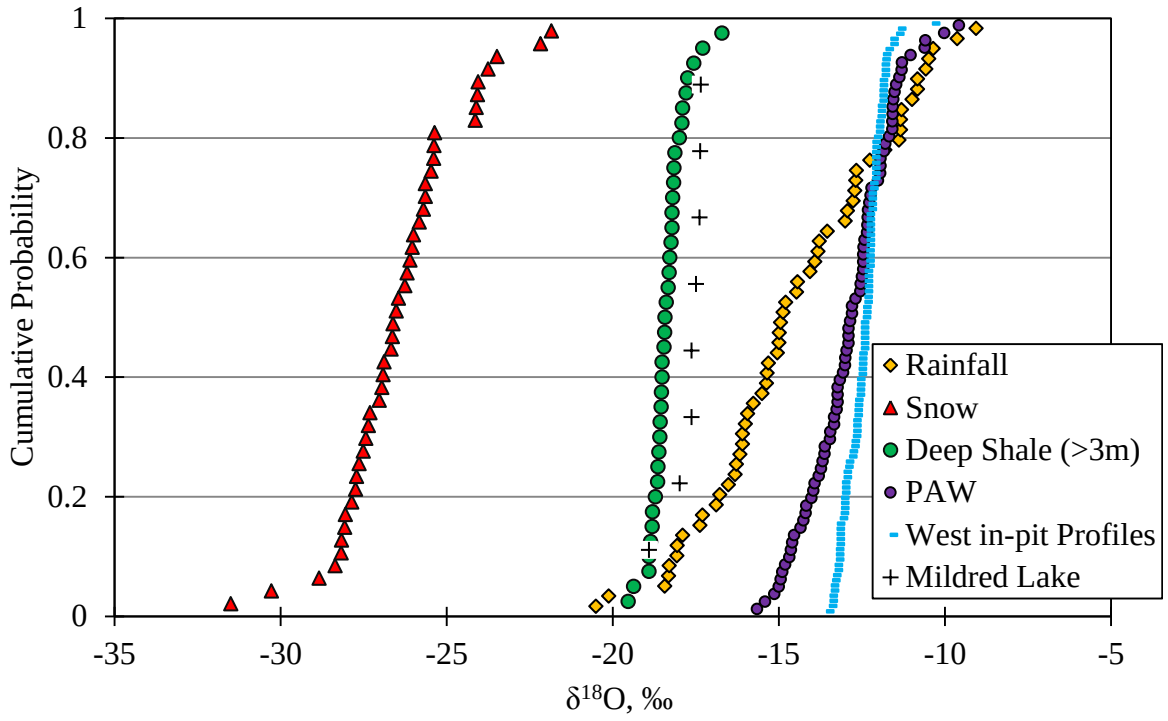

Figure 4.7: Experimental cumulative distribution functions of Mildred Lake mine waters for $\delta^{18}O$

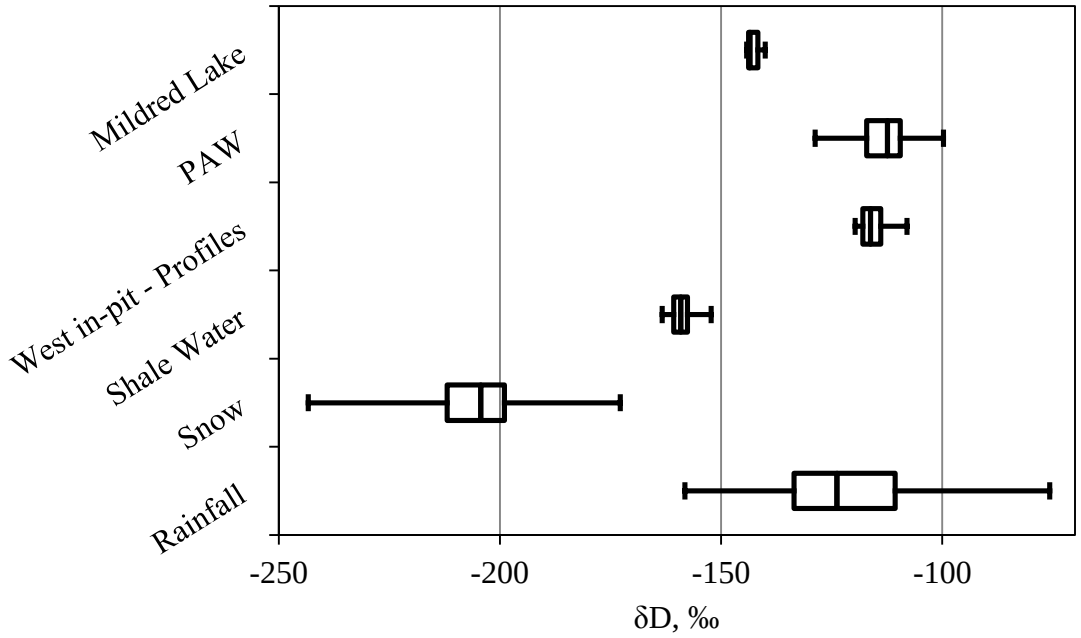

Figure 4.8: Box and whisker plot of δD values for Mildred Lake mine waters

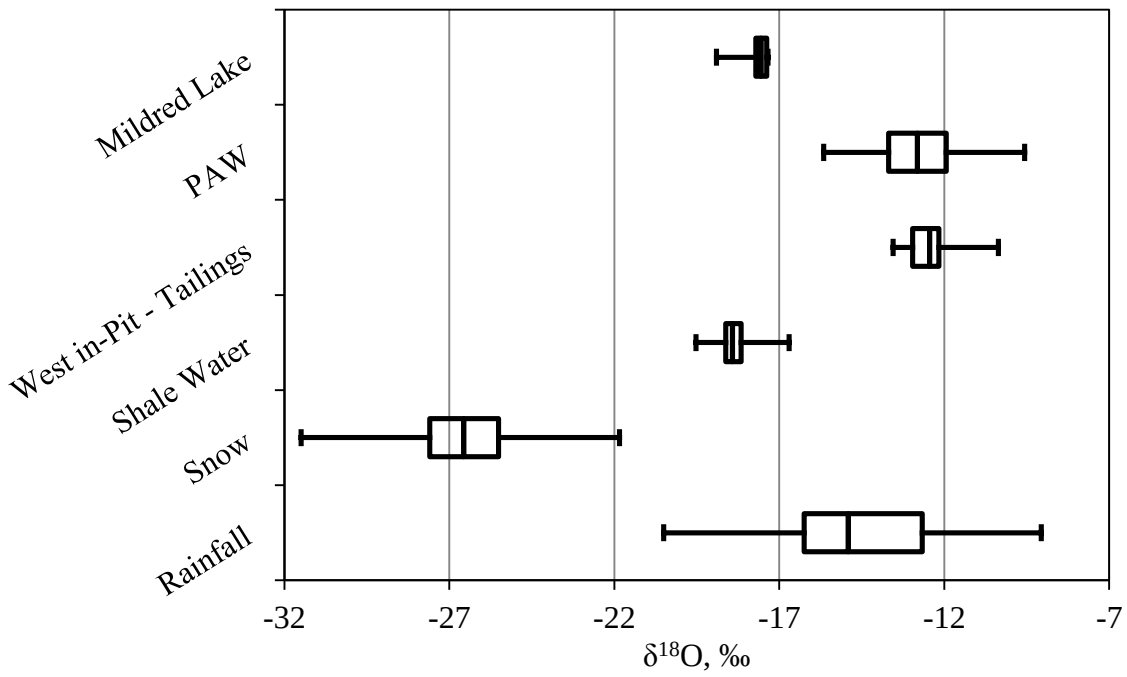

Figure 4.9: Box and whisker plot of $\delta^{18}O$ for Mildred Lake mine waters

The CDFs shown in Figures 4.6 and 4.7 are summarized in Table 4.5 by displaying the normal distribution average and standard deviations for each source water. The figures and table highlight that there is a clear distinction between each of the primary groups of mine site waters which should allow for unique δD and $\delta^{18}O$ signatures to be assigned to each water source. Additionally, the t-tests generated to statistically compare the data sets highlight that these data sets are distinct from each other.

Table 4.5: Averages and standard deviations of water characterizations

	δD, ‰		$\delta^{18}O$, ‰	
Sample	**Average**	**Std Dev**	**Average**	**Std Dev**
Rainfall*	-126.0	20.0	-15.3	2.7
Snow	-204.7	13.4	-26.4	1.9
Mildred Lake/Athabasca River	-142.7	1.6	-17.7	0.5
Deep Shale (>3m) (Hilderman 2011)	-158.9	2.4	-18.4	0.5
West in Pit (WIP)- Tailings Profiles	-115.8	2.6	-12.5	0.5
Surface PAW**	-113.6	6.5	-12.9	1.3

* Averages are amount weighted averages
**Excluding Effluent Pond samples

The following sections will describe the characterizations in more detail by drawing comparisons and differences between the data sets and providing further explanations where necessary in regards to isotope signatures of the waters and their existence within closure landforms.

4.4.2 Rainfall

Rainfall has the largest variance of all water sources as demonstrated in Figures 4.6 to 4.9, with isotope values ranging from -155 to -75‰ in δD. This range of values overlaps with the signature for interstitial shale water, Mildred Lake and PAW/tailings signatures which could cause issues when developing isotopic characterizations.

There is an observed seasonal trend in precipitation which results in cold weather (spring and fall) precipitation being more depleted than warm weather (summer) precipitation (Clark and Fritz 1997). Glancing at the rainfall data set (shown in Appendix E) verifies this relationship. A majority of the enriched precipitation values occur in late-June, July and August and are usually associated with small amounts of rainfall.

It is well established that the primary source of groundwater recharge semi-arid and arid regions is associated with snowmelt rather than rainfall. (e.g.: Ireson et al. 2013, Hayashi et al. 2003, Maule et al. 1994, Earman et al. 2006). There are several reasons for this, which include:

- Rain events are often short, high intensity events which results in more runoff than recharge. Snowmelt on the other hand, occurs over a longer duration, allowing recharge to take place (Earman et al. 2006).
- Rainfall occurs during the warmer seasons, when evaporation and transpiration are at its highest, resulting in significant losses before rainfall has a chance to infiltrate (Earman et al. 2006, Clark and Fritz 1997).
- Soils are more saturated during snowmelt than during the summer resulting in a higher rate of infiltration (Clark and Fritz 1997).

Considering these factors it is clear that rainfall alone likely does not make up a large component of recharge but may be stored in near surface soils or surface water where it is available for transpiration or evaporation. In some cases, late season rainfall may also be stored within the soil profile and later mixed with snowmelt infiltration as demonstrated by Kelln et al. (2007) and Hilderman (2011).

If rainfall is stored near or at the surface and subject to evaporation it is likely to be subject to fractionation events. These fractionation effects are described by Gat and Tzar (1967) and Gat (1996) and mainly involve evaporation of surface water and shallow groundwater, which results in the modification and enrichment of the rainfall signature.

Considering these factors, it is unlikely that recharge through closure landforms will have δD and $\delta^{18}O$ signatures consistent with that of rainfall. Rainfall is more likely to contribute to snowmelt recharge by mixing with snowmelt at the surface or within the soil matrix.

4.4.3 Snow

Snow is clearly the lightest of all the signatures with average values of -205 and -26.4‰ for δD and $\delta^{18}O$, respectively. The snow samples plot right along the LMWL and have δD values ranging from -243 and -172‰. Snowmelt will often undergo enrichment during melting as described previously in Section 2.3.3 and this enrichment can result in an underestimation of snowmelt contribution to recharge (Earman 2006).

Snowmelt enrichment is demonstrated by the two snow samples that are noticeably more enriched than the other snow samples in Figure 4.5. Both these samples were collected at South Bison Hills, one on March 29, 2009, the other on March 21, 2012.

According to 2012 weather data collected by O'Kane Consultants (O'Kane 2013), daily high temperatures at South Bison Hills reached above 0°C consistently around March 10. All samples except for one were collected before March 10 and had more typical snow δD and $\delta^{18}O$ values. The one exception was a snow sample collected on March 21, 2012. This sample was collected during snowmelt which likely contributed to enriched δD and $\delta^{18}O$ values.

The snow samples collected in 2009 were all collected between March 26 and 29. At this time, recorded daily high temperatures were just past the freezing point, with temperatures between 0 to 5°C. Only one snow sample from this set was significantly enriched. A possible explanation for the enriched sample is that the sample location may have been on an open south facing slope where there was more sunlight and warmer temperatures throughout the day, promoting melting.

Estimating the enrichment of snowmelt can be difficult; this problem is compounded greatly by considering that snowmelt enrichment is temporal and a continuous enrichment occurs throughout melting (Lee et al. 2010). This concept is out of the scope of this project. Instead,

more attention will be given to establishing and estimating an average value of snowmelt based on the data collected.

One method to estimate the isotopic signature of snowmelt is to use the point of intersection of the natural evaporation line and LMWL to determine the δD and $\delta^{18}O$ composition of pond source water as discussed by Gat (1996) and Gibson et al. (2005). The South Bison Hill ponds that were used to derive the natural evaporation line in Figure 4.4 are considered perched ponds and receive very little groundwater from the landscape. The main inputs into the ponds include snowmelt runoff and rainfall. Therefore, the point of intersection can be used to theoretically estimate the average value of snowmelt, keeping in mind that rainfall contributes to the source water signature. The rainfall contribution would cause an enrichment of the source water mixture of snow and rainfall. As a result, snowmelt is likely more depleted than the point of intersection. In Figure 4.4, the intersection point occurs at δD and $\delta^{18}O$ values of -175 and -22.2‰, respectively.

The LMWL/natural evaporation line intersect provides a rough theoretical estimate of the maximum average δD and $\delta^{18}O$ signatures of snowmelt. Table 4.6 shows comparisons of this estimate with select samples collected at the mine site. The minimum interflow value is comparable to the LMWL/natural evaporation line intersect. However, interflow must flow laterally through the shallow soil medium before it is collected. Therefore, interflow likely always consists of a mixture of snowmelt and antecedent rainwater. This would result in enriched interflow compositions compared to snowmelt.

Like the interflow, the most enriched snow sample is comparable to the LMWL/natural evaporation line intersect. The enriched snow values are likely not a good indicator of a snowmelt signature due to the continuous and transient enrichment of snow and snowmelt during melting. Nonetheless, this value provides an indicator of the extent of snow enrichment during melting.

Table 4.6: Comparison of LMWL/natural evaporation line intersect with samples collected on site

Method	δD, ‰	$\delta^{18}O$, ‰
LMWL/natural evaporation line Intersect	-174	-22.2
Interflow Minimum	-169	-22
Snow Maximum	-173	-22.1
Fen P13-Minimum	-190	-24.2
Fen P13- Maximum*	-179	-22.4
Fen P13 Average	-184	-23.1

*Maximum value taken as isotope values where it was obvious no evaporation fractionation had occurred

A soil profile collected on the Fen at Piezometer 13 (P13) is perhaps the most interesting and informative sample set which demonstrates the isotope signature of snowmelt. The soil profile was collected on May 1, 2013, shortly after snowmelt. The profile is shown in Figure 4.10. From the profile it can be seen that there is a depletion in δD and $\delta^{18}O$ values with increasing depth below ground from about 50 to 200 cm. At samples collected above 50 cm, the samples plot along the LMWL but are significantly enriched in comparison to deeper values, meaning this soil water is likely derived from spring rainfall. The soil, which was mainly sandy would allow for relatively fast infiltration with little evaporative fractionation. Figure 4.10 displays a range of $\delta^{18}O$ values from -24.2 to -22‰. These values are similar to those observed by Kelln (2008), who established $\delta^{18}O$ values between -22 to -20‰ for shallow groundwater at South Bison Hills. Two other profiles collected from the Fen (P30) and Coke Beach (Mildred Lake Settling Basin Cell 5) sites had minimum δD values of -186 and -174‰, respectively, further verifying the snowmelt signature.

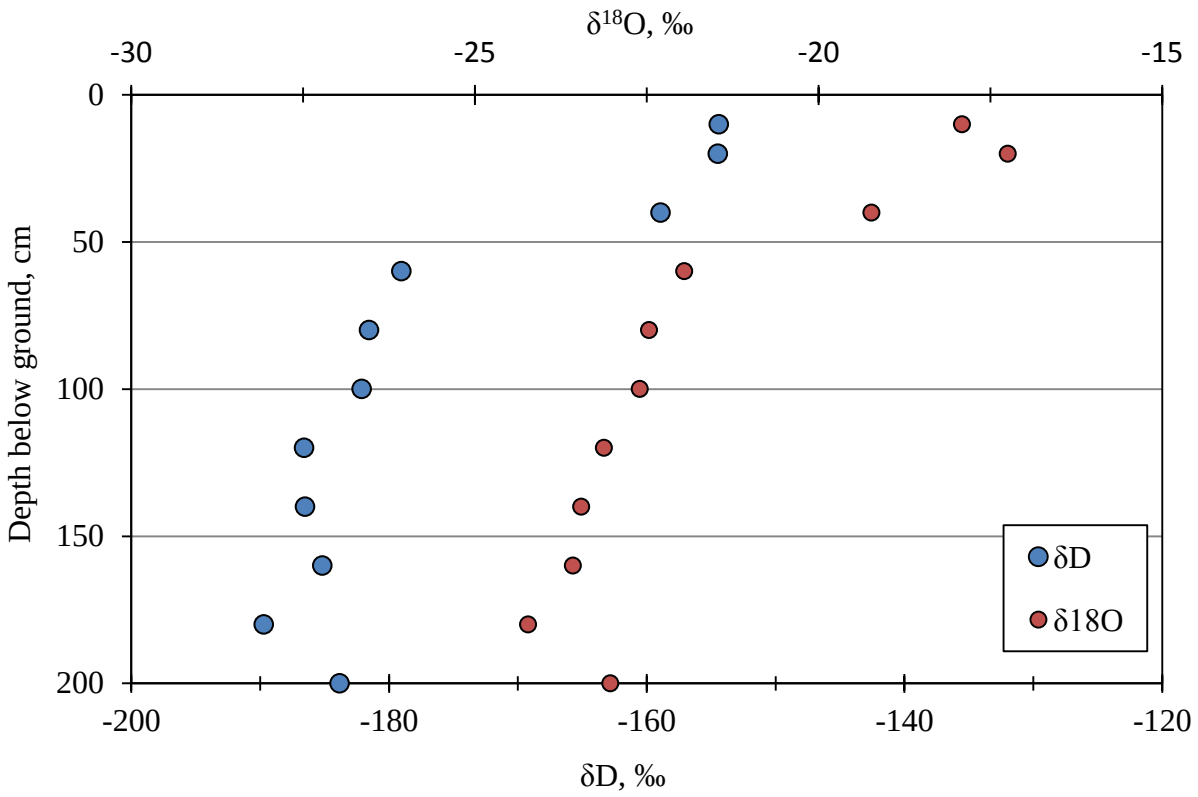

Figure 4.10: Vertical soil profile of Fen piezometer 13(P13). Soil samples collected on May 1, 2013

Much like the interflow samples, the snowmelt likely mixes with antecedent pore water as it infiltrates, causing an isotopic enrichment. However, the interflow mainly travels horizontally through the ground several meters to tens of meters before it was collected. Conversely, the snowmelt in the soil profiles likely only travelled a short distance vertically, indicating minimal mixing with antecedent pore water likely occurred.

With these points in mind, the soil profile provides a relatively good indicator to the isotope signature of snowmelt. Table 4.6 summarizes the isotope values of the profile. Average values of -184 and -23.1‰ for δD and $\delta^{18}O$, respectively were calculated for the profile. These values are slightly depleted compared to the LMWL/natural evaporation line intersect.

Based on the LMWL/natural evaporation line intersect and the samples discussed, an estimated average value of snowmelt can be established. The estimated composition of snowmelt was established at -185 and -23‰ for δD and $\delta^{18}O$, respectively. A summary showing the average value of snow, snowmelt and the total enrichment is shown in Table 4.7.

These values were defined by taking into consideration that the source water for the ponds at South Bison Hills likely has a rain component. Making a rough adjustment for this would result in a more depleted snowmelt value. This adjustment was made by taking into consideration the isotope values of the soil profile previously discussed in this section.

The $\delta^{18}O$ enrichment of snowmelt falls within the range of 3 to 5‰ established by Taylor et al. (2002) and is similar to the 4‰ enrichment utilized by Kelln (2008). The δD enrichment is comparable to enrichments of 15 to 30‰ found by Hooper and Shoemaker (1986).

Table 4.7: Average values of snow, snowmelt and total enrichment

Signature	δD, ‰	$\delta^{18}O$, ‰
Snow	-205	-26.4
Snowmelt	-185	-23
Enrichment	20	3.4

As mentioned briefly in Section 4.4.2, snowmelt recharge will likely mix with antecedent summer rainfall. The estimated snowmelt signature does not take into account mixing of snowmelt with antecedent rainwater as it infiltrates. Snowmelt, like rainfall may also contribute to surface water or shallow groundwater for a period of time before it infiltrates fully. This meltwater may go through similar evaporative fractionation processes as rainfall as it infiltrates, as described in Section 4.4.2. This would result in snowmelt enrichment before recharge occurs. These factors can alter or even eliminate the signatures of snowmelt within closure landforms.

4.4.4 Interstitial Shale Water

Hilderman (2011) assumed a δD and $\delta^{18}O$ of water signature for interstitial pore water in the shale prior to excavation and placement in an overburden dump based on a series of analyses conducted on a deep profile into the shale at South Bison Hills. In this study, interstitial shale water values were determined from soil samples collected from South Bison Hills in 2009 by Hilderman (2011). There is little variance in this data set indicating consistent, constrained isotope values with average δD and $\delta^{18}O$ values of -159 and -18.4‰, respectively. These values are more depleted than the volume weighted average of precipitation (δD= -145‰ and $\delta^{18}O$= -17.9‰). This may signify that interstitial shale water either originates from meteoric waters of a

different climate or is derived from modern precipitation with a high component of snowmelt.

It is difficult to tell if the shale values reported are representative of interstitial water found in the undisturbed shale formations. There is no known attempt to establish in-situ δD and $\delta^{18}O$ values for groundwater within the Clearwater Formation in the Fort McMurray region although recent drilling of intact shale at the Mildred Lake mine site has been recently completed with analyses of the natural stable isotopes of water for these samples pending (Barbour, oral communication).

Hendry and Wassenaar (1999) have shown that clays and tills in the Bear Paw Formation in southern Saskatchewan have δD and $\delta^{18}O$ values that are more depleted than the volume weighted average of precipitation in the region. The Bearpaw Formation is present from 80 m to about 160 m below ground and has a consistent baseline δD value of -144‰ at depths exceeding 110 m below ground. However, above the established baseline depth, δD values become more depleted as depth decreases and approaches a δD value of approximately -163‰ at 80 m below ground.

The till at the Mildred Lake mine has thicknesses of approximately 12 m (Chapman 2008), while the shale layer is approximately 20 to 40 m thick (Hilderman 2011). The varying geologies at each area may contribute to the varying δD and $\delta^{18}O$ values between the two locations. Despite this, the upper 40 m of Hendry and Wassenaar's (1999) shale profile and the Mildred Lake shale signature are comparable and relatively similar.

In a similar study conducted by Hendry et al. (2011), seven vertical δD profiles collected in southern Saskatchewan showed similar shale baseline values between -145 to -140‰. All profiles were located within 300 km from the profile in Hendry and Wassenaar (1999). The till-shale interface ranged between 11 to 78.5 m below ground and diffusive δD transport between the till and shale was evident through all the vertical profiles. Mathematical models for all profiles were created by Hendry et al. (2011) to demonstrate diffusive transport through the formations over time.

The diffusion trend between the till and shale is probable for the shale formations at the Mildred Lake mine as well. Several of the modelled vertical profiles in Hendry et al. (2011) had glacial till thicknesses between 11 to 13 m, which is comparable to the mine site. δD and $\delta^{18}O$ values of shale from these profiles ranged from -158 to -145‰ at a depth of 0 to 40 m below the till-shale interface. Integrating one of the profiles up to 40 m provides an average δD value estimate of

approximately -152‰ at shale depths between 0 to 40 m below the interface. This value is slightly more enriched compared to the interstitial shale value of -159‰ established in this study. However, the range of δD values are quite comparable between the two studies, with the Mildred Lake shale having δD values ranging from -163 to -152‰, further verifying the δD and $\delta^{18}O$ signatures of interstitial shale water at the mine site.

Lemay (2002) sampled select wells throughout Alberta in an attempt to characterize formation waters. Through this study, a series of groundwater samples were collected from the McMurray and Clearwater Formations. The Clearwater Formation samples had average δD and $\delta^{18}O$ values of -147 and -19.3‰, respectively. The McMurray Formation had similar average isotope values of -144 and -19.6‰ for δD and $\delta^{18}O$, respectively. One of the McMurray Formation samples was significantly enriched compared to the other samples (δD= -118‰; and $\delta^{18}O$= -16.7‰). Excluding this sample, the average δD and $\delta^{18}O$ values for the McMurray Formation is -152 and -20.5‰, respectively.

The values reported by Lemay (2002) are more enriched than the δD and $\delta^{18}O$ values of shale observed in this study and are more comparable to average values modelled by Hendry et al. (2011). The comparatively enriched δD and $\delta^{18}O$ values observed in Lemay's (2002) may be due to groundwater sample collection occurring south of Fort McMurray. Additionally, Hilderman (2011) points out that Lemay (2002) sampled from more permeable divisions within the formations, which could explain the differences observed.

A summary of the range of shale values observed in this study and other studies is shown in Table 4.8. Overall, the shale values in this study are slightly more depleted in comparison to the shale isotope signatures observed by Lemay (2002), Hendry and Wassenaar (1999) and Hendry et al. (2011). However, all three studies were conducted south of the study area which may play a factor in the enriched isotope values. The range of isotope values within the upper shale formations observed by Hendry and Wassenaar (1999) and Hendry et al. (2011) are comparable to values obtained in this study, verifying the isotopic signature of interstitial shale water.

Table 4.8: Summary of shale δD and $\delta^{18}O$ values observed in Alberta and Saskatchewan

Region	Range of Shale Values		Reference
	δD, ‰	$\delta^{18}O$, ‰	
Mildred Lake Mine	-163 to -152	-19.5 to -16.7	Hilderman (2011)
South Saskatchewan- shale/till interface 80 m below ground	-163 to -144	N/A	Hendry and Wassenaar (1999)
South Saskatchewan- shale/till interface approximately 12 m below ground	-158 to -145	N/A	Hendry et al. (2011)
Alberta- Between Edmonton and Fort McMurray	-157 to -149	-21 to -20.3	Lemay (2002)

4.4.5 Mildred Lake

Mildred Lake was sampled between the months of May to August 2012 and 2013. Throughout this time consistent isotope values were established with average δD and $\delta^{18}O$ values of -143 and -17.7‰, respectively. The variances for this data set were relatively small and tightly bound.

In another study conducted by Gibson et al. (2011), the Athabasca River was sampled north of Fort McMurray, AB. Sampling in this study consisted of river bed seeps collected in August and November 2009. River water was sampled at mid-channel and mid-depth in September and November 2009. Water samples were also taken at the bed interface in June 2009.

A comparison of Athabasca River δD and $\delta^{18}O$ values published by Gibson et al. (2011) and the δD and $\delta^{18}O$ values for Mildred Lake obtained from this study are shown in Figure 4.11. The Athabasca River δD and $\delta^{18}O$ values are generally located above the LMWL. This likely indicates that the river water is derived from a different region, most likely from the Jasper, AB area where the Athabasca River is sourced. Figure 4.11 also demonstrates that the δD and $\delta^{18}O$ values between the two surface waters are generally within the same range. However, Gibson et al.'s (2011) Athabasca River values show greater spread and variance.

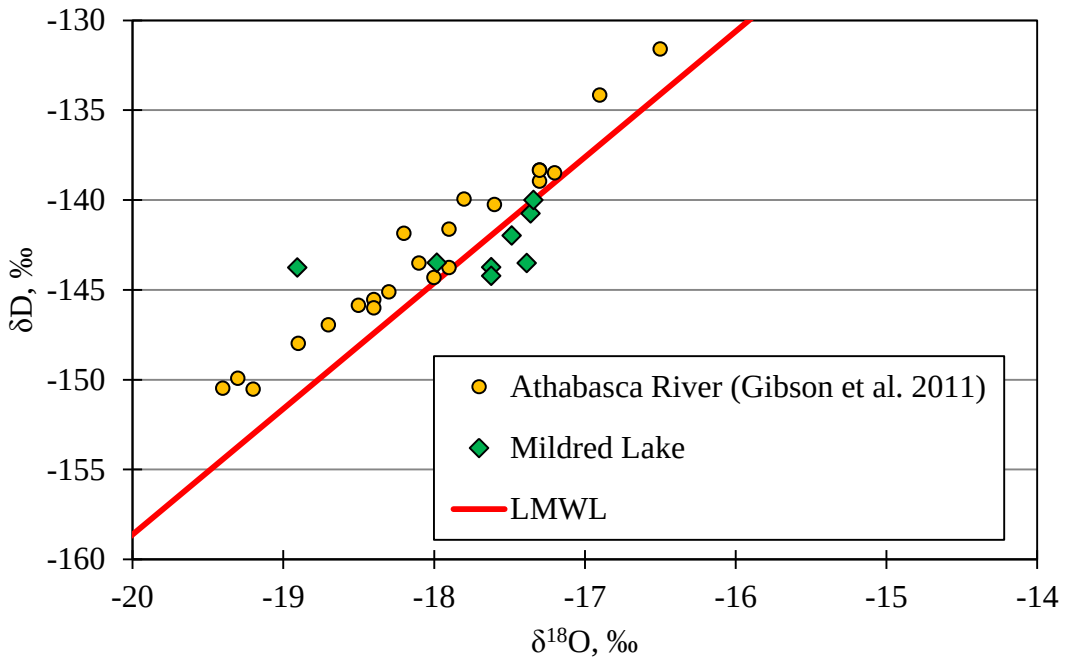

Figure 4.11: Mildred Lake and Athatbasca River water plotted with the LMWL

The wider spread may be attributed to several of Gibson et al.'s (2011) river samples being collected from beneath or just above the river bed and the extended duration of sampling (six months as compared to four months) which together may contribute to the higher variance observed in the δD and $\delta^{18}O$ values.

Additionally, the Mildred Lake reservoir may act as a "buffer" that restricts fluctuations in isotope composition. The Athabasca River, on the other hand, will have isotope compositions with more seasonal variations. This would produce a more consistent data set with less spread and fluctuations. This "buffer" concept is demonstrated further in Appendix J, which goes through basic mass balance concepts to show that the volume of water contained in Mildred Lake is capable of "buffering" alterations in δD and $\delta^{18}O$ due to seasonal variations in the Athabasca River.

The results of the calculations estimate that a snowmelt pulse of -165‰ in the Athabasca River over two months would alter the δD values of Mildred Lake from its average of -143‰ to approximately -154‰. This demonstrates that the Mildred Lake water volume is capable of partially "buffering" seasonal alterations of Athabasca River input water. This "buffer" effect results in less significant seasonal variations in δD and $\delta^{18}O$ values at Mildred Lake.

More depleted δD values in the range of -154‰ were not observed in any of the samples collected from Mildred Lake. This may be due to samples being collected mainly during the summer months when the Athabasca River input water had more enriched δD and $\delta^{18}O$ values. Additionally, the estimates did not take into account inflow/outflow components due to groundwater recharge/discharge and the effects that these components would have on the seasonal distribution of δD and $\delta^{18}O$ values.

4.4.6 PAW/Tailings

The PAW surface water and West in-pit tailings profiles make up the dataset that define the δD and $\delta^{18}O$ characterization for PAW/tailings. From this point on, PAW surface water will be referred to as PAW.

It should be noted that the PAW data set did not include samples collected from the Effluent Pond. The Effluent Pond is a reservoir that contains "sour" water and is high in nitrogen and sulfur compounds. These compounds may have an effect on the isotope composition and consequently are interpreted separately from the PAW data set. More information on the isotope signatures of Effluent Pond will be provided later on in this chapter.

The PAW and West in-pit data sets have similar signatures and make up the most enriched waters on the mine site. Additionally, the variances for the PAW and the West in-pit profiles are relatively small, indicating well constrained isotope signatures.

The West in-pit profiles have less variance than the PAW data set. This is expected for several reasons. The PAW samples were collected at the surface in the active water recycle circuit while the West in-pit tailings profiles originate from tailings dredged from deeper in Mildred Lake Settling Basin and discharged to West in-pit (Zubot 2010); the PAW samples are also open to the atmosphere and undergo evaporation in the summer and fall and mixing with snowmelt in the spring, and; the PAW samples were collected from tailings areas across site while the tailings profiles were collected at West in-pit only.

4.4.6.1 Seasonality and evaporative trend of PAW signatures

Table 4.9 displays the average monthly values of PAW samples, which illustrates the seasonality of PAW signatures. The most depleted signatures occur in the month of May, which is shortly after snowmelt generally occurs. During this time, snowmelt will flow into the tailings areas,

resulting in a shift in the surface water δD and $\delta^{18}O$ values to a more depleted signature. Throughout summer, the surface PAW evaporates, and fractionation contributions from the process water results in an enrichment throughout the summer months.

Table 4.9: Average monthly δD and $\delta^{18}O$ values of PAW

	Average	
Month	**δD, ‰**	**$\delta^{18}O$, ‰**
January	-112.6	-12.8
February	-111.6	-13.0
March	-115.1	-13.4
April	-118.7	-14.0
May	-125.8	-15.0
June	-119.8	-13.5
July	-115.2	-13.2
August	-104.9	-11.0
September	-108.1	-12.1
October	-107.0	-11.6
November	-108.8	-12.0
December	-112.2	-12.5

When the average values in Table 4.9 are plotted with the LMWL (Figure 4.12), an evaporative trend is evident. Plotting a (y-on-x) regression line through this data produces an evaporation line with a slope of 5.3, which is identical to the natural evaporation line developed in Section 4.2. This indicates that natural evaporation is likely one of the primary driving forces that defines the δD and $\delta^{18}O$ values of PAW.

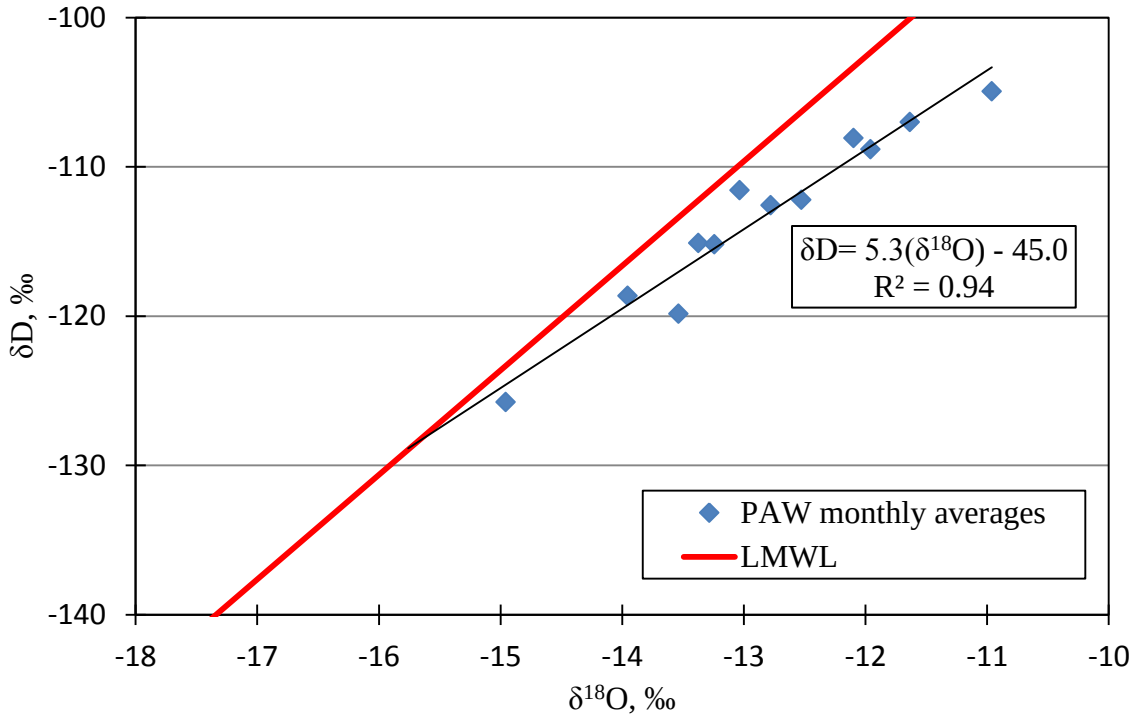

Figure 4.12: Average monthly PAW values plotted with LMWL

It is important to note that the evaporation lines for the ponds and PAW intersect the LMWL at different points. The PAW evaporation line intersects the LMWL (δD= -127‰; $\delta^{18}O$= -15.5‰) at a much more enriched value than the natural evaporation line established for the ponds at South Bison Hills. This suggests that the pre-event (pre-evaporation) water that makes up PAW is more enriched than the pre-event water for the ponds at South Bison Hills.

The LMWL/natural evaporation line intersect is much more enriched than typical δD and $\delta^{18}O$ values of Mildred Lake (average) precipitation. This signifies that PAW may go through evaporation cycles through the process water circuit may cause source water to fractionate parallel to the LMWL.

The process water circuit is described in Section 2.5. Evaporation fractionation is evident through particular components of the circuit, most notably during extraction and upgrading. Throughout these processes evaporative steam losses occur, signalling fractionation. Throughout extraction, temperatures range from 35°C in the Aurora hydrotransport stage to 75°C in the Mildred Lake extraction plant. For upgrading, raw Mildred Lake water is used as cooling water (Zubot 2010). Both these processes are high temperature systems which promote significant

steam losses and are likely a contributor to the fractionation of PAW and the resulting δD and $\delta^{18}O$ signatures of PAW and tailings.

A sensitivity analysis was conducted on the evaporation line model derived in Section 3.4.3 to illustrate how fractionation may occur in the recycle water circuit and contribute to the unique δD and $\delta^{18}O$ signatures of PAW/tailings.

The constant input parameters for the sensitivity analysis are shown in Table 4.10, with all symbols being previously described in Section 4.2. The isotopic composition of the source water was taken as the average isotopic composition of Mildred Lake water. Atmospheric δD and $\delta^{18}O$ values were derived in the same manner as in Section 4.2. The relative humidity is assumed to be high within the process water circuit due to the large volumes of steam produced by the systems and was given a value of 99%.

With these parameters, the slope of the evaporation line was then estimated over a range of typical temperatures observed in the recycle circuit. The results are shown in Figure 4.13.

Table 4.10: Constant input parameters for the evaporation line analysis of the recycle water circuit

Input	Value
Relative Humidity [%]	99
δD_l [‰]	-145
$\delta^{18}O_l$ [‰]	-17.7
δD_a [‰]	-214
$\delta^{18}O_a$ [‰]	-29.4

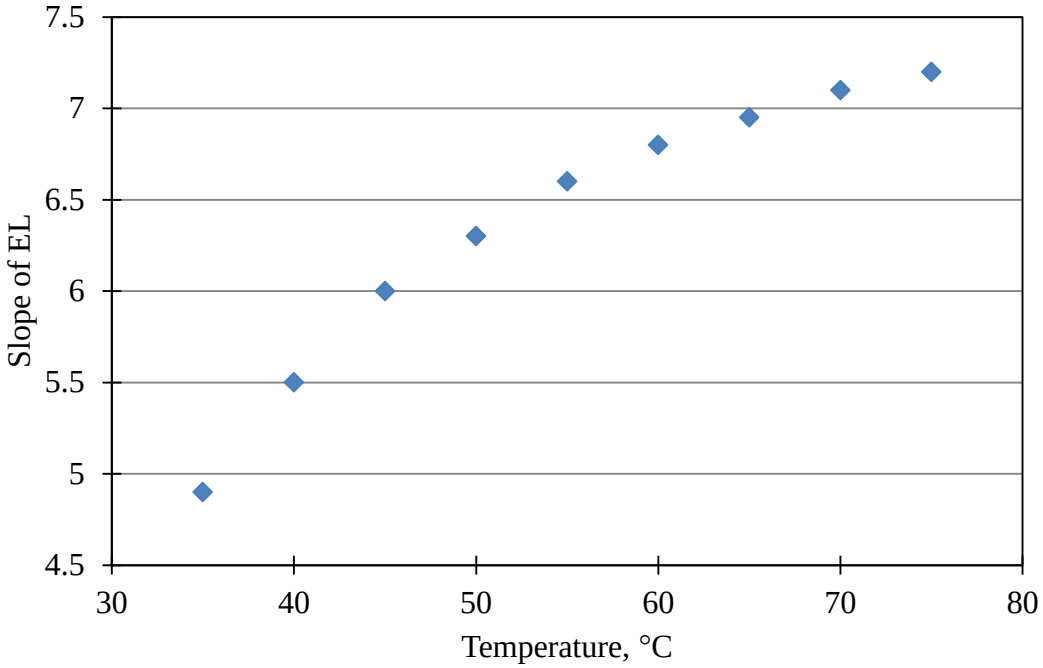

Figure 4.13: Slope of evaporation line at h=100% over a range of temperatures observed in the process water circuit

The results of the estimates show that the slope of the evaporation line increases as temperature increases. The modelled evaporation line slopes vary from 4.9 to 7.2 over the typical temperatures of the water circuit. At high temperatures, the slope of the evaporation line approaches a value similar to that of the LMWL. Evaporation occurring in this manner would result in fractionation that would shift the water signatures up along the LMWL. This verifies the hypothesis that the process water circuit causes fractionation of PAW such that δD and $\delta^{18}O$ values move up along the LMWL.

Figure 4.14 shows the surface PAW samples plotted with two evaporation lines that originate from the average isotope value of Mildred Lake. The first evaporation line has a slope of 5.3 and represents the natural evaporation line. The second evaporation line has a slope of 7.0 and represents fractionation due to the process water circuit. A majority of the PAW samples plot within the two lines, illustrating fractionation events from both natural evaporation and the process water circuit contribute and control the signature of surface PAW. This is further demonstrated conceptually in Figure 4.15.

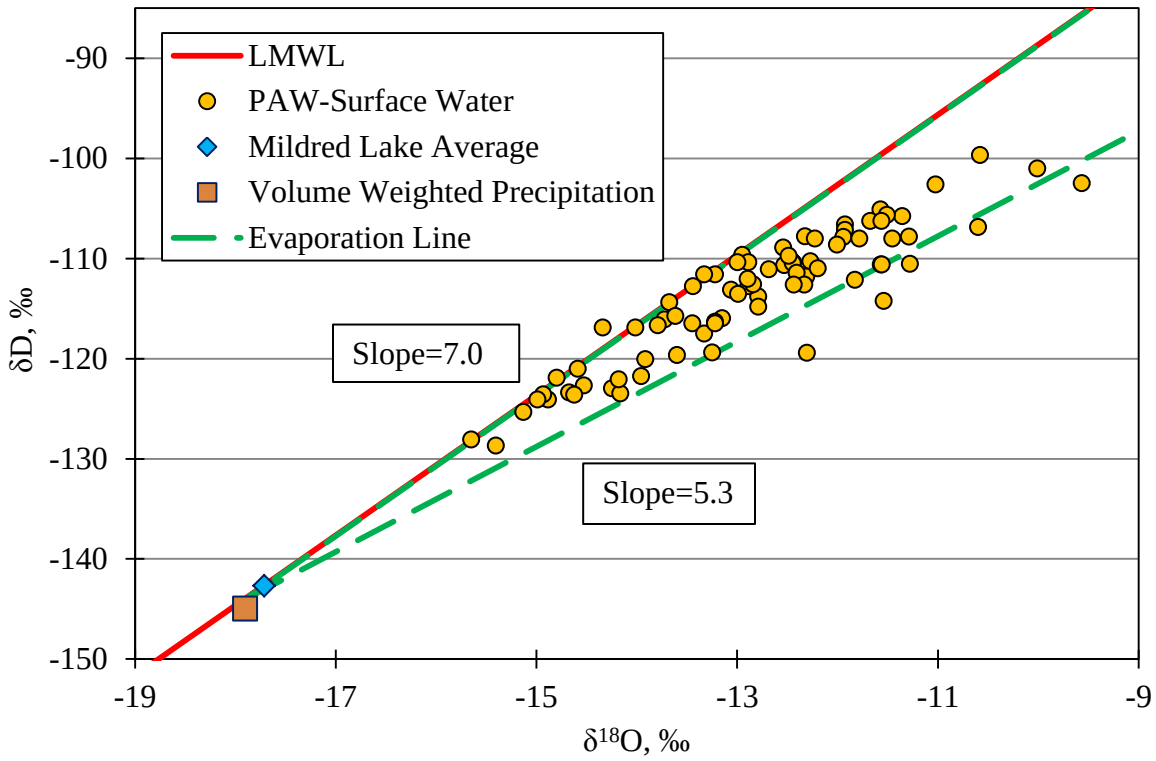

Figure 4.14: Surface PAW samples plotted with evaporation lines with slopes of 5.3 and 7.0, representing natural evaporation and process water circuit fractionation, respectively

When water from Mildred Lake is drawn into the process water circuit, it will fractionate along the fractionation line designated for the recycle water circuit (designated by a (1) in Figure 4.15). Once that water is discharged it will go through natural evaporation processes and fractionate at a slope equal to the natural evaporation line (designated by (2)). Natural water inputs (i.e. precipitation, snowmelt, Mildred Lake make-up water) will likely cause a slight depletion throughout the year (designated by (3)). These three processes would then cycle through continuously and generally balance out, resulting in the unique stable water isotope signature typically observed in PAW. Figure 4.15 is meant to be a conceptual model to break down the processes that control the δD and $\delta^{18}O$ values of water. The extent of fractionation caused by the processes may not be accurately portrayed and in reality these processes may occur simultaneously, rather than separately as shown in Figure 4.15.

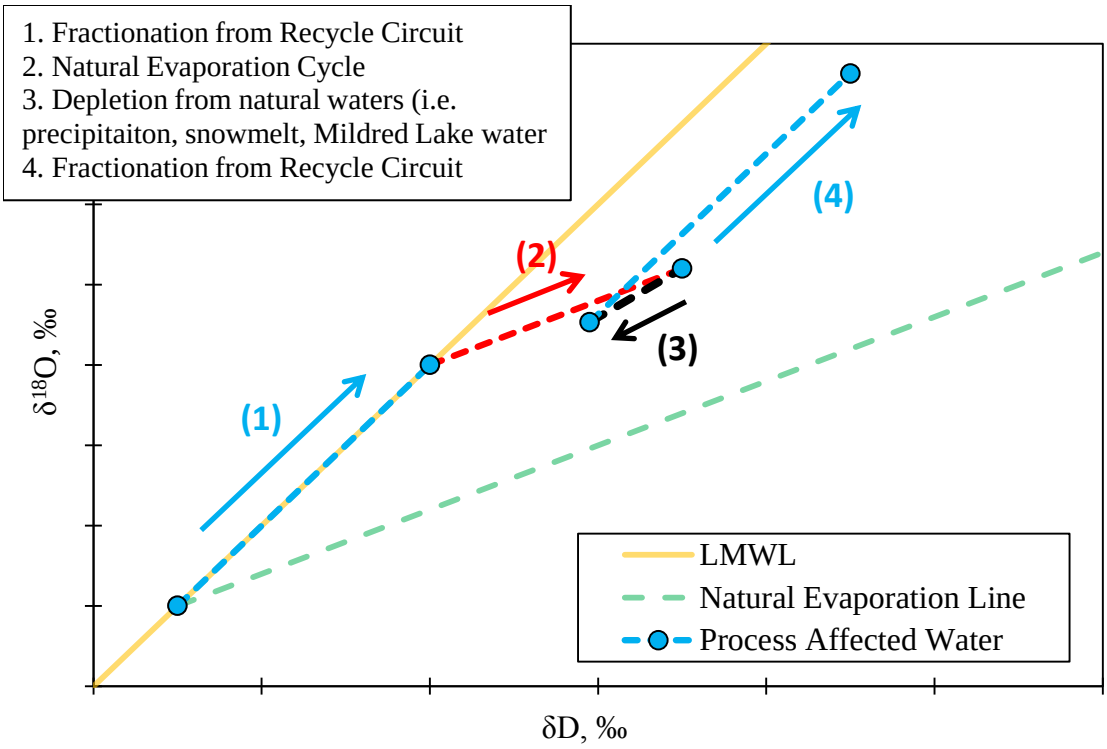

Figure 4.15: Conceptual illustration of fractionation of PAW

4.4.6.2 Evaporative enrichment and signature of tailings profiles

Vertical profiles were also obtained through fluid fine tailings at the Aurora Settling Basin. This project focuses on studying the Mildred Lake mine and as a result, the Aurora Settling Basins are not individually discussed or analyzed extensively to develop characterizations. However, more insight may be obtained by analyzing the Aurora Settling Basin along with the West in-pit profiles and drawing comparisons between the two tailings areas.

Figure 4.16 shows the West in-pit and Aurora Settling Basin datasets plotted with the LMWL, PAW surface samples and average values of precipitation and Mildred Lake water. A regression line through all samples is shown to represent the overall evaporation line among the data sets.

Similar to the PAW samples, the vertical tailings profiles lie below the LMWL, indicating evaporatively enriched waters. The bulk evaporation line coincidentally has a slope of 5.3, which is identical to the modelled and empirical slope of the natural evaporation line.

The bulk evaporation line (Figure 4.16) presented provides a general overview of the fractionation processes experienced by all tailings basins and PAW across the mine site.

However, this bulk evaporation line may not reflect or represent the tailings basins individually. Individual basins likely fractionate differently due to different atmospheric conditions, recycle water processes and basin geometries which would ultimately affect the isotope composition of input waters and the natural evaporation processes controlling fractionation.

West in-pit and Aurora Settling Basin have unique and distinct isotope signatures, signifying that the two tailings basins may be derived of varying degrees of recycle water and fresh water (Mildred Lake water and precipitation) and/or undergo different fractionation processes due to natural evaporation.

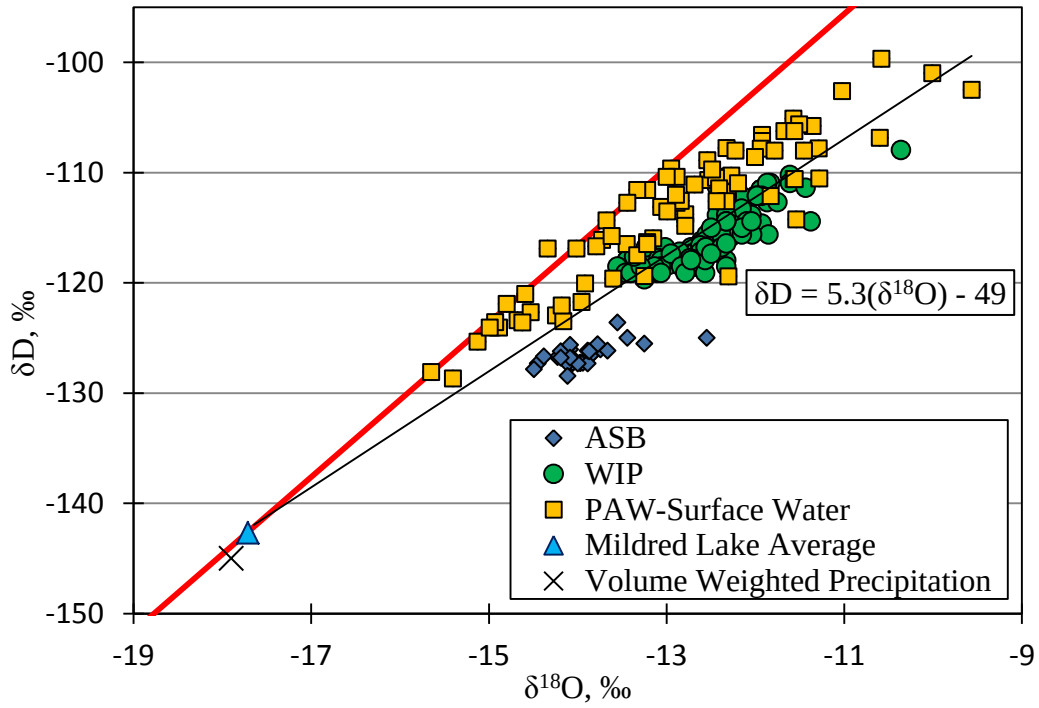

Figure 4.16: Comparison of West in-pit and Aurora Settling Basin profiles

This study will not go into detail developing individual evaporation lines for individual tailings basins, but it is noteworthy to recognize that the fractionating processes among tailings basins may be unique due to distinct conditions and characteristics at each basin. Evaporation line slopes may vary for different tailings basins due to different atmospheric conditions at each tailings basin. Parameters such as elevation, pond area and pond size may affect the relative humidity, temperature and the isotopic composition of atmospheric vapour which would ultimately alter the slope of the evaporation line between basins. As well, separate basins may be

composed of varying components of fresh water (precipitation and Mildred Lake) and recycle water, producing contrasting LMWL/evaporation line intersects. These factors would contribute to different evaporation lines and produce unique isotope signatures among the different tailings areas. This is demonstrated by the unique West in-pit and Aurora Settling Basin tailings signatures shown in Figure 4.16.

The evaporative isotopic enrichment of tailings and mine waste has been observed previously. Pellicori et al. (2005) conducted isotope analyses on tailings sampled collected at an abandoned metal mine in Butte, Montana. In that study, both tailings surface and profile samples were collected. Parallel to this study, Pellicori et al. (2005) found that both tailings surface and profile samples showed signs of enrichment through evaporation and that the isotope composition of tailings was essentially vertically homogenous. Pellicori et al. (2005) also determined that shallower tailings ponds were more enriched compared to deeper ponds.

In another study, Jasechko et al. (2012) observed evaporative enrichment of coarse tailings and tailings ponds in the Athabasca oil sands region. In this study, several PAW samples were collected from different mine sites, including the Mildred Lake mine and mines operated by Suncor, Canadian Natural Resources Ltd (CNRL) and Shell. The Mildred Lake mine and Suncor mine δD and $\delta^{18}O$ values obtained by Jasechko et al. (2012) are comparable to the ones in this study. However, the values of PAW at other mine sites are more depleted and have comparable isotope values to the Aurora Settling Basin profiles in this study.

Gibson et al. (2011) attributes the enrichment of tailings ponds to natural evaporation as well as evaporation through the process and recycle water circuit. The differences in enrichments were attributed to different residence times of PAW and differences in the mine water circuits between sites.

4.4.6.3 Comparison of Aurora Settling Basin and West in-Pit profiles

Figure 4.16 also illustrates that the tailings in West in-Pit are more enriched than Aurora Settling Basin tailings. This is puzzling because West in-pit and Aurora Settling Basin are both part of the same water circuit, indicating tailings and PAW should generally have similar δD and $\delta^{18}O$ signatures. However, there are many factors that could contribute to the different signatures of Aurora Settling Basin and West in-Pit tailings. The two main distinctions between the two tailings areas are elevation and age. Aurora Settling Basin is an above ground tailings area with

an elevation of 342 m while West in-pit is an in-pit tailings area with an elevation of 305 m. West in-pit and Aurora Settling Basin became operational in 1995 and 2000 respectively (Zubot 2010).

The age of the tailings areas likely has a major impact. An older pond indicates that the PAW and tailings have had more time to evaporate resulting in more enhanced fractionation and more enriched δD and $\delta^{18}O$ values. The elevation difference may result in differing atmospheric conditions such as temperature and humidity which would affect evaporation and the evaporation line, as discussed previously in Section 4.4.6.2.

4.4.6.4 Estimating δD and $\delta^{18}O$ values of tailings at depth in other tailings areas

Estimating the δD and $\delta^{18}O$ values of other deep tailings on site is difficult without being able to define the processes that control the signature of the deep tailings. However, a few points can be highlighted to support the suggestion that the tailings signatures are consistent throughout the Mildred Lake mine site. All surface PAW that is available for the mine circuit is re-circulated throughout all the tailings areas through the Recycle Pond. This indicates a similar signature should be present throughout the tailings.

T-test comparisons were conducted on the δD and $\delta^{18}O$ values between individual tailings areas (i.e. West in-pit vs. East in-pit). The t-tests produced P-values>0.1, indicating δD and $\delta^{18}O$ values amongst tailings areas are relatable (P-values>0.1) at a 95% confidence interval. Despite these similarities, each tailings area differs in elevation, depth, and size which could cause alterations in the δD and $\delta^{18}O$ values of tailings.

It is evident when the surface West in-pit surface samples and tailings profiles are compared that the surface samples are slightly more enriched than the tailings profiles. T-tests conducted between the two data sets highlight comparable $\delta^{18}O$ signatures but dissimilar δD signatures. No surface Aurora Settling Basin samples were collected to provide a comparison with the Aurora Settling Basin profiles. By assuming all tailings ponds have a similar trend as the West in-pit surface and tailings profiles, signatures of tailings at depth in other containments can be estimated by applying a correction to the surface signature of a tailings pond.

4.4.6.5 Summary of PAW/tailings signatures

In conclusion, tailings/PAW signatures are tightly confined and a consistent signature can be established. These waters have the most enriched signature in comparison to all other source water characterizations on the mine site. The δD and $\delta^{18}O$ signatures of surface PAW varies seasonally, with enriched values in the summer from evaporation and depleted values in the spring from snowmelt. Tailings profiles from West in-pit and Aurora Settling Basin demonstrate that the tailings in each individual pit have a constrained signature. However, different signatures are evident upon comparisons between the West in-pit and Aurora Settling Basin tailings profiles. The reasons for these differences occur are hypothesized to be due to differences in age, elevation and residence times between the ponds.

The PAW/tailings signatures consistently fall below the LMWL, indicating evaporative enrichment. The enrichment is mainly attributed to natural evaporation of tailings ponds and steam and evaporative losses generated through the extraction and upgrader water circuit. PAW from all tailings ponds are recirculated through the Recycle Pond, resulting in a well-mixed water circuit. This is demonstrated by the statistically similar signatures of surface PAW from individual tailings ponds.

The isotope signature of surface PAW is on average -114‰ and -12.9‰ for δD and $\delta^{18}O$, respectively. The seasonality of surface PAW should be considered when applying these characterizations to other applications. The signatures of tailings are vertically consistent as demonstrated through the signatures of Aurora Settling Basin and West in-pit tailings. However, the signatures of the West in-pit and Aurora Settling Basin profiles are noticeably different, demonstrating individual tailings basins may have unique signatures of δD and $\delta^{18}O$.

4.4.7 Source water characterization summary

A summary of the isotopic signatures of source waters on site is shown in Table 4.11. However, there are some important implications which could alter the signature for certain applications.

Table 4.11: Summary of δD and $\delta^{18}O$ characterizations

Sample	δD, ‰	$\delta^{18}O$, ‰
Rainfall	-126	-15.3
Snow	-205	-26.4
Snowmelt (Estimated)	-185	-23.0
Mildred Lake/Athabasca River	-143	-17.7
Deep Shale (>3m) (Hilderman 2011)	-159	-18.4
West in Pit (WIP)- Tailings	-116	-12.5
Surface PAW	-114	-12.9

These implications include:

- Seasonal variations of rainfall. Rainfall in the summer months is usually heavier than rainfall in the spring and fall. Additionally, rainfall has a highly variable signature.
- Snowmelt occurs over a period of weeks and the resulting snow and snowmelt will become progressively enriched. This results in a highly variable snow and snowmelt signature during this duration.
- Meteoric water may undergo evaporative fractionation processes while it is present on the surface or the shallow groundwater.
- Mildred Lake water will have seasonal variations, most notably a depleted pulse as snowmelt from the mountains passes through the Fort McMurray region;
- Surface PAW is generally enriched in summer months due to evaporation and depleted in spring from snowmelt runoff.
- Comparing the West in-pit and Aurora Settling Basin tailings signatures demonstrates the potential for a high variability of δD and $\delta^{18}O$ signatures between tailings basins. Caution should be used when applying the tailings signatures to other tailings areas.

Despite these implications, the δD and $\delta^{18}O$ variations between source waters suggest that these signatures can be used for hydrological applications on closure landforms.

4.5 Other Characterizations and Additional Data

This section will present other relevant data that was collected through the field portion of this study. Samples include groundwater, interflow, soil and underdrain samples from Southwest Sands Storage (SWSS) Cells 32 and 46, the Fen and South Bison Hills. The additional data is

presented by plotting samples with the LMWL. Additional analyses on select data will be presented in Chapter 5.

4.5.1 South Bison Hills- interflow and soil samples

Interflow samples were collected in the spring and summer months in 2003 to 2007 by Kelln (2008), in 2009 by Hilderman (2011) and in 2012 and 2013 as part of this project. The resulting combined sample set is plotted against the LMWL in Figure 4.17 along with the snow samples for comparison. The interflow essentially represents water that moves horizontally through shallow soil. The interflow collectors do not generally collect interflow in the summer and winter months, signifying that snowmelt triggers water movement in shallow soils at South Bison Hills.

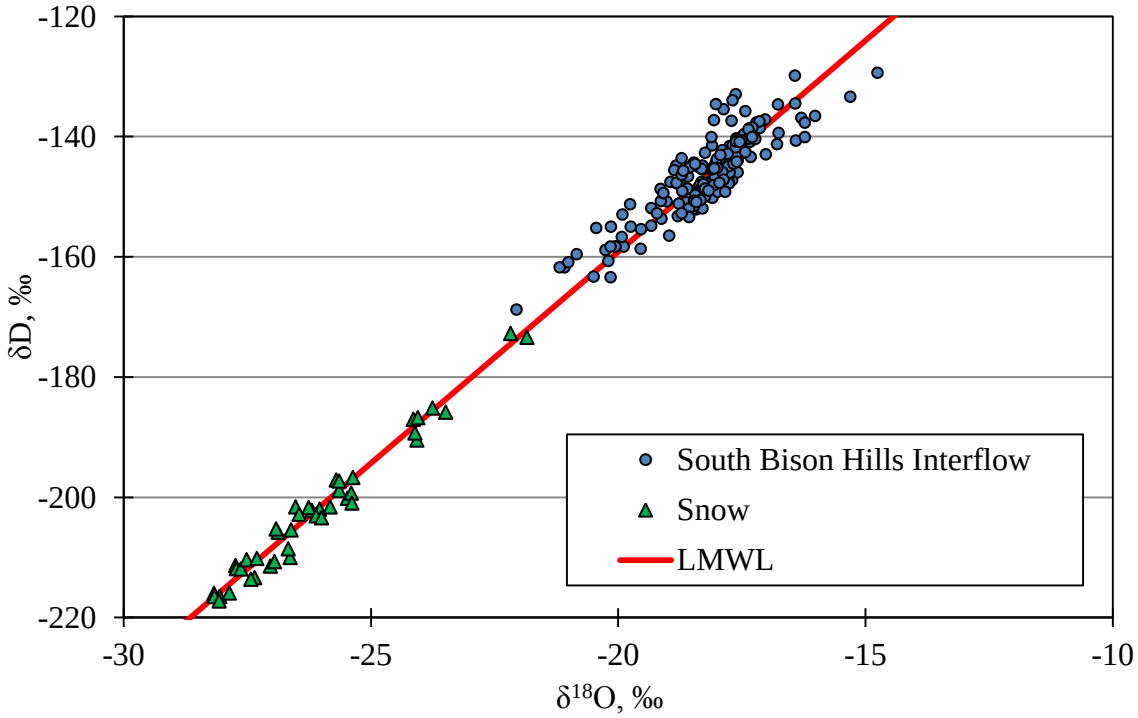

Figure 4.17: Interflow dataset plotted with snow data set

The typical interflow values are more enriched than snow and the snowmelt δD and $\delta^{18}O$ signatures established in Section 4.4.3. This indicates that snowmelt mixes with pore water as it travels through shallow soil. Kelln (2008) calculated components of snowmelt and pore water in interflow were using a two component mixing model.

The three interflow collection systems on South Bison Hills are located on three different study areas called D1, D2 and D3. Each area has differing depths of soil covers which are summarized in Table 3.1. The δD and $\delta^{18}O$ values observed in each interflow system from 2003 to 2013 is shown in Figure 4.18.

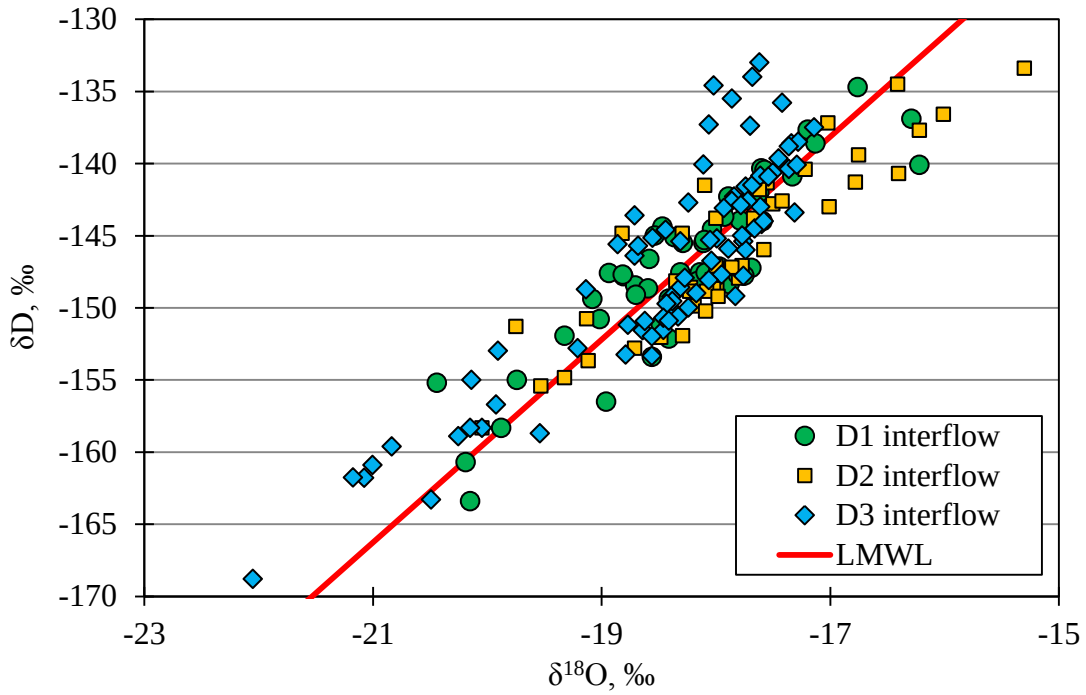

Figure 4.18: Interflow isotope values through D1, D2 and D3 soil covers

Additionally the evolution of δD and $\delta^{18}O$ values observed in each interflow system throughout the spring and summer is shown in Figure 4.19 and 4.20. Generally, the δD and $\delta^{18}O$ values observed in the interflow collected started off with more depleted values and gradually became more enriched throughout the spring. The only major exceptions are the spikes in the D2 and D3 covers on June 3, 2013. The gradual enrichment of interflow isotope signatures has been observed through these covers by Kelln (2008) for the 2005 season. Kelln (2008) attributed this to preferential flow paths within frozen soils, which allow for snowmelt to infiltrate into the frozen soils. The melt water, having a more depleted signature, flows through shallow soil and is first collected by the interflow system. As the ground thaws, the snowmelt and antecedent pore water mix, causing enrichments in δD and $\delta^{18}O$ in the interflow throughout the spring.

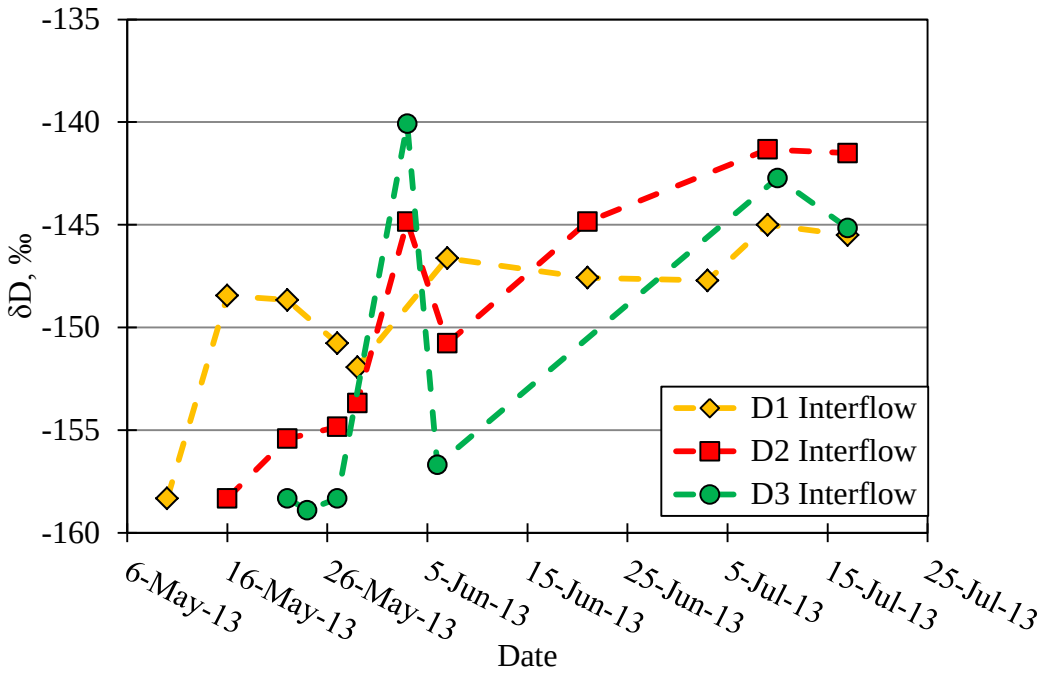

Figure 4.19: Evolution of δD in each interflow collection system throughout 2013

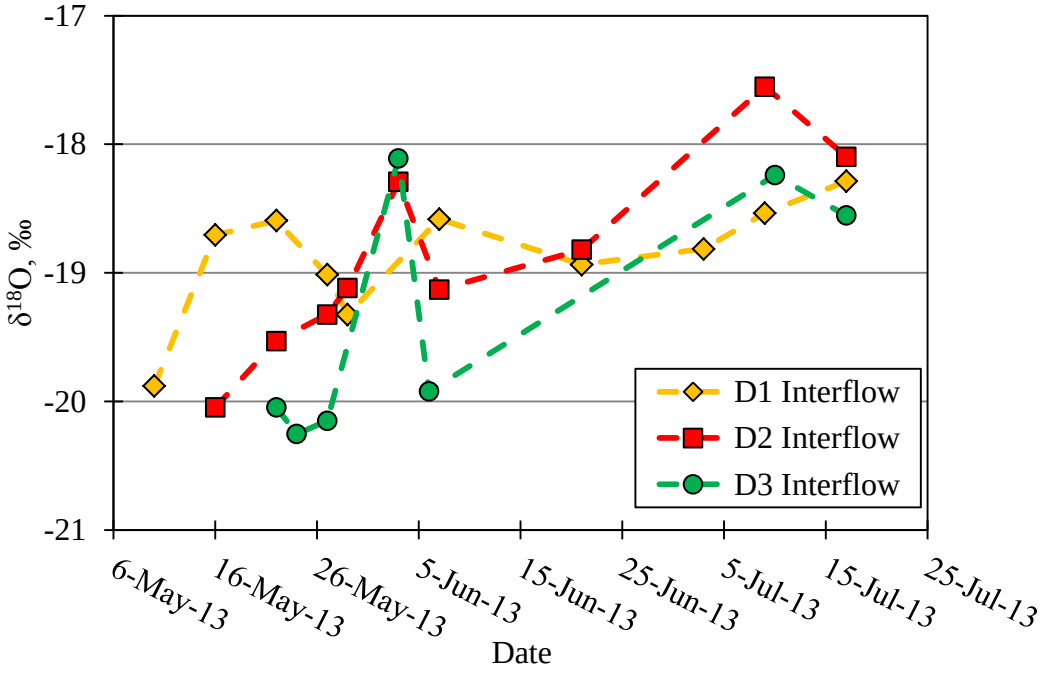

Figure 4.20: Evolution of $\delta^{18}O$ in each interflow collection system throughout 2013

Vertical soil profiles were also collected in December 2008 by Hilderman (2011) and September 2012 as part of a Syncrude capping study. A majority of soil samples collected in 2008 and 2012 were shallow samples, with maximum depths reaching 3 m and 1.8 m below ground,

respectively. One profile collected in December 2008 reached a depth of 9.1 m below ground and was used to establish the interstitial shale water characterization in Section 4.4.4. The soil samples plotted with the interflow dataset is shown in Figure 4.21.

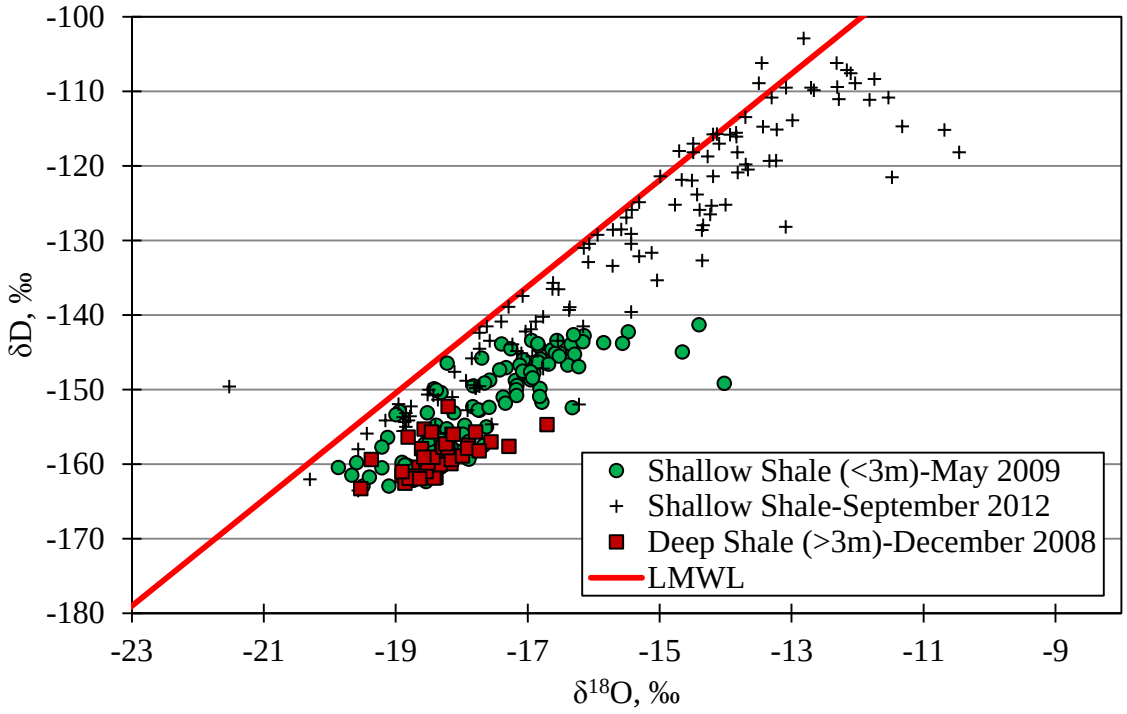

Figure 4.21: Soil samples and interflow collected at South Bison Hills

A majority of the 2012 samples were collected from the D1, D2 and D3 covers; of the 125 samples collected, 83 of them were collected from within the covers. The remainder were collected along a transect running south of D1. The samples from 2008 were mainly sampled within the D3 soil cover with the exception of a transect that ran south of D3 and the deep profile which was located just north of D3. Overall, a majority of the samples collected from the 2008/09 and 2012 years were collected in similar locations, but at different times of the year. Sampling depths in 2012 ranged from 0 to 180 cm below ground, while the shallow samples collected in 2008 had depths of 0 to 300 cm below ground.

The shallow soil samples follow a trend which falls below the LMWL. This signifies evaporative enrichment and is likely due to natural evaporation from the soil surface. The samples collected in September 2012 have a much wider spread and are generally more enriched compared to the 2008 samples. This illustrates that there may be a seasonal δD and $\delta^{18}O$ shift in shallow soils

which is driven by evaporation or the varying δD and $\delta^{18}O$ values of precipitation that occurs throughout the year. The samples in 2012 were collected in September, possibly indicating the shallow pore water had an opportunity to evaporate throughout the summer months or enriched summer rain infiltrated into the soil during this time.

4.5.2 Effluent Pond

The Effluent Pond was not included in the PAW data set because the signatures were noticeably unique compared to the surface PAW and tailings datasets. Figure 4.22 displays this data along with the LMWL to compare the Effluent Pond samples are located above the PAW/tailings and above the LMWL.

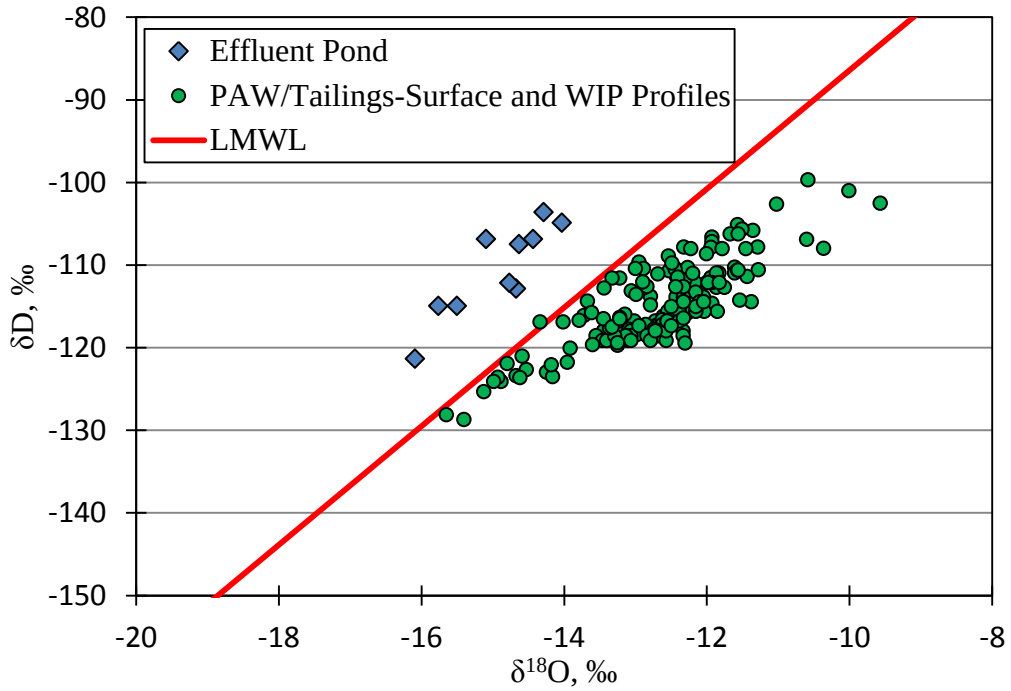

Figure 4.22: Effluent Pond comparison with PAW and tailings

As mentioned briefly in Section 4.4.6, the Effluent Pond is a reservoir for "sour" water which is extremely high in sulfur and nitrogen compounds. The concentration of these compounds may be high enough to cause noticeable fractionation of the Effluent Pond water.

Water exchange with hydrocarbons, methane (CH_4) and hydrogen sulfide (H_2S) results in a δD enrichment (Horita 2005). δD enrichment of leachate waters in landfills similar to those found in the Effluent Pond have been observed by Bennett (1998) and Hackley et al. (1996). Both studies

attributed the enrichment to methanogenesis consuming lighter water molecules causing a δD enrichment of the water reservoir. Similar reactions involving carbon, nitrogen and sulfur compounds may cause a δD enrichment in the Effluent Pond.

Although tailings contain hydrocarbons and produce methane, the amount of water in these reservoirs likely greatly exceeds the amount of hydrocarbons and therefore noticeable fractionation effects are limited. However, in the Effluent Pond, fractionating compounds are likely present in high enough concentrations to induce substantial chemical reactions that cause a noticeable alteration in δD and $\delta^{18}O$ compositions.

4.5.3 Sandhill Fen

Soil samples at the Fen were collected during the summer of 2012 and on May 1, 2013. The isotopic compositions of the soil samples are shown Figure 4.23.

The range of isotope values for soil samples collected on May 1, 2013 is greater than the sample set of 2012. The soil samples collected on May 1, 2013 were shallow soil profiles of 2 m. Because sampling occurred right after snowmelt, soil water likely consisted of enriched pre-event soil water and depleted snowmelt, possibly explaining the wide range of values.

The soil samples collected in 2012 ranged in depths from the ground surface to 11 m below ground. Some of the deep soil samples were collected in the tailings zone beneath the reclamation site, producing enriched values. Because sample collection occurred during the summer months, shallower samples were likely evaporatically enriched. These factors likely contributed to enriched and more confined isotope values.

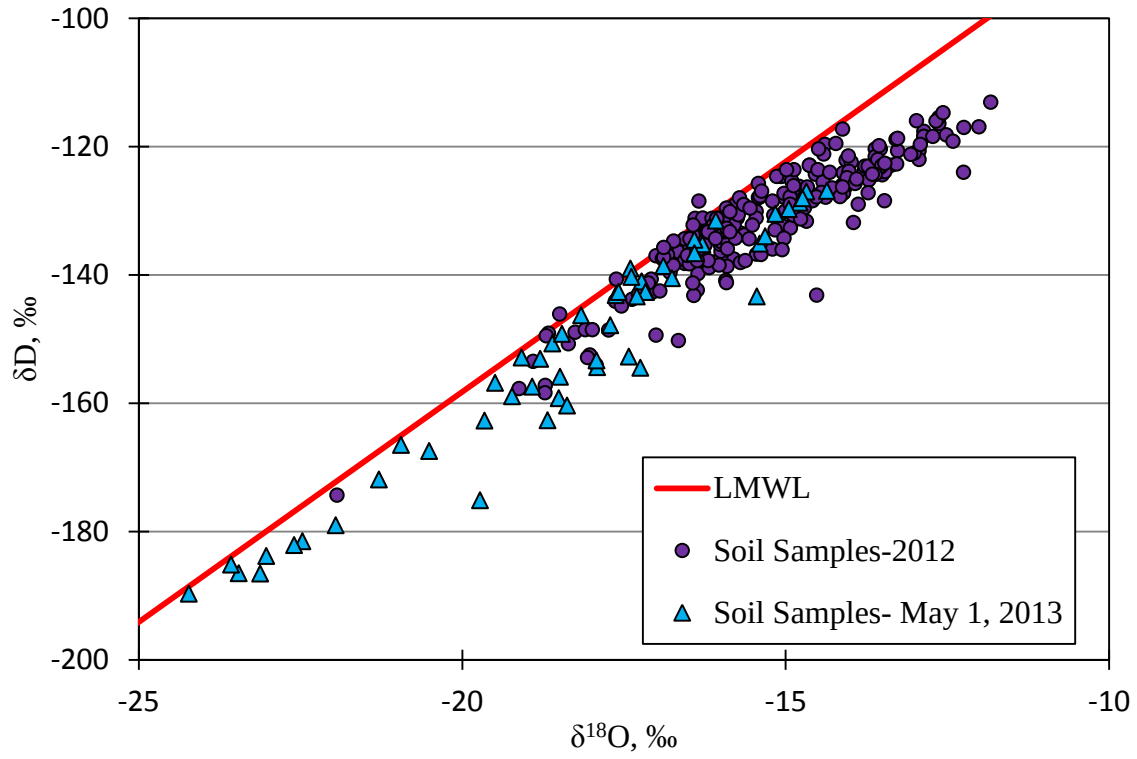

Figure 4.23: Fen soil samples plotted with the LMWL

Additional samples collected at the Fen include groundwater samples from wells installed by BGC, piezometers installed by the University of Alberta and sump samples which act as a discharge point for the underdrain system. These samples are plotted along with the Fen soil samples in Figure 4.24.

All of the BGC wells sampled are well into the tailings zone underneath the reclamation site. This results in enriched δD and $\delta^{18}O$ values that are more similar to the PAW/tailings signatures. Statistically comparing the BGC well data set to the surface PAW data set through a t-test produces P-values greater than 0.05, demonstrating that the data sets are comparable at a 95% confidence interval.

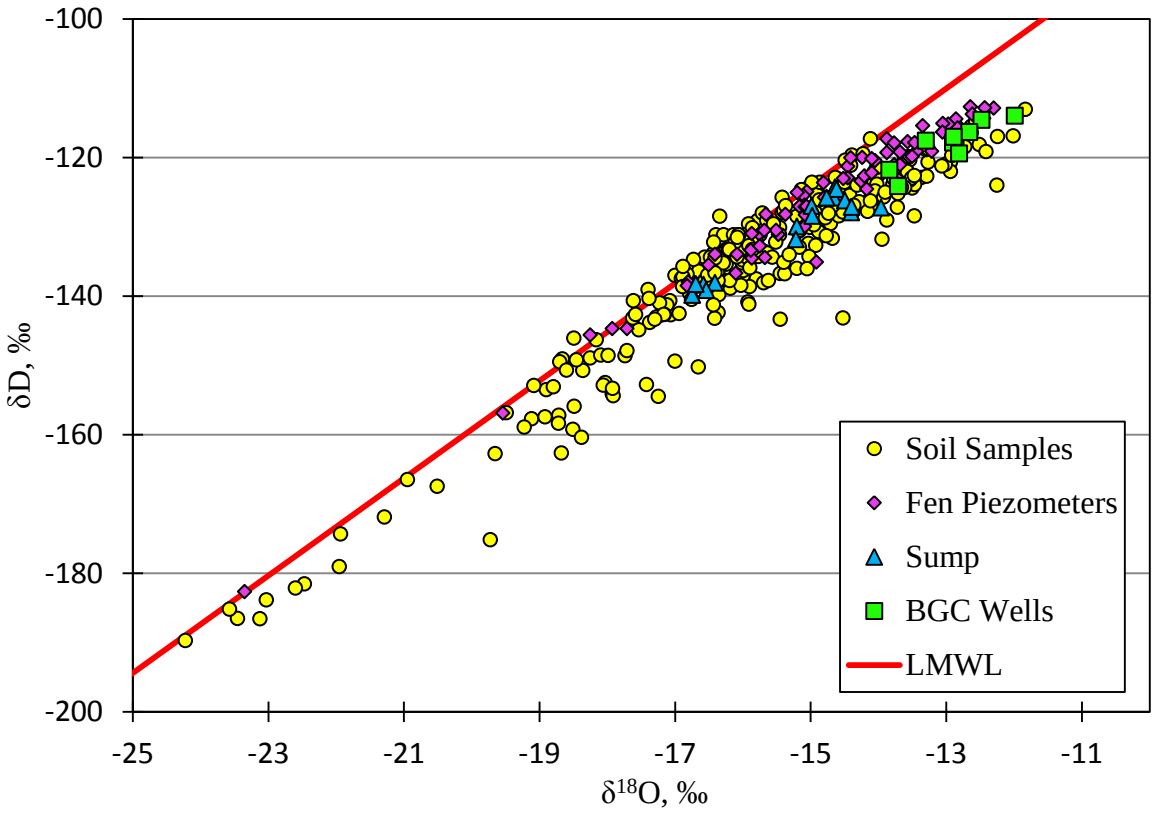

Figure 4.24: Fen sump, groundwater and soil samples plotted in δD vs. $\delta^{18}O$ space

A majority of the shallow piezometers were dry, especially on hummocks. The isotope values of water samples collected from piezometers had a wide range of δD and $\delta^{18}O$ values. A majority of the deeper installations had δD and $\delta^{18}O$ compositions that were similar to the BGC wells, indicating these piezometers are in the tailings zone. More depleted values in shallower zones signify waters that are mixtures of meteoric, Mildred Lake and/or PAW/tailings.

The sump acts as a discharge and collection point for the underdrain systems at the Fen. δD and $\delta^{18}O$ values were consistently lighter than the BGC wells, signifying waters other than PAW/tailings being collected by the drainage system.

4.5.4 Southwest Sands Storage (SWSS)

Groundwater from SWSS Cells 32 and 46 were sampled from piezometers and underdrains. A majority of shallow piezometers, especially at higher elevations were dry. Deeper piezometers were sampled and underdrains were sampled at the discharge points. Figure 4.25 displays δD and $\delta^{18}O$ values of each sample along with the LMWL. The majority of samples fall below the

LMWL and have δD values of approximately -118 to -130‰, with a few samples showing more depleted isotope values. The heavier samples likely contain a high percentage of PAW, resulting in a heavier signature. A majority of the depleted samples were collected from deep wells that intruded below the tailings structure and into glacial till. These samples are displayed as a separate data set in Figure 4.25. The depleted values signify high compositions of interstital groundwater within the natural landscape. A select few of the depleted samples were collected closer to the surface, indicating high compositions of meteoric water.

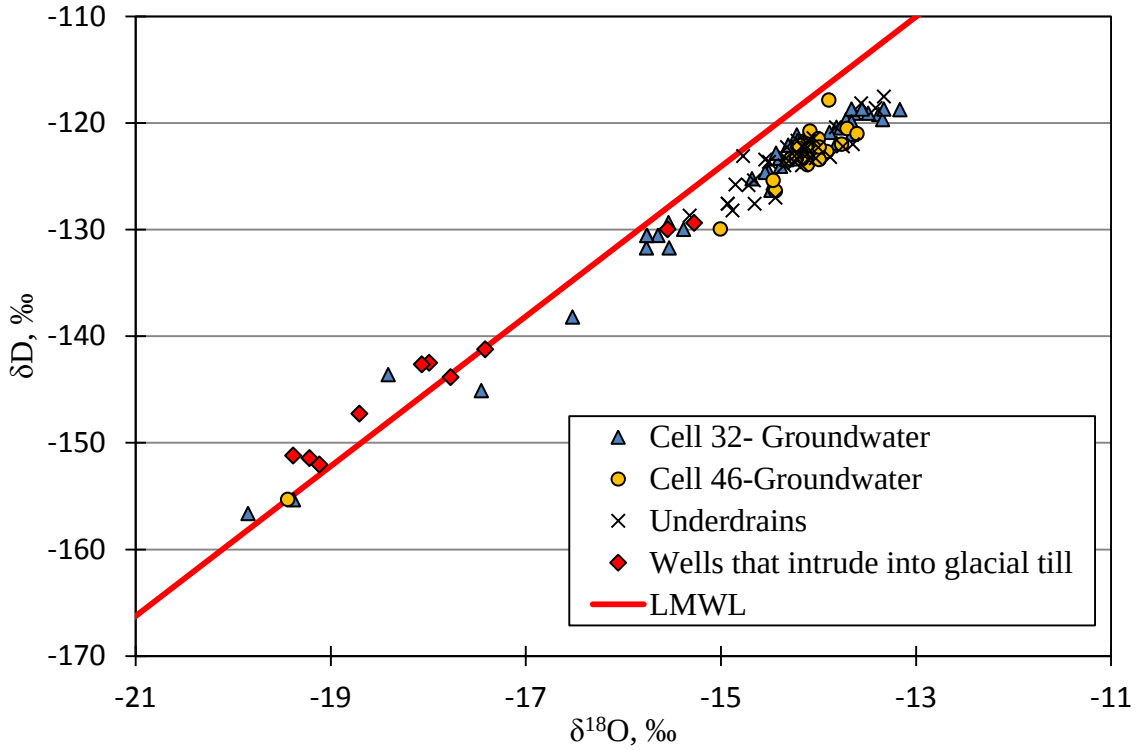

Figure 4.25: SWSS groundwater samples collected from underdrains and piezometers

4.6 Vapour Sampling

Vapour samples were collected from select piezometers at SWSS Cell 32 on July 12, 2012. This activity was executed as a preliminary study to attempt to determine the isotopic composition of pore water in unsaturated soil by converting the isotopic composition of vapour equilibrated with the unsaturated soils. The vapours to liquid conversions were calculated using isotope theory presented in Section 3.4.5.

Vapour samples were collected from both “dry” and “wet” piezometers. A water sample was

also collected from wet piezometers to compare the water sample to the corresponding theoretical conversion. Overall, twenty seven vapour samples and eight water samples were collected. Methane interference was observed by the Picarro upon analysis of several of the vapour samples. These samples were discarded from the data set, leaving a total of twenty two vapour samples; four of the remaining samples had a corresponding water sample for comparison.

Once δD and $\delta^{18}O$ analysis of all vapour samples was complete, liquid isotope values were theoretically calculated from the vapour values using techniques described in Section 3.4.5. The corrected liquid δD and $\delta^{18}O$ values along with the experimental liquid values are compared in Table 4.12. A table showing the correction calculations for all vapour samples is shown in Appendix K.

Table 4.12: Comparison of actual liquid δD and $\delta^{18}O$ values and liquid δD and $\delta^{18}O$ values calculated from theoretical correction of vapour samples

		Actual liquid isotope values		Theoretical liquid isotope values from vapour isotope values	
Sample	**Temperature, °C**	**δD, ‰**	**$\delta^{18}O$, ‰**	**δD, ‰**	**$\delta^{18}O$, ‰**
GW-15-07	9.5	-152	-18.7	-136	-16.2
GW-11-07	7.0	-161	-20.5	-138	-17.3
GW-09-06	7.1	-130	-15.5	-167	-13.4
GW-10-07	7.0	-136	-16.4	-171	-11.5

Analyzing Table 4.12 shows that there is little correlation between the actual liquid δD and $\delta^{18}O$ values and the theoretically calculated δD and $\delta^{18}O$ values. All comparisons show that the vapour to liquid conversions is significantly different than the actual liquid values.

Figure 4.26 graphically displays a summary of results obtained for the vapour to liquid theoretical conversion. Despite not being able to produce comparable results with the vapour to liquid conversion, the theoretical conversion established produced several estimates that plotted near the LMWL and within a range of δD and $\delta^{18}O$ values observed in groundwater at SWSS Cell 32. However, no liquid comparisons were available for a majority of these samples. GW-15-07 and GW-11-07 plotted along the LMWL but the actual liquid isotope values were significantly different.

Several estimates also plotted well below the LMWL, possibly indicating non-equilibrium conditions between the vapour and liquid phases during sampling or methane interference during lab analysis.

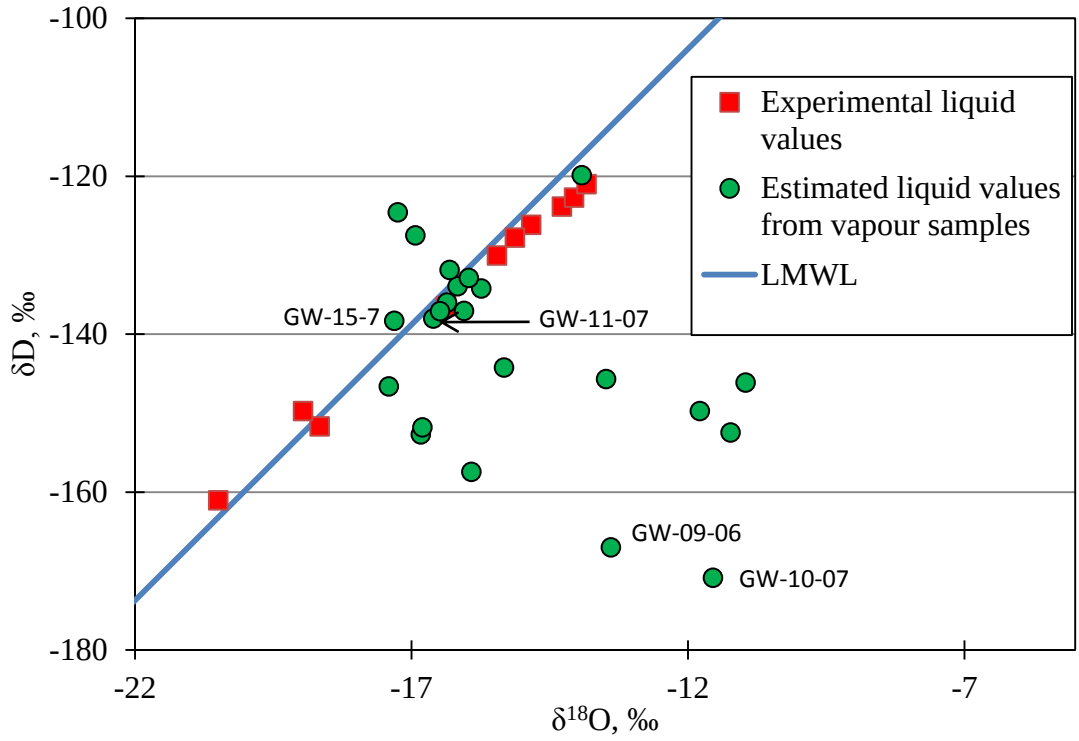

Figure 4.26: Summary of vapour analysis plotted with the LMWL

The inconsistent results obtained from this study may be due to several reasons. The first and most probable is sampling the vapour itself may have thrown the liquid-vapour system out of equilibrium. Throughout sampling, the specific humidity of the air may have lowered and thrown the vapour and liquid phases into a non-equilibrium condition.

It is possible that atmospheric air may have been collected along with the vapour sample through leaks in the sample apparatus. Atmospheric interference was prevented by covering the piezometer top at all times during sampling and ensuring connections between the tubing, pump and sample bag was tight to prevent atmospheric air from short circuiting into the piezometers. However, small amounts of atmospheric air may still have been collected along with the vapour sample through small leaks between connections or the piezometer cap.

The purpose of this study was to develop a preliminary methodology to sample vapour. Although

this study did not produce promising results, there were many learning outcomes and recommendations can be made for future work on this topic. These conclusions are presented and described in Chapter 6.

This technique has the potential to be a powerful tool on the Mildred Lake mine due to a majority of shallow piezometers being dry on closure landforms. By being able to effectively sample vapour and estimate the liquid δD and $\delta^{18}O$ values, dry piezometers and vapour sampling tubes on closure landforms can be utilized effectively. Additionally, sampling vapour to determine unsaturated soil water δD and $\delta^{18}O$ values is a non-destructive sampling approach. Other techniques to sample unsaturated water mainly consist of destructive sampling that disturbs the landscapes and soils.

4.7 Geochemistry

Basic chemistry of the primary source waters was obtained from various literature sources to provide an additional comparison upon the source waters. A summary of the source water chemistry is shown in Table 4.13. Precipitation (rain and snow) were assumed to have minimal anion and cation concentrations and therefore basic chemical data was not obtained for these waters.

The Athabasca River is relatively pure and has the lowest anion/cation concentrations and electrical conductivity along with the highest pH. Alternatively, PAW and interstitial shale water have higher anion/cation concentrations, relatively higher electrical conductivity values and lower pHs. PAW display a lower range of anion/cation concentrations and EC in comparison to shale water. The electrical conductivity for PAW varies by little more than 2000 μS/cm, while shale water has electrical conductivity values that cover a range of over 10000 μS/cm. Similarly, the PAW anion/cation concentrations vary by tens to hundreds of mg/L for while shale water has values that vary by hundreds to thousands of mg/L.

A majority of the PAW chemical data falls within the range of values observed within the interstitial shale water, making it difficult to chemically characterize the mine site source waters. Exceptions to this include calcium and magnesium concentrations, in which PAW consistently has lower concentrations than interstitial shale water. Alternatively, the isotopic signatures developed in this study show that interstitial shale water and PAW are unique and can be

classified with naturally occuring stable water isotopes.

Additionally, concentrations of chloride and bromide and chloride:bromide are typically used as tracers to characterize waters due to the wide variations typically observed in both natural and anthropogenic sourced waters (Davis et al. 1998).

Table 4.13: Summary of source water geochemistry

Source Water	West in-Pit PAW	Interstitial Shale Water	Athabasca River- Upstream of Mildred Lake
Years	1997-2007	2002-2003	2000-2011
pH	7.8-8.2	6.9-7.6	7.8-9
EC [uS/cm]	2750-4800	1468-15100	200-350
Na^+	690-1020	85-4250	7-20
K^+	7.0-20.4	0.1-38.6	0.8-2.0
Mg^{2+}	5.5-11.7	21.6-321	6.8-11.2
Ca^{2+}	8.2-18.0	57.6-364	23-39
Cl^-	375-970	13-1980	1-13
SO_4^{2-}	26-370	26-9230	13-39
CO_3^{2-}	0-25.8	----	5
HCO_3^-	795-1290	227-3030	115-162
Reference	Zubot (2010)	Chapman (2008)	RAMP (2013)

**Cation/Anion chemistry expressed in units of mg/L

5 ANALYSIS

This section will provide examples to demonstrate that the δD and $\delta^{18}O$ characterizations developed for source waters can be applied to estimate mixing processes and water balance components within closure landforms. The examples provided include estimates of two component mixing and evaporation from surface water on closure landforms

5.1 Mixing

The mixing examples provided will utilize two component mixing equations and mass balance equations to estimate the PAW components within closure landforms. Similar techniques have been utilized by Kelln (2008) to estimate components of antecedent pore water and snowmelt within a soil cover at South Bison Hills. The examples take place at the Sandhill Fen and Southwest Sands Storage Cell 32.

5.1.1 Sandhill Fen

As mentioned in Section 3.1.5, the Sandhill Fen contains an underdrain system which was installed to prevent upward movement of PAW into the plant root zone. Conceptually, the underdrain collects PAW from below and fresh water from above and discharges it to a sump. The fresh water source would have been completely meteoric in origin until July 7, 2012. After this day, Mildred Lake water was pumped into the Fen to provide fresh water to the area. The pumps were then shut off for the winter and pumping started again on May 29, 2012. Fresh water collected by the underdrains after this point would be a mixture of meteoric water and Mildred Lake water.

The Fen underdrain mixture is illustrated in Figure 5.1. Each component of the model has a flow rate and an $\delta^{18}O$ and δD composition (both) associated with it.

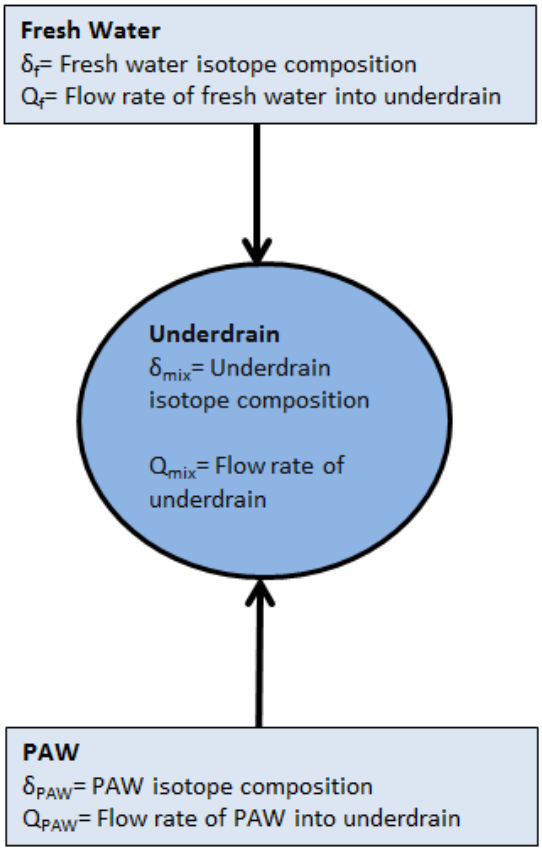

Figure 5.1: Illustration of Fen underdrain mixing model

The corresponding mixing equations include:

$$Q_{mix} = Q_{PAW} + Q_f \tag{5.1}$$

$$Q_{mix}\delta_{mix} = Q_{PAW}\delta_{PAW} + Q_f\delta_f \tag{5.2}$$

where each of the variables are as described in Figure 5.1. These two equations can be manipulated by techniques shown in Section 2.4 to estimate the components of PAW and fresh water flow collected by the underdrain system with the δD and $\delta^{18}O$ compositions of the mixture, PAW and fresh water. The calculations involved in this section will utilize $\delta^{18}O$ values.

The $\delta^{18}O$ values of the underdrain mixture were developed from sampling the sump into which the underdrain network discharges. Sump sampling occurred periodically from June 2012 to June 2013 with $\delta^{18}O$ values ranging from -14.4‰ in February and March 2013 to -16.6‰ in June 2013.

PAW signatures were established by sampling the BGC wells that intruded into the tailings zone. The average $\delta^{18}O$ values were -12.9‰, respectively. T-testing the BGC wells against the West in-pit tailings profiles at the 95% confidence interval statistically demonstrated that these data sets are relatable at the 95% interval. It was assumed that the $\delta^{18}O$ values of the PAW were constant throughout the study period.

The recharge signature was assumed to vary temporally based on seasonal variations, which included taking into consideration:

- a snowmelt pulse during the spring freshet (and before Mildred Lake water was pumped into the Fen) that would result in a relatively depleted signature, and;
- a relatively more enriched signature in the summer and fall due to summer precipitation and Mildred Lake water being pumped into the Sandhill Fen.

The more enriched (summer) $\delta^{18}O$ signature was developed with the $\delta^{18}O$ values of Mildred Lake and the volume weighted average of precipitation. These two source water signatures are relatively similar and the fresh water signature was established by taking the average of the two signatures, resulting in $\delta^{18}O$ values -17.8‰ for fresh water during the late spring and summer months.

In 2013, pumping of Mildred Lake water into the Fen began on May 29, 2013. This signifies that the high amount of fresh water collected in the early spring (late April to May) is likely a snowmelt pulse infiltrating through the soil. In this situation, recharge is likely made up primarily of snowmelt with a small portion of antecedent pore water, resulting in a more depleted fresh water signature. During this time, the fresh water signature was adjusted during this time to account for this snow pulse. Kelln (2008) established an infiltrating water $\delta^{18}O$ value of -21.2‰ from shallow groundwater samples collected at South Bison Hills shortly after snowmelt. Using similar values observed by Kelln (2008), the snow pulse was established as having a $\delta^{18}O$ value of -21.2‰ during this time.

Using these established isotopic signatures of water, along with Equations 5.1 and 5.2, the fraction of PAW and fresh water collected by the underdrain network over time were estimated. The results of the calculations are shown in Figure 5.2 and provide an estimate of the PAW component in water collected by the underdrain system. Results were approximately similar when δD values were used in the calculations. The remaining water fraction is made up of fresh

water. A table showing the calculations can be found in Appendix L. The fraction of PAW throughout the study time is fairly consistent and ranges from approximately 0.5 to 0.7.

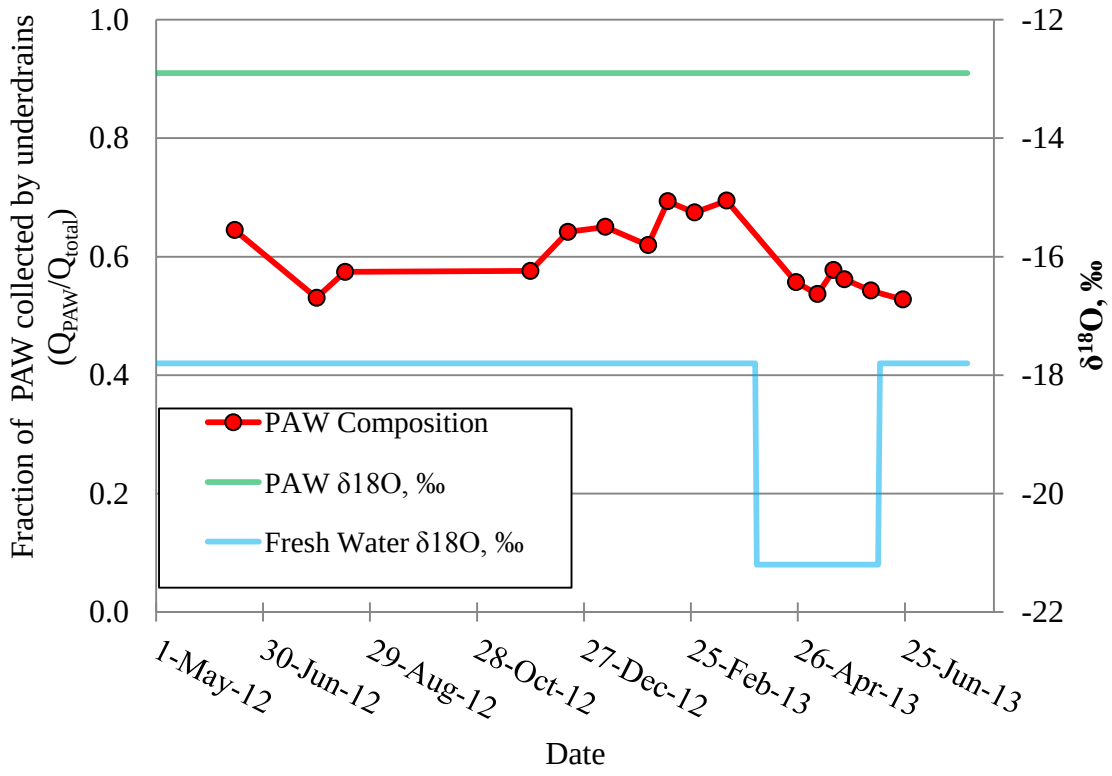

Figure 5.2: Fraction of PAW/tailings collected by Fen underdrain system

Table 5.1 demonstrates how the estimates of PAW and fresh water components collected by the underdrains can be combined with meteorological data and flow data to calculate water balances. Outflow data from the Sandhill Fen was used to estimate the water volume collected by the underdrain system from April 8, 2013 to June 6, 2013. The component of fresh water in the underdrains was estimated from Figure 5.2 and given a value of 0.45. This value was used to calculate the total volume of fresh water collected by the drains. Using precipitation data (O'Kane 2013) and estimating the area of the Fen provides a volume of fresh water inputs during the spring of 2013. Subsequently the total percentage and volumes of snowmelt and rainfall lost to the underdrains can be calculated.

An estimated 22% of snowmelt and rainfall was lost to the underdrain systems from April 8 to June 6, 2013, amounting to a total volume loss of 16,600 m^3. This is a relatively significant

quantity of fresh water that could be potentially utilized to sustain vegetation on the Sandhill Fen.

Table 5.1: Water balance and flow calculations to estimate fraction of snowmelt and rainfall lost to the underdrain system from April 8 to June 6, 2013

Parameter	Value
Total water volume collected by underdrains [m^3]	36,900
Fraction of fresh water collected by underdrains	0.45
Fresh water collected by underdrains [m^3]	16,605
Fen 2013 snow-water equivalent [m]	0.145
Fen rainfall from April 1, 2013 to June 6, 2013 [m]	0.04
Estimated area of Fen [m^2]	408,750
Volume snowmelt and rainfall on Fen [m^3]	75,619
Percentage of fresh water lost to underdrains [%]	22

This example demonstrates that isotope characterizations can be utilized effectively to estimate mixing processes within closure landforms. Through this example fractions of PAW and freshwater were estimated. As well, it was shown that variations in δD and $\delta^{18}O$ values may occur and need to be accounted for when making estimates. Combining the estimations of PAW and freshwater components with flow and meteorological data allowed for water balance calculations to estimate the quantity of fresh water lost to the underdrain system.

5.1.2 Southwest Sands Storage (SWSS) Cell 32 Underdrains

Much like the Fen, SWSS Cell 32 contains a series of underdrains along each bench which discharge to a ditch at the toe of the sand tailings structure. A similar mixing model can be established in which the underdrain collects PAW and meteoric water infiltrating through the soil.

Flow nets of SWSS Cell 32 (Price 2005) show that a majority of PAW water moving through SWSS Cell32 originate from tailings located at depth within SWSS. The PAW signature was established by comparing the West in-pit and SWSS datasets (shown in Table 5.2). The surface

water sampled from West in-pit and SWSS have similar δD and $\delta^{18}O$ ranges. Assuming this trend continues at depth between the two tailings areas enables an estimation of δD and $\delta^{18}O$ values in SWSS tailings from the West in-Pit data sets. The SWSS tailings were given the same isotope values as West in-pit tailings profiles, with δD and $\delta^{18}O$ values of -116‰ and -12.5‰, respectively.

Table 5.2: Summary of PAW signatures used to develop PAW characterization for mixing model

	Average Values	
Dataset	**δD, ‰**	**$\delta^{18}O$, ‰**
West in-pit - Surface Water	-111	-12.2
West in-Pit - Tailings	-116	-12.5
SWSS - Surface Water	-112	-12.2

The meteoric water signature was established as being the volume weighted average of precipitation, with δD and $\delta^{18}O$ values of -144‰ and -17.9‰, respectively. An additional analysis was done by applying a snowmelt bias to infiltrating meteoric water to account for recharge that is synonymous with snowmelt. These values were established from recharge values presented by Kelln (2008) and Hilderman (2011). The underdrain discharges were sampled periodically throughout May to August 2012 and represent the mixture. The input parameters for the mixing calculations are shown in Table 5.3.

Table 5.3: Input parameters for SWSS mixing model

	Parameter for Mixing Calculations	
Parameter	**δD, ‰**	**$\delta^{18}O$, ‰**
Bench A Underdrain	-123	-14.3
Bench B Underdrain	-125	-14.6
Bench C Underdrain	-128	-14.8
PAW/Sand Tailings	-116	-12.5
Infiltrating Meteoric Water-Volume Weighted Precipitation	-144	-17.9
Infiltrating Meteoric Water-with Snowmelt bias	-157	-21.2

The results of the calculations are shown in Table 5.4. The δD and $\delta^{18}O$ analyses produce slightly different results but a trend is evident between the analyses. In both cases, the lower bench (Bench A) had more enriched δD and $\delta^{18}O$ values and therefore higher PAW compositions, while the higher bench (Bench C) had more depleted values and a lower PAW fraction.

Table 5.4: Results of SWSS mixing model

	Fraction PAW-Volume weighted precipitation		**Fraction PAW- snowmelt bias**	
	δD Analysis	**$\delta^{18}O$ Analysis**	**δD Analysis**	**$\delta^{18}O$ Analysis**
Bench A	0.75	0.67	0.83	0.79
Bench B	0.69	0.62	0.79	0.76
Bench C	0.58	0.57	0.71	0.73

Price (2005) modelled the hydrogeology of SWSS Cell 32 from groundwater data collected in 2002 and 2003 as well as the flushing of dissolved solids through the landform over. In the flushing model, Price (2005) projected that upon closure of the SWSS tailings area dissolved solids in the upper benches would flush before the lower benches. As well, it was shown through the current groundwater data that water flushes through the landform from the upper benches to the lower benches, causing an accumulation of dissolved solids as water moves through the landform.

The PAW fractions obtained from this study coincide with the Price's (2005) models. The low PAW fractions in the upper benches indicate that a higher component of fresh water moves through the upper benches. As the fresh water moves through the upper benches, it will accumulate dissolved solids and flush the landforms. The higher components of fresh water suggest that the upper benches will flush faster than the lower benches, which was demonstrated in Price's (2005) model.

The estimated components of PAW and infiltration collected by the underdrains were combined with flow discharge data to approximate the volume of water lost during the sampling duration of June to August 2012. Table 5.5 shows the results of these calculations. The total average fresh water flow rate into the underdrains is approximately 0.56 and 0.36 L/s for the volume weighted

precipitation and snowmelt bias calculations, respectively. This amounts to volumes of approximately 2800 and 4300 m^3 of fresh water infiltration collected by the underdrains between June and August 2012.

Table 5.5: Average flow rate [L/s] of SWSS Cell 32 underdrains from June to August 2012

		Volume Weighted Precipitation		Snomelt Bias	
	Total Flow	**PAW**	**Infiltration**	**PAW**	**Infiltration**
Bench A	0.39	0.28	0.11	0.32	0.07
Bench B	0.76	0.50	0.26	0.59	0.17
Bench C	0.43	0.25	0.18	0.31	0.12
Total	1.58	1.02	0.56	1.22	0.36

Similar to the Sandhill Fen example, this illustration further demonstrates that natural stable isotope tracers can be utilized effectively in closure landform studies. Supplementing the results of the analysis with hydrological and flow data can be used to estimate water balance components within closure landforms. It was also shown that the results of this simple analysis coincided with a numerical model which estimated flushing through SWSS Cell 32. This signifies that δD and $\delta^{18}O$ signatures can be applied to hydrological model applications to verify and enhance numerical models.

5.2 Evaporation estimates: perched ponds at South Bison Hills

Techniques to estimate the evaporation to inflow ratio (E/I ratio) developed by Gonfiantini (1986) were presented in Section 3.4.4. These procedures will be utilized in this section to make an estimate of evaporation from Peat Pond, one of the perched ponds on South Bison Hills. Hydrological data will be combined with the δD and $\delta^{18}O$ data and E/I estimates to approximate total evaporation losses from Peat Pond in 2012.

Equation 3.11 was used to estimate E/I ratios over a range of $\delta^{18}O$ values that were observed in ponds at South Bison Hills. Input parameters for the calculations are equivalent to the ones use in modelling and developing the natural evaporation line and are shown in Table 4.4. The $\delta^{18}O$ value of input water (δ_I) was taken as the point of intersection between the natural evaporation line and LMWL, resulting in a value of -22.2‰.

A table showing the results of these calculations can be found in Appendix M. The results are summarized graphically in Figure 5.3 along with the observed isotopic composition of perched ponds during 2003 to 2004 (Kelln 2008), 2009 (Hilderman 2011) and 2012.

Figure 5.3 provides a simple and time efficient method to estimate the E/I ratios of the ponds at South Bison Hills at a specific time. Upon δD and $\delta^{18}O$ analysis of a water sample, the sample values can be plotted on the graph to estimate the E/I ratio. As a water body evaporates it becomes more enriched, signifying a higher E/I ratio and this is verified by Figure 5.3 which shows that more enriched waters result in a higher E/I ratio.

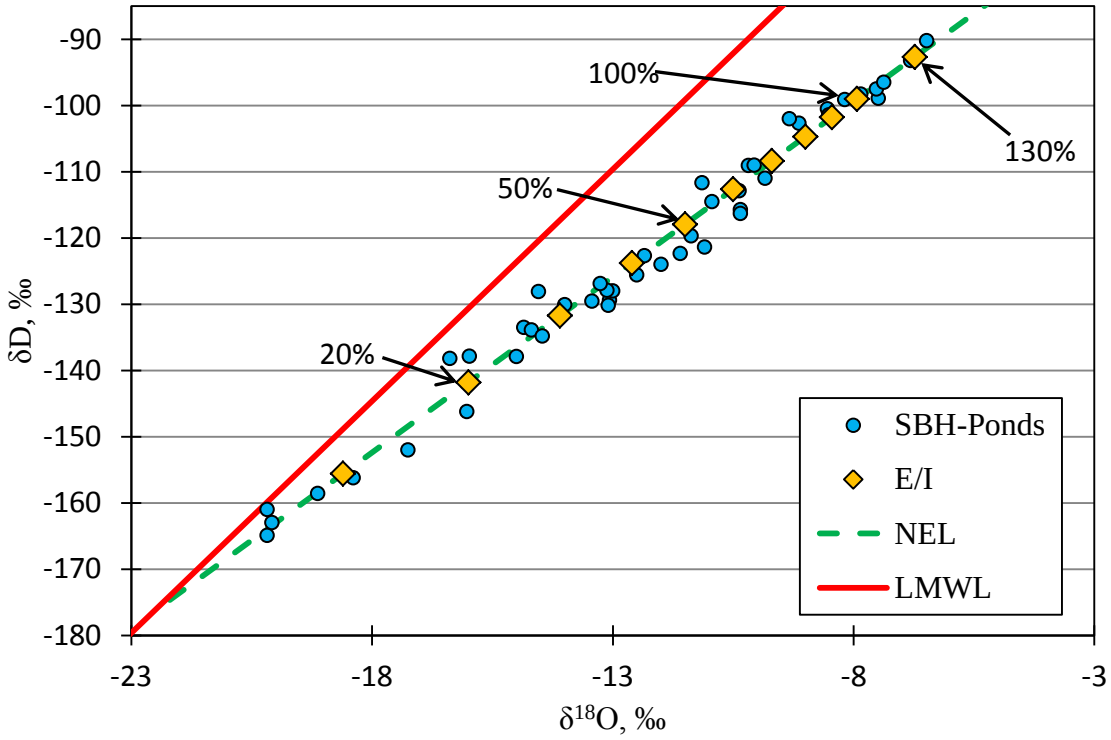

Figure 5.3: Estimated E/I ratios of ponds at South Bison Hills using $\delta^{18}O$ values for analysis. Observed isotopic compositions of ponds are plotted with the E/I ratios

Generally, a wide range of δD and $\delta^{18}O$ values are observed throughout the spring and summer. δD and $\delta^{18}O$ compositions of the ponds are generally more depleted in the early spring from snowmelt and runoff contributions and become progressively more enriched throughout the summer when evaporation dominates. Overall, a majority of the samples have E/I ratios between 0.2 and 0.8. A select few samples show E/I ratios over 1, indicating evaporation losses exceeds the inflow volume, signifying a water volume loss.

Rainfall, flow and runoff data is available for Peat Pond during the 2012 season. This data was used along with E/I values to approximate evaporation losses at different times of the year 2012. The calculations were done for August 14, 2012 and July 9, 2012. The results of the calculations are summarized in Table 5.6.

Table 5.6: Summary of evaporation calculations for Peat Pond on August 14, 2012 and July 9, 2012

Parameter	14-Aug-2012	9-Jul-2012
$\delta^{18}O$ of Peat Pond on August 14, 2012 [‰]	-6.8	-7.8
E/I ratio on August 14, 2012	1.28	1.0
Peat Pond Area [m^2]	7070	7070
Runoff Volume [m^3]	308	308
	44	44
Rainfall Volume [mm]	228	228
[m^3]	1612	1612
Snow Volume [mm]	57	57
[m^3]	403	403
Inflows (Snow+Rain+Runoff) [mm]	329	329
Evaporation [mm]	420	329

The E/I ratios were calculated from the observed $\delta^{18}O$ values of the samples. The rainfall and runoff volumes were calculated from meteorological data collected by O'Kane Consultants (O'Kane 2013). Runoff input volumes were calculated from flow data collected from weirs upstream and downstream of Peat Pond during snowmelt. The input volume was calculated by subtracting the volume passing through the Peat Pond Outlet Weir from the estimated total runoff volume of the contributing runoff area. These calculations are shown in Appendix N.

Once the total volume of inflows was quantified, evaporation losses were directly calculated from the E/I ratio and the total inflow volume. The cumulative estimated evaporation losses for the year were 420 mm and 330 mm for August 14, 2012 and July 9, 2012, respectively.

These values were compared with evaporation estimates calculated by Syncrude Canada Ltd. utilizing Penman's (1948) equation and daily meteorological data such as relative humidity, net

radiation and temperature. The cumulative potential evaporation estimates from the beginning of the year to July 9, 2012 and August 14, 2012 were approximately 330 mm and 450 mm, respectively.

As shown in Table 5.7, the evaporation estimates utilizing E/I ratios are similar to the evaporation depths calculated with the Penman (1948) equation (O'Kane 2013). E/I ratios also provide information on volume changes and water balance processes, such as when evaporation exceeds input volumes. An E/I ratio above one indicates that evaporation losses exceeds inflow volumes, likely resulting in overall water volume losses and decreasing pond levels.

Table 5.7: Comparison of evaporation estimates from δD and $\delta^{18}O$ analysis and Penman's (1948) equation

Date	Cumulative annual evaporation loss [mm]	
	δD and $\delta^{18}O$ Analysis	**Penman's (1948) Equation**
July 9, 2012	330	330
August 14, 2012	420	450

The 2012 year was the only year that produced E/I ratios that exceeded 1. This could be explained by analyzing snow and runoff data over various years. The snow-water equivalent measured during the 2012 melt year was 57 mm, which is significantly lower than the 126 mm and 93 mm measured in 2013 and 2009, respectively. These increased snow depths resulted in a total water volume of nearly 3000 m^3 passing through Peat Pond Inlet Weir, which is considerably more than the volume of 248 m^3 measured in 2012. The decreased runoff and snowmelt inputs into Peat Pond may be the contributing factor for the enriched δD and $\delta^{18}O$ values observed in 2012. A combination of the enriched values, high E/I ratios and below average snowfall and runoff values signifies a moisture deficit in 2012.

The example demonstrated in this section first estimated the E/I ratios of perched ponds on South Bison hills from observed δD and $\delta^{18}O$ compositions of the ponds. The E/I ratios were calculated by combining isotope theory and lake balance concepts suggested by Gonfiantini (1986) and Ferguson et al. (2007). The E/I ratios were then supplemented with flow and precipitation data to calculate evaporation losses. The estimates produced comparable values to evaporation

calculations using Penman's (1948) equation. The similar results between the two methods verifies that stable natural isotope tracers can be used to accurately estimate evaporation from a surface water body. As well, it was shown that hydrological and natural stable isotope data can be combined to provide further information on the water balance of water bodies such as evidence of water volume reductions through extensive evaporation and low inflow rates.

6 CONCLUSIONS AND RECOMMENDATIONS

This chapter will initially restate the objectives of this study and then go through the main learning outcomes of this research. Recommendations for future research and work will be discussed.

6.1 Conclusion

The main objective of this study was to assemble a catalogue of natural stable water isotope signatures across the Mildred Lake mine and use this catalogue to characterize source waters on oil sands closure landforms. The δD and $\delta^{18}O$ signatures developed were then applied to identify mixing and flushing processes within mine closure landforms to demonstrate that these signatures have the potential to be useful and powerful tools when studying the hydrogeology of closure landforms.

A range of surface water, groundwater, soil and vapour samples were collected to adequately represent different source waters on the mine site and the typical δD and $\delta^{18}O$ ranges found in groundwater across oil sands closure landforms. After sample collection, δD and $\delta^{18}O$ compositions for all samples were determined with a Picarro cavity ring down spectrometer isotope analyzer. The collected data was used in conjunction with data collected by Kelln (2008) and Hilderman (2011) to initiate a catalogue of δD and $\delta^{18}O$ signatures across the Mildred Lake mine, develop source water characterizations, refine the local meteoric water line (LMWL) and demonstrate applications of using the characterizations and signatures developed.

6.1.1 Development of local meteoric water line and natural evaporation line

This study refined the local meteoric water line (LMWL) for the region which was first established by Hilderman (2011) based on rain and snow data collected in 2009. In addition to Hilderman's (2009) data, the LMWL was refined with rain data collected throughout 2012 and snow data collected in 2012 and 2013. The refined LMWL was developed utilizing a volume

weighted average approach similar to Peng et al. (2004) and Athanasopoulos (2009). The resulting LMWL equation is:

$$\delta D = 7.0 \cdot \delta^{18}O - 18.6 \quad (6.1)$$

A natural evaporation line was established for the mine site based on observed δD and δ^{18}O compositions of three perched ponds at South Bison Hills. The natural evaporation line had a slope of 5.3 and was compared to natural evaporation lines observed by Gibson et al. (2005), Wassenaar et al. (2011) and Gammons et al. (2006). The natural evaporation line was further analyzed with Gonfiantini's (1986) model which estimates the natural evaporation line by approximating enrichment and fractionation factors from meteorological data. The model output a natural evaporation line with a slope of 5.25, which is comparable to the empirical natural evaporation line slope of 5.3.

6.1.2 Characterizing mine site source waters

This study identified five primary source waters on the mine site. These source waters included rainfall, snow, Mildred Lake/Athabasca River water, interstitial shale water and process affected water (PAW). Uniqueness among the δD and δ^{18}O signatures of source waters as demonstrated in Figures 4.5 to 4.9 allowed for characterizations to be established from the isotopic distinctions. A summary of the normal distribution average and standard deviation δD and δ^{18}O values of source waters is shown in Table 6.1.

The summary of average isotope values and standard deviations also demonstrates distinctions exist between source waters. The low standard deviations observed in the PAW/tailings, interstitial shale water and Mildred Lake datasets indicate tightly confined natural stable water isotope signatures. Rainfall and snow have a greater variance signifying more variable signatures.

Table 6.1: Summary of average δD and $\delta^{18}O$ values and standard deviations of primary source waters

	δD, ‰		$\delta^{18}O$, ‰	
Sample	**Average**	**Std. Dev.**	**Average**	**Std. Dev.**
Rainfall*	-126	20	-15.3	2.7
Snow	-205	13.5	-26.4	1.9
Mildred Lake/Athabasca River	-143	1.4	-17.7	0.5
Interstitial Shale Water (Hilderman 2011)	-159	2.4	-18.4	0.5
West in Pit - Tailings	-116	2.6	-12.5	0.5
Surface PAW	-114	6.5	-12.9	1.3

*Averages are volume weighted

Snow had the most depleted δD and $\delta^{18}O$ signature and was more depleted than spring and summer rainfall. This demonstrates the seasonality in signatures of precipitation. Interstitial shale water had signatures that were more depleted than the volume weighted average of precipitation (δD= -145‰ and $\delta^{18}O$= -17.9‰). This signifies that shale water is likely derived from meteoric water from a different climate or made up of modern day recharge that is composed primarily of snowmelt.

PAW had the most enriched δD and $\delta^{18}O$ values and were located below the LMWL, signifying evaporative enrichment of PAW. Similar evaporative enrichments of PAW have been observed by Gibson et al. (2010) and Pellicori et al. (2005). Evaporative enrichments were attributed to a combination of natural evaporation from the ponds and steam losses from the process water circuit.

A range of evaporation lines were estimated for the process water circuit to show that fractionations from the process water circuit and natural evaporation are unique. The process water circuit is a high temperature (35 to 75°C) and high relative humidity system that results in an evaporation line slope between 4.9 and 7.2. The steeper slopes are observed at higher temperatures (60 to 75°C) are similar to the slope of the LMWL, indicating that evaporative fractionation at these temperatures would cause isotope signatures to move up along the LMWL.

Surface PAW and vertical profiles of Aurora Settling Basin and West in-pit had varying δD and $\delta^{18}O$ ranges, signifying that each of these waters experiences differing fractionation processes that control the signature of each basin. The unique signatures may be due to differing compositions of source water inputs (recycle and tailings water vs. precipitation). As well,

varying natural evaporation processes at individual tailings basins may contribute to the differing signatures among the West in-pit and Aurora Settling Basin tailings. The varying evaporation processes were hypothesized as being due to unique atmospheric conditions at each tailings basin resulting in varying evaporative enrichments. Size, age and depth of tailings areas may have also attributed to the varying signatures between basins.

6.1.3 Applications of natural stable water isotope characterizations

Once characterizations for source waters was established, these characterizations were applied to different hydrogeological situations on closure landforms to demonstrate that the isotope characterizations developed can be used in practical applications. This study presented three examples, two of which estimated fresh water/precipitation and PAW components within closure landforms. The third example estimated evaporation losses from perched ponds at South Bison Hills using water balances and isotope theory.

The first example estimated fractions of PAW and freshwater collected by an underdrain system at the Sandhill Fen. Isotopic characterizations of snowmelt, precipitation and PAW along with isotopic compositions of the underdrain discharge were input into a two component mixing model to estimate fractions of PAW. The results from the mixing model was supplemented with hydrological and flow data to estimate volumes of freshwater collected and subsequently lost to the underdrain system.

The second example, much like the first, estimated fractions of recharge water and PAW collected by the underdrain system at Southwest Sands Storage (SWSS) Cell 32. Flow data was incorporated into this study as well to estimate volumes of recharge lost to the underdrains. Additionally, the results were compared with Price's (2009) research which estimated the long term flushing of contaminants of SWSS Cell 32. The mixing model verified that contaminants would first be flushed from the top benches of SWSS Cell 32, followed by the lower benches.

An evaporation model was created based on methods developed by Gonfiantini (1986) and Ferguson et al. (2007) to estimate evaporation/input (E/I) ratios using $\delta^{18}O$ values. Evaporation losses were calculated from the E/I ratios and precipitation and flow data. The evaporation losses were comparable with estimates using Penman's (1948) equation. On July 9, 2012 the cumulative evaporation estimates was similar between the two analyses. On August 14, 2012 the two analyses produced slightly different evaporation losses but were still relatively comparable

and within an acceptable range.

The examples described above demonstrate that the natural stable water isotope catalogue and characterizations generated from this study are useful tools that can be applied to hydrogeological studies of oil sands closure landforms. The results from this study have a wide variety of applications when combined with hydrological and meteorological data which include identifying flow characteristics, mixing and flushing within closure landforms which can be used to verify and enhance models and predict the hydrogeological evolution of these landforms over time.

6.2 Opportunities for future work and research

This study successfully established source water characterizations based on natural δD and $\delta^{18}O$ signatures. Opportunities for future research exist based on the findings in this study that can further validate the effectiveness of natural isotope tracers as a tool to further understand the hydrogeology of closure landforms and mine site processes.

6.2.1 Recommended future sampling

The findings from this research illustrated that natural stable isotope signatures of water have the potential to be valuable and powerful tools when studying the hydrogeology of closure landform. Because of this sampling and isotopic analysis of mine site waters should be consistently continued in the future.

As a minimum, snow and rainfall samples from at least one location should be sampled year round to further characterize the meteoric water signatures and to further establish the LMWL.

Periodic δD and $\delta^{18}O$ analysis of groundwater from closure landforms across site is also recommended. This data along with the isotope characterizations developed in this study can be used to identify mixing, flushing, and flow paths within closure landforms.

Any additional natural stable water isotope analyses conducted on mine site waters can be put into the "catalogue" created from this study to further develop source water characterizations and further identify different fractionation processes and hydrological characteristics of the mine site.

6.2.2 Supplementing natural stable water isotope data with geochemical data

Supplementing the natural stable water isotope data obtained in this study with geochemical data would provide further insight into hydrogeological and geochemical processes occurring within the mine site. Geochemical data would provide another set of data and an additional viewpoint to interpret the data.

In the future, it would be beneficial to conduct both geochemical and natural stable water isotope analyses to provide that extra viewpoint when analyzing and interpreting data. Geochemical parameters that should be considered include basic cations (calcium, sodium, magnesium and potassium), basic anions (chloride, sulphate, bicarbonate and carbonate) and chloride:bromide ratios.

6.2.3 Further establishing Mildred Lake and shale water signatures

Only eight samples were collected from Mildred Lake and all samples were collected between May and August. More consistent sampling of Mildred Lake is recommended to fully define the isotopic signature of Mildred Lake and identify the seasonal variations, if any, of the freshwater reservoir. As well, sampling of Athabasca River water being pumped into Mildred Lake is recommended to identify seasonal variations of the Mildred Lake input water.

Additionally, the interstitial shale values were established from soil samples collected from South Bison Hills, which consists of disturbed shale formations. To verify the characterizations of interstitial shale water, soil sampling of natural and undisturbed shale formations is recommended. This will provide more data to further establish and characterize interstitial shale water signatures. Recently, a drilling program has sampled intact and undisturbed shale formations at the Mildred Lake mine with δD and $\delta^{18}O$ analysis of soil samples pending (Barbour, oral communication). The results of the drilling program can be combined with those from this study to characterize interstitial shale water.

6.2.4 Natural stable water isotope signatures of recharge

This study developed water isotope signatures for both rainfall and snow. However, as meteoric water infiltrates into the groundwater, the δD and $\delta^{18}O$ compositionz may alter through fractionation processes discussed by Gat and Tzur (1967) or mix with antecedent pore water. As a result the signatures of recharge are more complicated to develop and pinpoint. Identifying the

δD and $\delta^{18}O$ signatures of recharge water was outside the scope of this study.

Developing natural stable water isotope characterizations for recharge would provide further insight into the hydrogeological processes of closure landforms. A signature for recharge would result in more defined and accurate model inputs which would further assist in identifying the hydrological characteristics and evolution of closure landforms. Processes controlling recharge into closure landforms may be hypothesized and the processes controlling the isotopic characterization of recharge could be determined and identified.

6.2.5 Processes and characteristics controlling the signature of PAW/tailings

The results of this study showed that the δD and $\delta^{18}O$ compositions of PAW/tailings fall below the LMWL, implying an evaporative enrichment of these waters. As well, individual tailings basins may be unique and distinct from each other. This was demonstrated through the different signatures observed at Aurora Settling Basin and West in-pit tailings profiles. Based on the information gathered from this research, it was challenging to identify and categorize the processes and characteristics that control the signatures of individual tailings basins.

Gathering additional natural stable water isotope data from multiple tailings basins on site would result in a greater understanding of the tailings basins and provide more insight into the processes controlling the signatures of PAW/tailings. Interpreting δD and $\delta^{18}O$ signatures of basins with meteorological data, atmospheric isotope compositions and characteristics of tailings basins and comparing the results of individual tailings basins would likely provide further understanding into the evaporation and fractionation events that define the signatures of tailings basins.

Differences in meteorological conditions, elevations, and basin size, depths and volumes may all define the evaporation characteristics of each basin and contribute to the δD and $\delta^{18}O$ values of PAW/tailings. Identifying the factors controlling the evaporative enrichment would result in more meaningful and accurate evaporation loss estimates from tailings basins. Ultimately this would lead to more accurate water balance models and calculations for tailings basins.

6.2.6 Estimating evaporation losses from tailings basins

Reasonable estimates of evaporation can be obtained by combining δD and $\delta^{18}O$ data with meteorological and pump data. The evaporation line of tailings basins and E/I ratios can be

modelled and calculated with atmospheric temperature, relative humidity and the δD and $\delta^{18}O$ compositions of atmospheric vapour and input (source) water. The range of δD and $\delta^{18}O$ values of atmospheric vapour can be measured in the field with an isotope analyzer over a period of time or estimated using theoretical approaches laid out by Gammons et al. (2006). An approximation of the δD and $\delta^{18}O$ composition of input/source water can be determined with the compositions and inflow rates/volumes of precipitation and the PAW discharged to the ponds. An evaporation line and E/I can be developed with this information along with temperature and relative humidity data as discussed in Sections 3.4.3 and 3.4.4. Once the E/I ratio is known, evaporation loss volumes can be calculated by supplementing the E/I estimates with inflow volume estimates.

6.2.7 Vapour sampling

Sampling of vapour in isotopic equilibrium with pore water in the unsaturated zone is necessary to fully understand the natural stable water isotope compositions of groundwater in the unsaturated zone. Because the in-situ vapour and liquid phases are in isotopic equilibrium, the δD and $\delta^{18}O$ compositions of the pore water can be estimated by applying a theoretical correction to the isotopic composition of a vapour sample. Vapour samples can be collected from "dry" wells and piezometers or gas sampling tubes.

The vapour sampling program executed did not produce meaningful results for the most part. Despite this, there were many learning outcomes from a sampling and theoretical perspective that can be applied to similar studies and applications moving forward.

First; a series of laboratory tests should be conducted to further understand different sampling systems and to confirm and establish theoretical corrections with empirical results. Laboratory experiments should be conducted which explore memory effects of tubing, purge times before sample collection, the effects of pumping and drawing a sample on the isotopic equilibrium between the liquid and vapour phases and the effect of varying relative humidity on the output of the isotope analyzer.

This study utilized a theoretical correction to estimate the liquid δD and $\delta^{18}O$ compositions from the vapour samples. However, it is likely possible to establish calibration curves over a range of typical temperatures. This can be achieved by equilibrating a series of known liquid standards over a range of temperatures. Once equilibrium is reached the vapour phase can be analyzed.

Calibration curves at different temperature can then be generated by plotting the δD and $\delta^{18}O$ compositions of liquid and vapour against each other. Upon analysis of a vapour sample, the liquid δD and $\delta^{18}O$ values can then be directly calculated from the corresponding calibration curves.

Several of the vapour samples contained methane which interfered with the isotope analyzer output. To alleviate this interference, a methane correction can be programmed into the isotope analyzer (Hendry, personal communication) or the methane can be burned off by running the vapour through a high temperature oven or coil before the vapour sample is ran through the isotope analyzer.

Improvements can be made to the field sampling system and procedures utilized in this study. The first recommendation is to ensure a sampling system in which minimal atmospheric air is collected with the sample. Although the sampling set up had tight connections between the tubing, pump and sampling bag, there may have been minor leaks which allowed for atmospheric air to leak into the system and mix with the vapour sample.

Another recommendation is an attempt should be made to sample vapour at very low pumping rates to ensure equilibrium conditions are maintained during sampling. Pumping at higher rates may cause a relative humidity deficit and induce non-equilibrium condition between the liquid and vapour phases, altering the isotopic fractionation between the two phases. Laboratory testing to test this hypothesis was recommended earlier in this section.

6.2.8 Application of natural stable water isotopes in closure landform water balance

Natural stable water isotopes have the potential to be a major contributor in the water balance of oil sands closure landforms. The characterizations developed in this study can be supplemented with additional geochemical, meteorological, hydrological and flow data to understand flow processes and characteristics through closure landforms. Chapter 5 presented several examples which demonstrated applications of natural stable isotopes to help understand flow systems and characteristics of closure landforms. There are several other applications of naturally occurring stable isotopic tracers or water that can be applied to further comprehend the hydrogeology and water balance of closure landforms. Clark and Fritz (1997) and IAEA (2001) are two good sources which cover a majority of applications in the realms of hydrology and hydrogeology, with many of the applications being beneficial to closure landform studies.

REFERENCES

Adomako, D., P. Maloszewski, C. Stumpp, S. Osae and T.T. Akiti. 2010. Estimating groundwater recharge from water isotope (δ^2H, $\delta^{18}O$) depth profiles in the Densu River basin, Ghana. Hydrological Sciences Journal 55(8): 1405-1416.

Allison, G.B., J.R. Gat, and F.W.J. Leaney. 1985. The relationship between deuterium and oxygen-18 delta values in leaf water. Chemical Geology 58: 145-156.

Athanasopoulos, P. 2009. Using stable isotopes to develop a regional hydrogeological model and characterize nitrate sources in groundwater. M. Sc. thesis, Department of Geological Sciences, University of Saskatchewan, Saskatoon, Saskatchewan.

Baertschi, P. 1976. Absolute ^{18}O content of standard mean ocean water. Earth and Planetary Science Letters 31: 341-344.

Barnes, C.J. and G.B. Allison. 1988. Tracing of water movement in the unsaturated zone using stable isotopes of hydrogen and oxygen. Journal of Hydrology 100: 143-176.

Bennett, P.J. 1998. The stable isotopic characterization of carbon and water cycling in municipal solid waste landfills. M.Sc. thesis, Department of Earth Sciences, University of Western Ontario, London, Ontario.

Boese, C.D. 2003. The design and installation of field instrumentation program for the evaluation of soil-atmosphere water fluxes in a vegetated cover over saline/sodic shale overburden. M.Sc. Thesis, Department of Civil Engineering, University of Saskatchewan, Saskatoon, Saskatchewan.

CAPP. 2011. Crude oil: forecasts, markets and pipelines, June 2011. Canadian Association of Petroleum Producers. Calgary, AB.

Chapman, D. 2008. Hydrogeologic characterization of a newly constructed saline-sodic clay overburden hill. M. Sc. thesis, Department of Civil and Geological Engineering, University of Saskatchewan, Saskatoon, Saskatchewan.

Clark, I. and P. Fritz. 1997. Environmental isotopes in hydrogeology. CRC Press: Boca Raton, FL.

Craig, H. 1961. Isotopic variations in meteoric waters. Science 133(3465): 1702-1703.

Craig H. and L.I. Gordon. 1965. Deuterium and oxygen-18 variations in the ocean and the marine atmosphere. In *Stable Isotopes in Oceanographic Studies and Paleotemperatures*, ed. E. Tongiorgi. C.N.R., Laboratorio di Geologia Nucleare, Pisa: 9-130.

Criss, R.E. and M.L. Davisson. 1996. Isotopic imaging of surface water/groundwater interactions, Sacramento Valley, California. Journal of Hydrology 178: 205-222.

de Wit J.C., C.M. Vander Straaten and W.G. Mook. 1980. Determination of the absolute hydrogen isotopic ratio of V-SMOW and SLAP. Geostandards Newsletter 4: 33-36.

Dansgaard, W. 1964. Stable isotopes in precipitation. Tellus XVI(4): 436-468.

Davis, S.M., D.O. Wittemore and J. Fabryka-Martin. 1998. Uses of chloride/bromide ratios in studies of potable water. Groundwater 36(2): 338-350.

Douglas, M.C. 1997. Mixing and temporal variation in the groundwater flow system at the Con Mine, Yellowknife, N.W.T. , Canada; an analogue for a nuclear waste repository. M. Sc. thesis, Department of Earth Sciences, University of Ottawa, Ottawa, Ontario.

Earman, S., A.R. Campbell, F.M. Phillips and B.D. Newman. 2006. Isotopic exchange between snow and atmospheric water vapor: Estimation of the snowmelt component of groundwater recharge in the southwestern United States. Journal of Geophysical Research 111, D09302, doi:10.1029/2005JD006470, 18 pages.

Ferguson, P.R., N. Weinrauch, L.I. Wassenaar, B. Mayer, and J. Veize. 2007. Isotope constraints on water, carbon, and heat fluxes from the northern Great Plains region of North America. Global Biogeochemical Cycles 21, GB2023, doi:10.1029/2006GB002702, 11 pages.

Friedman, I., L. Machta and R. Soller. 1962. Water vapour exchange between a water droplet and its environment. Journal of Geophysical Research 7: 2761-2766.

Gammons, C.H., S.R. Poulson, D.A. Pellicori, P.J. Reed, A.J. Roesler and E.M. Petrescu. 2006. The hydrogen and oxygen isotopic composition of precipitation, evaporated mine water, and river water in Montana, USA. Journal of Hydrology 328: 319-330.

Gat, J.R. and T. Tzar. 1967. Modification of the isotopic composition of rainwater by processes which occur before groundwater recharge. In *Isotopes in Hydrology, Symposium Proceedings*, Vienna, Austria, 1966, IAEA Publication 83: 49-59.

Gat, J.R. 1981. Lakes. In Stable Isotope Hydrology: Deuterium and Oxygen-18 in the Water Cycle. In *Technical Report Series no. 210*, ed. J.R. Gat and R. Gonfiantini. IAEA: Vienna.

Gat, J.R. and E. Matsui. 1991. Atmospheric water balance in the Amazon basin: an isotopic evapotranspiration model. Journal of Geophysical Research 96(7): 13179-13188.

Gat, J.R., C.J. Bowser and C. Kendall. 1994. The contribution of evaporation from the Great Lakes to the continental atmosphere: estimate based on stable isotope data. Geophysical Research Letters 21(7): 557-560.

Gat, J.R., 1995. Stable isotopes and the water balance of fresh and saltwater lakes. In *Physics and Chemistry of Lakes, 2nd Edition*, ed. A. Lerman, D.M. Imboden and J.R. Gat. Springer: Verlag, Berlin.

Gat, J.R. 1996. Oxygen and hydrogen isotopes in the water cycle. Annual Review of Earth and Planetary Sciences 24: 225-262.

Gat, J.R., A. Shemesh, E. Tziperman, A. Hecht, D. Georgopoulos and O. Basturk. 1996. The stable isotope composition of waters in the eastern Mediterranean Sea. Journal of Geophysical Research 101: 6441-6451.

Gat, J.R. 2005. Some classic concepts of isotope hydrology. In *Isotopes in the Water Cycle: Past, Present and Future of a Developing Science*, ed. P.K. Aggarwal, J.R. Gat and K.F.O. Froehlich. Springer: Dordecht, NL

Gat, J.R. 2010. Isotope hydrology: a study of the water cycle. Imperial College Press: London, UK.

Gibson, J.J., T.W.D Edwards, G.G. Bursey and T.D. Prowse. 1993. Estimating evaporation using stable isotopes: quantitative results and sensitivity analysis for two catchments in northern Canada. Nordic Hydrology 24:79-94.

Gibson, J.J. and T.W.D Edwards. 2002. Regional water balance trends and evaporation-transpiration partitioning from a stable isotope survey of lakes in northern Canada. Global Biochemical Cycles 16(2), 1026, doi:10.1029/2001GB001839, 18 pages.

Gibson, J.J., T.W.D. Edwards, S. J. Birks, N. A. St. Amour, W. M. Buhay, P. McEachern, B. B. Wolfe and D. L. Peters. 2005. Progress in isotope tracer hydrology in Canada. Hydrological Processes 19: 303-327.

Gibson, J.J., S.J. Birks, M. Moncur, Y. Yi, K. Tattrie, S. Jasechko, K. Richardson and P. Eby. 2011. Isotopic and Geochemical Tracers for Fingerprinting Process-Affected Waters in the Oil Sands Industry: A Pilot Study. Oil Sands Research and Information Network, University of Alberta, School of Energy and the Environment, Edmonton, Alberta. OSRIN Report No. TR-12.

Google. 2013a. Google Maps Canada. Available at: https://maps.google.ca/maps?hl=en&tab=wl (Accessed 20 March 2013).

Google. 2013b. Google Maps Canada. Available at: https://maps.google.ca/ (Accessed 1 November 2013).

Gonfiantini, R. 1986. Environmental isotopes in lake studies. In *Handbook of Environmental Isotope Geochemistry, The Terrestrial Environment (2B)*, ed. P. Fritz and J. Ch. Fontes. Elsevier, Amsterdam: 113–168.

Government of Alberta. 2012a. Oil sands: the resource. Available at: http://www.oilsands.alberta.ca/FactSheets/Resource_FSht_June_2012_Online.pdf (Accessed 13 February 2013).

Government of Alberta. 2012b. Oil sands: reclamation. Available at: http://www.oilsands.alberta.ca/FactSheets/Reclamation_FSht_June_2012_Online.pdf (Accessed 13 February 2013).

Government of Alberta. 2013. Facts and Statistics. Available at: http://www.energy.alberta.ca/OilSands/791.asp (Accessed 14 February 2013).

Hayashi, M., G. van der Kamp and R. Schmidt. 2003. Focused infiltration of snowmelt water in partially frozen soil under small depressions. Journal of Hydrology 270: 214-229.

Hackely, K.C., C.L. Liu and D.D. Coleman. 1996. Environmental isotope characteristics of landfill leachate and gases. Ground Water 34: 827-836.

Hendry, M.J. and L.I. Wassenaar. 1999. Implications of the distribution of δD in pore waters for groundwater flow and the timing of geologic events in a thick aquitard system. Water Resources Research 35(6): 1751-1760.

Hendry, M.J., S.L. Barbour, J. Zettl, V. Chostner, and L.I. Wassenaar. 2011. Controls on the long-term downward transport of δ^2H of water in a regionally extensive, two-layered aquitard system. Water Resources Research 47, W06505, doi:10.1029/2010WR010044, 13 pages.

Hildermann, J. 2011. Net percolation as a function of topographic variation in a reclamation cover over a saline-sodic overburden dump. M. Sc. thesis, Department Civil and Geological Engineering, Univeristy of Saskatchewan, Saskatoon, Saskatchewan.

Hoefs, J. 2009. Stable isotope geochemistry, 6th ed. Springer: Verlag Berlin Heidelberg, DE.

Hooper, R.P. and C.A. Shoemaker. 1986. A comparison of chemical and isotope hydrograph separation. Water Resources Research 22: 1444-1454.

Horita, J. and D.J. Wesolowski. 1994. Liquid-vapour fractionation of oxygen and hydrogen isotopes of water from freezing to the critical temperature. Geochimica et Cosmochimica Acta 58: 3425-3437.

Horita, J. 2005. Saline Waters. In *Isotopes in the Water Cycle: Past, Present and Future of a Developing Science*, ed. P.K. Aggarwal, J.R. Gat and K.F.O. Froehlich: 39-51. Springer: Dordecht, NL.

Isaac, B.A., M.B. Dusseault, G.D. Lobb and J.D. Root. 1982. Characterization of the lower cretaceous overburden for oil sands surface mining within Syncrude Canada Ltd. leases northeast Alberta, Canada. In *Proceedings of the IV International Association of Engineering Geology II*, New Delhi, India. A.A. Balkema, Rotterdam, Netherlands.

Jacob, H. and C. Sonntag. 1991. An 8-year record of seasonal variation of ^{2}H and ^{18}O in atmospheric water vapour and precipitation at Heidelberg, Germany. Tellus 43B: 291-300.

Jasechko, S., J.J. Gibson, S.J. Birks and Y. Yi. 2012. Quantifying saline groundwater seepage to surface waters in the Athabasca oil sands region. Applied Geochemistry 27: 2068-2076.

Kelln, C.J., S.L. Barbour, A. Elshorbagy and C. Qualizza. 2006. Long-term performance of a reclamation cover: the evolution of hydraulic properties and hydrologic response. Unsaturated Soils: 813-824.

Kelln, C., L. Barbour and C. Qualizza. 2007. Preferential flow in a reclamation cover: hydrological and geochemical response. Journal of Geotechnical and Geoenvironmental Engineering 133:1277-1289.

Kelln, C. 2008. The effects of meso-scale topography on the performance of engineered soil covers. PhD thesis, Department of Civil and Geological Engineering, University of Saskatchewan, Saskatoon, Saskatchewan.

Kendall, C. and E.A. Caldwell. 1998. Fundamentals of isotope geochemistry. In *Isotope Tracers in Catchment Hydrology*, ed. C. Kendall and J.J. McDonnell. Elsevier: Amsterdam.

Kendall, C. and T.B. Coplen. 2001. Distribution of oxygen-18 and deuterium in river waters across the United States. Hydrological Processes 15: 1363–1393.

Kendall, C. and D.H. Doctor. 2011. Stable isotope applications in hydrologic studies. In *Isotope Geochemistry, from the treatise on geochemistry*, ed. H.D. Holland and K.K. Turekian: 181-226. Elsevier: Oxford, UK.

International Atomic Energy Association (IAEA). 2001. Environmental isotopes in the hydrological cycle – Principles and applications. In *IHP-V, Technical Documents in Hydrology No. 39*, ed. W.G. Mook. UNESCO, Amsterdam.

Ireson, A.M., G. van der Kamp, G. Ferguson, U. Nachshon and H.S. Wheater. 2013. Hydrogeological processes in seasonally frozen northern latitudes: understanding, gaps and challenges. Hydrogeology Journal 21: 53-66.

Lee, J., X. Feng, A.M. Faiia, E.S. Posmentier, J.W. Kirchner, R. Osterhuber and S. Taylor. 2010. Isotopic evolution of a seasonal snowcover and its melt by isotopic exchange between liquid water and ice. Chemical Geology 270:126-134.

Lemay, T.G. 2002. Geochemical and isotope data for formation water from selected wells, Cretaceous to Quaternary succession, Athabasca Oil Sands (in situ) Area, Alberta. EUB/AGS Geo-Note 2002-02. Alberta Energy and Utilities Board, Alberta Geological Survey, Edmonton, AB. December 2002.

Majoube, M. 1971. Fractionnement en oxyge`ne-18 et en deuterium entre l'eau et sa vapeur. Journal of Physical Chemistry 68: 1423–1436.

Maule, C.P., D.S. Chanasyk and K. Muehlenbachs. 1994. Isotopic determination of snow-water contribution to soil water and groundwater. Journal of Hydrology, 155: 73-91.

Mayr, C., A. Lucke, W. Stichler, P. Trimborn, B. Ercolano, G. Oliva, C. Ohlendorf, J. Soto, M. Fey, T. Haberzettl, S. Janssen, F. Schabitz, G.H. Schleser, M. Wille, B. Zolitschka. 2007. Precipitation origin and evaporation of lakes in semi-arid Patagonia (Argentina) inferred from stable isotopes ($\delta^{18}O$, $\delta^{2}H$). Journal of Hydrology 334: 53-63.

Merlivat, L. and J. Jouzel. 1979. Global climatic interpretation of the deuterium–oxygen 18 relationship for precipitation. Journal of Geophysical Research 84: 5029–5033.

Microsoft. 2010. Excel 2010. Mississauga, Ontario, Canada.

MiniTab Incorporated. 2012. MiniTab 16. State College, Pennsylvania, USA.

Mook, W.G. 2001a. Environmental isotopes in the hydrological cycle – Principles and applications, Vol. 1 – Introduction, theory, methods and review. In *IHP-V, Technical Documents in Hydrology No. 39*, ed. W.G. Mook. UNESCO, Amsterdam.

Mook, W.G. 2001. Environmental isotopes in the hydrological cycle – Principles and applications, Vol. 1 – Introduction, theory, methods and review. In *IHP-V, Technical Documents in Hydrology No. 39*, ed. W.G. Mook. UNESCO, Amsterdam.

Mook, W.G. 2006. Introduction to isotope hydrology. Taylor & Francis Group: London, UK.

Moser, H. and W. Stichler. 1975. Deuterium and oxygen-18 contents as index of the properties of snow blankets. In *Snow Mechanics, Proceedings, Grindelwald Symposium*, April 1974, IAHS Publication 114: 122-135.

O'Kane. 2013. Watershed Research Database. Available at: http://portal.projectlinesolutions.net/syncrude/pages/default.aspx (Restricted Access, Last Accessed 16 March 2014).

Pellicori, D.A., C.H. Gammons and S.R. Poulson. 2005. Geochemistry and stable isotope composition of the Berkeley pit lake and surrounding mine waters, Butte, Montana. Applied Geochemistry 20: 2116-2137.

Peng, H., B. Mayer, S. Harris and H.R. Krouse. 2004. A 10-yr record of stable isotope ratios of hydrogen and oxygen in precipitation at Calgary, Alberta, Canada. Tellus 56B: 147-159.

Penman, H.L. 1948. Natural evapotranspiration from open water, bare soil and grass. Proceedings of the Royal Society of London, Series A, 193: 120-145.

Picarro. 2009. Picarro L1102-i isotopic liquid water and water vapour analyzer: User's guide. Sunnyvale, CA.

Price, A. 2005. Evaluation of groundwater flow and salt transport within an undrained tailings sand dam. M. Sc. thesis, Department of Earth and Atmospheric Sciences, University of Alberta, Edmonton, Alberta.

RAMP (Regional Aquatics Monitoring Program). 2013. RAMP water quality data report. Available at: http://www.ramp-alberta.org/data/Water/WaterReport.aspx?siteid=ATR-SR-W&from=Map (Accessed 4 October 2013).

Rock, L. and B. Mayer. 2007. Isotope hydrology of the Oldman River basin, southern Alberta, Canada. Hydrological Processes 21, 3301-3315.

Rose, S. E. 1995. Introduction to Isotope Hydrology, Principles and Applications. Atlanta, Georgia. Environmental Education Enterprises, Columbus, Ohio.

Rothfuss, Y., H. Vereecken and N. Bruggemann. 2013. Monitoring water stable isotopic composition in soils using gas-permeable tubing and infrared laser absorption spectroscopy. Water Resources Research 49: 3747–3755, doi:10.1002/wrcr.20311.

RSC (Royal Society of Canada). 2011. Environmental and health impacts of Canada's oil sands industry: December 2010. Ottawa, ON.

Savin, S.M. 1980. Oxygen and hydrogen isotope effects in low-temperature mineral water interactions. In *Handbook of Environmental Isotope Geochemistry 1, The Terrestrial Environment (A)*, ed. P. Fritz and J.C. Fontes. Elsevier, Amsterdam: 283-327.

Schmidt, M., K. Maseyk, C. Lett, P. Biron, P. Richard, T. Bariac and U. Seibt. 2010. Concentration effects on laser-based $\delta^{18}O$ and $\delta^{2}H$ measurements and implications for the calibration of vapour measurements with liquid standards. Rapid Communications in Mass Spectrometry 24: 3553–3561.

Syncrude. 2010. 2010 Key Sustainability Metrics: Syncrude. Available at: http://www.syncrude.ca/users/folder.asp?FolderID=5713 (Accessed: 31 May 2012).

Syncrude. 2012a. 2010/2011 Sustainability Report. Available at: http://www.syncrude.ca/users/folder.asp?FolderID=5713 (Accessed 7 March 2013).

Syncrude. 2012b. Finance and operations: performance overview. Available at: http://www.syncrudesustainability.com/2011/media/pdf/sections/SycrudeCSR_Finance-Operations.pdf (Accessed 27 February 2013).

Taylor, S., X. Feng, J.W. Kirchner, R. Osterhuber, B. Klaue and C.E. Renshaw. 2001. Isotopic evolution of a seasonal snowpack and its melt. Water Resources Research 37(3): 759-769.

Taylor, S., X. Feng, M. Williams and J. McNamara. 2002. How isotopic fractionation of snowmelt affects hydrograph separation. Hydrological Processes 16: 2683-3690.

Wassenaar, L.I., M.J. Hendry, V.I. Chostner and G.P. Lis. 2008. High Resolution Pore Water $\delta^{2}H$ and $\delta^{18}O$ Measurements by $H_2O_{(liquid)}$-$H_2O_{(vapor)}$ Equilibration Laser Spectroscopy. Environmental Science Technology 42: 9262-9267

Wassenaar, L.I., P. Athanasoupoulos and M.J. Hendry. 2011. Isotope hydrology of precipitation,nsurface and ground waters in the Okanagan Valley, British Columbia, Canada. Journal or Hydrology 411: 27-48.

Wolfe, B.B., T.L. Karst-Riddoch, R.I. Hall, T.W.D. Edwards, M.C. English, R. Palmini, S. McGowan, P.R. Leavitt and S.R. Vardy. 2007. Classification of hydrological regimes of northern floodplain basins (Peace–Athabasca Delta, Canada) from analysis of stable isotopes ($\delta^{18}O$, $\delta^{2}H$) and water chemistry. Hydrological Processes 21: 151-168.

Zimmermann, U., K.O Munnich and W. Roether. 1967. Downward movement of soil moisture traced by means of hydrogen isotopes. In *Isotope Techniques in the Hydrologic Cycle, Geophysical Monograph Series 11*, American Geophysical Union.

Zubot, W. 2010. Removal of naphthenic acids from oil sands process water using petroleum coke. M. Sc. Thesis, Department of Civil and Environmental Engineering, University of Alberta, Edmonton, Alberta.

APPENDICES

Contents

APPENDIX A: Los Gatos and Picarro Comparison

Table A1: Comparison of Picarro and Los Gatos istope analyzer

		Los Gatos		Picarro		Absolute Difference	
Sample	Date Sampled	δD	$\delta^{18}O$	δD	$\delta^{18}O$	δD	$\delta^{18}O$
SWSS - South West Sands	1-Dec-11	-113.79	-12.79	-112.6	-12.14	1.18	0.65
RCW 110 MLSB	5-Jun-12	-112.1	-11.83	-112.1	-11.97	0.00	0.14
WIP - West in Pit	7-Nov-11	-107.85	-11.94	-109.5	-11.63	1.63	0.31
WIP - West in Pit	1-Dec-11	-111.0	-10.39	-110.6	-11.28	0.40	0.89
SEP - South East Pit	1-Dec-11	-114.3	-11.54	-114.7	-11.35	0.47	0.19
Fen sump	1-Dec-11	-127.3	-13.96	-126.9	-14.00	0.38	0.04
Fen GW BGC 08 05C June 13 2012	13-Jun-12	-114.01	-11.99	-113.9	-11.90	0.13	0.09
Fen GW BGC 08 08B June 13 2012	13-Jun-12	-117.57	-13.3	-117.2	-13.32	0.33	0.02
Fen GW BGC 08 04C June 13 2012	13-Jun-12	-117.88	-12.9	-119.0	-12.57	1.10	0.33
SEP - South East Pit	7-Nov-11	-99.68	-10.58	-98.6	-9.97	1.11	0.61
Precip SWSS Cell 32 June 12 2012	12-Jun-12	-126.42	-14.99	-127.1	-15.18	0.66	0.19
Precip Ucell June 4 2012	4-Jun-12	-127.56	-16.51	-129.1	-16.89	1.57	0.38
Precip 30-T May 16 2012	16-May-12	-112.8	-15.06	-114.0	-15.04	1.20	0.02
Precip 30T June 12 2012	12-Jun-12	-121.64	-14.87	-120.1	-14.97	1.51	0.10
Bench C Drain LC3 SWSS June 11 2012	11-Jun-12	-127.81	-15.31	-127.6	-14.93	0.24	0.38
Fort Hills North Snow	7-Mar-12	-185.52	-23.92	-185.8	-23.48	0.33	0.44
South Hills 30W	2-Mar-12	-204.87	-26.45	-201.9	-26.03	2.93	0.42
Precip 30T June 12 2012	12-Jun-12	-121.64	-14.87	-120.1	-14.97	1.51	0.10
Golden Pond June 11 2012	11-Jun-12	-100.81	-8.12	-99.1	-8.18	1.69	0.06
RCW 120-North Mine Ditch	5-Jun-12	-116.0	-13.01	-117.35	-13.56	1.31	0.55
					Average=	**0.98**	**0.29**
					Std. Deviation=	**0.73**	**0.24**

APPENDIX B: Example- calculating liquid isotope values from experimental vapour isotope values

On July 13, 2013, A vapour sample was drawn from a piezometer GW-15-7 on SWSS Cell 32. The temperature measured at the sampling depth was 9.5°C. The sample was analyzed with the Picarro isotope analyzer at the University of Saskatchewan and the following readings were obtained: δD= -200.5‰; δ18O= -25‰ and specific humidity=11700.

Knowing these values, the first correction (Equation 3.12) can be applied to the δD and $\delta^{18}O$ values:

$$\delta D_{cor} = \delta D_{exp} - 14.5‰ = -200.5‰ - 14.5‰ = \mathbf{215}‰$$

$$\delta^{18}O_{cor} = \delta^{18}O_{exp} - 4.2‰ = -25‰ - 4.2‰ = \mathbf{29.2}‰$$

The second correction (Equation 3.13) to correct for specific humidity differences can then be applied:

$$\delta D_{cor2} = \delta D_{cor} + \left(30000 - SH_{sample}\right) * 0.08 \frac{‰}{1000\ ppm}$$

$$\delta D_{cor2} = -215‰ + (30000 - 11700) * 0.08 \frac{‰}{1000\ ppm} = -213.4‰$$

$$\delta^{18}O_{cor2} = \delta^{18}O_{cor} + \left(30000 - SH_{sample}\right) * 0.131 \frac{‰}{1000\ ppm}$$

$$\delta^{18}O_{cor2} = \delta^{18}O_{cor} + (30000 - 11700) * 0.131 \frac{‰}{1000\ ppm} = -26.8‰$$

The last correction is calculated using Equation 3.13 and Equations 2.4 and 2.5 to calculate the equilibrium fractionation factors. At a temperature of 9.5°C, the equilibrium fractionation factors for δD and $\delta^{18}O$ are 1.098 and 1.011, respectively. The liquid isotope values can then be calculated:

$$\delta D_L = (\delta_{cor2} + 1000) * \alpha_{l/v} - 1000 = (-213.4 + 1000) * 1.098 - 1000 = -136‰$$

$$\delta^{18}O_L = (\delta_{cor2} + 1000) * \alpha_{l/v} - 1000 = (-26.8 + 1000) * 1.011 - 1000 = -16.4‰$$

APPENDIX C: Isotope values of water and soil samples

Water Samples

Tailings Profiles

Sample	Depth, m	δD, ‰	$\delta^{18}O$, ‰
ASB-12-11-12.9	12.9	-123.6	-13.55
ASB-12-11-14.9	14.9	-126.0	-14.11
ASB-12-11-16.9	16.9	-126.0	-14.11
ASB-12-11-18.9	18.9	-125.0	-12.55
ASB-12-11-20.9	20.9	-127.3	-13.97
ASB-12-11-22.9	22.9	-127.3	-13.97
ASB-12-11-24.9	24.9	-127.3	-13.97
ASB-12-11-26.9	26.9	-127.3	-13.97
ASB-12-11-28.9	28.9	-127.3	-14.06
ASB-12-11-30.9	30.9	-127.3	-14.06
ASB-12-11-32.9	32.9	-127.3	-14.06
ASB-12-11-34.9	34.9	-125.5	-13.25
ASB-12-11-36.9	36.9	-127.3	-13.94
ASB-12-11-38.9	38.9	-126.6	-14.20
ASB-12-11-40.9	40.9	-126.0	-14.09
ASB-12-11-42.9	42.9	-126.0	-13.74
ASB-12-11-44.9	44.9	-126.6	-13.86
ASB-12-11-46.9	46.9	-126.6	-13.86
ASB-12-11-48.9	48.9	-126.6	-14.09
ASB-12-8-11.7	11.7	-127.3	-14.45
ASB-12-8-13.7	13.7	-126.2	-13.67
ASB-12-8-15.7	15.7	-125.6	-13.78
ASB-12-8-17.7	17.7	-126.7	-14.22
ASB-12-8-19.7	19.7	-127.3	-13.89
ASB-12-8-21.7	21.7	-126.2	-13.89
ASB-12-8-23.7	23.7	-127.3	-14.11
ASB-12-8-25.7	25.7	-128.5	-14.11
ASB-12-8-27.7	27.7	-127.3	-14.00
ASB-12-8-29.7	29.7	-125.0	-13.44
ASB-12-8-31.7	31.7	-126.2	-14.19
ASB-12-8-33.7	33.7	-125.6	-14.09
ASB-12-8-35.7	35.7	-126.8	-14.09
ASB-12-8-37.7	37.7	-126.8	-14.19
ASB-12-8-39.7	39.7	-126.2	-13.87
ASB-12-8-41.7	41.7	-126.7	-14.38
ASB-12-8-43.7	43.7	-127.9	-14.49

Sample	Depth, m	δD, ‰	$\delta^{18}O$, ‰
AEPN-E-01-5.2		-129.0	-14.71
AEPN-E-01-8.2		-127.9	-14.38
AEPN-E-01-11.2		-129.6	-14.92
AEPN-E-03-5.5		-124.3	-14.06
AEPN-E-03-8.5		-126.6	-14.60
AEPN-E-03-11.5		-118.2	-11.44
WIP-12-12-4.6	4.6	-111.3	-12.43
WIP-12-12-7	7	-110.2	-11.61
WIP-12-12-9	9	-111.5	-12.27
WIP-12-12-11	11	-111.5	-11.94
WIP-12-12-13	13	-112.1	-11.94
WIP-12-12-15	15	-113.3	-12.38
WIP-12-12-17	17	-113.3	-12.27
WIP-12-12-19	19	-112.7	-12.22
WIP-12-12-21	21	-113.3	-12.22
WIP-12-12-23	23	-113.9	-12.43
WIP-12-12-25	25	-112.1	-12.00
WIP-12-12-27	27	-113.3	-12.32
WIP-12-12-29	29	-113.3	-12.16
WIP-12-12-31	31	-111.0	-11.83
WIP-12-12-33	33	-111.5	-11.94
WIP-12-12-35	35	-112.1	-12.16
WIP-12-12-37	37	-111.0	-11.61
WIP-12-12-39	39	-111.5	-11.87
WIP-12-11-4.8	4.8	-111.0	-11.87
WIP-12-11-6.8	6.8	-112.1	-11.98
WIP-12-11-8.8	8.8	-112.7	-11.87
WIP-12-11-10.8	10.8	-112.7	-11.75
WIP-12-11-12.8	12.8	-111.4	-11.44
WIP-12-11-14.8	14.8	-114.1	-12.16
WIP-12-11-16.8	16.8	-114.1	-12.16
WIP-12-11-18.8	18.8	-114.6	-11.93
WIP-12-11-20.8	20.8	-115.8	-12.27
WIP-12-11-22.8	22.8	-116.8	-12.50
WIP-12-11-24.8	24.8	-116.2	-12.38
WIP-12-11-26.8	26.8	-116.2	-12.50
WIP-12-11-28.8	28.8	-116.8	-12.72
WIP-12-11-30.8	30.8	-116.2	-12.50
WIP-12-11-32.8	32.8	-117.4	-12.72
WIP-12-11-34.8	34.8	-118.5	-12.61

Sample	Depth, m	δD, ‰	$\delta^{18}O$, ‰
WIP-12-11-38.8	38.8	-116.2	-12.38
WIP-12-11-40.8	40.8	-115.0	-12.38
WIP-12-11-42.8	42.8	-116.2	-12.50
WIP-12-11-44.8	44.8	-116.2	-12.61
WIP-12-01-6.5	6.5	-112.1	-11.93
WIP-12-01-9	9	-113.9	-12.04
WIP-12-01-11	11	-114.4	-12.16
WIP-12-01-13	13	-113.3	-12.16
WIP-12-01-15	15	-108.0	-10.36
WIP-12-01-17	17	-116.8	-13.02
WIP-12-01-19	19	-119.1	-13.23
WIP-12-01-21	21	-117.9	-13.02
WIP-12-01-23	23	-117.9	-13.23
WIP-12-01-25	25	-117.9	-13.34
WIP-12-01-27	27	-117.9	-13.23
WIP-12-01-29	29	-117.9	-13.44
WIP-12-01-31	31	-117.9	-13.44
WIP-12-01-35	35	-116.8	-13.23
WIP-12-01-37	37	-118.5	-13.55
WIP-12-01-38.5	38.5	-119.1	-13.22
WIP-12-03-4.2	4.2	-112.1	-12.33
WIP-12-03-6.2	6.2	-115.6	-12.55
WIP-12-03-8.2	8.2	-117.9	-12.77
WIP-12-03-10.2	10.2	-119.0	-13.09
WIP-12-03-12.2	12.2	-119.1	-13.11
WIP-12-03-14.2	14.2	-117.3	-12.68
WIP-12-03-16.2	16.2	-116.6	-12.62
WIP-12-03-18.2	18.2	-117.2	-12.62
WIP-12-03-20.2	20.2	-117.2	-12.86
WIP-12-03-22.2	22.2	-119.0	-13.09
WIP-12-03-24.2	24.2	-117.8	-13.09
WIP-12-03-26.2	26.2	-117.8	-12.74
WIP-12-03-28.2	28.2	-116.6	-12.39
WIP-12-03-30.2	30.2	-118.4	-12.97
WIP-12-03-32.2	32.2	-117.9	-13.06
WIP-12-03-34.2	34.2	-118.5	-13.06
WIP-12-03-36.2	36.2	-119.1	-13.40
WIP-12-03-40.2	40.2	-119.1	-13.46
WIP-12-03-42.2	42.2	-117.4	-12.95

Sample	Depth, m	δD, ‰	$\delta^{18}O$, ‰
WIP-12-08-4.6	4.6	-114.4	-12.10
WIP-12-08-7	7	-113.9	-12.33
WIP-12-08-9	9	-115.6	-12.44
WIP-12-08-11	11	-115.6	-12.33
WIP-12-08-13	13	-117.9	-12.67
WIP-12-08-15	15	-118.5	-12.69
WIP-12-08-17	17	-118.5	-12.69
WIP-12-08-19	19	-119.1	-12.57
WIP-12-08-21	21	-117.9	-12.33
WIP-12-08-23	23	-118.5	-12.33
WIP-12-08-25	25	-117.9	-12.57
WIP-12-08-27	27	-116.2	-12.33
WIP-12-08-29	29	-115.6	-12.33
WIP-12-08-31	31	-114.4	-11.38
WIP-12-08-33	33	-115.6	-11.85
WIP-12-08-35	35	-115.6	-12.04
WIP-12-08-37	37	-115.6	-12.27
WIP-12-08-39	39	-115.6	-12.39
WIP-12-08-43	41	-115.6	-12.15
WIP-12-08-41	43	-115.0	-12.15
WIP-12-08-45	45	-116.8	-12.56
WIP-12-08-47	47	-116.8	-12.56
WIP-12-10-4.9	4.9	-112.1	-11.98
WIP-12-10-7	7	-114.4	-12.33
WIP-12-10-9	9	-114.4	-12.33
WIP-12-10-11	11	-115.0	-12.50
WIP-12-10-15	15	-114.4	-12.04
WIP-12-10-17	17	-116.8	-12.38
WIP-12-10-19	19	-118.5	-12.84
WIP-12-10-21	21	-117.4	-12.50
WIP-12-10-23	23	-119.1	-12.79
WIP-12-10-25	25	-119.1	-13.25
WIP-12-10-27	27	-119.7	-13.25
WIP-12-10-29	29	-119.1	-13.25
WIP-12-10-31	31	-118.5	-13.13
WIP-12-10-33	33	-119.1	-13.29
WIP-12-10-35	35	-117.9	-12.72
WIP-12-10-37	37	-119.1	-13.40
WIP-12-10-39	39	-118.5	-13.29
WIP-12-10-41	41	-119.1	-13.06
WIP-12-10-43	43	-116.4	-12.33

Sample	Depth, m	δD, ‰	$\delta^{18}O$, ‰
WIP-12-10-45	45	-117.6	-13.36

PAW

Sample	Date	δD, ‰	$\delta^{18}O$, ‰
SWS - South West Sands	7-Nov-11	-105.11	-11.57
SWSS - South West Sands	1-Dec-11	-113.79	-12.79
RCW 150-SWSS	5-Jun-12	-107.8	-11.29
RCW 150-SWSS	10-Jul-12	-105.8	-11.36
RCW 150 SWSS	8-Aug-12	-102.5	-9.57
RCW 150 SWSS	oct/dec 12	-112.8	-12.89
RCW 150 SWSS	5-Nov-12	-106.9	-10.60
RCW 150 SWSS	8-Jan-13	-110.4	-12.45
RCW 150- SWSS	5-Feb-13	-110.4	-12.45
RCW150-SWSS	8-Mar-13	-116.5	-13.45
RCW 150-SWSS	2-Apr-13	-116.1	-13.72
RCW 150-SWSS	7-May-13	-123.4	-14.68
RCW 150 SWSS	2-Jul-13	-119.6	-13.60
MLSB - Mildred Lake Settling Basin	7-Nov-11	-108.9	-12.54
MSLB - Mildred Lake Settling Basin	1-Dec-11	-113.13	-13.06
RCW 110 MLSB	5-Jun-12	-112.1	-11.83
RCW 110 MLSB	10-Jul-12	-109.7	-12.95
RCW 110- MLSB	8-Aug-12	-106.2	-11.67
RCW 110 MLSB	12-Sep	-106.6	-11.93
RCW 110 MLSB	6-Nov-12	-110.3	-12.27
RCW 110-MLSB	8-Mar-13	-114.4	-13.68
RCW 110-MLSB	2-Apr-13	-116.9	-14.34
RCW 110-MLSB	7-May-13	-125.3	-15.13
RCW 110-MLSB	4-Jun-13	-121.8	-13.96
RCW 110 MLSB	2-Jul-13	-120.1	-13.91
RW - Recycle Water	7-Nov-11	-110.68	-12.53
RP - Recycle Water	1-Dec-11	-112.57	-12.84
RCW 200 Recycle Pond	10-Jul-12	-112.0	-12.90
RCW 200 Recycle Pond	8-Aug-12	-105.7	-11.51
RCW 200 Recycle Pond	Sep-12	-110.5	-12.44
RCW 200 Recycle Pond	2-Oct-12	-107.8	-12.32
RCW 200-Recycle Pond	6-Nov-12	-110.6	-11.57
RCW 200 Recycle Pond	11-Dec-12	-110.4	-12.89
RCW 200-Recycle Pond	5-Feb-13	-111.6	-13.22
RCW 200-Recycle Pond	8-Mar-13	-116.7	-13.79
RCW 200-Recycle Pond	2-Apr-13	-121.9	-14.80

Sample	Date	δD, ‰	$\delta^{18}O$, ‰
Recycle Pond	7-May-13	-128.1	-15.65
RCW 200-Recycle Pond	4-Jun-13	-124.1	-14.89
RCW 230 North Mine	10-Jul-12	-111.1	-12.68
RCW 230- North Mine Train2	8-Aug-12	-106.2	-11.56
RCW 230 NMT	12-Sep	-107.1	-11.93
RCW 230 NMT	2-Oct-12	-110.6	-11.56
RCW 230- North Mine Train 2	8-Nov-12	-108.0	-12.23
RCW 230- North Mine train 2	11-Dec-12	-110.4	-13.00
RCW 230- North Mine Train 2	8-Jan-13	-111.6	-13.33
RCW 230- North Mine train 2	5-Feb-13	-112.8	-13.44
RCW 230- North mine train	8-Mar-13	-116.9	-14.01
RCW 230- North mine train	2-Apr-13	-123.6	-14.93
RCW 230-North Mine Train 2	7-May-13	-128.7	-15.40
RCW 230- North Mine Train	4-Jun-13	-124.1	-14.99
RCW 230 NMT	2-Jul-13	-122.7	-14.53
WIP - West in Pit	7-Nov-11	-107.85	-11.94
WIP - West in Pit	1-Dec-11	-110.6	-11.28
WIP June 5 2012	5-Jun-12	-111.81	-12.31
RCW 010 WIP	10-Jul-12	-111.4	-12.41
RCW 010 WIP	8-Aug-12	-108.0	-11.45
RCW 010-WIP	6-Nov-12	-109.7	-12.49
RCW 010-WIP	8-Mar-13	-112.6	-12.33
RCW 010-WIP	2-Apr-13	-112.6	-12.44
RCW 010- WIP	7-May-13	-116.0	-13.15
SEP - South East Pit	7-Nov-11	-99.68	-10.58
SEP - South East Pit	1-Dec-11	-114.3	-11.54
RCW 220 SEP	10-Jul-12	-111.0	-12.20
RCW 220 SEP	8-Aug-12	-101.0	-10.01
RCW 220 SEP	2-Oct-12	-102.6	-11.02
RCW 220-SEP	6-Nov-12	-119.4	-13.25
RCW-220- SEP	11-Dec-12	-116.3	-13.22
RCW 220 SEP	8-Jan-13	-117.5	-13.33
RCW 220-SEP	2-Apr-13	-123.0	-14.25
RCW 220-SEP	4-Jun-13	-119.4	-12.30
RCW 220 SEP	2-Jul-13	-115.8	-13.62
RCW 130-SWIP	11-Dec-12	-108.0	-11.78
RCW 130 SWIP	8-Jan-13	-108.6	-12.00
RCW 130-SWIP	2-Apr-13	-116.5	-13.22
RCW 130-SWIP	8-Mar-13	-113.6	-12.99
RCW 130-SWIP	7-May-13	-123.6	-14.62
RCW 130- SWIP	4-Jun-13	-123.5	-14.16

Sample	Date	δD, ‰	$\delta^{18}O$, ‰
RCW 130 SWIP	2-Jul-13	-121.0	-14.59
RCW 020-Tailings Slurry	8-Jan-13	-114.8	-12.79
RCW 020 Tailings Slurry	2-Jul-13	-122.1	-14.18
RCW 120-North Mine Ditch	5-Jun-12	-116.0	-13.01
RCW 120 North Mine Ditch	10-Jul-12	-125.8	-15.44
RCW 120-North Mine Ditch	8-Aug-12	-119.3	-13.77
RCW 120 NMD	12-Sep	-112.5	-13.91
RCW 120-North Mine Ditch	2-Oct-12	-118.7	-14.10
RCW 120-North Mine Ditch	8-Nov-12	-138.3	-16.49
RCW 120-North Mine Ditch	2-Apr-13	-169.1	-21.44
RCW 120-NMD	7-May-13	-156.9	-19.18
RCW 120 NMD	4-Jun-13	-139.2	-15.92
RCW 010-WIP	4-Jun-13	-133.9	-16.12
RCW 200-SEP	7-May-13	-135.1	-16.08
RCW 300 Effluent Pond	10-Jul-12	-104.9	-14.03
RCW 300 Effluent Pond	8-Aug-12	-106.8	-14.43
RCW 300-Effluent Pond	12-Sep	-103.6	-14.29
RCW 300-Effluent Pond	6-Nov-12	-112.8	-14.67
RCW 300 Effluent Pond	11-Dec-12	-107.5	-14.63
RCW 300 Effluent Pond	8-Jan-13	-106.8	-15.10
RCW 300 Effluent Pond	5-Feb-13	-112.2	-14.77
RCW 300-Effluent Pond	8-Mar-13	-114.9	-15.50
RCW 300-Effluent Pond	2-Apr-13	-114.9	-15.76
Effluent Pond	7-May-13	-121.3	-16.09

Sandhill Fen

Sample	Date	δD, ‰	$\delta^{18}O$, ‰
Fen 31-04	30-Sep-12	-125.9	-14.55
Fen 11-11	30-Sep-12	-131.1	-15.48
Fen 55-07	30-Sep-12	-130.0	-15.09
Fen 20-09	30-Sep-12	-112.7	-12.64
Fen 39-09	29-Sep-12	-112.9	-12.30
Fen 42-06	30-Sep-12	-115.2	-12.84
Fen 43-09	30-Sep-12	-114.4	-12.86
Fen 57-09	30-Sep-12	-123.1	-13.71
SH-GW-53-04	16-May-13	-134.4	-15.68
SH-GW-63-03	16-May-13	-121.3	-14.45
SH-GW-46-04	16-May-13	-125.1	-14.65
SH-GW-30-3.5	16-May-13	-156.9	-19.54

Sample	Date	δD, ‰	$\delta^{18}O$, ‰
SH-GW-58-06	16-May-13	-122.9	-14.45
SH-GW-44-08	16-May-13	-119.9	-13.55
SH-GW-52-04	16-May-13	-128.3	-15.08
SH-GW-57-05	16-May-13	-116.0	-12.99
SH-GW-19-07	16-May-13	-136.7	-16.10
SH-GW-20-09	16-May-13	-115.4	-13.35
SH-GW-11-11	25-Apr-13	-134.6	-15.87
SH-GW-45-1.5	13-May-13	-131.0	-15.76
SH-GW-43-09	16-May-13	-115.8	-12.83
SH-GW-18-04	16-May-13	-134.0	-16.41
SH-GW-26-04	16-May-13	-125.7	-14.80
SH-GW-48-09	16-May-13	-123.4	-14.26
SH-GW-20-09	25-Apr-13	-115.2	-12.97
SH-GW-20-07	16-May-13	-123.6	-14.81
SH-GW-34-04	16-May-13	-135.5	-16.50
SH-GW-54-08	16-May-13	-130.5	-15.51
SH-GW-19-07	25-Apr-13	-138.0	-16.81
SH-GW-43-05	16-May-13	-125.0	-15.06
SH-GW-43-07	16-May-13	-120.4	-14.05
SH-GW-57-09	16-May-13	-125.5	-15.11
SH-GW-41-05	16-May-13	-120.0	-14.24
SH-GW-39-09	16-May-13	-115.1	-13.05
SH-GW-07-3.5	16-May-13	-145.6	-18.25
SH-GW-06-04	16-May-13	-131.0	-15.87
SH-GW-41-07	16-May-13	-119.1	-13.22
SH-GW-20-07	25-Apr-13	-122.0	-13.77
SH-GW-63-06	25-Apr-13	-114.4	-12.45
SH-GW-46-04	25-Apr-13	-119.1	-13.44
SH-GW-44-04	16-May-13	-125.1	-15.20
SH-GW-40-02	16-May-13	-122.7	-14.21
SH-GW-36-3.5	16-May-13	-117.3	-13.88
SH-GW-54-04	16-May-13	-126.8	-15.09
SH-GW-40-04	16-May-13	-117.9	-13.77
SH-GW-47-04	16-May-13	-117.3	-13.33
SH-GW-03-03	15-May-13	-128.2	-15.66
SH-GW-35-1.5	16-May-13	-135.1	-14.91
SH-GW-11-11	15-May-13	-134.0	-16.08
SH-GW-63-06	16-May-13	-113.8	-12.62
SH-GW-04-04	15-May-13	-144.7	-17.71
SH-GW-18-02	16-May-13	-144.7	-17.93
SH-GW-39-07	16-May-13	-120.0	-14.41
SH-GW-31-02	16-May-13	-117.7	-13.57

Sample	Date	δD, ‰	$\delta^{18}O$, ‰
SH-GW-57-07	16-May-13	-117.9	-13.47
SH-GW-61-03	16-May-13	-120.2	-14.10
SH-GW-38-02	16-May-13	-133.4	-15.88
SH-GW-39-05	16-May-13	-123.0	-14.52
SH-GW-37-02	16-May-13	-119.9	-13.50
SH-GW-11-09	15-May-13	-124.6	-14.17
SH-GW-35-04	16-May-13	-116.3	-13.05
SH-GW-01-03	16-May-13	-121.0	-13.77
SH-GW-42-06	16-May-13	-119.3	-13.88
SH-GW-45-04	16-May-13	-122.2	-14.10
SH-GW-54-06	16-May-13	-132.8	-15.75
SH-GW-42-03	16-May-13	-119.2	-13.68
SH-GW-28-04	16-May-13	-127.1	-15.17
SH-GW-02-05	16-May-13	-130.5	-15.68
SH-GW-31-04	16-May-13	-128.2	-15.37
SH-GW-17-04	16-May-13	-138.5	-16.82
SH-GW-04-6	15-May-13	-127.1	-15.08
SH-GW-31-02	16-May-13	-182.7	-23.35
SH-GW-15B-Clay	25-Apr-13	-121.1	-13.68
SH-GW-15C-Sand	16-May-13	-112.8	-12.43
SH-GW-15B-Clay	16-May-13	-127.1	-15.06
Fen sump	1-Dec-11	-127.3	-13.96
Fen sump	14-Jun-12	-124.34	-14.64
Fen Sump	30-Jul-12	-130.0	-15.20
Fen Sump	15-Aug-12	-127.0	-14.99
Fen Sump	27-Nov-12	-128.4	-14.98
Fen Sump	18-Dec-12	-125.8	-14.66
Fen Sump	8-Jan-13	-124.6	-14.61
Fen Sump	1-Feb-13	-125.8	-14.77
Fen Sump	12-Feb-13	-127.9	-14.40
Fen Sump	27-Feb-13	-126.2	-14.49
Fen Sump	17-Mar-13	-127.2	-14.40
Fen Sump	25-Apr-13	-138.4	-16.58
Fen Sump	7-May-13	-139.8	-16.74
Fen Sump	16-May-13	-138.1	-16.41
Fen Sump	22-May-13	-139.2	-16.54
Fen Sump	6-Jun-13	-138.3	-16.70
Fen Sump	24-Jun-13	-131.8	-15.22
Fen GW BGC 08 05C June 13 2012	13-Jun-12	-114.01	-11.99
Fen GW BGC 08 05D June 13 2012	13-Jun-12	-117.61	-12.86
Fen GW BGC 08 08D June 14 2012	14-Jun-12	-121.81	-13.84
Fen GW BGC 08 08B June 13 2012	13-Jun-12	-117.57	-13.3

Sample	Date	δD, ‰	$\delta^{18}O$, ‰
Fen GW BGC 08 04C June 13 2012	13-Jun-12	-117.88	-12.9
Fen GW BGC 08 04D June 14 2012	14-Jun-12	-124.16	-13.71
Fen GW BGC 08 02C June 13 2012	13-Jun-12	-114.61	-12.48
Fen GW BGC 08 02D June 13 2012	13-Jun-12	-119.42	-12.81
Fen GW BGC 08 10D June 13 2012	13-Jun-12	-116.36	-12.66
Fen GW BGC 08 06A June 13 2012	13-Jun-12	-117.02	-12.89
Surface water by P15	16-May-13	-141.5	-15.57
FenPond Surface Water	13-May-13	-146.9	-17.53
Fen Surface Water by P15	25-Apr-13	-155.2	-18.92

SWSS

Sample	Date	δD, ‰	$\delta^{18}O$, ‰
SWSS-C32-P10-07	29-Sep-12	-130.0	-15.38
SWSS-C32-P11-27	29-Sep-12	-129.4	-15.28
SWSS-C32-P5-08	29-Sep-12	-118.8	-13.17
SWSS-C32-P09-8	29-Sep-12	-122.8	-14.14
SWSS-C32-P43-10	29-Sep-12	-120.4	-13.81
SWSS-C32-P8-7	29-Sep-12	-119.2	-13.38
SWSS-C32-P03-15	29-Sep-12	-152.0	-19.12
SWSS-C32-P04-8	29-Sep-12	-121.6	-14.09
SWSS-C32-P07-21	29-Sep-12	-142.5	-17.99
SWSS-C32-P12-6	29-Sep-12	-119.7	-13.34
SWSS-C32-P02-7	29-Sep-12	-142.6	-18.07
SWSS-C32-P13-9	29-Sep-12	-122.7	-14.22
SWSS-C32-39-7	25-Jul-12	-125.2	-14.68
SWSS-C32-48-8	25-Jul-12	-138.2	-16.52
SWSS-C32-52-5	25-Jul-12	-121.9	-13.81
SWSS-C32-11-27	23-Jul-12	-130.0	-15.55
SWSS-C32-37-8	25-Jul-12	-130.6	-15.64
SWSS-C32-44-5.5	25-Jul-12	-130.6	-15.76
SWSS C32-52-4	25-Jul-12	-145.1	-17.46
SWSS-C32-37-7	25-Jul-12	-131.7	-15.53
SWSS-C32-46-10	25-Jul-12	-121.7	-14.11
SWSS-C32-58-6	25-Jul-12	-121.1	-14.22
SWSS-C32-45-5	25-Jul-12	-124.1	-14.39
SWSS-C32-01-3	25-Jul-12	-124.5	-14.53
SWSS-C32-47-10	25-Jul-12	-122.1	-14.31
SWSS-C32-48-10	25-Jul-12	-129.3	-15.54
SWSS-C32-41-7	25-Jul-12	-119.1	-13.64
SWSS-C32-40-6.5	25-Jul-12	-126.3	-14.49
SWSS-C32-38-7	24-Jul-12	-125.7	-14.47

Sample	Date	δD, ‰	$\delta^{18}O$, ‰
SWSS-C32-47-8	25-Jul-12	-124.6	-14.51
SWSS-C32-15-15WT	24-Jul-12	-131.7	-15.76
SWSS-C32-13-6	24-Jul-12	-123.3	-14.40
SWSS-C32-05-08	24-Jul-12	-119.7	-13.72
SWSS-C32-07-15	24-Jul-12	-119.1	-13.49
SWSS-C32-15-7	24-Jul-12	-155.3	-19.38
SWSS-C32-15-24	24-Jul-12	-120.9	-13.89
SWSS-C32-08-7	24-Jul-12	-118.7	-13.66
SWSS-C32-09-8	24-Jul-12	-123.4	-14.32
SWSS-C32-04-6	24-Jul-12	-121.1	-14.10
SWSS-C32-02-7	24-Jul-12	-143.6	-18.41
SWSS-C32-12-6	24-Jul-12	-118.7	-13.33
SWSS-C32-4-8	24-Jul-12	-121.7	-14.21
SWSS-C32-10-7	24-Jul-12	-130.6	-15.76
SWSS-C32-11-23	24-Jul-12	-118.7	-13.55
SWSS-C32-15-33	24-Jul-12	-141.2	-17.42
SWSS-C32-3-9	24-Jul-13	-122.8	-14.43
SWSS-C32-3-8	24-Jul-12	-120.5	-13.77
SWSS-C32-02-5	25-Jul-12	-124.6	-14.54
SWSS-C32-03-6	24-Jul-12	-121.1	-13.66
SWSS-C32-11-15	24-Jul-12	-119.9	-13.66
SWSS-C32-11-7	24-Jul-12	-156.6	-19.85
SWSS-C46-P16-4	29-Sep-12	-122.8	-14.09
SWSS-C46-P17-12	30-Sep-12	-151.4	-19.22
SWSS-C46-P22-8	30-Sep-12	-123.9	-14.11
SWSS-C46-P19-9	29-Sep-12	-122.0	-14.09
SWSS-C46-P23-19	29-Sep-12	-120.8	-14.09
SWSS-C46-P21-7	29-Sep-12	-117.9	-13.89
SWSS-C46-P18-7	29-Sep-12	-121.5	-14.00
SWSS-C46-23-7	26-Jul-12	-126.4	-14.44
SWSS-C46-19-5	26-Jul-12	-120.5	-13.71
SWSS-C46-23-5	26-Jul-12	-155.3	-19.44
SWSS-C46-23-12	26-Jul-12	-130.0	-15.00
SWSS -C46-16-2	26-Jul-12	-125.4	-14.46
SWSS-C46-17-4	26-Jul-12	-122.2	-14.06
SWSS-C46-23-19	26-Jul-12	-123.4	-14.17
SWSS-C46-21-7	26-Jul-12	-121.0	-13.60
SWSS-C46-17-12	26-Jul-12	-151.2	-19.39
SWSS-C46-7-6	26-Jul-12	-122.1	-14.20
SWSS-C46-19-7	26-Jul-12	-122.7	-13.91
SWSS-C46-19-16	26-Jul-12	-143.8	-17.77
SWSS-C46-18-5	26-Jul-12	-122.0	-13.76

Sample	Date	δD, ‰	$\delta^{18}O$, ‰
SWSS-C46-23-25	25-Jul-12	-147.3	-18.70
SWSS-C46-18-7	26-Jul-12	-123.4	-14.28
SWSS-C46-19-9	26-Jul-12	-123.4	-14.23
SWSS-C46-22-8	26-Jul-12	-123.4	-13.99
SWSS-C46-22-6	26-Jul-12	-122.3	-13.99
SWSS-C46-Drain-QC3	26-Jun-12	-124.0	-14.17
SWSS-C46-Drain-QC3	7-Jul-12	-122.9	-14.11
SWSS-C46-Drain-QC3	26-Jul-12	-122.9	-14.22
SWSS-C46-Drain-QC3	13-Aug-12	-121.7	-14.21
SWSS-C46 Drainage Channel	26-Jun-12	-118.2	-13.56
SWSS-C46-Channel-Upstream	7-Jul-12	-123.6	-14.51
SWSS-C46-Drainage Channel-Upstream	26-Jul-12	-118.6	-13.42
SWSS-C46-Channel-upstream	13-Aug-12	-117.5	-13.33
Bench A Drain LA3 SWSS June 11 2012	11-Jun-12	-123.96	-14.35
SWSS-C32-Drain-Bench A-LA3	26-Jun-12	-123.1	-14.77
SWSS-C32-Drain-Bench A-LA3	7-Jul-12	-123.3	-14.33
SWSS-C32-Drain-Bench A-LA3	25-Jul-12	-122.0	-13.65
SWSS-C32-Drain-Bench A-LA3	13-Aug-12	-122.3	-14.32
SWSS Drain MA1 June 11 2012	11-Jun-12	-120.41	-13.82
SWSS-C32-Drain-Bench A-MA1	26-Jun-12	-122.2	-14.17
SWSS-C32-Bench A Drain MA1	25-Jul-12	-122.3	-14.11
SWSS-C32-Drain-Bench A-MA1	8-Aug-12	-121.7	-14.10
Bench B Drain LB3 SWSS June 11 2012	11-Jun-12	-125.38	-14.66
SWSS-C32-Drain-Bench B-LB3	26-Jun-12	-125.8	-14.72
SWSS-C32-Drain-Bench B-LB3	7-Jul-12	-125.8	-14.85
SWSS-C32-Bench B Drain-LB3	25-Jul-12	-123.3	-14.03
SWSS-C32-Drain-Bench B-LB3	13-Aug-12	-123.4	-14.54
SWSS Drain MB1 June 11 2012	11-Jun-12	-121.43	-14.05
SWSS-C32-Drain-Bench B-MB1	26-Jun-12	-122.3	-14.00
SWSS-C32-Bench B Drain-MB1	25-Jul-12	-122.2	-13.75
SWSS-C32-Drain-Bench B-MB1	13-Aug-12	-121.7	-14.10
SWSS LC3 Algae June 11 2012	11-Jun-12	-127.6	-14.93
Bench C Drain LC3 SWSS June 11 2012	11-Jun-12	-127.6	-14.93
SWSS-C32-Drain-Bench C-LC3	26-Jun-12	-127.0	-14.44
SWSS-C32-Drain-Bench C-LC3	7-Jul-12	-128.7	-15.32
SWSS C32-Bench C Drain-LC3	25-Jul-12	-128.2	-14.88
SWSS-C32-Drain-Bench C-LC3	13-Aug-12	-127.6	-14.66
SWSS Drain MC1 June 11 2012	11-Jun-12	-123.67	-14.24
SWSS-C32-Drain-Bench C-MC1	26-Jun-12	-123.3	-14.22
SWSS-C32-Bench C Drain-MC1	25-Jul-12	-123.2	-13.88
SWSS-C32-Drain-Bench C-MC1	13-Aug-12	-123.4	-14.10

South Bison Hills and W1

Sample	Date	δD, ‰	$\delta^{18}O$, ‰
W1 Dump 200-10m	26-Jul-12	-150.3	-19.06
W1 Dump 201-30	26-Jul-12	-148.7	-19.11
Peat Pond 109W	30-Sep-12	-142.9	-17.06
Peat Pond 103-3	30-Sep-12	-147.9	-17.99
Peat Pond 115-7	30-Sep-12	-149.9	-18.51
Bills Lake 005-W	29-Sep-12	-133.6	-16.86
Bills Lake 18-W	29-Sep-12	-142.8	-17.88
SBH 136-30	29-Sep-12	-143.4	-18.44
Peat Pond 103-W	30-Sep-12	-140.2	-17.30
SBH-005-2A	27-Jul-12	-140.1	-17.41
SBH-005-3	23-Jul-12	-146.5	-18.51
SBH-136-10	23-Jul-12	-147.1	-18.73
30D-103-W	23-Jul-12	-142.8	-17.68
30D-103-2	23-Jul-12	-145.7	-17.79
SBH-015-1	23-Jul-12	-116.0	-11.93
30D-131-10	23-Jul-12	-146.1	-17.88
SBH-004-5	23-Jul-12	-147.1	-18.55
SBH-135-30	23-Jul-12	-144.5	-18.36
SBH-015-W	23-Jul-12	-113.4	-10.84
SBH-005-3A	23-Jul-12	-145.1	-18.03
SBH-005-W	23-Jul-12	-142.2	-17.71
SBH-004-W	23-Jul-12	-144.0	-18.14
SBH-103-5	23-Jul-12	-142.5	-17.63
SBH-119-7	23-Jul-12	-159.2	-20.15
SBH-004-3	23-Jul-12	-140.0	-17.41
SBH-103-W2	23-Jul-12	-144.4	-18.08
30D-005-W3	23-Jul-12	-135.1	-16.30
SBH-005-W2	23-Jul-12	-146.1	-18.14
SBH- SP011730-11	31-Aug-12	-146.0	-18.41
SBH- SP011730-10-Glass	31-Aug-12	-145.6	-17.66
SBH- SP011730-10-Plastic	31-Aug-12	-140.7	-17.40
SBH-SP011730-01	31-Aug-12	-147.1	-19.01
SBH-SP011730-20	31-Aug-12	-149.9	-19.14
PP outlet 4 April 2012	4-Apr-12	-164.93	-20.18
PP Inlet 4 April 2012	4-Apr-12	-161	-20.18
Peat Pond June 11 2012	11-Jun-12	-100.51	-8.54
Peat Pond	26-Jun-12	-98.9	-7.48
Peat Pond	9-Jul-12	-98.3	-7.85
Peat Pond	23-Jul-12	-97.5	-7.52
Peat Pond	14-Aug-12	-93.2	-6.81

Sample	Date	δD, ‰	$\delta^{18}O$, ‰
Bills Lake June 11 2012	11-Jun-12	-115.71	-10.35
Bills Lake	26-Jun-12	-112.9	-10.38
Bills Lake	9-Jul-12	-111.7	-11.15
Bills Lake	23-Jul-12	-109.1	-10.18
Bills Lake	14-Aug-12	-102.7	-9.13
Golden Pond 24 April 2012	24-Apr-12	-162.99	-20.08
Golden Pond June 11 2012	11-Jun-12	-99.1	-8.18
Golden Pond	9-Jul-12	-101.4	-8.51
Golden Pond	23-Jul-12	-96.5	-7.37
Golden Pond	14-Aug-12	-90.2	-6.48
SBH D1 Interflow	10-Jul-12	-144.4	-18.47
SBH D2 Interflow	10-Jul-12	-140.3	-17.60
SBH-D3-Interflow #3	10-Jul-12	-140.5	-17.58
SBH-D3-Interflow	21-Jun-12	-144.0	-17.79
SBH-Interflow-D3	10-Jul-12	-145.1	-18.36
SBH-Interflow D3	10-Jul-12	-144.5	-18.03
SBH-Interflow D3	20-Jun-12	-147.8	-18.81
SBH-Interflow D3	21-Jun-12	-143.7	-17.93
SBH-Interflow-D2	12-Jul-12	-137.7	-17.20
D1 Interflow	10-May-13	-158.3	-19.88
D1 Interflow	29-May-13	-151.9	-19.32
D1 Interflow	27-May-13	-150.8	-19.01
D3 Interflow	24-May-13	-158.9	-20.25
D2 Interflow	22-May-13	-155.4	-19.53
D3 Interflow	27-May-13	-158.3	-20.15
D1 Interflow	22-May-13	-148.7	-18.59
D2 Interflow	16-May-13	-158.3	-20.05
D2 Interflow	27-May-13	-154.8	-19.32
D3 Interflow	22-May-13	-158.3	-20.05
D2 Interflow	29-May-13	-153.7	-19.12
D1 Interflow	16-May-13	-148.5	-18.70
D1 Int	7-Jun-13	-146.6	-18.58
D2 Int	7-Jun-13	-150.8	-19.13
D1 Int	21-Jun-13	-147.6	-18.94
D3 Int	10-Jul-13	-142.7	-18.24
D3 Int	17-Jul-13	-145.2	-18.55
D3 Int	6-Jun-13	-156.7	-19.92
D2 Int	17-Jul-13	-141.5	-18.10
D1 Int	9-Jul-13	-145.0	-18.53
D1 Int	3-Jul-13	-147.7	-18.81
D3 Int	3-Jun-13	-140.1	-18.11
D1 Int	17-Jul-13	-145.5	-18.29

Sample	Date	δD, ‰	$\delta^{18}O$, ‰
D2 Int	3-Jun-13	-144.9	-18.29
D2 int	9-Jul-13	-141.3	-17.55
D2 Int	21-Jun-13	-144.9	-18.82

Base Mine Lake/WIP

Sample	Date	δD, ‰	$\delta^{18}O$, ‰
BML12-MW02	3-Oct-12	-153.4	-19.02
BML12-MW05	16-Oct-12	-178.8	-24.17
BML12-MW17	30-Sep-12	-144.6	-18.13
BML12-MW20	4-Oct-12	-157.2	-20.20
BML12-MW14	4-Oct-12	-157.2	-20.42
BML12-MW14	1-Oct-12	-157.1	-19.87
BML12-MW01	3-Oct-12	-145.6	-17.81
BML12-MW03	2-Oct-12	-146.5	-19.03
BML12-MW04	2-Oct-13	-147.0	-19.14

Precipitation

Sample	Date Sampled	δD, ‰	$\delta^{18}O$, ‰
Rain C32 May 16 2012	16-May-12	-109.8	-11.3
Precip SWSS Cell 32 June 11 2012	11-Jun-12	-123.6	-13.54
Precip SWSS Cell 32 June 12 2012	12-Jun-12	-126.4	-14.99
C32 Precipitation	20-Jun-12	-130.6	-16.09
SWSS-C32-Precip	25-Jun-12	-81.3	-11.33
SWSS-C32-Precipitation	7-Jul-12	-126.9	-16.09
SWSS-C32-Precip	24-Jul-12	-122.8	-14.99
SWSS-C32-Precip	9-Aug-12	-92.0	-10.35
SWSS-C32-Precip	31-Aug-12	-98.1	-11.81
C32 Precip	9-Jul-13	-121.5	-15.76
Precip Ucell June 4 2012	4-Jun-12	-127.6	-16.51
Ucell- Precipitation	20-Jun-12	-143.5	-18.07
Ucell Precip	25-Jun-12	-82.4	-11.33
Ucell Precip	10-Jul-12	-128.8	-16.78
Ucell- Precipitation	12-Jul-12	-78.0	-9.06
Ucell-Precip	20-Jul-12	-139.4	-18.30
Ucell-Precip	9-Aug-12	-106.3	-12.71
Ucell Precip	23-Aug-12	-90.9	-10.49
Ucell Precip	7-Sep-12	-105.5	-13.82
Ucell Precip	18-Sep-12	-124.1	-16.17
Precip 30-T May 16 2012	16-May-12	-114.0	-15.04
Precip 30T May 29 2012	29-May-12	-158.1	-20.5

Sample	Date	δD, ‰	$\delta^{18}O$, ‰
Precip 30T June 11 2012	11-Jun-12	-130.0	-15.5
Precip 30T June 12 2012	12-Jun-12	-121.6	-14.87
30T-Precip	21-Jun-12	-149.4	-18.44
30T-Precip	25-Jun-12	-75.7	-9.62
30T Precip	9-Jul-12	-131.7	-17.30
30T Precip	23-Jul-12	-129.4	-16.31
30T-Precip	2-Aug-12	-114.0	-14.43
30T-Precip	9-Aug-12	-105.6	-12.26
30T-Preciptiation	14-Aug-12	-95.6	-10.82
30T Precip	31-Aug-12	-95.1	-11.38
30T Precip	12-Sep-12	-113.4	-14.94
South Hills 30W	2-Mar-12	-201.9	-26.03
Capping St Aurora Site	7-Mar-12	-190.5	-24.07
C32 Station Snow	5-Mar-12	-200.2	-25.47
Coke Beach Snow	6-Mar-12	-197.1	-25.7
U Cell Snow	28-Feb-12	-198.9	-25.64
Sandhill Fen Snow	29-Feb-12	-189.3	-24.11
W1 Dump Snow	5-Mar-12	-196.7	-25.36
C46 Station Snow	5-Mar-12	-205.8	-26.88
Fort Hills North Snow	7-Mar-12	-185.8	-23.48
SIB Snow	6-Mar-12	-202.2	-26.19
30T Snow	21-Mar-12	-172.8	-22.17
Snow-Jack Pine	9-Jan-13	-201.7	-26.25
Snow-Coke Beach	9-Jan-13	-205.2	-26.92
Ucell-Precip	9-Jan-13	-211.3	-27.74
Snow-Fort Hills Aurora	10-Jan-13	-201.6	-26.52
Snow-W1	20-Feb-13	-215.9	-28.17
Snow-SBH	20-Feb-13	-216.5	-28.05
Snow-Fort Hills Aurora	21-Feb-13	-187.0	-24.14
Snow-SWSS-C46	25-Feb-13	-216.5	-28.16
Snow-SWSS-C32	25-Feb-13	-211.8	-27.72
Snow-Ucell	26-Feb-13	-205.4	-26.61
Snow-Sulfur Blocks	26-Feb-13	-230.5	-30.28
Snow-Coke Beach	12-Mar-13	-211.9	-27.63
Snow-C32	12-Mar-13	-203.1	-26.10
Snow-Fen	20-Mar-13	-243.3	-31.50
Snow-Ucell	12-Mar-13	-202.8	-26.45
Snow-SBH	14-Mar-13	-220.3	-28.35
Snow-C46	12-Mar-13	-210.4	-27.51
Snow-Jack Pine	12-Mar-13	-199.3	-25.39
Snow-W1	12-Mar-13	-197.3	-25.64

Sample	Date	δD, ‰	$\delta^{18}O$, ‰
Snow-Fort Hills	26-Mar-13	-217.2	-28.07
Snow-Aurora	26-Mar-13	-210.2	-27.30

Mildred Lake/Beaver Creek

Sample	Date Sampled	δD, ‰	$\delta^{18}O$, ‰
MLR PI 23-May-13	13-May-13	-143.5	-17.39
MLR PI 30-May-13	30-May-13	-143.7	-17.62
MLR PI 6-Jun-13	6-Jun-13	-144.2	-17.62
MLR PI 22-Jun-13	22-Jun-13	-143.8	-18.91
MLR PI 5-Jul-13	5-Jul-13	-142.0	-17.48
MLR PI 8-Jul-13	8-Jul-13	-140.8	-17.36
Mildred Lake	15-Aug-12	-140.0	-17.34
Mildred Lake	19-May-13	-143.5	-17.98
BCR PI 23-May-13	23-May-13	-154.8	-18.84
BCR PI 30-May-13	30-May-13	-152.1	-18.24
BCR PI 6-Jun-13	6-Jun-13	-151.5	-18.12
BCR PI 8-Jul-13	8-Jul-13	-138.5	-16.75

Soil Samples

Sample Name	Date	Soil	Depth [ft]	Depth [m]	δD, ‰	$\delta^{18}O$, ‰
Fen P01 30cm	27-Jun-12	Peat		0.30	-136.8	-15.45
Fen P1 60 cm	27-Jun-12	Tailings		0.60	-126.2	-14.79
Fen P01 12 ft	1-Jul-12	Tailings	12	3.66	-123.9	-13.79
Fen P2 11ft	1-Jul-12	Moist Sand	11	3.36	-120.7	-12.94
Fen P2 18 ft	1-Jul-12	Sticky Sand	18	5.49	-116.9	-12.01
Fen P03 5 ft	1-Jul-12	Wet/Sticky sand	5	1.53	-130.1	-14.90
Fen P03 11ft	1-Jul-12	Sticky Sand	11	3.36	-132.4	-15.03
Fen P04 3 ft	1-Jul-12	Moist Sand	3	0.92	-128.5	-14.65
Fen P04 15 ft	1-Jul-12	Wet/Sticky sand	15	4.58	-142.4	-16.36
Fen P4 21 Feet	1-Jul-12	Wet/Sticky sand	21	6.41	-137.5	-15.80
Fen P06 30 cm	28-Jul-12	Peat		0.30	-140.9	-15.93
Fen P06 1m	28-Jul-12	Peat		1.00	-148.6	-17.74
Fen P06 1.1m	28-Jul-12	Peat/Clay		1.10	-143.8	-17.37
Fen P06 1.5 m	28-Jul-12	Clay		1.50	-138.2	-16.56
Fen P06 1.7m	28-Jul-12	Moist Sand		1.70	-136.4	-16.65
Fen P06 2.1 m	28-Jul-12	Tailings		2.10	-137.7	-16.56
Fen P06 13ft	28-Jul-12	Tailings	13.00	3.96	-131.2	-15.75
Fen P07 30 cm	8-Jul-12	Moist Sand		0.30	-139.8	-16.36
Fen P07 60 cm	8-Jul-12	Moist Sand		0.60	-136.8	-15.38
Fen P07 1 m	8-Jul-12	Moist Sand		1.00	-138.0	-16.16
Fen P07 1.5m	8-Jul-12	Moist Sand		1.50	-134.2	-15.90
Fen P07 2.0 m	8-Jul-12	Clay		2.00	-137.2	-16.00
Fen P07 2.5 m	8-Jul-12	Wet/Sticky sand		2.50	-136.3	-16.00
Fen P07 3 m	8-Jul-12	Sticky Sand		3.00	-133.5	-15.70
Fen P07 3.7 m	8-Jul-12	Sticky Sand/Tailings		3.70	-135.3	-16.01
Fen P07 4.2 m	8-Jul-12	Tailings		4.20	-134.8	-16.00
Fen p09 2 ft	2-Jul-12	Eng Coarse Sand	2	0.61	-131.8	-13.95
Fen P09 9 ft	2-Jul-12	Moist Sand	9	2.75	-125.7	-14.03
Fen P10 1 ft	2-Jul-12	Eng Coarse Sand	1	0.31	-128.5	-13.47
Fen P10 90 cm	2-Jul-12	Moist Sand		0.90	-127.9	-14.38
Fen P09 8 ft	2-Jul-12	Moist Sand	8	2.44	-122.1	-14.06
Fen P10 15 ft	2-Jul-12	Moist Sand	15	4.58	-120.7	-13.27
Fen P11 1 ft	2-Jul-12	Coarse Sand	1	0.31	-141.2	-15.91
Fen P11 70 cm	2-Jul-12	Moist Sand		0.70	-130.1	-15.01
Fen P11 8 ft	2-Jul-12	Moist sand	8	2.44	-131.3	-14.83
Fen P11 12 ft	2-Jul-12	coarse sand	12	3.66	-117.6	-12.86
Fen P11 18 ft	2-Jul-12	Moist Sand	18	5.49	-118.4	-12.86
Fen P11 24 ft	2-Jul-12	Moist Sand	24	7.32	-132.7	-14.93

Sample Name	Date	Soil	Depth [ft]	Depth [m]	δD, ‰	$\delta^{18}O$, ‰
Fen P11 30 ft	2-Jul-12	Wet Sand	30	9.14	-133.3	-16.25
Fen P11 36 ft	30-Jul-12	Wet Sand	36	11	-134.4	-15.94
Fen P11 40 cm	30-Jul-12	Moist Sand		0.40	-128.0	-15.01
Fen P11 1.0m	30-Jul-12	Moist Sand		1.00	-133.8	-15.64
Fen P11 1.5m	30-Jul-12	Moist Sand		1.50	-137.0	-16.50
Fen P11 1.9m	30-Jul-12	Moist Fine Sand		1.90	-133.3	-15.95
Fen P12 2 ft	2-Jul-12	Moist coarse sand	2	0.61	-157.2	-18.72
Fen P12 8 ft	2-Jul-12	Loose Sand	8	2.44	-124.1	-14.11
Fen P12 15 ft	2-Jul-12	Moist Sand	15	4.58	-118.2	-12.51
Fen P12 21 ft	2-Jul-12	Moist Sand	21	6.41	-122.0	-12.94
Fen P18 9 ft	27-Jun-12	Sand	9	2.75	-142.7	-17.06
Fen P18 15 ft	27-Jun-12	sticky sand	15	4.58	-138.3	-16.49
Fen P19 2.5 feet	27-Jun-12	Moist Sand	2.5	0.76	-124.4	-13.50
Fen P19 9 ft	27-Jun-12	Moist Sand	9	2.75	-121.0	-13.01
Fen P26 30 cm	29-Jul-12	Dark Loose Sand		0.30	-126.3	-14.66
Fen P26 0.6m	29-Jul-12	Moist Fine Sand		0.60	-128.0	-14.72
Fen P26 80cm	29-Jul-12	loose Sand		0.80	-135.9	-15.90
Fen P26 1.3m	29-Jul-12	Moist Fine Sand		1.30	-140.7	-17.08
Fen P26 2.0m	29-Jul-12	Sticky Sand		2.00	-152.5	-18.03
Fen P26 14ft	29-Jul-12	Tailings	14	4.27	-127.9	-15.40
Fen P27 30cm	29-Jul-12	Coarse Sand		0.30	-127.0	-14.89
Fen P27 55 cm	29-Jul-12	Moist Fine Sand		0.55	-128.5	-16.34
Fen P27 90 cm	29-Jul-12	Moist Fine Sand		0.90	-131.2	-16.40
Fen P27 1.25m	29-Jul-12	Moist Sand		1.25	-131.2	-16.28
Fen P27 1.6m	29-Jul-12	Moist fine Sand		1.60	-137.0	-17.00
Fen P27 2m	29-Jul-12	Moist Fine sand		2.00	-137.5	-16.91
Fen P27 14 ft	29-Jul-12	Moist Sand	14	4.27	-124.3	-14.54
Fen P27 21ft	29-Jul-12	Tailings	21	6.40	-130.1	-15.46
Fen P28 30cm	29-Jul-12	Clay		0.30	-135.4	-16.49
Fen P28 70cm	29-Jul-12	Coarse moist sand		0.70	-133.3	-16.04
Fen P28 1.1m	29-Jul-12	Fine Moist Sand		1.10	-133.3	-16.13
Fen P28 1.5 m	29-Jul-12	Fine sticky sand		1.50	-124.7	-15.07
Fen P28 2m	29-Jul-12	Moist Fine Sand		2.00	-128.0	-15.42
Fen P28 14 ft	29-Jul-12	Moist Fine Sand	14	4.27	-131.2	-16.14
Fen P30 30 cm	6-Jul-12	Clay		0.30	-123.4	-13.71
Fen P30 55 cm	6-Jul-12	Moist Sand		0.55	-125.5	-14.42
Fen P30 1m	6-Jul-12	Moist Sand		1.00	-124.5	-15.05
Fen P30 1.7m	6-Jul-12	Moist Sand		1.70	-126.3	-14.12
Fen P30 1.95 m	6-Jul-12	Clay		1.95	-123.1	-13.77
Fen P30 2.7 m	6-Jul-12	Moist Sand		2.70	-130.7	-15.18
Fen P30 3.2 m	6-Jul-12	Tailings		3.20	-157.7	-19.12

Sample Name	Date	Soil	Depth [ft]	Depth [m]	δD, ‰	$\delta^{18}O$, ‰
Fen P30 3.7 m	6-Jul-12	Tailings		3.70	-174.4	-21.94
Fen P31 30 cm	28-Jul-12	Black Soil		0.30	-138.9	-16.18
Fen P31 70cm	28-Jul-12	Peat		0.70	-149.1	-18.66
Fen P31 1m	28-Jul-12	Sticky Sand		1.00	-146.1	-18.49
Fen P31 1.3m	28-Jul-12	Moist Sand		1.30	-149.5	-18.70
Fen P31 2m	28-Jul-12	Tailings		2.00	-140.7	-17.62
Fen P32 30 cm	28-Jul-12	Peat		0.30	-150.8	-18.36
Fen P32 70 cm	28-Jul-12	Moist Sand		0.70	-133.8	-16.28
Fen P32 1.1m	28-Jul-12	Moist Sand		1.10	-124.9	-14.93
Fen P32 1.5m	28-Jul-12	Moist Fine Sand		1.50	-124.7	-15.07
Fen P32 2.0 m	28-Jul-12	Moist Fine Sand		2.00	-125.8	-15.42
Fen P32 13ft	28-Jul-12	Tailings	13	3.96	-122.9	-14.63
Fen P32 18ft	28-Jul-12	Tailings	18	5.49	-129.1	-15.79
Fen P34 30 cm	27-Jul-12	Peat		0.30	-134.4	-15.56
Fen P34 50 cm	27-Jul-12	Moist Sand		0.50	-133.8	-16.43
Fen P34 80cm	27-Jul-12	Moist Fine Sand		0.80	-128.0	-15.71
Fen P34 1.2m	27-Jul-12	Loose Sand		1.20	-131.7	-16.04
Fen P34 1.5m	27-Jul-12	Clay		1.50	-132.2	-15.80
Fen P34 2.0 m	27-Jul-12	Moist Sand		2.00	-129.6	-15.92
Fen P34 2.8 m	27-Jul-12	Moist Sand		2.80	-130.6	-15.73
Fen P34 3.5m	27-Jul-12	Tailings		3.50	-133.3	-16.03
Fen P34 4.0m	29-Jul-12	Tailings		4.00	-132.2	-16.12
Fen P35 30cm	27-Jul-12	Peat		0.30	-134.4	-16.56
Fen P35 65 cm	27-Jul-12	Clay		0.65	-142.7	-17.21
Fen P35 90 cm	27-Jul-12	Clay		0.90	-143.0	-17.27
Fen P35 1.4m	27-Jul-12	Tailings		1.40	-149.0	-18.25
Fen P35 13ft	28-Jul-12	Tailings	13	3.96	-124.7	-15.14
Fen P36 55 cm	3-Jul-12	Loose Peat		0.55	-150.2	-16.66
Fen P36 80 cm	3-Jul-12	Peat		0.80	-143.2	-14.52
Fen P36 90 cm	3-Jul-12	Supersat. Clay		0.90	-126.1	-14.13
Fen P36 15 ft	3-Jul-12	Tailings (CT?)	15	4.58	-116.4	-12.63
Fen p37 20 cm	3-Jul-12	Eng Coarse Sand		0.20	-154.1	-17.93
Fen P37 3 ft	3-Jul-12	Sticky Sand	3	0.92	-153.5	-18.90
Fen P37 8 ft	3-Jul-12	Tailings	8	2.44	-130.7	-14.88
Fen P38 8 ft	3-Jul-12	Tailings	8	2.44	-120.4	-13.54
Fen P39 35 cm	5-Jul-12	Moist Eng/coarse Sand		0.35	-122.9	-14.63
Fen P39 70 cm	5-Jul-12	Moist Sand		0.70	-131.7	-14.68
Fen P39 75 cm	5-Jul-12	Wet Sand		0.75	-158.4	-18.72
Fen P39 1 m	5-Jul-12	Moist Sand		1.00	-143.2	-16.42
Fen P39 5ft	5-Jul-12	Moist Sand	5	1.53	-141.3	-16.44
Fen P39 11 ft	5-Jul-12	Moist Sand	11	3.36	-122.9	-13.37

Sample Name	Date	Soil	Depth [ft]	Depth [m]	δD, ‰	$\delta^{18}O$, ‰
Fen P39 18 ft	5-Jul-12	Tailings	18	5.49	-118.9	-13.29
Fen P39 24 ft	5-Jul-12	Tailings	24	7.32	-115.5	-12.63
Fen P39 30 ft	29-Jul-12	Tailings	30	9.14	-119.7	-14.39
Fen P39 30 cm	29-Jul-12	Coarse loose Sand		0.30	-123.6	-14.50
Fen P39 70 cm	29-Jul-12	Sticky Sand		0.70	-128.5	-15.20
Fen P39 1m	29-Jul-12	Moist Sand		1.00	-125.4	-14.90
Fen P40 25 cm	5-Jul-12	Moist coarse sand		0.25	-124.0	-12.25
Fen P40 55 cm	5-Jul-12	Moist Sand		0.55	-129.0	-13.87
Fen P40 80 cm	5-Jul-12	Moist Sand		0.80	-138.1	-15.69
Fen P40 3 ft	5-Jul-12	Moist Sand	3	0.92	-138.7	-15.90
Fen P40 8 ft	5-Jul-12	Tailings	8	2.44	-126.3	-14.08
Fen P40 15 ft	5-Jul-12	Tailings	15	4.58	-118.7	-13.27
Fen P41 30cm	28-Jul-12	Peat		0.30	-137.8	-15.62
Fen P41 50cm	28-Jul-12	Clay/Peat		0.50	-137.0	-16.52
Fen P41 90 cm	28-Jul-12	Fine Moist Sand		0.90	-139.6	-16.78
Fen P41 1.3m	28-Jul-12	Fine Moist Sand		1.30	-133.3	-16.22
Fen P41 1.8 m	28-Jul-12	Wet Sand		1.80	-127.3	-15.02
Fen P41 2m	28-Jul-12	Tailings		2.00	-126.4	-14.28
Fen P41 11ft	28-Jul-12	Tailings	11	3.35	-122.4	-13.99
Fen P41 21 ft	23-Jul-12	Tailings	21	6.40	-119.5	-14.22
Fen P41 30 ft	28-Jul-12	Tailings	30	9.14	-117.3	-14.12
Fen P42 30cm	28-Jul-12	Peat		0.30	-136.0	-15.20
Fen P42 50cm	28-Jul-12	Peat		0.60	-136.6	-16.28
Fen P42 80 cm	28-Jul-12	Wet Sand		0.80	-144.1	-17.63
Fen P42 1.1m	28-Jul-12	Tailings		1.10	-136.9	-16.82
Fen P42 11ft	28-Jul-12	Wet Sand	11	3.35	-121.2	-14.41
Fen P42 21ft	28-Jul-12	Tailings	21	6.40	-123.6	-14.87
Fen P43 40 cm	6-Jul-12	Peat/Clay		0.40	-129.6	-14.71
Fen P43 60 cm	6-Jul-12	Clay		0.60	-128.4	-14.86
Fen P43 85 cm	6-Jul-12	Moist sand		0.85	-127.9	-14.93
Fen P43 1.25m	6-Jul-12	Moist Sand		1.25	-126.1	-14.87
Fen P43 2.3 m	6-Jul-12	Sand		2.30	-123.9	-13.46
Fen P43 2.85 m	6-Jul-12	Moist fine Sand		2.85	-123.3	-13.54
Fen P43 3.15 m	6-Jul-12	Moist Fine Sand		3.15	-123.1	-13.72
Fen P43 18 ft	6-Jul-12	Tailings	18	5.49	-123.9	-14.02
Fen P43 24 ft	6-Jul-12	Tailings	24	7.32	-123.6	-14.98
Fen P43 30 ft	30-Jul-12	Tailings	30	9.14	-120.4	-14.49
Fen P43 30 cm	30-Jul-12	Clay		0.30	-137.7	-16.29
Fen P43 60 cm	30-Jul-12	Brown Sugar		0.60	-131.2	-15.96
Fen P43 1m	30-Jul-12	Moist Sand		1.00	-132.2	-16.43
Fen P43 1.5m	30-Jul-12	Moist Fine Sand		1.50	-138.6	-16.73
Fen P44 15 ft	30-Jun-12	Tailings	15	4.58	-116.0	-12.67

Sample Name	Date	Soil	Depth [ft]	Depth [m]	δD, ‰	$\delta^{18}O$, ‰
Fen P44 27 ft	30-Jun-12	Tailings	27	8.24	-120.4	-13.62
Fen P45 30 cm	27-Jul-12	Peat		0.30	-135.4	-16.25
Fen P45 60cm	27-Jul-12	Peat		0.60	-144.9	-17.54
Fen P45 90 cm	27-Jul-12	Wet Sand		0.90	-136.6	-16.37
Fen P45 1.6m	27-Jul-12	Tailings		1.60	-133.3	-16.20
Fen P45 2.0m	27-Jul-12	Tailings		2.00	-134.4	-16.48
Fen P45 13ft	15-Aug-12	Tailings	13	3.96	-129.1	-15.65
Fen P46 0.3m	15-Aug-12	Peat		0.30	-141.3	-17.12
Fen P46 60 cm	15-Aug-12	Moist Fine Sand		0.60	-134.3	-15.77
Fen P46 1m	15-Aug-12	Loose Fine Sand		1.00	-130.2	-15.86
Fen P46 1.5m	15-Aug-12	Loose Sand		1.50	-137.3	-16.89
Fen P46 1.8m	15-Aug-12	Sticky Sand		1.80	-134.7	-16.73
Fen P46 2.1m	15-Aug-12	Moist Sand		2.10	-132.8	-15.91
Fen P46 14ft	15-Aug-12	Tailings	14	4.27	-127.7	-15.40
Fen P47 3 ft	30-Jun-12	Moist Sand	3	0.92	-149.4	-17.00
Fen P47 6 ft	30-Jun-12	Loose Sand	6	1.83	-131.3	-14.77
Fen P47 15 ft	30-Jun-12	Sand	15	4.58	-121.6	-13.61
Fen P47 27 Feet	30-Jun-12	Tailings	27	8.24	-117.0	-12.24
Fen P48 35 cm	8-Jul-12	Clay		0.30	-138.5	-16.03
Fen P48 70 cm	8-Jul-12	Moist sand		0.70	-129.0	-14.93
Fen P48 3 ft	8-Jul-12	Moist Sand	3	0.92	-128.5	-14.58
Fen P48 5 Ft	8-Jul-12	Moist Sand	5	1.53	-124.0	-14.32
Fen P48 11 ft	8-Jul-12	Moist Sand	11	3.36	-122.0	-13.57
Fen P48 18 ft	8-Jul-12	Moist Sand	18	5.49	-118.4	-12.86
Fen P48 24 Feet	8-Jul-12	Moist sand	24	7.32	-114.7	-12.56
Fen P48 30ft	30-Jul-12	Sticky Sand	30	9.15	-131.2	-15.46
Fen P48 30 cm	30-Jul-12	Peat		0.30	-133.3	-15.86
Fen P48 70 cm	30-Jul-12	Moist Sand		0.70	-131.2	-16.06
Fen P48 1.1m	30-Jul-12	Moist Fine Sand		1.10	-131.2	-16.06
Fen P48 1.5m	30-Jul-12	Moist Sand		1.50	-129.6	-15.55
Fen P48 2.0m	30-Jul-12	Fine Moist Sand		2.00	-127.0	-15.37
Fen p51 9 ft	29-Jun-12	Loose Sand	9	2.75	-123.0	-13.51
Fen P51 15 ft	29-Jun-12	Sticky Sand	15	4.58	-124.8	-14.05
Fen P51 27 ft	29-Jun-12	Tailings	27	8.24	-116.0	-12.98
Fen P52 8 ft	29-Jun-12	Sticky sand	8	2.44	-137.8	-16.20
Fen P52 15 ft	29-Jun-12	Tailings	15	4.58	-125.2	-13.71
Fen P53 8 ft	29-Jun-12	Loose Sand	8	2.44	-133.0	-15.16
Fen P53 15 ft	29-Jun-12	Moist Sand	15	4.58	-127.2	-13.72
Fen P54 8 ft	29-Jun-12	Moist Sand	8	2.44	-127.3	-14.10
Fen P54 15 ft	29-Jun-12	Moist Sand	15	4.58	-127.8	-14.16
Fen P54 21 ft	29-Jun-12	Loose Sand	21	6.41	-119.9	-13.55
Fen P54 27ft	29-Jun-12	Tailings	27	8.24	-125.7	-13.92

Sample Name	Date	Soil	Depth [ft]	Depth [m]	δD, ‰	$\delta^{18}O$, ‰
Fen P55 15 ft	30-Jun-12	Loose sand	15	4.58	-127.1	-14.44
Fen P55 27 feet	30-Jun-12	Tailings	27	8.24	-119.7	-12.92
Fen P56 30cm	15-Aug-12	Peat		0.30	-134.3	-15.02
Fen P56 80cm	15-Aug-12	Moist Sand		0.80	-137.8	-16.37
Fen P56 1m	15-Aug-12	Moist Fine Sand		1.00	-142.5	-16.94
Fen P56 1.5m	15-Aug-12	Wet Sand		1.50	-135.8	-16.89
Fen P56 1.9m	15-Aug-12	Loose fine sand		1.90	-132.2	-15.51
Fen P56 2.15m	15-Aug-12	Moist Sand		2.15	-134.3	-16.08
Fen P56 13 ft	15-Aug-12	Loose Sand	13	3.96	-125.0	-13.90
Fen P57 5 ft	28-Jun-12	Moist Sand	5	1.53	-126.3	-14.12
Fen P57 12 ft	28-Jun-12	Moist Sand	12	3.66	-127.9	-14.52
Fen P57 18 ft	28-Jun-12	Sticky fine sand	18	5.49	-124.3	-13.61
Fen P57 24 ft	28-Jun-12	Sticky Sand	24	7.32	-124.3	-13.66
Fen P57 30 ft	28-Jun-12	Tailings	30	9.15	-122.7	-13.28
Fen P58 9 ft	28-Jun-12	Moist Sand	9	2.75	-121.2	-13.06
Fen P58 15ft	28-Jun-12	Moist Sand	15	4.58	-118.4	-12.73
Fen P58 21 ft	28-Jun-12	tailings	21	6.41	-119.2	-12.41
Fen P61 12 Feet	28-Jun-12	Wet/Sticky sand	12	3.66	-122.6	-13.47
P63 50 cm	3-Jul-12	Loose Peat		0.50	-148.5	-18.09
Fen P63 3 ft (met stn)	3-Jul-12	Sat Clay	3	0.92	-148.6	-17.99
Fen P63 Frost/Snow 1m	3-Jul-12	Water		1.00	-152.9	-18.06
Fen P63 1.1 m	3-Jul-12	Clay		1.10	-136.1	-15.05
Fen P63 11 ft	3-Jul-12	Tailings	11	3.36	-121.5	-14.03
Fen P63 21 feet	3-Jul-12	Tailings	21	6.41	-113.1	-11.83

South Bison Hills

Sample Name	Depth [cm]	Soil	δD, ‰	$\delta^{18}O$, ‰
T1C 0-18	0-18	Peat	-108.4	-11.74
T1C 18-33	18-33	Clay	-111.1	-12.28
T1C 33-48	33-48	Clay	-124.9	-15.31
T1C 48-63	48-63	Clay	-139.4	-16.37
T1C 63-78	63-78	Clay	-149.5	-17.73
T1C 78-93	78-93	Clay	-149.8	-17.79
T1C 93-108	93-108	Clay	-149.8	-17.79
T1C 108-123	108-123	Clay	-149.4	-17.81
T1C 123-138	123-138	Clay	-147.2	-16.76
T1U 0-19	0-19	Peat	-119.3	-13.23
T1U 19-34	19-34	Clay	-109.5	-13.08
T1U 34-55	34-55	Clay	-125.3	-14.21
T1U 55-70	55-70	Clay	-141.9	-16.95
T1U 70-85	70-85	Clay	-140.9	-16.88
T1M 0-16	0-16	Peat	-118.2	-10.46
T1M 16-31	16-31	Peat	-118.7	-14.27
T1M 31-45	31-45	Clay	-123.9	-14.43
T1M 45-60	45-60	Clay	-128.5	-15.58
T1M 60-75	60-75	Clay	-133.4	-15.71
T1L 0-11	0-11	Peat	-117.5	-11.67
T1L 11-26	11-26	Clay	-109.5	-12.70
T1L 26-45	26-45	Clay	-125.2	-14.00
T1L 45-60	45-60	Clay	-156.3	-19.30
T1L 60-75	60-75	Clay	-162.0	-20.30
T2C 0-19	0-19	Organics	-114.7	-11.32
T2C 19-34	19-34	Clay/Peat	-121.9	-14.66
T2C 34-49	34-49	Clay/Peat	-141.5	-17.62
T2C 49-64	49-64	Clay	-150.0	-18.49
T2C 64-79	64-79	Clay	-153.7	-18.89
T2C 79-94	79-94	Clay	-155.9	-19.44
T2C 94-109	94-109	Sandy soil	-151.3	-18.36
T2C 109-124	109-124	Clay	-148.8	-17.93
T2C 124-139	124-139	Clay	-143.4	-16.54
T2C 139-154	139-154	Clay	-139.6	-15.43
T2U 0-15	0-15	Peat/Organics	-111.2	-11.82
T2U 15-32	15-32	Organics	-119.3	-13.34
T2U 32-47	32-47	Clay	-143.5	-17.57
T2U 47-62	47-62	Clay	-142.2	-17.03
T2M 0-13	0-13	Peat/Organics	-120.5	-13.66
T2M 13-28	13-28	Peat	-107.1	-12.16

Sample Name	Depth [cm]	Soil	δD, ‰	$\delta^{18}O$, ‰
T2M 28-44	28-44	Clay	-126.0	-14.33
T2M 44-59	44-59	Clay	-125.2	-14.76
T2M 59-74	59-74	Clay	-130.4	-15.43
T2L 0-10	0-10	Organics	-110.8	-11.53
T2L 10-24	10-24	Peat	-121.4	-14.19
T2L 24-39	24-39	Clay	-136.5	-16.62
T2L 39-54	39-54	Clay	-135.7	-16.61
T3C 0-9	0-9	Organics	-118.2	-13.82
T3C 9-24	9-24	Clay	-107.6	-12.10
T3C 24-39	24-39	Clay	-115.5	-13.84
T3C 39-54	39-54	Clay	-115.8	-13.48
T3C 54-69	54-69	Clay	-117.0	-14.49
T3C 69-84	69-84	Clay	-118.2	-14.49
T3C 84-99	84-99	Clay	-115.8	-13.93
T3C 99-114	99-114	Clay	-117.0	-14.10
T3U 0-13	0-13	Peat	-122.2	-12.50
T3U 13-28	13-28	Peat/Clay	-106.2	-12.32
T3U 28-43	28-43	Clay	-131.0	-16.15
T3U 43-58	43-58	Sand-clay mix	-140.9	-17.40
T3U 58-73	58-73	Clay	-145.8	-17.85
T3U 73-88	73-88	Clay	-152.2	-18.77
T3U 88-103	88-103	Clay	-153.6	-18.78
T3U 103-118	103-118	Clay	-152.0	-18.96
T3U 118-133	118-133	Clay	-154.4	-18.87
T3U 133-150	133-150	Clay	-149.9	-18.28
T3U 150-165	150-165	Clay	-149.2	-17.23
T3U 165-180	165-180	Clay	-149.2	-16.94
T3M 0-7	0-7	Organics	-128.6	-14.36
T3M 7-22	7-22	Peat	-109.8	-12.66
T3M 22-37	22-37	Clay	-137.4	-17.07
T3M 37-52	37-52	Clay	-150.8	-18.43
T3M 52-67	52-67	Clay	-154.1	-19.16
T3M 67-82	67-82	Clay	-153.2	-18.84
T3M 82-97	82-97	Samd/clay mix	-154.0	-18.32
T3M 106-121	106-121	Clay	-155.0	-18.85
T3M 121-136	121-136	Clay	-152.8	-17.91
T3L 0-5	0-5	Peat	-132.7	-14.35
T3L 5-20	5-20	Peat	-121.4	-14.99
T3L 20-35	20-35	Clay	-106.2	-13.45
T3L 35-50	35-50	Clay	-102.9	-12.82
T3L 50-71	50-71	Clay	-108.9	-13.49
T3L 71-86	71-86	Clay	-129.2	-15.94

Sample Name	Depth [cm]	Soil	δD, ‰	$\delta^{18}O$, ‰
T3L 86-101	86-101	Clay	-143.9	-17.23
T8P1 0-10	0-10	Organics	-128.0	-14.34
T8P1 10-25	10-25	Peat	-115.1	-13.22
T8P1 25-40	25-40	Clay	-134.0	-14.81
T8P1 40-55	40-55	Clay	-135.7	-16.02
T8P1 55-70	55-70	Clay	-140.2	-16.76
T8P1 70-85	70-85	Sandy clay	-144.5	-17.73
T8P1 85-100	85-100	Clay	-143.9	-16.87
T8P1 100-115	100-115	Clay	-145.6	-16.93
T8P1 115-130	115-130	Clay	-144.8	-17.16
T8P1 130-145	130-145	Clay	-145.2	-17.10
T8P2 0-7	0-7	Organics	-131.6	-15.12
T8P2 7-22	7-22	Peat	-128.6	-15.71
T8P2 22-37	22-37	Clay	-118.0	-14.70
T8P2 37-52	37-52	Clay	-110.8	-13.30
T8P2 52-67	52-67	Clay	-113.5	-13.70
T8P2 67-82	67-82	Clay	-119.0	-14.27
T8P2 82-97	82-97	Clay	-125.9	-15.42
T8P2 97-112	97-112	Clay	-130.4	-16.07
T8P2 112-127	112-127	Clay	-138.9	-16.36
T8P2 127-142	127-142	Clay	-141.5	-16.16
T8C 0-12	0-12	Organics	-129.1	-15.43
T8C 12-27	12-27	Peat	-109.4	-12.31
T8C 27-42	27-42	Peat	-112.2	-13.41
T8C 42-57	42-57	Clay	-113.9	-12.98
T8C 57-72	57-72	Clay	-115.7	-14.13
T8C 72-87	72-87	Clay	-122.0	-14.51
T8C 87-102	87-102	Clay	-121.1	-14.31
T8C 102-117	102-117	Clay	-128.2	-14.60
T8C 117-132	117-132	Clay	-132.1	-15.31
T8M 0-15	0-15	Organics	-115.2	-10.46
T8M 15-30	15-30	Peat	-125.9	-14.39
T8M 30-45	30-45	Clay	-138.9	-17.29
T8M 45-60	45-60	Clay	-151.0	-18.14
T8M 60-75	60-75	Peat	-154.1	-18.80
T8M 75-90	75-90	Clay	-162.1	-19.13
T8T 0-17	0-17	Organics	-108.9	-12.04
T8T 17-32	17-32	Organics	-120.9	-13.81
T8T 32-47	32-47	Clay	-136.6	-16.53
T8T 47-62	47-62	Clumpy Organics	-150.4	-17.35
T8T 62-77	62-77	Crumbly Peat	-155.6	-18.89
T8T 77-92	77-92	Loose clay	-155.9	-18.25

Sample Name	Depth [cm]	Soil	δD, ‰	$\delta^{18}O$, ‰
T8T 92-107	92-107	Loose Clay	-155.0	-18.40

Fen and Mildred Lake Settling Basin C4- Spring 2013

Sample	Date	Soil Type	Depth	δD, ‰	$\delta^{18}O$,‰
Fen P11-10	1-May-13	moist sand	10	-162.7	-18.68
Fen P11-20	1-May-13	moist sand	20	-159.2	-18.51
Fen P11-30	1-May-13	moist fine sand	30	-155.9	-18.49
Fen P11-40	1-May-13	moist fine sand	40	-153.1	-18.79
Fen P11-50	1-May-13	moist fine sand	50	-147.9	-17.71
Fen P11-60	1-May-13	wet fine sand	60	-150.7	-18.60
Fen P11-70	1-May-13	moist sand	70	-149.2	-18.45
Fen P11-80	1-May-13	wet fine sand	80	-131.5	-16.08
Fen P11-90	1-May-13	moist sand	90	-138.7	-16.89
Fen P11-100	1-May-13	wet fine sand	100	-143.2	-17.62
Fen P11-110	1-May-13	wet fine sand	110	-135.2	-16.29
Fen P11-120	1-May-13	wet fine sand	120	-139.1	-17.40
Fen P11-130	1-May-13	moist sand	130	-141.0	-17.23
Fen P11-140	1-May-13	wet fine sand	140	-140.3	-17.38
Fen P11-150	1-May-13	moist fine sand	150	-142.7	-17.58
Fen-P11-160	1-May-13	wet fine sand	160	-142.7	-17.16
Fen P11-170	1-May-13	wet sand	170	-146.3	-18.16
Fen P11-180	1-May-13	wet fine sand	180	-140.5	-16.76
Fen P11-190	1-May-13	wet sand	190	-142.7	-17.17
Fen P11-200	1-May-13	moist sand	200	-143.4	-17.30
Fen P12-100	1-May-13	moist sand	10	-157.5	-18.92
Fen P12-20	1-May-13	moist fine sand	20	-143.4	-15.45
Fen P12-40	1-May-13	moist fine sand	40	-128.7	-14.78
Fen P12-60	1-May-13	loose sand	60	-126.9	-14.36
Fen P12-80	1-May-13	moist fine sand	80	-127.0	-14.68
Fen P12-100	1-May-13	sand	100	-135.1	-15.40
Fen p12-130	1-May-13	wet sand	130	-128.1	-14.74
Fen P12-140	1-May-13	wet fine sand	140	-130.5	-15.16
Fen P12-160	1-May-13	moist sand	160	-129.7	-14.95
Fen P12-180	1-May-13	wet fine sand	180	-134.5	-16.41
Fen P12-200	1-May-13	wet fine sand	200	-152.9	-19.08
Fen P13-200	1-May-13	moist fine sand	20	-154.5	-17.24
Fen P13-10	1-May-13	dry peat/organics	10	-154.4	-17.91
Fen-P13-40	1-May-13	Moist fine sand	40	-158.9	-19.23
Fen P13-60	1-May-13	moist fine sand	60	-179.0	-21.95
Fen P13-80	1-May-13	wet sand	80	-181.5	-22.47

Sample	Date	Soil Type	Depth	δD, ‰	$\delta^{18}O$,‰
Fen P13-100	1-May-13	moist fine sand	100	-182.1	-22.60
Fen P13-120	1-May-13	wet fine sand	120	-186.6	-23.12
Fen P13-140	1-May-13	wet fine sand	140	-186.5	-23.45
Fen P13-160	1-May-13	moist sand	160	-185.2	-23.57
Fen P13-180	1-May-13	wet fine sand	180	-189.7	-24.22
Fen P13-200	1-May-13	wet fine sand	200	-183.8	-23.03
Fen P14-10	1-May-13	peat	10	-153.3	-17.92
Fen P14-20	1-May-13	peat	20	-152.8	-17.42
Fen P14-40	1-May-13	peat	40	-160.4	-18.38
Fen P14-60	1-May-13	clay/peat	60	-175.2	-19.72
Fen P14-80	1-May-13	clay	80	-162.7	-19.66
Fen P14-100	1-May-13	clay	100	-167.4	-20.51
Fen P14-120	1-May-13	moist sand	120	-166.5	-20.95
Fen P14-140	1-May-13	moist sand	140	-156.9	-19.49
Fen P14-160	1-May-13	wet fine sand	160	-136.6	-16.41
Fen P14-180	1-May-13	wet sticky sand	180	-134.0	-15.32
Fen P14-200	1-May-13	wet sticky sand-tailings	200	-171.9	-21.29
MLSB-C4-up-0-20	14-May-13	peat	20	-167.4	-14.85
MLSB-C4-Up-20-30	14-May-13	peat	30	-177.4	-17.08
MLSB-C4-up-30-40	14-May-13	peat	40	-164.5	-16.65
MLSB-C4-Up-40-50	14-May-13	Peat/organic	50	-155.7	-17.81
MLSB-C4-up-50-60	14-May-13	clay	60	-154.7	-19.39
MLSB-C4-up-60-70	14-May-13	loose clay	70	-157.7	-19.67
MLSB-C4-up-70-80	14-May-13	dirt	80	-159.8	-19.83
MLSB-C4-up-80-90	14-May-13	dry dirt	90	-159.2	-19.52
MLSB-C4-up-90-100	14-May-13	dry dirt	100	-160.6	-19.83
MLSB-C4-up-100-110	14-May-13	clay dirt mix	110	-161.8	-19.89
MLSB-C4-mid-0-20	14-May-13	peat/clay	20	-174.2	-17.34
MLSB-C4-mid-20-30	14-May-13	clay	30	-157.2	-18.77
MLSB-C4-Mid-30-40	14-May-13	clay	40	-140.8	-16.75
MLSB-C4-mid-40-50	14-May-13	moist sand	50	-153.9	-19.27
MLSB-C4-Mid-50-60	14-May-13	moist fine sand-	60	-166.1	-19.99
MLSB-C4-Mid-60-70	14-May-13	moist sand	70	-163.9	-20.47
MLSB-C4-mid-70-80	14-May-13	Wet sand	80	-164.7	-20.42
MLSB-C4-Mid-80-90	14-May-13	moist fine sand	90	-166.5	-21.21
MLSB-C4-mid-90-100	14-May-13	wet sand	100	-171.2	-21.78
MLSB-C4-mid-100-110	14-May-13	fine wet sand	110	-185.6	-23.57
MLSB-C4-Lowe-0-20	14-May-13	Peat/organics	20	-171.8	-18.80
MLSB-C4-low-20-30	14-May-13	Peat/organics	30	-147.3	-17.06
MLSB-C4-Low-30-40	14-May-13	dry peat/organics	40	-143.1	-16.98
MLSB-C4-low-40-50	14-May-13	dry peat/organics	50	-145.0	-15.88
MLSB-C4-low-50-60	14-May-13	dry peat/organics	60	-147.8	-16.77

Sample	Date	Soil Type	Depth	δD, ‰	$\delta^{18}O$,‰
MLSB-C4-Lower-60-70	14-May-13	dry peat/organics	70	-153.1	-17.28
MLSB-C4-low-70-80	14-May-13	dry peat/organics	80	-152.8	-16.54
MLSB-C4-Low-80-90	14-May-13	dry peat/organics	90	-156.9	-17.79
MLSB-C4-Low-90-100	14-May-13	dry peat/organics	100	-156.6	-17.60
MLSB-C4-Low-100-110	14-May-13	dry peat/organics	110	-159.7	-17.73
MLSB-C4-Low-110-120	14-May-13	dry peat/organics	120	-159.8	-19.04

Hilderman's (2011) Water and Soil Samples

Water Samples

Sample	Date	δD, ‰	$\delta^{18}O$, ‰
D1 Interflow	30-Apr-09	-149.4	-18.41
D1 Interflow	2-May-09	-148.5	-18.07
D1 Interflow	11-May-09	-147.6	-18.31
D1 Interflow	12-May-09	-148.4	-18.18
D1 Interflow	13-May-09	-148.2	-18.07
D1 Interflow	14-May-09	-148.3	-17.92
D1 Interflow	15-May-09	-148.1	-18.02
D1 Interflow	16-May-09	-151.2	-18.48
D1 Interflow	25-May-09	-147.5	-18.14
D1 Interflow	27-May-09	-147.2	-17.97
D1 Interflow	28-May-09	-148.1	-18.16
D1 Interflow	29-May-09	-147.5	-18.05
D1 Interflow	30-May-09	-147.6	-18.09
D1 Interflow	6-Jun-09	-147.8	-17.86
D1 Interflow	14-Jun-09	-147.2	-17.69
D1 Interflow	21-Jun-09	-152.2	-18.41
D1 Interflow	28-Jun-09	-148.4	-17.88
D1 Interflow	5-Jul-09	-147.7	-17.81
D1 Interflow	12-Jul-09	-147.8	-17.75
D2 Interflow	30-Apr-09	-148.3	-18.31
D2 Interflow	2-May-09	-149.9	-18.19
D2 Interflow	11-May-09	-148.2	-18.35
D2 Interflow	12-May-09	-148.7	-17.99
D2 Interflow	13-May-09	-147.9	-17.80
D2 Interflow	14-May-09	-147.3	-17.87
D2 Interflow	15-May-09	-148.1	-18.03
D2 Interflow	16-May-09	-148.6	-18.22
D2 Interflow	25-May-09	-148.7	-18.02
D2 Interflow	27-May-09	-147.1	-17.77
D2 Interflow	28-May-09	-147.1	-18.00

Sample	Date	δD, ‰	$\delta^{18}O$, ‰
D2 Interflow	29-May-09	-148.9	-18.08
D2 Interflow	30-May-09	-148.9	-18.23
D2 Interflow	6-Jun-09	-152.1	-18.48
D2 Interflow	14-Jun-09	-150.2	-18.09
D2 Interflow	28-Jun-09	-152.0	-18.29
D2 Interflow	5-Jul-09	-146.0	-17.58
D2 Interflow	12-Jul-09	-149.2	-17.98
D3 Interflow	2-May-09	-147.9	-18.27
D3 Interflow	11-May-09	-150.4	-18.35
D3 Interflow	12-May-09	-151.5	-18.46
D3 Interflow	13-May-09	-151.6	-18.64
D3 Interflow	14-May-09	-150.9	-18.62
D3 Interflow	15-May-09	-151.2	-18.77
D3 Interflow	16-May-09	-148.1	-18.06
D3 Interflow	25-May-09	-149.2	-18.39
D3 Interflow	27-May-09	-149.5	-18.38
D3 Interflow	28-May-09	-150.0	-18.24
D3 Interflow	29-May-09	-149.7	-18.43
D3 Interflow	30-May-09	-150.6	-18.33
D3 Interflow	6-Jun-09	-152.0	-18.56
D3 Interflow	14-Jun-09	-153.3	-18.79
D3 Interflow	28-Jun-09	-150.7	-18.46
D3 Interflow	5-Jul-09	-150.9	-18.41
D3 Interflow	12-Jul-09	-153.3	-18.56
D3 Interflow (recharge)	30-Apr-09	-146.8	-18.04
D3 Interflow (stagnant)	30-Apr-09	-148.6	-18.31
Peat Pond	2-May-09	-125.6	-12.50
Peat Pond	16-May-09	-124.0	-12.00
Peat Pond	30-May-09	-122.4	-11.60
Golden Pond	3-May-09	-133.9	-14.69
Golden Pond	16-May-09	-129.5	-13.43
GP weir 1	1-May-09	-137.9	-15.98
GP weir 2	1-May-09	-134.8	-14.46
Bill's Lake	2-May-09	-156.2	-18.39
Bill's Lake	16-May-09	-152.0	-17.25
Bill's Lake	30-May-09	-146.2	-16.03
Rainfall	18-May-09	-136.9	-16.88
Rainfall	1-Jun-09	-156.8	-18.32
Rainfall	11-Jun-09	-113.1	-10.98
Rainfall	20-Jun-09	-138.1	-15.37
Rainfall	27-Jun-09	-131.5	-14.79
Rainfall	28-Jun-09	-118.9	-12.93

Sample	Date	δD, ‰	$\delta^{18}O$, ‰
Rainfall	1-Jul-09	-148.4	-17.37
Rainfall	9-Jul-09	-129.3	-14.46
Rainfall	19-Jul-09	-133.8	-15.31
Rainfall	30-Jul-09	-117.4	-12.68
Rainfall	2-Aug-09	-115.5	-12.66
Rainfall	5-Aug-09	-135.7	-16.27
Rainfall	14-Aug-09	-136.1	-16.00
Rainfall	23-Aug-09	-124.0	-13.91
Rainfall	26-Aug-09	-124.4	-15.35
Rainfall	9-Sep-09	-114.0	-14.06
Rainfall	16-Sep-09	-88.5	-10.57
Rainfall	28-Sep-09	-114.6	-12.76
Rainfall	7-Oct-09	-143.5	-17.89
Rainfall	13-Oct-09	-199.8	-26.20
Rainfall	17-Oct-09	-201.6	-26.23
Rainfall	27-Oct-09	-141.5	-18.06
Rainfall	5-Nov-09	-154.8	-20.12
Snow	26-Mar-09	-210.0	-26.63
Snow	26-Mar-09	-208.6	-26.67
Snow	26-Mar-09	-213.4	-27.35
Snow	26-Mar-09	-215.9	-27.86
Snow	26-Mar-09	-223.3	-28.84
Snow	26-Mar-09	-203.4	-26.00
Snow	29-Mar-09	-211.4	-27.03
Snow	29-Mar-09	-200.9	-25.38
Snow	29-Mar-09	-210.7	-26.95
Snow	29-Mar-09	-213.6	-27.43
Snow	29-Mar-09	-173.4	-21.84
Snow	29-Mar-09	-186.7	-24.05
Snow	29-Mar-09	-201.6	-25.82
Snow	29-Mar-09	-185.1	-23.75

Soil Samples

Sample	Depth, m	δD, ‰	$\delta^{18}O$, ‰
Pro 50 #6.	110	-144.1	-16.84
Pro 50 #7.	127	-143.9	-17.39
Pro 50 #9.	157	-148.8	-17.19
Pro 50 #10.	170	-147.7	-17.04
Pro 50 #11.	185	-147.1	-17.32
Pro 50 #12.	197	-151.0	-17.37
Pro 50 #13.	210	-154.8	-17.95

Sample	Depth, m	δD, ‰	$\delta^{18}O$, ‰
Pro 50 #14.	222	-157.8	-18.28
Pro 50 #15.	235	-158.2	-18.09
Pro 50 #16.	245	-152.8	-17.73
Pro 50 #17.	260	-159.8	-18.90
Pro 50 #18.	270	-160.2	-18.82
Pro 50 #19.	282	-159.8	-19.59
Pro 50 #20.	295	-160.4	-19.87
Pro 52 #3.	95	-143.9	-16.34
Pro 52 #4.	105	-145.2	-16.29
Pro 52 #5.	115	-143.4	-16.94
Pro 52 #6.	127	-144.5	-17.25
Pro 52 #7.	142	-145.1	-16.51
Pro 52 #8.	157	-147.4	-16.96
Pro 52 #9.	172	-153.1	-18.12
Pro 52 #10.	185	-149.9	-18.42
Pro 52 #11.	195	-162.2	-18.73
Pro 52 #12.	205	-162.9	-19.49
Pro 52 #13.	215	-160.5	-19.21
Pro 52 #14.	227	-161.7	-19.40
Pro 54 #5.	127	-145.9	-16.81
Pro 54 #6.	142	-144.7	-16.63
Pro 54 #7.	155	-145.1	-16.58
Pro 54 #8.	165	-146.0	-17.06
Pro 54 #9.	175	-147.8	-17.06
Pro 54 #10.	185	-148.7	-17.58
Pro 54 #11.	195	-152.3	-17.83
Pro 54 #12.	205	-154.8	-18.38
Pro 54 #13.	215	-156.1	-18.47
Pro 54 #14.	225	-155.3	-18.22
Pro 54 #15.	235	-157.7	-18.16
Pro 54 #16.	245	-146.5	-18.22
Pro 54 #17.	257	-156.4	-19.12
Pro 54 #18.	270	-156.0	-18.49
D3-02 #5.	127	-153.1	-18.52
D3-02 #6.	142	-145.8	-17.70
D3-02 #7.	157	-143.4	-16.55
D3-02 #8.	172	-141.3	-14.40
D3-02 #9.	185	-149.8	-16.81
D3-02 #10.	195	-142.3	-15.48
D3-02 #11.	205	-142.8	-16.14
D3-02 #12.	215	-143.6	-16.16

Sample	Depth, m	δD, ‰	$\delta^{18}O$, ‰
D3-02 #13.	225	-143.7	-15.85
D3-02 #14.	235	-145.0	-14.65
D3-02 #15.	250	-149.5	-17.16
D3-02 #16.	270	-146.7	-16.39
D3-02 #17.	290	-146.9	-16.23
D3-04 #4.	110	-157.7	-19.21
D3-04 #5.	125	-152.7	-17.75
D3-04 #6.	140	-151.8	-17.34
D3-04 #7.	150	-150.0	-17.17
D3-04 #8.	160	-145.5	-16.52
D3-04 #9.	175	-143.8	-15.56
D3-04 #10.	195	-143.9	-16.85
D3-04 #11.	225	-142.6	-16.30
D3-04 #12.	247	-161.5	-19.67
D3-04 #13.	265	-146.7	-17.12
D3-04 #14.	277	-149.5	-17.82
D3-04 #15.	292	-150.4	-18.31
D3-05 #5.	105	-156.0	-17.98
D3-05 #6.	127	-157.2	-18.55
D3-05 #7.	152	-157.0	-17.90
D3-05 #8.	170	-159.4	-18.12
D3-05 #9.	190	-157.8	-18.51
D3-05 #10.	210	-158.7	-18.18
D3-05 #11.	230	-159.0	-17.95
D3-08 #9.	150	-152.9	-18.94
D3-08 #10.	162	-152.4	-17.59
D3-08 #11.	175	-150.8	-17.17
D3-08 #12.	255	-156.7	-18.48
D3-08 #13.	285	-148.7	-16.95
D3-08 A #14.	195	-147.7	-16.91
D3-08 A #15.	225	-147.6	-17.08
D3-08 A # 16.	247	-153.4	-19.00
D3-08 A #17.	262	-146.3	-16.84
D3-08 A #18.	277	-147.4	-17.42
D3-08 A # 19.	292	-147.6	-16.95
D3-10 #10.	157.0	-156.8	-18.31
D3-10 #11.	187.0	-159.2	-17.92
D3-10 #12.	202.0	-158.8	-17.88
D3-10 #13.	217.0	-160.1	-18.86
D3-10 #14.	232.0	-160.4	-18.31
D3-10 #15.	250.0	-150.1	-18.38
D3-10 #16.	270.0	-163.0	-19.10

Sample	Depth, m	δD, ‰	$\delta^{18}O$, ‰
D3-10 #17.	290.0	-161.0	-18.76
Deep #4.	90	-149.1	-17.65
Deep #5.	110	-148.4	-16.92
Deep #6.	125	-146.6	-16.68
Deep #7.	135	-151.7	-16.78
Deep #8.	145	-150.9	-16.82
Deep #9.	155	-152.4	-16.32
Deep #10.	165	-155.0	-17.62
Deep #11.	175	-157.5	-17.67
Deep #12.	210	-149.2	-14.02
Deep #13.	247	-159.3	-17.89
Deep #14.	262	-161.5	-18.44
Deep #15.	277	-162.4	-18.54
Deep #16.	292	-161.4	-18.51
Deep #17.	307	-157.9	-18.60
Deep #18.	322	-161.8	-18.39
Deep #19.	337	-159.3	-18.51
Deep #20.	352	-161.6	-18.90
Deep #21.	367	-158.8	-18.19
Deep #22.	382	-160.4	-18.65
Deep #23.	397	-157.6	-17.28
Deep #24.	412	-159.8	-18.30
Deep #25.	430	-161.9	-18.42
Deep #26.	450	-159.9	-18.16
Deep #27.	470	-159.4	-18.53
Deep #28.	490	-157.5	-17.89
Deep #29.	510	-161.6	-18.71
Deep #30.	530	-161.0	-18.54
Deep #31.	550	-162.6	-18.86
Deep #32.	570	-161.9	-18.80
Deep #33.	590	-162.0	-18.64
Deep #34.	605	-161.0	-18.90
Deep #35.	615	-163.3	-19.53
Deep #36.	627	-159.4	-19.37
Deep #37.	637	-160.1	-18.33
Deep #38.	650	-159.4	-18.16
Deep #39.	660	-159.8	-18.51
Deep #40.	672	-159.1	-18.43
Deep #41.	685	-158.9	-17.98
Deep #42.	692	-157.8	-18.28
Deep #43.	707	-155.7	-17.79
Deep #44.	722	-159.1	-18.57

Sample	Depth, m	δD, ‰	$\delta^{18}O$, ‰
Deep #45.	737	-157.8	-18.21
Deep #46.	750	-157.0	-17.55
Deep #47.	762	-156.4	-18.81
Deep #48.	775	-157.3	-18.24
Deep #49.	785	-157.9	-17.91
Deep #50.	800	-155.3	-18.57
Deep #51.	815	-152.3	-18.21
Deep #52.	835	-156.0	-18.13
Deep #53.	855	-154.7	-16.71
Deep #54.	880	-158.2	-17.74
Deep #55.	910	-155.7	-18.46

Kelln's (2008) interflow samples

Sample	Date	δD, ‰	$\delta^{18}O$, ‰
D1 interflow	5-Jun-03	-148.7	-18.24
D1 interflow	11-Jun-03	-144.0	-17.59
D1 interflow	19-Jun-03	-149.1	-18.70
D1 interflow	8-Jul-03	-142.0	-17.62
D2 interflow	21-May-03	-133.4	-15.30
D2 interflow	5-Jun-03	-142.8	-17.50
D2 interflow	11-Jun-03	-143.8	-17.67
D2 interflow	19-Jun-03	-151.3	-19.75
D2 interflow	8-Jul-03	-142.6	-17.78
D2 interflow	16-Sep-03	-140.7	-16.40
D3 interflow	5-Jun-03	-149.0	-18.17
D3 interflow	11-Jun-03	-145.4	-17.76
D3 interflow	19-Jun-03	-142.6	-17.72
D3 interflow	25-Jun-03	-146.0	-17.74
D3 interflow	2-Jul-03	-142.6	-17.86
D3 interflow	12-Jul-03	-145.0	-17.77
D3 interflow	17-Jul-03	-147.8	-17.76
D3 interflow	24-Jul-03	-149.2	-17.83
D3 interflow	31-Jul-03	-144.5	-17.66
D3 interflow	16-Sep-03	-144.0	-17.58
D1 interflow	25-May-04	-163.4	-20.15
D1 interflow	31-May-04	-134.7	-16.76

Sample	Date	δD, ‰	$\delta^{18}O$, ‰
D1 interflow	10-Jun-04	-136.9	-16.29
D1 interflow	17-Jun-04	-140.1	-16.22
D2 interflow	25-May-04	-141.3	-16.78
D2 interflow	31-May-04	-139.4	-16.75
D2 interflow	10-Jun-04	-137.7	-16.22
D2 interflow	17-Jun-04	-136.6	-16.01
D2 interflow	24-Jun-04	-129.9	-16.42
D2 interflow	30-Jun-04	-134.5	-16.41
D3 interflow	12-May-04	-142.3	-17.84
D3 interflow	20-May-04	-143.4	-17.31
D3 interflow	25-May-04	-145.9	-17.89
D3 interflow	31-May-04	-133.0	-17.62
D3 interflow	10-Jun-04	-141.6	-17.74
D3 interflow	17-Jun-04	-143.0	-17.61
D3 interflow	24-Jun-04	-144.2	-17.60
D3 interflow	30-Jun-04	-141.5	-17.68
D1 Interflow: April 7	7-Apr-05	-160.7	-20.19
D1 Interflow: April 10	10-Apr-05	-156.5	-18.96
D1 Interflow: April 13	13-Apr-05	-153.4	-18.56
D1 Interflow: April 15	15-Apr-05	-145.5	-18.11
D1 Interflow: April 16	16-Apr-05	-145.3	-18.10
D1 Interflow: April 18	18-Apr-05	-142.3	-17.89
D1 Interflow: April 23	23-Apr-05	-140.9	-17.33
D1 Interflow: April 28	28-Apr-05	-138.6	-17.13
D2 Interflow: April 7	7-Apr-05	-152.8	-18.71
D2 Interflow: April 10	10-Apr-05	-143.8	-18.00
D2 Interflow: April 13	13-Apr-05	-147.2	-17.86
D2 Interflow: April 15	15-Apr-05	-141.8	-17.62
D2 Interflow: April 16	16-Apr-05	-142.6	-17.42
D2 Interflow: April 18	18-Apr-05	-140.4	-17.22
D2 Interflow: April 23	23-Apr-05	-143.0	-17.01
D2 Interflow: April 28	28-Apr-05	-137.2	-17.02
D3 Interflow: March 6	6-Mar-05	-129.4	-14.75
D3 Interflow: April 7	7-Apr-05	-163.3	-20.49
D3 Interflow: April 10	10-Apr-05	-158.7	-19.54
D3 Interflow: April 13	13-Apr-05	-152.8	-19.21
D3 Interflow: April 15	15-Apr-05		-18.27
D3 Interflow: April 16	16-Apr-05	-145.4	-18.31
D3 Interflow: April 18	18-Apr-05	-147.7	-17.95
D3 Interflow: April 23	23-Apr-05	-138.6	-17.34
D3 Interflow: April 28	28-Apr-05	-137.5	-17.14
D3 Int May 19	19-May-05	-142.9	-17.78

Sample	Date	δD, ‰	$\delta^{18}O$, ‰
D3 Int June 6	6-Jun-05	-145.2	-17.99
D3 Int June 15	15-Jun-05	-143.1	-17.93
D3 Int June 21	21-Jun-05	-145.3	-18.05
D3 Int June 24	24-Jun-05	-137.4	-17.70
D3 Int July 17	17-Jul-05	-138.5	-17.28
D3 Int July 25	25-Jul-05	-135.8	-17.42
D3 Int Aug 3	3-Aug-05	-135.5	-17.86
D3 Int Aug 18	18-Aug-05	-137.3	-18.06
D3 Int Sept 5	5-Sep-05	-134.6	-18.02
D3 Int Sept 28	28-Sep-05	-134.0	-17.68
D3 Interflow	27-Apr-06	-140.9	-17.61
D3 Interflow	3-May-06	-139.7	-17.45
D3 Interflow	11-May-06	-140.4	-17.36
D3 Interflow	9-May-06	-138.8	-17.36
D3 Interflow	16-May-06	-140.6	-17.50
D3 Interflow	17-May-06	-140.9	-17.54
D3 Interflow	20-Jun-06	-140.1	-17.29
D3 Int 4/11/07	11-Apr-07	-168.8	-22.05
D3 Int 4/13/07	13-Apr-07	-161.8	-21.08
D3 Int 4/15/07	15-Apr-07	-159.6	-20.84
D3 Int 4/17/07	17-Apr-07	-161.8	-21.17
D3 Int 4/19/07	19-Apr-07	-160.9	-21.00
D3 Int4/23/07	23-Apr-07	-155.0	-20.14
D3 Int 4/25/07	25-Apr-07	-153.0	-19.91
D3 Int 5/1/07	1-May-07	-148.7	-19.14
D3 05/03/07	3-May-07	-145.6	-18.86
D3 05/08/07	8-May-07	-144.6	-18.44
D3 05/13/07	13-May-07	-143.6	-18.71
D3 05/17/07	17-May-07	-146.4	-18.71
D3 05/31/07	31-May-07	-145.7	-18.68
D1 05/13/07	13-May-07	-155.2	-20.44
D1 05/17/07	17-May-07	-155.0	-19.74
D1 05/31/07	31-May-07	-149.4	-19.08

APPENDIX D: Sampling locations and dates

Table D1: Sampling location and dates for the Sandhill Fen

Location	Easting	Northing	Soil Sampling Date	Water Sampling Date
SH-GW-01	0463619	6321864	27-Jun-12	16-May-13
SH-GW-02	0463829	6321934	1-Jul-12	16-May-13
SH-GW-03	0463704	6321860	1-Jul-12	16-May-13
SH-GW-04	0463722	6321855	1-Jul-12	16-May-13
SH-GW-06	0463798	6321761	28-Jul-12	16-May-13
SH-GW-07	0463801	6321773	8-Jul-12	16-May-13
SH-GW-09	0463824	6321914	2-Jul-12	16-May-13
SH-GW-10	0463829	6321934	2-Jul-12	16-May-13
SH-GW-11	0463835	6321969	2-Jul-12, 30-Jul-12, 1-May-13	30-Sept-12, 16-May-13
SH-GW-12	0463847	6322001	2-Jul-12, 1-May-13	16-May-13
SH-GW-13	0463858	6322029	1-May-13	16-May-13
SH-GW-14	0463858	6322030	1-May-13	--
SH-GW-15	0463828	6322097	--	16-May-13
SH-GW-16	0463828	6322125	--	16-May-13
SH-GW-17	0463824	6322143	--	16-May-13
SH-GW-18	0464016	6322219	27-Jun-12	16-May-13
SH-GW-19	0464027	6322185	27-Jun-12	16-May-13
SH-GW-20	0464038	6322155	--	30-Sept-12, 16-May-13
SH-GW-26	0464043	6321940	29-Jul-12	16-May-13
SH-GW-27	0464026	6321919	29-Jul-12	16-May-13
SH-GW-28	0464007	6321885	29-Jul-12	16-May-13
SH-GW-30	0463942	6321781	6-Jul-12	16-May-13
SH-GW-31	0463950	6321770	28-Jul-12	30-Sept-12, 16-May-13
SH-GW-32	0463943	6321717	28-Jul-12	16-May-13
SH-GW-34	0464009	6321806	27-Jul-12	16-May-13
SH-GW-35	0464024	6321796	27-Jul-12	16-May-13
SH-GW-36	0464112	6321810	3-Jul-12	16-May-13
SH-GW-37	0464099	632187	3-Jul-12	16-May-13
SH-GW-38	0464108	6321922	3-Jul-12	16-May-13
SH-GW-39	0464202	6321878	5-Jul-12, 29-Jul-12	30-Sept-12, 16-May-13
SH-GW-40	0464251	6321866	5-Jul-12	16-May-13
SH-GW-41	0464344	6321694	28-Jul-12	16-May-13
SH-GW-42	0464343	6321733	28-Jul-12	30-Sept-12, 16-May-13
SH-GW-43	0464519	6321823	6-Jul-12, 30-Jul-12	30-Sept-12, 16-May-13
SH-GW-44	0464517	6321920	30-Jun-12	16-May-13

Location	Easting	Northing	Soil Sampling Date	Water Sampling Date
SH-GW-45	0464546	6321927	27-Jul-12	16-May-13
SH-GW-46	0464527	6322119	15-Aug-12	16-May-13
SH-GW-47	0464500	6322124	30-Jun-12	16-May-13
SH-GW-48	0464419	6322146	8-Jul-12, 30-Jul-12	16-May-13
SH-GW-51	0464350	6322133	29-Jun-12	16-May-13
SH-GW-52	0464364	6322172	29-Jun-12	16-May-13
SH-GW-53	0464407	6322212	29-Jun-12	16-May-13
SH-GW-54	0464437	6322226	30-Jun-12	16-May-13
SH-GW-55	0464463	6322238	30-Jun-12	30-Sept-12, 16-May-13
SH-GW-56	0464492	6322242	15-Aug-12	16-May-13
SH-GW-57	0464239	6322201	28-Jun-12	30-Sept-12, 16-May-13
SH-GW-58	0464272	6322208	28-Jun-12	16-May-13
SH-GW-61	0464313	6322230	28-Jun-12	16-May-13
SH-GW-63	0464231	6321782	3-Jul-12	16-May-13

UTM coordinates courtesy of Dr. Carl Mendoza, University of Alberta

Table D2: Sampling location and dates for South Bison Hills

Location	Easting	Northing	Soil Sampling Date
T1C	462345	6316960	13-Sep-12
T1U	462320	6317000	13-Sep-12
T1M	462280	6317030	13-Sep-12
T1L	462260	6317080	13-Sep-12
T2C	462380	6316900	13-Sep-12
T2U	462360	6317030	13-Sep-12
T2M	462330	6317070	13-Sep-12
T2L	462305	6317100	13-Sep-12
T3C	462425	6317020	13-Sep-12
T3U	462395	6317055	13-Sep-12
T3M	462370	6317100	13-Sep-12
T3L	462345	6317135	13-Sep-12
T8-P1	462375	6316875	13-Sep-12
T8-P2	462420	6316820	13-Sep-12
T8C	462460	6316780	13-Sep-12
T8M	462460	6316760	13-Sep-12
T8T	462475	6316745	13-Sep-12

Table D3: Soil sampling locations for Hilderman's (2011) study

Location	Easting	Northing	Soil Sampling Date
D3-2	462331	6317148	12-Dec-08
D3-4	462351	6317119	12-Dec-08
D3-5	462362	6317105	12-Dec-08
D3-8	462393	6317061	12-Dec-08
D3-10	462415	6317033	9-Dec-08
Pro 50	462486	6316901	9-Dec-08
Pro 52	462456	6316967	9-Dec-08
Pro 54	462465	6316988	9-Dec-08
Deep	462307	6317197	13-Dec-08

UTM coordinates and sampling dates referenced from Hilderman (2011)

**All UTM co-ordinates are in UTM NAD 83

APPENDIX E: Weighted means of precipitation to modify the LMWL

May- June 10

Sample	Date Sampled	δD, ‰	$\delta^{18}O$, ‰	Volume [mm]	Normalized Volume [mm/mm]	Weighted averages δD, ‰	Weighted averages $\delta^{18}O$, ‰
Rain C32 May 16 2012	16-May-12	-109.8	-11.3	18	0.0261	-2.864	-0.295
Precip SWSS Cell 32 June 1	11-Jun-12	-123.64	-13.54	18	0.0261	-3.225	-0.353
Precip Ucell June 4 2012	4-Jun-12	-127.56	-16.51	21	0.0304	-3.882	-0.502
Precip 30-T May 16 2012	16-May-12	-114.0	-15.04	4.5	0.0065	-0.743	-0.098
Precip 30T May 29 2012	29-May-12	-158.14	-20.5	11.5	0.0167	-2.636	-0.342
Precip 30T June 11 2012	11-Jun-12	-130.04	-15.5	10.5	0.0152	-1.979	-0.236
	18-May-09	-136.9	-16.88	5	0.0227	-3.111	-0.384
	1-Jun-09	-156.79	-18.32	6.5	0.0295	-4.632	-0.541
	11-Jun-09	-113.08	-10.98	1.5	0.0068	-0.771	-0.075
	26-May-09	-136.92	-15.94	2	0.0091	-1.245	-0.145
	26-May-09	-113.46	-13	2	0.0091	-1.031	-0.118
	28-May-09	-132.42	-13.78	0.5	0.0023	-0.301	-0.031
Average		-130.0	-15.4	101	0.2006	-26.42195	-3.120313
			Weighted Averages			-131.7	-15.6

June 11-June 25

Sample	Date Sampled	δD, ‰	$\delta^{18}O$, ‰	Amount [mm]	Normalized Volume [mm/mm]	Weighted averages δD, ‰	Weighted averages $\delta^{18}O$, ‰
Precip SWSS Cell 32 June 1	12-Jun-12	-126.42	-14.99	7.5	0.0109	-1.374	-0.163
C32 Precipitation	20-Jun-12	-130.6	-16.09	24.5	0.0355	-4.635	-0.571
SWSS-C32-Precip	25-Jun-12	-81.3	-11.33	12	0.0174	-1.413	-0.197
Ucell- Precipitation	20-Jun-12	-143.5	-18.07	44	0.0638	-9.152	-1.152
Ucell Precip	25-Jun-12	-82.4	-11.33	14	0.0203	-1.672	-0.230
Precip 30T June 12 2012	12-Jun-12	-121.64	-14.87	8.5	0.0123	-1.498	-0.183
30T-Precip	21-Jun-12	-149.4	-18.44	39	0.0565	-8.446	-1.042
30T-Precip	25-Jun-12	-75.7	-9.62	13	0.0188	-1.426	-0.181
	20-Jun-09	-138.08	-15.37	6.5	0.0295	-4.080	-0.454
	27-Jun-09	-131.53	-14.79	55	0.2500	-32.883	-3.698
Average		-118.1	-14.5	216.5	0.5151	-65.2	-7.7
			Weighted Averages			-126.599	-14.966

June 26 to July 12

Sample	Date Sampled	δD, ‰	$\delta^{18}O$, ‰	Volume [mm]	Normalized Volume [mm/mm]	Weighted averages δD, ‰	Weighted averages $\delta^{18}O$, ‰
SWSS-C32-Precipitation	7-Jul-12	-126.9	-16.09	80	0.1159	-14.716	-1.865
Ucell Precip	10-Jul-12	-128.8	-16.78	73	0.1058	-13.627	-1.775
30T Precip	9-Jul-12	-131.7	-17.30	75	0.1087	-14.318	-1.880
	28-Jun-09	-118.87	-12.93	18	0.0818	-9.726	-1.058
	1-Jul-09	-148.41	-17.37	6	0.0273	-4.048	-0.474
	9-Jul-09	-129.31	-14.46	6.5	0.0295	-3.821	-0.427
Average		-130.7	-15.8	258.5	0.4691	-60.255	-7.479
			Weighted Averages			-128.5	-15.9

July 13 to July 23

Sample	Date Sampled	δD, ‰	$\delta^{18}O$, ‰	Volume [mm]	Normalized Volume [mm/mm]	Weighted averages δD, ‰	Weighted averages $\delta^{18}O$, ‰
SWSS-C32-Precip	24-Jul-12	-122.8	-14.99	18	0.0261	-3.205	-0.391
Ucell-Precip	20-Jul-12	-139.4	-18.30	21	0.0304	-4.244	-0.557
	19-Jul-09	-133.81	-15.31	13.5	0.0614	-8.211	-0.939
30T Precip	23-Jul-12	-129.4	-16.31	14	0.0203	-2.625	-0.331
Ucell- Precipitation	12-Jul-12	-78.0	-9.06	2.5	0.0036	-0.283	-0.033
Average		-120.7	-14.8	69	0.1418	-18.567	-2.251
			Weighted Averages			-130.9	-15.9

July 24 to August 9

Sample	Date Sampled	δD, ‰	$\delta^{18}O$, ‰	Volume [mm]	Normalized Volume [mm/mm]	Weighted averages δD, ‰	Weighted averages $\delta^{18}O$, ‰
Ucell-Precip	9-Aug-12	-106.3	-12.71	16.5	0.0239	-2.541	-0.304
30T-Precip	2-Aug-12	-114.0	-14.43	18	0.0261	-2.973	-0.377
30T-Precip	9-Aug-12	-105.6	-12.26	9	0.0130	-1.378	-0.160
SWSS-C32-Precip	9-Aug-12	-92.0	-10.35	9.5	0.0138	-1.267	-0.142
	30-Jul-09	-117.35	-12.68	7	0.0318	-3.734	-0.403
	2-Aug-09	-115.49	-12.66	14	0.0636	-7.349	-0.806
	5-Aug-09	-135.65	-16.27	2	0.0091	-1.233	-0.148
	14-Aug-09	-136.11	-16	4.5	0.0205	-2.784	-0.327
Average		-117.0	-13.4	80.5	0.2018	-23.259	-2.667
			Weighted Averages			-115.3	-13.2

Aug 10 to Aug 31

Sample	Date Sampled	δD, ‰	$\delta^{18}O$, ‰	Volume [mm]	Normalized Volume [mm/mm]	Weighted averages δD, ‰	Weighted averages $\delta^{18}O$, ‰
	14-Aug-09	-136.11	-16	4.5	0.0205	-2.784	-0.327
	23-Aug-09	-123.98	-13.91	12.5	0.0568	-7.044	-0.790
	26-Aug-09	-124.36	-15.35	27	0.1227	-15.262	-1.884
30T-Preciptiation	14-Aug-12	-95.6	-10.82	8	0.0116	-1.108	-0.125
30T Precip	31-Aug-12	-95.1	-11.38	1.0	0.0014	-0.138	-0.016
SWSS-C32-Precip	31-Aug-12	-98.1	-11.81	12	0.0174	-1.706	-0.205
Ucell Precip	23-Aug-12	-90.9	-10.49	1	0.0014	-0.132	-0.015
Average		-104.7	-12.3	66	0.2319	-28.174	-3.364
			Weighted Averages			-121.5	-14.5

Sept

Sample	Date Sampled	δD, ‰	$\delta^{18}O$, ‰	Volume [mm]	Normalized Volume [mm/mm]	Weighted averages δD, ‰	Weighted averages $\delta^{18}O$, ‰
Ucell Precip	7-Sep-12	-105.5	-13.82	30	0.0435	-4.588	-0.601
Ucell Precip	18-Sep-12	-124.1	-16.17	54	0.0783	-9.713	-1.265
30T Precip	12-Sep-12	-113.4	-14.94	9.0	0.0130	-1.480	-0.195
	9-Sep-09	-113.96	-14.06	4	0.0182	-2.072	-0.256
	16-Sep-09	-88.52	-10.57	4	0.0182	-1.609	-0.192
	28-Sep-09	-114.61	-12.76	3.5	0.0159	-1.823	-0.203
Average		-110.9	-13.7	104.5	0.1871	-21.286	-2.712
			Weighted Averages			-113.8	-14.5

Oct-Nov

Sample	Date Sampled	δD, ‰	$\delta^{18}O$, ‰	Volume [mm]	Normalized Volume [mm/mm]	Weighted averages δD, ‰	Weighted averages $\delta^{18}O$, ‰
	7-Oct-09	-143.53	-17.89	1	0.0045	-0.652	-0.081
	13-Oct-09	-199.77	-26.2	1	0.0045	-0.908	-0.119
	17-Oct-09	-201.62	-26.23	0	0.0000	0.000	0.000
	27-Oct-09	-141.48	-18.06	17.5	0.0795	-11.254	-1.437
	5-Nov-09	-154.81	-20.12	0	0.0000	0.000	0.000
Average		-168.2	-21.7	19.5	0.0886	-12.815	-1.637
			Weighted Averages			-144.6	-18.5

Snow

Sample	Date Sampled	δD, ‰	$\delta^{18}O$, ‰
South Hills 30W	2-Mar-12	-201.9	-26.03
Capping St Aurora Site	7-Mar-12	-190.46	-24.07
C32 Station Snow	5-Mar-12	-200.16	-25.47
Coke Beach Snow	6-Mar-12	-197.09	-25.7
U Cell Snow	28-Feb-12	-198.88	-25.64
Sandhill Fen Snow	29-Feb-12	-189.3	-24.11
W1 Dump Snow	5-Mar-12	-196.7	-25.36
C46 Station Snow	5-Mar-12	-205.77	-26.88
Fort Hills North Snow	7-Mar-12	-185.8	-23.48
SIB Snow	6-Mar-12	-202.16	-26.19
30T Snow	21-Mar-12	-172.76	-22.17
	Average	**-194.6**	**-25.0**
Snow-Jack Pine	9-Jan-13	-201.7	-26.25
Snow-Coke Beach	9-Jan-13	-205.2	-26.92
Ucell-Precip	9-Jan-13	-211.3	-27.74
Snow-Fort Hills Aurora	10-Jan-13	-201.6	-26.52
Snow-W1	20-Feb-13	-215.9	-28.17
Snow-SBH	20-Feb-13	-216.5	-28.05
Snow-Fort Hills Aurora	21-Feb-13	-187.0	-24.14
Snow-SWSS-C46	25-Feb-13	-216.5	-28.16
Snow-SWSS-C32	25-Feb-13	-211.8	-27.72
Snow-Ucell	26-Feb-13	-205.4	-26.61
Snow-Sulfur Blocks	26-Feb-13	-230.5	-30.28
	Average	**-209.4**	**-27.3**
Snow-Coke Beach	12-Mar-13	-211.9	-27.63
Snow-C32	12-Mar-13	-203.1	-26.10
Snow-Fen	20-Mar-13	-243.3	-31.50
Snow-Ucell	12-Mar-13	-202.8	-26.45
Snow-SBH	14-Mar-13	-220.3	-28.35
Snow-C46	12-Mar-13	-210.4	-27.51
Snow-Jack Pine	12-Mar-13	-199.3	-25.39
Snow-W1	12-Mar-13	-197.3	-25.64
Snow-Fort Hills	26-Mar-13	-217.2	-28.07
Snow-Aurora	26-Mar-13	-210.2	-27.30
	Average	**-211.6**	**-27.4**

Hilderman- Snow

Date Sampled	δD, ‰	$\delta^{18}O$, ‰
26-Mar-09	-210.01	-26.63
26-Mar-09	-208.58	-26.67
26-Mar-09	-213.37	-27.35
26-Mar-09	-215.88	-27.86
26-Mar-09	-223.33	-28.84
26-Mar-09	-203.37	-26
29-Mar-09	-211.42	-27.03
29-Mar-09	-200.92	-25.38
29-Mar-09	-210.66	-26.95
29-Mar-09	-213.6	-27.43
29-Mar-09	-173.35	-21.84
29-Mar-09	-186.72	-24.05
29-Mar-09	-201.57	-25.82
29-Mar-09	-185.14	-23.75

2009 Snow Ave	**-204.1**	**-26.1**

Total Average	**-205.2**	**-26.6**
2012 Snow Ave	**-194.6**	**-25.0**
2013 Snow Ave	**-210.5**	**-27.4**

Sample	δD, ‰	$\delta^{18}O$, ‰
May- June 10	-131.7	-15.6
June 11-June 25	-126.6	-15.0
June 26 to July 12	-128.5	-15.9
July 13 to July 23	-130.9	-15.9
July 24 to August 9	-115.3	-13.2
Aug 10 to Aug 31	-121.5	-14.5
Sept	-113.8	-14.5
Oct-Nov	-144.6	-18.5
2009 Snow Ave	-204.1	-26.1
2012 Snow Ave	-194.6	-25.0
2013 Snow Ave	-210.5	-27.4

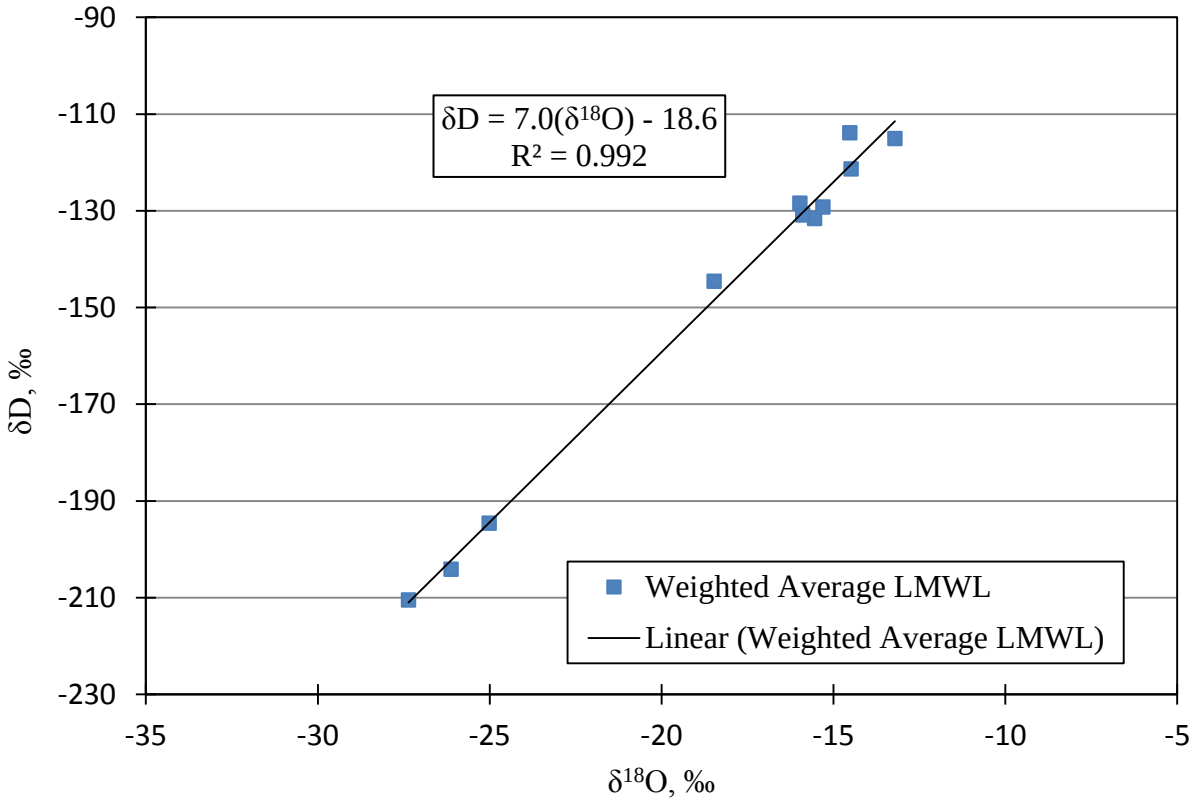

Figure E1: Development of LMWL using weighted average values of precipitation

APPENDIX F: Individual NEL for Peat Pond, Golden Pond and Bill's Lake

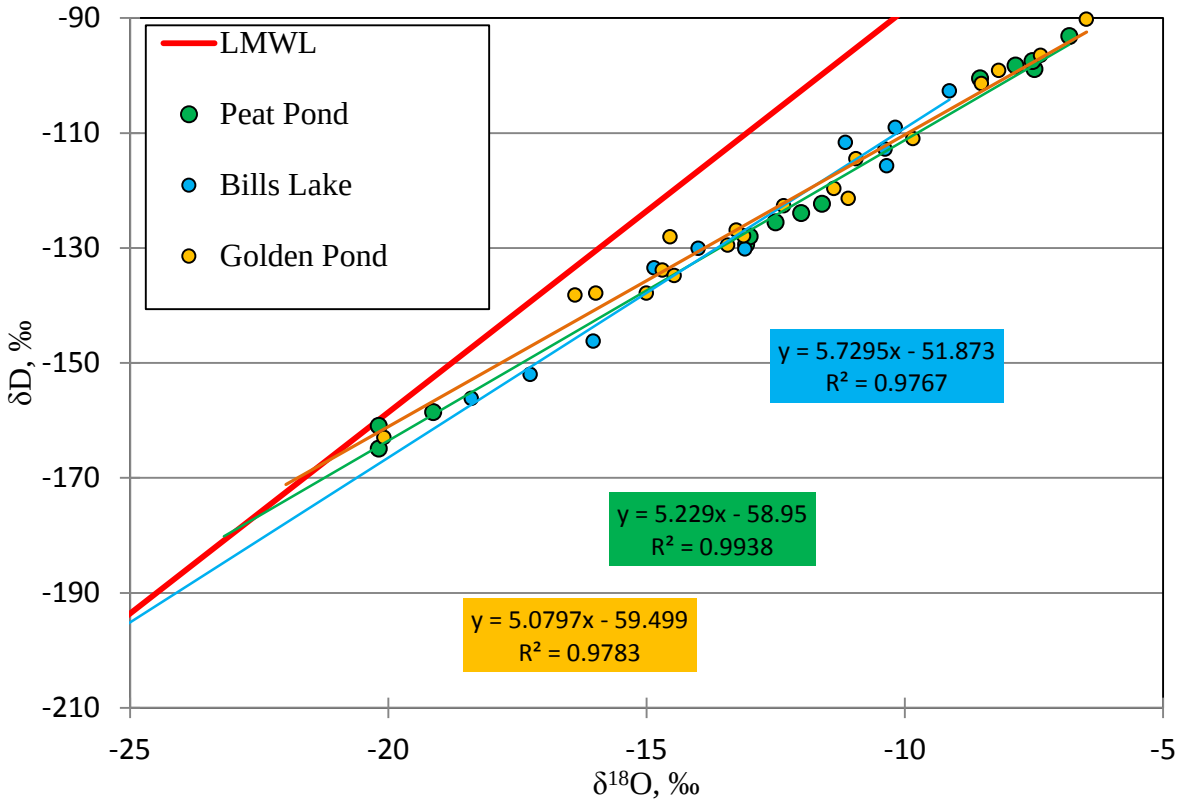

Figure F1: NEL for Peat Pond, Bill's Lake and Golden Pond

APPENDIX G: Summary of quantile plot results

Table G1: Summary of quantile plot Results

Dataset	δD, ‰			$\delta^{18}O$, ‰		
	Average	Std Dev	P-Value	Average	Std Dev	P-Value
Rainfall	-120.5	20.0	0.18	-14.5	2.7	0.43
Snow	-204.7	13.4	0.16	-26.4	1.9	0.20
West in-pit (WIP)- Tailings Profiles	-115.8	2.6	<0.005	-12.5	0.5	0.02
Aurora Settling Basin (ASB)- Tailings Profiles	-126.6	0.9	0.01	-14.0	0.3	<0.005
Surface PAW-Excluding Effluent Pond	-113.6	6.5	0.02	-12.9	1.3	0.71
Southwest in-pit (SWIP)	-116.4	6.6	0.39	-13.3	1.2	0.42
Southeast pit (SEP)	-114.6	10.1	0.33	-12.6	1.7	0.20
North mine drainage (NMD)	-132.9	19.7	0.20	-15.9	2.8	0.17
Effluent Pond	-110.6	5.6	0.40	-14.9	0.7	0.56
Soutwest Sands Storage (SWSS)	-111.6	6.1	0.90	-12.3	1.4	0.88
Mildred Lake Settling Basin (MLSB)	-113.8	6.1	0.56	-13.1	1.1	0.70
West in-pit (WIP)	-111.2	2.5	0.68	-12.2	0.6	0.21
Recycle pond	-114.0	6.7	0.02	-13.2	1.3	0.21
North Mine Train	-114.9	7.4	0.06	-13.4	1.3	0.28
Deep Shale (>3m) (Hilderman 2011)	-158.9	2.4	0.69	-18.4	0.5	0.10
Shallow Shale (<3m) (Hilderman 2011)	-151.9	6.2	<0.005	-17.6	1.1	0.26
2012/13 Interflow	-148.1	6.2	0.02	-18.7	0.8	0.49
2009 Interflow (Hilderman 2011)	-149.1	1.8	<0.005	-18.2	0.3	0.85
2003-2007 Interflow (Kelln 2008)	-144.7	7.9	<0.005	-18.0	1.3	<0.005
Combined Interflow	-146.7	6.6	0.02	-18.2	1.0	<0.005
Mildred Lake/Athabasca River	-142.7	1.6	0.05	-17.7	0.5	0.01
BGC Wells	-118.0	3.1	0.40	-12.9	0.6	0.43

APPENDIX H: Experimental and theoretical CDFs of select data sets

Rainfall

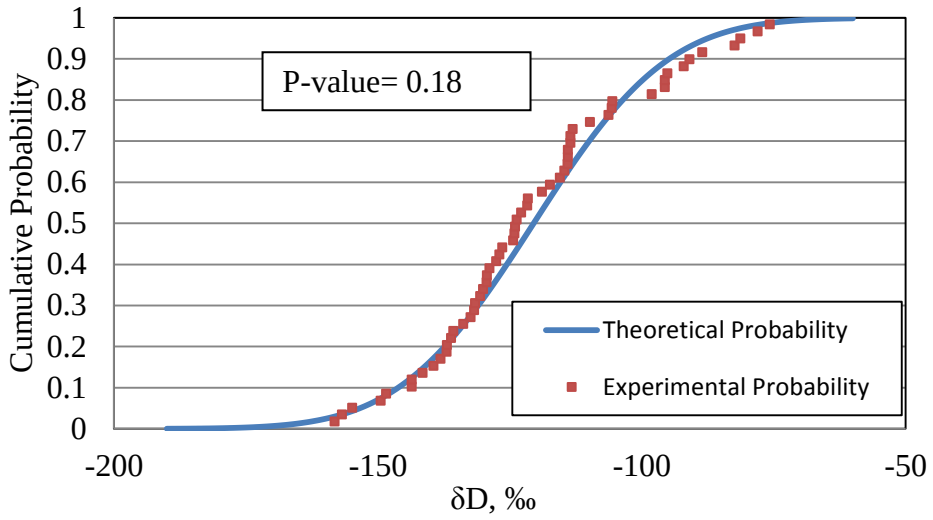

Figure H1: CDF of rainfall data set, δD

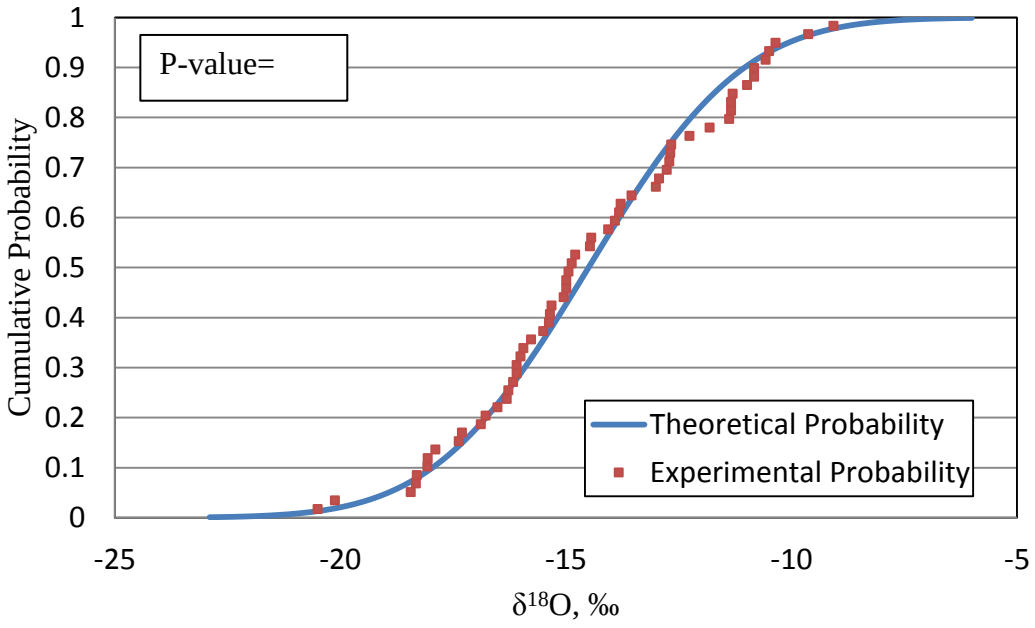

Figure H2: CDF of rainfall data set, $\delta^{18}O$

Snow

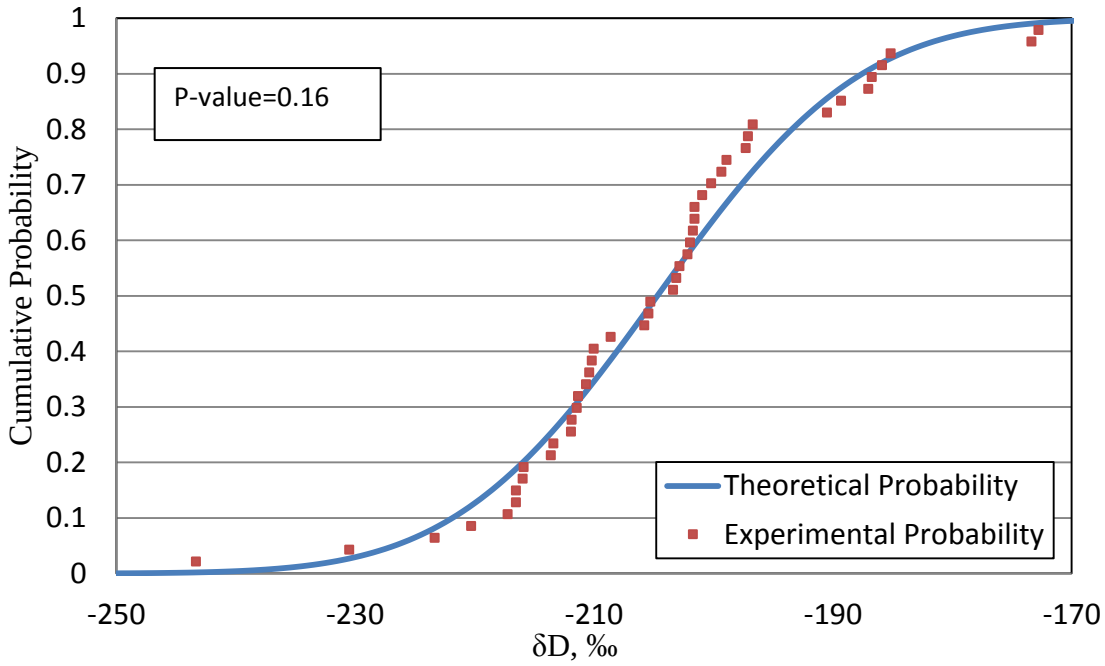

Figure H3: CDF of snow data set, δD

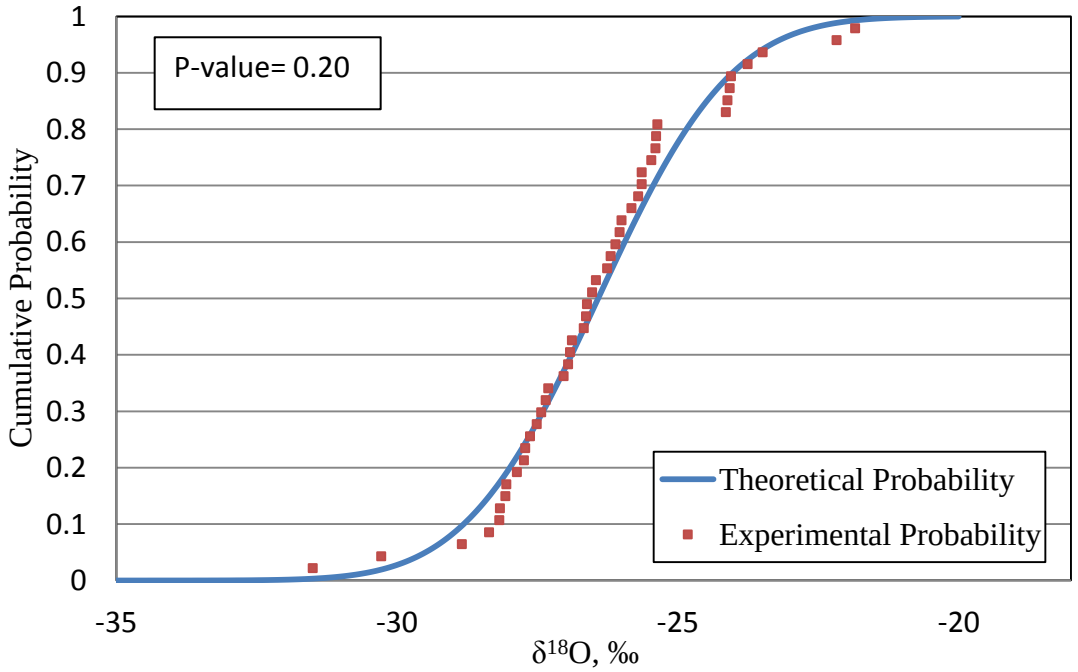

Figure H4: CDF of snow data set, $\delta^{18}O$

Interstitial shale water

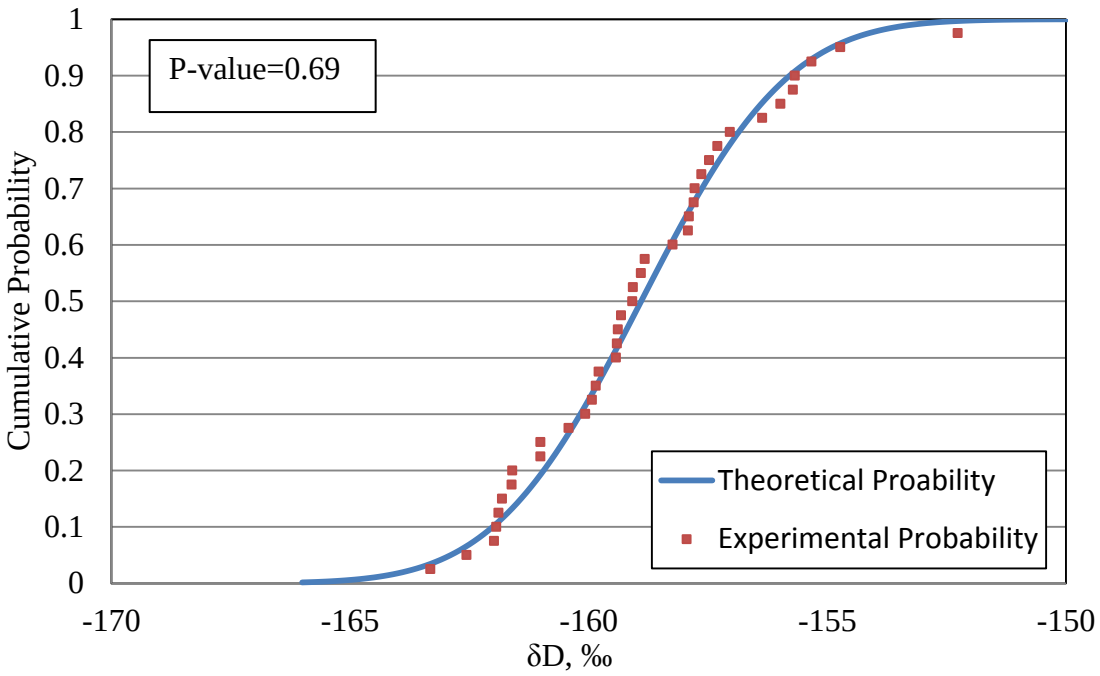

Figure H5: CDF of interstitial shale water data set, δD

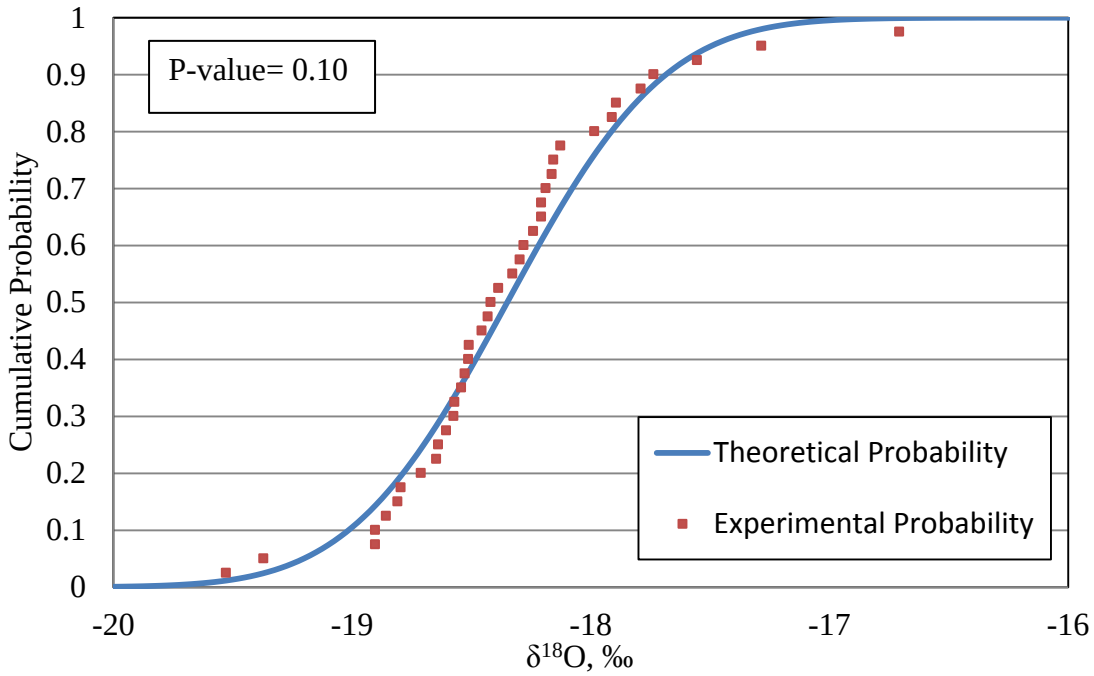

Figure H6: PDF of interstitial shale water data set, $\delta^{18}O$

Mildred Lake

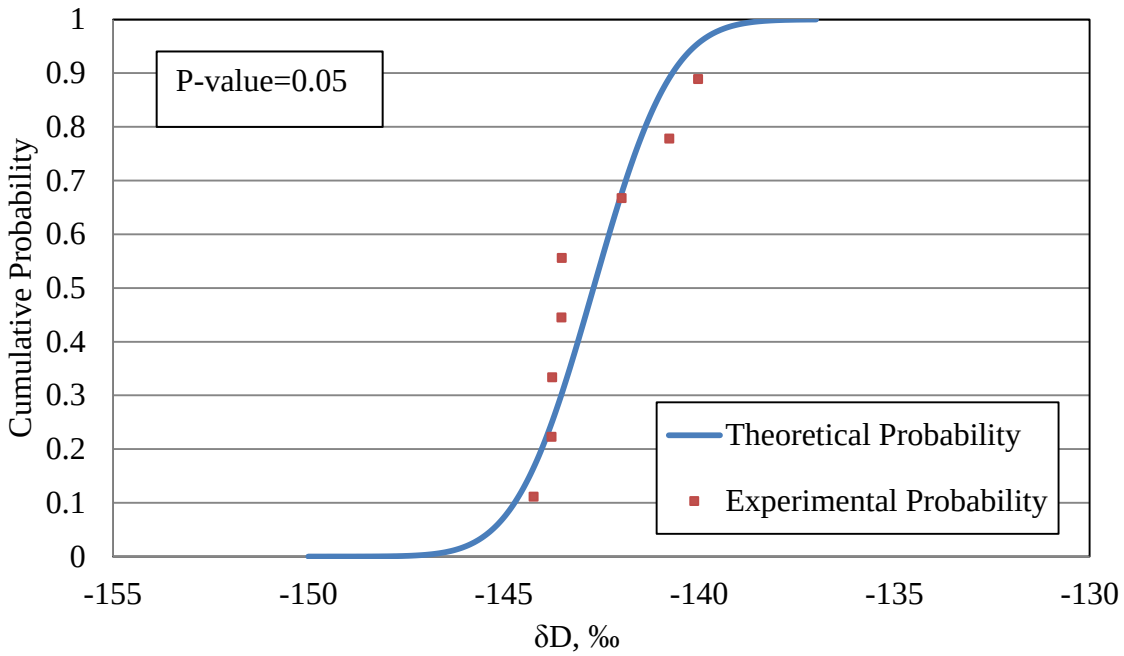

Figure H7: CDF of Mildred Lake water data set, δD

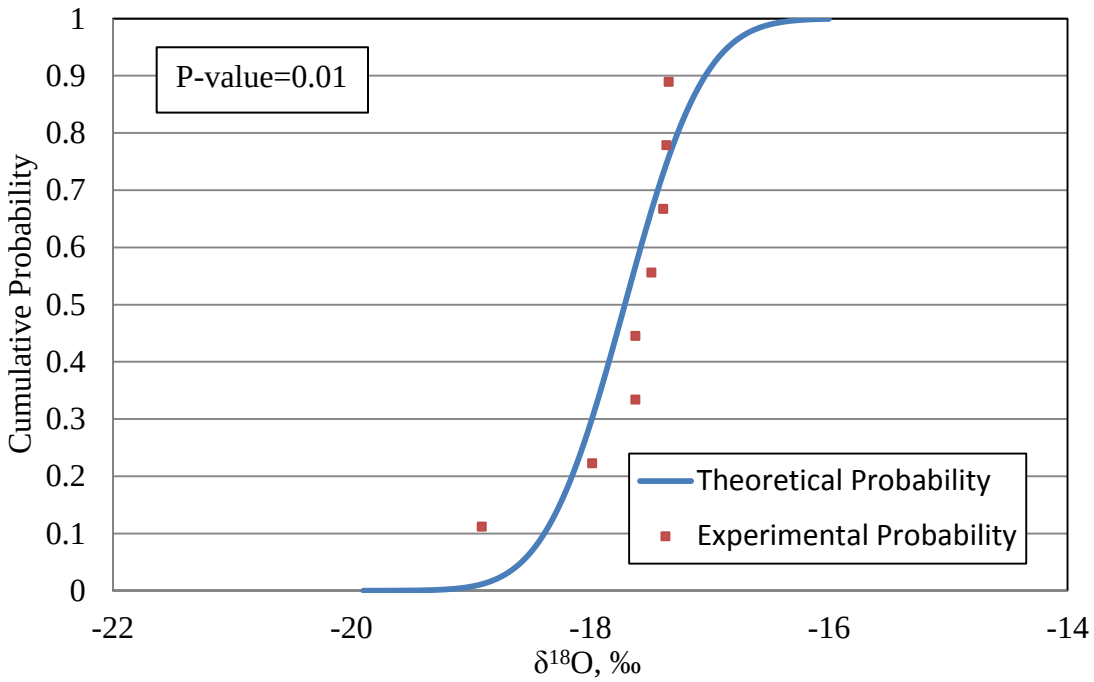

Figure H8: CDF of Mildred Lake water data set, $\delta^{18}O$

Process affected water (PAW)/tailings

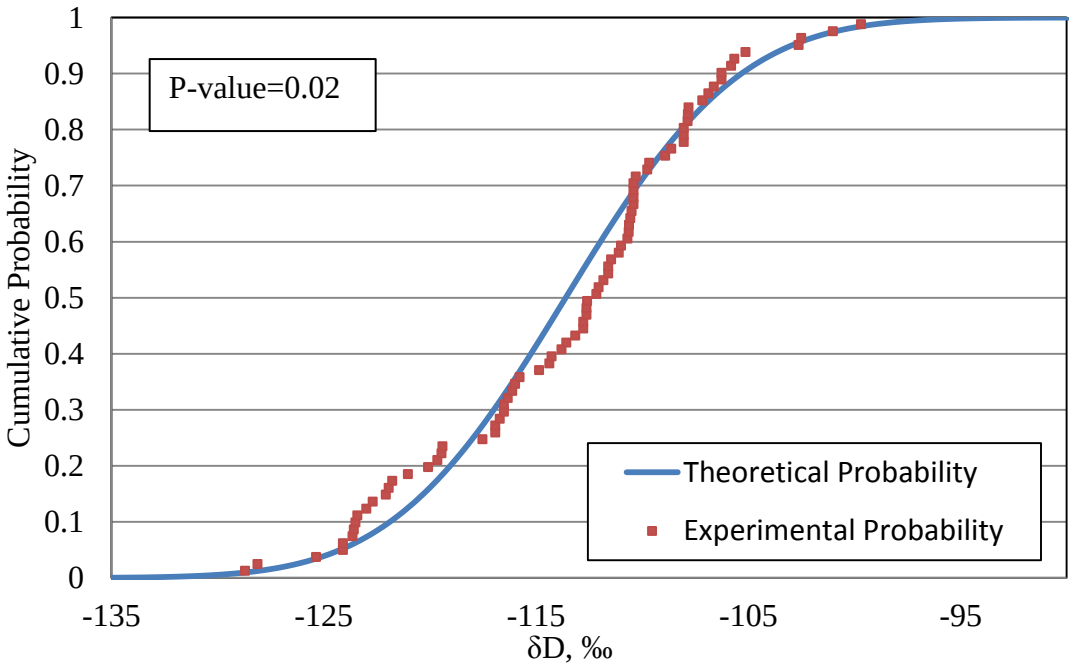

Figure H9: CDF of PAW data set, δD

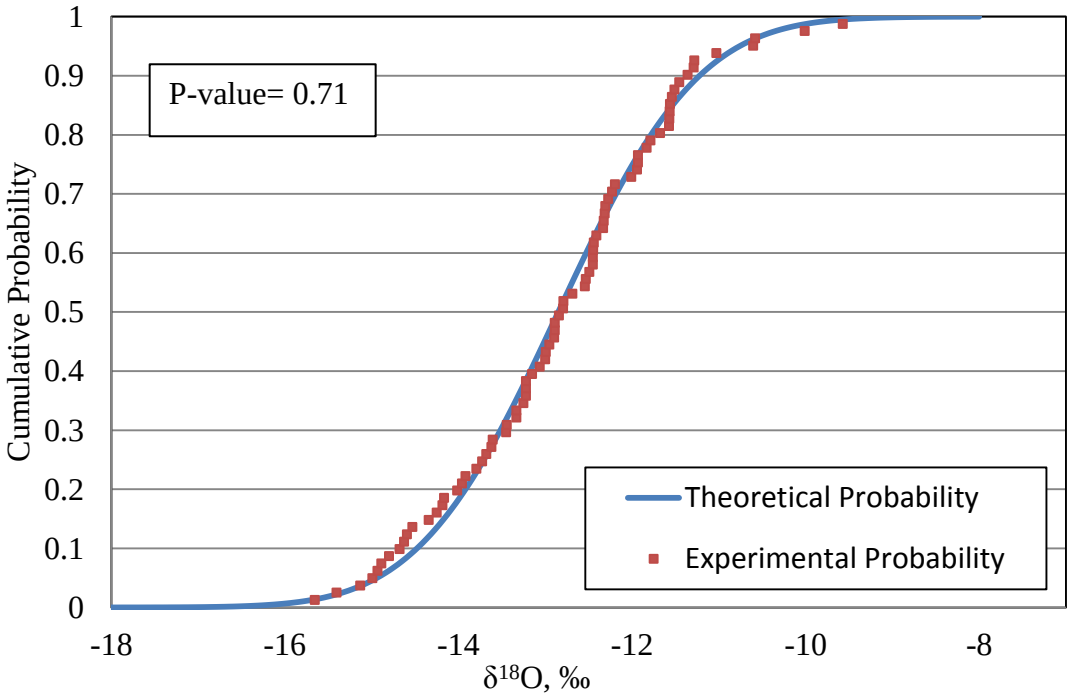

Figure H10: PDF of PAW data set, $\delta^{18}O$

West in-pit Tailings

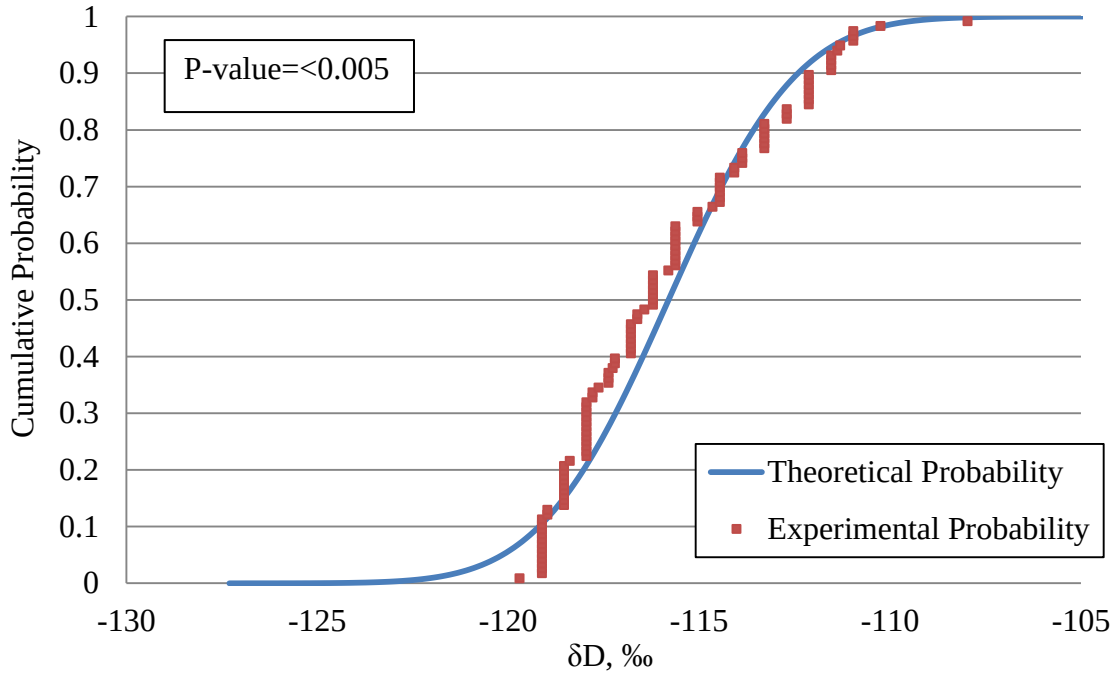

Figure H11: CDF of West in-pit data set, δD

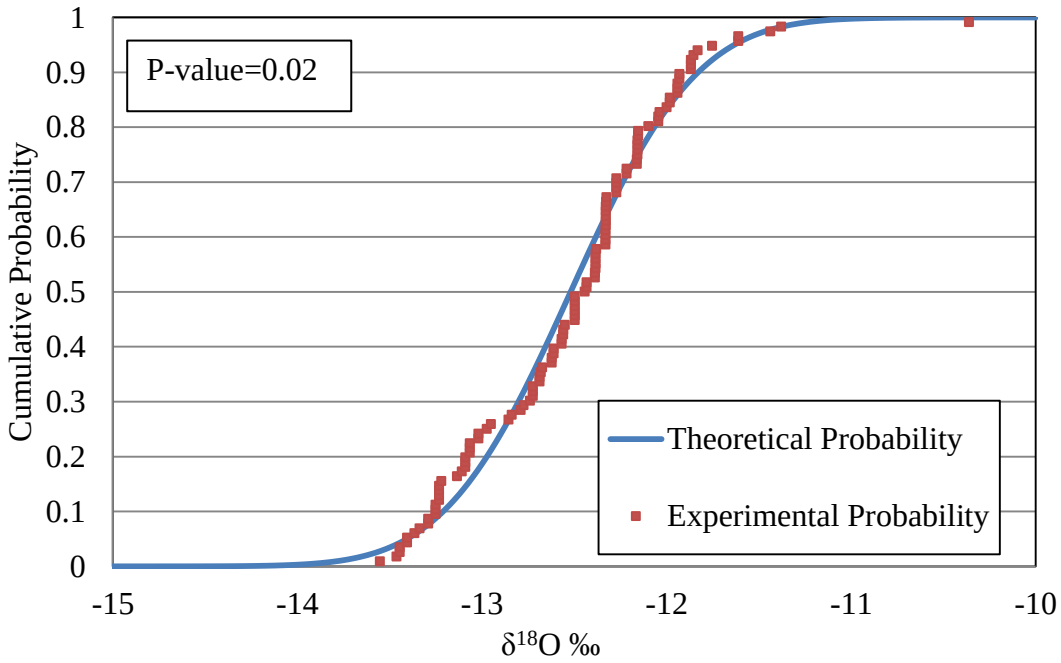

Figure H12: CDF of West in-pit data set, $\delta^{18}O$

Summary of t-tests- δD

			Equal Variance				Unequal Variance			
Sample 1	Sample 2	μ1-μ2	95% Lower CI	95% upper CI	T-value	P-value	95% Lower CI	95% upper CI	T-value	P-value
Precipitation	Snow	84.2	77.4	91.08	24.5	0.000	77.7	90.8	25.61	0
Precipitation	PAW	-6.9	-11.7	-2.19	-2.9	0.004	-12.4	-1.5	-2.5	0.014
Snow	PAW	-91.2	-94.7	-87.68	-51.5	0.000	-95.4	-87.0	-43.4	0
PAW	WIP-Tailings	2.3	0.9	3.59	3.4	0.001	0.7	3.8	3.0	0.004
PAW	ASB	13.0	10.9	15.16	12.0	0.000	11.5	14.5	17.6	0
ASB	WIP-Tailings	-10.7	-11.6	-9.86	-23.9	0.000	-11.3	-10.17	-36.9	0
Precipitation	WIP-Tailings	-4.7	-8.41	-0.9	-2.5	0.015	-10.0	0.6	-1.8	0.083
Precip	Deep shale	38.4	32.0	44.83	11.9	0.0	33.1	43.7	-14.4	0
Snow	Deep Shale	-45.8	-50.1	-41.50	-21.1	0.0	-49.9	-41.80	-22.8	0.0
Deep Shale	Shallow Shale	-7.0	-9.0	-4.95	-6.8	0.0	-8.3	-5.5	-9.7	0
BGC	WIP-Tailings	-2.2	-4.0	-0.47	-2.5	0.0	-4.5	0.0	-2.2	0.052
BGC	PAW	-4.5	-8.6	-0.35	-2.2	0.034	-7.0	-2.0	-3.7	0.001
Interflow	Shallow Shale	5.2	3.7	6.80	6.6	0.0	3.7	6.8	6.8	0
Precipitaiton	Mildred Lake	22.2	7.9	36.45	3.1	0.0	16.8	27.6	8.3	0
PAW	SWSS	-1.9	-5.8	1.87	-1.0	0.3	-5.9	2.0	-10.1	0.309
PAW	MLSB	0.2	-3.7	4.17	0.1	0.9	-3.9	4.3	0.11	0.91
WIP	WIP-Tailings	4.6	2.8	6.45	5.1	0.0	2.7	6.6	5.3	0
SEP	BGC	3.5	-3.5	10.38	1.0	0.3	-3.2	10.1	1.1	0.28
SWSS	MLSB	2.2	-2.9	7.23	0.9	0.4	-2.9	7.3	0.9	0.388
PAW	Effluent	-3.0	-7.2	1.27	-1.4	0.2	-7.1	1.2	-1.6	0.144
PAW	NMD	19.3	13.3	25.30	6.4	0.0	4.1	34.5	2.9	0.019
Recycle Pond	SWSS	-2.4	-7.6	2.77	-1.0	0.3	-7.6	2.8	-1.0	0.346
Recycle Pond	MLSB	-0.26	-5.6	5.06	-0.1	0.919	-5.6	5.1	-0.1	0.919
Recycle Pond	WIP	-2.87	-7.8	2.04	-1.2	0.237	-7.2	1.5	-1.4	0.179
Recycle Pond	SEP	0.54	-6.5	7.56	0.2	0.874	-6.7	7.8	0.16	0.877
Recycle Pond	SWIP	2.36	-4.2	8.92	0.8	0.461	-4.4	9.1	0.8	0.464
SWSS	WIP	-0.44	-4.98	4.1	-0.2	0.841	-4.5	3.6	-0.2	0.819
SWSS	SWIP	4.78	-1.43	10.99	1.62	0.123	-1.9	11.4	1.6	0.142
SWSS	SEP	3.0	-3.9	9.81	0.9	0.4	-4.1	10.1	0.9	0.391
WIP	SEP	3.4	-3.8	10.60	1.0	0.3	-3.2	10.0	1.1	0.282
Effluent	WIP	5.243	3.3	7.18	5.4	0	1.2	9,28	2.9	0.016

Summary of t-tests- $\delta^{18}O$

			Equal Variance				Unequal Variance			
Sample 1	Sample 2	µ1-µ2	95% Lower CI	95% upper CI	T-value	P-value	95% Lower CI	95% uppe	T-value	P-value
Precipitation	Snow	11.90	10.98	12.85	25.4	0	11.02	12.81	26.5	0
Precipitation	PAW	-1.65	-2.3	-0.97	-4.8	0.0	-2.4	-0.9	-4.3	0
Snow	PAW	-13.57	-14.1	-13.01	-48.4	0.0	-14.2	-12.9	-43.8	0
PAW	WIP-Tailings	-0.33	-0.6	-0.07	-2.5	0.0	-0.63	-0.04	-2.2	0.029
PAW	ASB	1.10	0.7	1.53	5.1	0.0	0.8	1.4	7.2	0
ASB	WIP-Tailings	-1.45	-1.6	-1.25	-15.0	0.0	-1.6	-1.3	-18.7	0
Precipitation	WIP-Tailings	-1.99	-2.5	-1.47	-7.6	0.0	-2.7	-1.3	-5.5	0
Precipitation	Deep Shale	3.85	3.0	4.72	8.8	0.0	3.1	4.6	10.5	0
Snow	Deep shale	-8.06	-8.7	-7.45	-26.1	0.0	-8.6	-7.5	-28.0	0
Deep Shale	Shallow Shale	-0.77	-1.1	-0.41	-4.2	0.0	-1.0	-0.5	-5.6	0
BGC	WIP-Tailings	-0.43	-0.8	-0.08	-2.4	0.0	-0.8	-2.4	-2.4	0.04
BGC	PAW	-0.09	-0.9	0.72	-0.2	0.8	-0.6	0.4	-0.4	0.681
Interflow	Shallow Shale	-0.63	-0.9	-0.38	-4.9	0.0	-0.9	-0.4	-4.8	0
Precipitation	Mildred Lake	3.21	1.3	5.14	3.3	0.0	2.4	4.0	8.0	0
PAW	SWSS	-0.51	-1.3	0.25	-1.3	0.2	-1.4	0.4	-1.2	0.239
PAW	MLSB	0.26	-0.5	1.02	0.7	0.5	-0.5	1.0	0.7	0.477
WIP	WIP-Tailings	0.32	-0.1	0.69	1.7	0.1	-0.1	0.76	1.6	0.1
SEP	BGC	0.33	-0.8	1.50	0.6	0.6	-0.8	1.5	0.6	0.541
SWSS	MLSB	0.77	-0.3	1.83	1.5	0.1	-0.3	1.8	1.5	0.144
PAW	Effluent	2.08	1.3	2.89	5.1	0.0	1.5	2.6	8.1	0
PAW	NMD	3.07	2.0	4.10	5.9	0.0	0.9	5.2	3.3	0.011
Recycle Pond	SWSS	-0.84	-1.9	0.25	-1.6	0.1	-1.9	0.3	-1.6	0.124
Recycle Pond	MLSB	-0.08	-1.1	0.91	-0.2	0.877	-1.1	0.9	-0.2	0.876
Recycle Pond	WIP	-0.98	-1.9	0.03	-2.2	0.043	-1.8	-0.1	-2.5	0.025
Recycle Pond	SEP	-0.56	-1.8	0.67	-0.9	0.355	-1.8	0.7	-0.9	0.362
Recycle Pond	SWIP	0.16	-10.6	1.38	0.3	0.788	-1.1	1.4	0.3	0.784
SWSS	WIP	-0.14	-1.184	0.906	-0.28	0.784	-1.1	0.8	-0.3	0.754
SWSS	SWIP	1.00	-0.319	2.32	1.59	0.129	-0.269	2.27	1.69	0.113
SWSS	SEP	0.28	-1.0	1.57	0.5	0.7	-1.0	1.6	0.4	0.663
WIP	SEP	0.42	-0.8	1.66	0.7	0.5	-0.7	1.5	0.8	0.442
Effluent	WIP	-2.41	-2.8	-2.05	-13.3	0	-2.9	-1.9	-11.1	0

APPENDIX J: Demonstration of Mildred Lake "buffering" capacity against δD and δ18O alterations

Table J1: Calculations estimating the Mildred Lake "buffering" capacity against δD and δ18O alterations

Descriptor	Value	Units
Inflow from Athabasca River	38.5×10^6 3.2×10^6	m^3/year m^3/month
Estimated Volume of Mildred Lake	7.2×10^6	m^3
Residence time of Mildred Lake water	2.25	months
Average δD of Mildred Lake	-143	‰
Estimated δD of Athabasca River during spring snowmelt	-165	‰
δD shift from Athabasca River during snowmelt pulse (assumed two months)	-154	‰

Note: 1) Volumes are estimated based on a survey from Halferdahl and Zubot (2003). The volume estimate assumes an elevation of Mildred Lake of 306.2 masl.

2) δD and $\delta^{18}O$ values of Athabasca River during snowmelt are unknown at this time. Values were approximated using a relatively conservative value.

APPENDIX K: Vapour sampling results- theoretical conversion

			Relative	Vapour Values		Machine Correction		PPMV Correction		Fractionation Factors		Liquid Values	
Sample	Temp [°C]	Temp [K]	Humidity [%]	δD [‰]	$\delta^{18}O$ [‰]	δD [‰]	$\delta^{18}O$ [‰]	δD [‰]	$\delta^{18}O$ [‰]	δD	$\delta^{18}O$	δD [‰]	$\delta^{18}O$ [‰]
GW-08-05	8.7	281.85	12750	-192	-23.3	-206.4	-27.5	-205.0	-25.2	1.099	1.011	-127.5	-16.9
GW-13-04	12	285.15	13850	-196	-24.3	-210.4	-28.5	-209.1	-26.4	1.095	1.011	-133.9	-16.2
GW-15-7	9.5	282.65	11700	-201	-25.0	-214.9	-29.2	-213.4	-26.8	1.098	1.011	-136.0	-16.4
GW-09-06	7.1	280.25	11650	-231	-22.3	-245.4	-26.5	-243.9	-24.1	1.102	1.011	-167.0	-13.4
GW-06-3.8	9.9	283.05	12800	-208	-23.8	-221.9	-28.0	-220.5	-25.8	1.098	1.011	-144.2	-15.3
GW-04-4	8.2	281.35	13300	-200	-24.3	-214.4	-28.5	-213.0	-26.3	1.100	1.011	-134.2	-15.7
Gw-05-3	11.9	285.05	13050	-199	-24.3	-213.4	-28.5	-212.0	-26.3	1.095	1.011	-137.0	-16.0
GW-03-3	12.9	286.05	12400	-206	-21.8	-220.4	-26.0	-219.0	-23.7	1.094	1.010	-145.7	-13.5
GW-11-7	7	280.15	12300	-205	-26.1	-219.4	-30.3	-218.0	-28.0	1.102	1.011	-138.3	-17.3
GW-05-2.2	10.9	284.05	13200	-214	-19.6	-228.4	-23.8	-227.0	-21.6	1.096	1.011	-152.5	-11.2
GW-11-6	7.7	280.85	12900	-188	-22.6	-201.9	-26.8	-200.5	-24.6	1.101	1.011	-119.9	-13.9
GW-10-7	7	280.15	13050	-235	-20.3	-248.9	-24.5	-247.5	-22.3	1.102	1.011	-170.9	-11.5
GW-10-2.5	10.9	284.05	13600	-212	-20.1	-225.9	-24.3	-224.6	-22.2	1.096	1.011	-149.8	-11.8
GW-05-1.5	12.2	285.35	13300	-207	-19.2	-221.4	-23.4	-220.0	-21.2	1.095	1.010	-146.1	-11.0
GW-09-2	11.6	284.75	13600	-208	-25.6	-222.4	-29.8	-221.1	-27.7	1.096	1.011	-146.6	-17.4
GW-10-3	11.2	284.35	13900	-201	-24.8	-214.9	-29.0	-213.6	-26.9	1.096	1.011	-138.0	-16.6
GW-13-2	12.1	285.25	14100	-194	-24.4	-208.4	-28.6	-207.1	-26.5	1.095	1.011	-131.9	-16.3
GW-11-5	9	282.15	13300	-198	-24.5	-212.4	-28.7	-211.0	-26.5	1.099	1.011	-132.9	-16.0
GW-06-5	8.5	281.65	11400	-221	-24.7	-235.4	-28.9	-233.9	-26.5	1.100	1.011	-157.5	-15.9
GW-03-4	9	282.15	11500	-202	-25.2	-216.4	-29.4	-214.9	-27.0	1.099	1.011	-137.1	-16.5
GW-06-06	6.7	279.85	10500	-193	-26.3	-207.4	-30.5	-205.8	-28.0	1.102	1.011	-124.6	-17.2
GW-13-2.5	12.7	285.85	13800	-213	-24.9	-226.9	-29.1	-225.6	-27.0	1.094	1.010	-152.7	-16.8

Machine Correction		Relative Humidity- Slope Correction	
δD [‰]=	14.4	δD [‰/1000ppm]=	0.083
$\delta^{18}O$ [‰]=	4.21	$\delta^{18}O$ [‰/1000 ppm]=	0.131

APPENDIX L: Sandhill Fen mixing example

Table K1: Estimates of PAW in Fen underdrains

				PAW Composition	
Sample	**Date**	**δD, ‰**	**$\delta^{18}O$, ‰**	**$\delta^{18}O$= -17.8 ‰**	**$\delta^{18}O$= -21.2‰**
Fen sump	14-Jun-12	-124.3	-14.64	0.645	0.785
Fen Sump	30-Jul-12	-130.0	-15.20	0.530	0.716
Fen Sump	15-Aug-12	-127.0	-14.99	0.574	0.742
Fen Sump	27-Nov-12	-128.4	-14.98	0.576	0.743
Fen Sump	18-Dec-12	-125.8	-14.66	0.642	0.783
Fen Sump	8-Jan-13	-124.6	-14.61	0.650	0.788
Fen Sump	1-Feb-13	-125.8	-14.77	0.619	0.770
Fen Sump	12-Feb-13	-127.9	-14.40	0.693	0.815
Fen Sump	27-Feb-13	-126.2	-14.49	0.675	0.803
Fen Sump	17-Mar-13	-127.2	-14.40	0.695	0.815
Fen Sump	25-Apr-13	-138.4	-16.58	0.249	0.546
Fen Sump	7-May-13	-139.8	-16.74	0.215	0.525
Fen Sump	16-May-13	-138.1	-16.41	0.284	0.567
Fen Sump	22-May-13	-139.2	-16.54	0.258	0.551
Fen Sump	6-Jun-13	-138.3	-16.70	0.225	0.531
Fen Sump	24-Jun-13	-131.8	-15.22	0.528	0.714

APPENDIX M: Estimated E/I over a range of δ18O

Table M1: Estimated E/I ratios over a range of $\delta^{18}O$

$\delta^{18}O$, ‰	E/I	$\delta^{18}O$, ‰	E/I	$\delta^{18}O$, ‰	E/I
-22.2	0.000	-14.8	0.262	-7.4	1.120
-22.0	0.005	-14.6	0.273	-7.2	1.172
-21.8	0.009	-14.4	0.284	-7.0	1.226
-21.6	0.014	-14.2	0.296	-6.8	1.285
-21.4	0.019	-14.0	0.308	-6.6	1.347
-21.2	0.024	-13.8	0.320	-6.4	1.414
-21.0	0.029	-13.6	0.333	-6.2	1.486
-20.8	0.035	-13.4	0.346	-6.0	1.564
-20.6	0.040	-13.2	0.360		
-20.4	0.045	-13.0	0.374		
-20.2	0.051	-12.8	0.388		
-20.0	0.057	-12.6	0.403		
-19.8	0.062	-12.4	0.419		
-19.6	0.068	-12.2	0.435		
-19.4	0.074	-12.0	0.452		
-19.2	0.081	-11.8	0.469		
-19.0	0.087	-11.6	0.487		
-18.8	0.093	-11.4	0.506		
-18.6	0.100	-11.2	0.525		
-18.4	0.107	-11.0	0.545		
-18.2	0.114	-10.8	0.566		
-18.0	0.121	-10.6	0.588		
-17.8	0.128	-10.4	0.611		
-17.6	0.135	-10.2	0.635		
-17.4	0.143	-10.0	0.659		
-17.2	0.151	-9.8	0.685		
-17.0	0.159	-9.6	0.712		
-16.8	0.167	-9.4	0.741		
-16.6	0.175	-9.2	0.770		
-16.4	0.184	-9.0	0.802		
-16.2	0.193	-8.8	0.834		
-16.0	0.202	-8.6	0.869		
-15.8	0.211	-8.4	0.905		
-15.6	0.221	-8.2	0.943		
-15.4	0.231	-8.0	0.984		
-15.2	0.241	-7.8	1.027		
-15.0	0.251	-7.6	1.072		

APPENDIX N: Calculations to estimate runoff component into Peat Pond for evaporation estimate

Flow data available for Peat Pond in 2012

Runoff Area Upstream=	11	ha
Runoff Area Downstream=	16.7	ha
Total water volume through upstream weir=	248	m^3
Total water volume through downstream weir=	68	m^3

1. Calculated the amount of runoff produced per hectare with the total water volume of upstream weir and upstream area

$$\frac{Runoff\ volume}{hectare} = \frac{248\ m^3}{11\ ha} = 22.5\frac{m^3}{ha}$$

2. Assuming the area upstream and downstream produce the same runoff volume per hectare, the total runoff volume can be calculated:

$$Total\ Runoff\ Volume = 22.5\frac{m^3}{ha} \cdot 16.7\ ha = 376\ m^3$$

3. Total runoff input into peat pond is calculated by subtracting volume passing through downstream weir from the total runoff volume:

$$Total\ Runoff\ Input\ into\ Peat\ Pond = 376\ m^3 - 68m^3 = 308\ m^3$$